Contributions to Gemology

No.10 May 2011

DISTINGUISHING NATURAL TIBETAN COPPER-BEARING ANDESINE FROM ITS DIFFUSION-TREATED COUNTERPARTS USING ADVANCED ANALYTICAL METHODS

Natural copper diffusion and sulfur-rich fluids

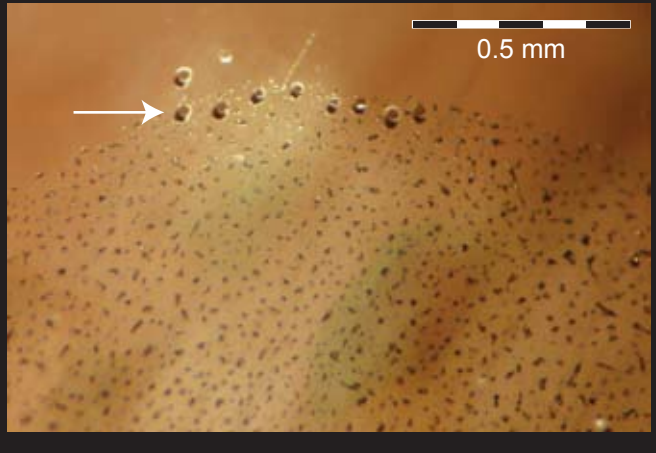

Fluid-inclusion analysis by LA-ICP-MS

Detail of treated surface by SEM

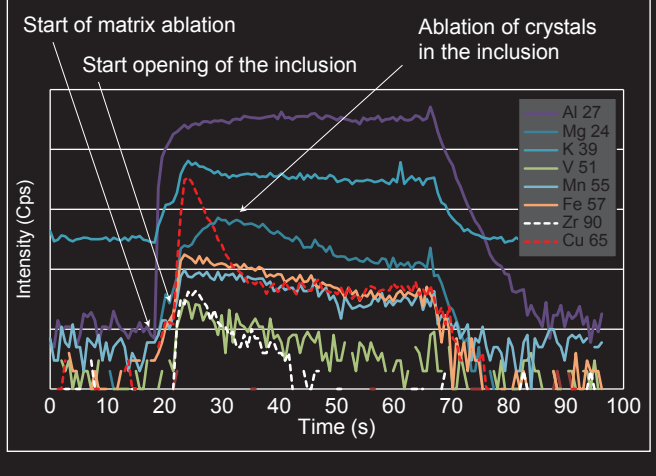

GRS GEMRESEARCH SWISSLAB

Editor

Dr. A. Peretti, FGG, FGA, EurGeol
GRS Gemresearch Swisslab AG, P.O.Box 3628, 6002 Lucerne, Switzerland

adolf@peretti.ch

Coming Soon

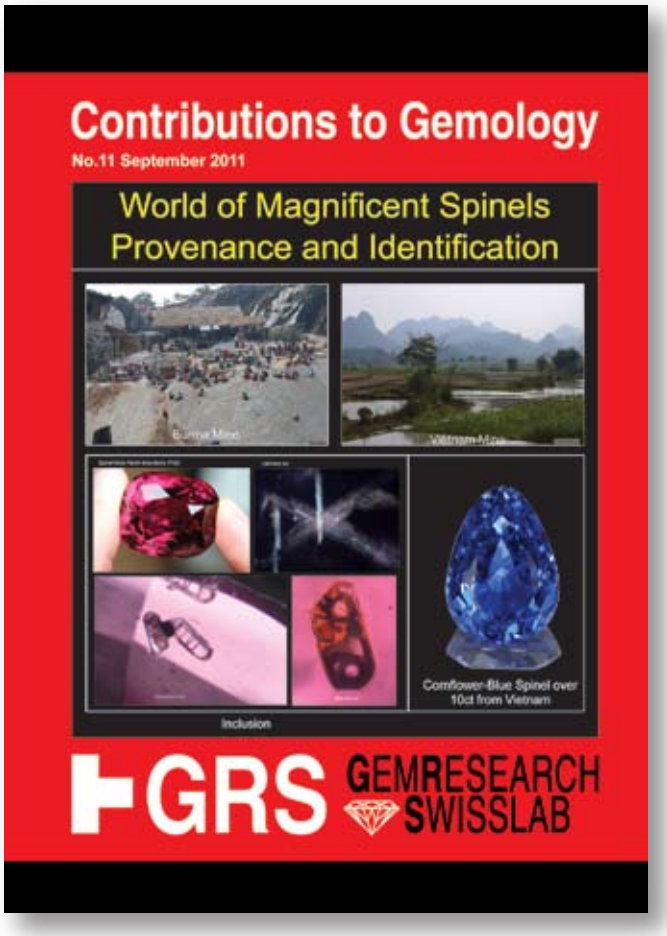

This journal follows the rules of the Commission on New Minerals and Mineral Names of the IMA in all matters concerning mineral names and nomenclature.

Distributor

GRS (Thailand) Co., LTD
257/919 Silom Rd., JTC Building
Bangkok 10500, Thailand.

This report is available online at www.gemresearch.ch

ISBN 978-3-9523867-0-5

Message from the Editors Desk

The identification of copper-bearing gem quality andesine ("red andesine") is of high interest to the gem industry as most of today's red andesine labeled as coming from Tibet is debated as potentially diffusion-treated. Separating diffusion-treated from natural gems turned out to be one of the most challenging research projects. Subsequent to an extensive analysis that was made during a PhD study at the "Eidgenössische Technische Hochschule" (Swiss Federal Institute of Technology) in Zurich (ETHZ) on samples from GRS. Additional samples were received 6 months ago from an expedition that reported to have found new mining spots in Tibet. Therefore, it was necessary to complement the previous research by analyzing the recently collected samples.

The breakthrough of our finding consists of a new element proxy (silver) complemented by copper isotope measurements using a state of the art femtosecond laser ablation-MC-ICP-MS instrument (D-CHAB, ETH Zurich). These analyses were further crosschecked by radiogenic Argon-measurements, crystal structure analyses (both at the University of Berne) and by an extensive suite of further tests including a detailed SEM-study on surface particles (University of Fribourg) and fluid inclusion analyses (again at D-CHAB, ETH Zurich).

The "Smoking Gun" was finally found in a sample that GRS collected itself earlier from one of the mines in Tibet in 2009. We were able to drill with a laser inside this sample and to open hidden fluid inclusions. It was possible than to analyze these "chemical fingerprints" in the fluids once trapped in Tibetan copper-bearing andesine when it formed in the depth of the Earth Millions of years ago. Clearly, a natural signature was found.

Based on our indepth research we are able to isolate a group of natural copper-bearing Tibetan andesines from the new material, these can be confirmed as authentic and these gems are not diffusion-treated.

Another surprising result, was that all of the gem-quality copper-bearing andesine that we have tested recently and that was labeled in the market as untreated materials coming from Tibet ("market stones") did not contain the elemental fingerprint including silver of natural copper-bearing Tibetan andesines. Therefore, none of these could be confirmed as authentic materials using non-destructive methods. Since our results allow us to identify natural Tibetan andesine mostly from the locality Yu Lin Gu, it remains unknown where the red, gem-quality materials widely available in the market are coming from, unless destructive methods can be used for testing.

"Absence of evidence is not evidence of absence" (Carl Sagen, 1934-1996) remains as a valid plea for the authenticity of the market stones.

Adolf Peretti

GRS Contents of Contributions to Gemology No.10

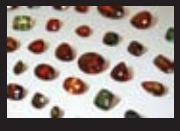

Introduction 1

Copper-bearing andesine from Tibet 2

Map of Tibet (China) with the major reported Tibetan andesine occurrences at the "new mines" (Zha Lin, Yu Lin Gu, Gyaca) and "old mines" (Bainang) 3

Mine locations (Fig. An04) 4

GRS Expedition: The Potala Palace, Landmark in Lhasa, Capital of Tibet (China) 5

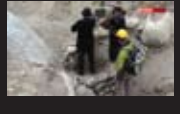

Expedition of GRS to a collection point of copper-andesine in Tibet (Gyaca). Clips are from the movie shown in Tucson at the GILC meeting in January 2011 6-13

The so-called "old mines" copper-bearing andesine occurrence at Bainang (Tibet) 14

The "sunstone" (copper-bearing labradorite) occurrences of Oregon (USA) 15-16

Mining operations at the Dust Devil Mining Company (DDMC) in Oregon (USA) 17-18

Comparison of two reported mining operations in Tibet and Oregon 19

Copper-bearing labradorite (sunstone) from Oregon 20

Sample source verification 21-28

Fluid inclusions in a copper-bearing andesine from Gyaca (Tibet) 29-34

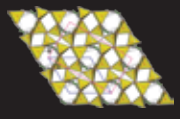

Structure model of copper-bearing andesine from Tibet 35

Lattice-parameters of feldspar from different provenances (treated and untreated) including copper-bearing andesine from Tibet 36-37

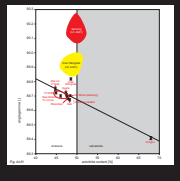

Conclusion crystallography 38

LA-ICP-MS analyses 39

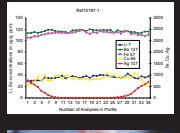

Concentration profiles natural Tibetan andesine 40-45

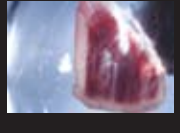

Diffusion-treated copper-bearing andesine samples of Chinese origin 46

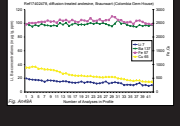

Concentration profiles of diffusion-treated copper-bearing andesine determined by LA-ICP-MS 47

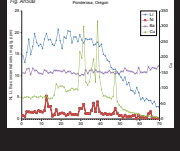

Concentration profiles of sunstone from Oregon by LA-ICP-MS 48-49

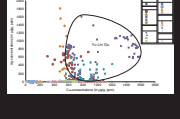

Ag-Cu- and Li-Cu-discrimination diagram for natural andesine, diffusion-treated andesine and sunstone from Oregon 50

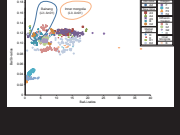

Ni-Cu- and Ba/Sr versus Ba/Li discrimination diagram and conclusion LA-ICP-MS analysis 51

Fluid inclusion analysis by LA-ICP-MS 52

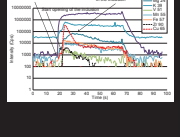

Analysis of individual fluid inclusions in andesine from Gyaca by LA-ICP-MS 53

Contents of Contributions to Gemology No.10

Results of fluid inclusion analysis by LA-ICP-MS 54

Scanning Electron Microscopy (SEM-EDX) analysis 55-74

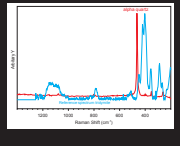

Raman analysis of surface particles 75

Raman spectra of inclusions (anatase, calcite and alpha-quartz) in an andesine from the Bainang mine (Tibet) 76

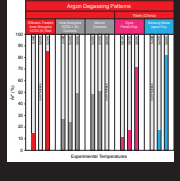

Radiogenic argon measurements of copper-bearing feldspar 77

Argon degassing patterns 78

Noble gas laboratory at the Institute of Geology, University of Berne (Switzerland) 79

K-Ar age determinations 80

Results Argon testing 81

K-Ar ages of feldspars from Tibet, Oregon, Mexico and Inner Mongolia 82

IR-UV-fs-MC-ICP-MS Instrumentation at the Research Group for "Trace Element and Micro Analysis" at the ETH Zurich, Switzerland 83-84

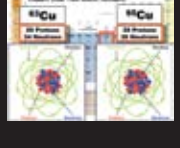

Copper isotope ratio analysis of copper-bearing andesine: Definitions and results 85-86

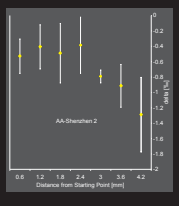

Copper isotope ratio measurements on diffusion treated samples (Xian, Shenzhen) using femtosecond laser ablation-MC-ICP-MS 87

Copper isotope ratio measurements on natural Tibetan samples (Gyaca) using femtosecond laser ablation-MC-ICP-MS 88

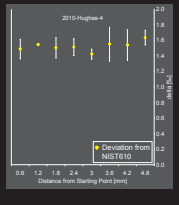

Copper isotope ratio measurements on natural Tibetan samples (Yu Lin Gu) using femtosecond laser ablation-MC-ICP-MS 89

Conclusion copper isotope ratio measurements 90

Interpretation of authenticity of Tibetan red andesine 91-92

Inclusion features in treated copper-bearing andesine 93

Microphotograph of experimentally diffusion-treated Inner Mongolia andesine 94

Tab. An06-An13 Chemical compositions 95-102

Literature 103

About the Authors and Acknowledgments 105

DISTINGUISHING NATURAL TIBETAN COPPER-BEARING ANDESINE FROM ITS DIFFUSION-TREATED COUNTERPARTS USING ADVANCED ANALYTICAL METHODS

Adolf Peretti (1) Igor Villa (2), Willy Bieri (1), Kathrin Hametner (3), Ladina Dorta (3), Gisela Fontaine (3) Mario Meier (4) and Detlef Günther (3)

(1) GRS Gemresearch Swisslab AG, Sempacherstr. 1, CH-6003 Lucerne, Switzerland
(2) University of Bern, Institute of Geological Sciences, Baltzerstrasse 3, 3012 Bern, Switzerland
(3) Laboratory of Inorganic Chemistry, ETH Hönggerberg, HCI, G113, CH-8093 Zurich, Switzerland
(4) Department of Geosciences, University of Fribourg, Chemin du Musée 6, Pérolles, 1700 Fribourg, Switzerland

INTRODUCTION

The diffusion-treatment of andesine-feldspar with copper transforms yellowish colored feldspar into a beautiful reddish-colored copper-bearing andesine (Lit. An10 and An44).
Untreated copper-bearing feldspar of beautiful red color is also found in nature (see for example Fig. An17) but it is extremely rare. These natural red copper andesines are regarded as gems and are highly valuable. The only widely acknowledged natural occurrence up to this date is found in the State of Oregon (USA). A further occurrence in Tibet is currently under investigation (Lit An1-7, An27 and An39-40).
The recent discovery of the treated copper-bearing andesine emerging from heat-treatment laboratories in the last 5 years has challenged the gemological community and it is regarded a difficult task to find a conclusive test for the identification of this treatment.
Before the question of testing could be addressed, the first challenge was to find natural andesine in the field, particularly from Tibet. Several expeditions were made to Tibet by various researchers, including one expedition by GRS to Gyaca (Tibet, 2009). This expedition resulted in one of the first international documentaries on a salted mine captured on DVD and was presented by GRS to the GILC-meeting in Tucson (Arizona) in January 2011. Additional discovery of various other salted copper-bearing andesine occurrences in Tibet have been reported (Lit. An47) that confirmed the findings of GRS. In September 2010, another expedition team finally confirmed the natural occurrence of copper-bearing andesine in Tibet approx. 350 km away from the occurrence visited by GRS one year earlier (Lit. An06-07 and Lit. An24). As mentioned in the first publication on the subject, material from this expedition was not available and was therefore not incorporated into our first report (Lit. An13). We have received the new mines material from the recent expedition in November 2010, including first hand collected material from the 2 new collection spots in Tibet from 2 different expedition members (See Acknowledgements). No samples of the new mines were obtained from other participants of the 2010 expedition. In addition, further rough sunstone materials from the provenance of Oregon (USA) were also received from different sources (Desert Devil Mine Co., Desert Sun Mining Co. and and from a new mine in Oregon, the Pana mine). Furthermore, different generations of diffusion-treated copper-bearing andesine samples were acquired (Xian University, China, production 2004-2005) and from other gem treating centers (Shenzhen or Tianjin) in early 2011 from two different sources. A detailed listing of the tested material is compiled in Tab. An01. Due to the large influx of new material after our first report appeared, it was necessary to revisit the entire andesine material that was previously analysed (Lit. An13, 14 and 28).
This report is the summary of our efforts to find a test that can separate natural from diffusion-treated copper-bearing andesines through the investigation of these newly acquired samples. We used the entire repertoire of state-of-the-art analytical techniques that were available at different Swiss Research Groups (University Fribourg, University Berne and ETH Zurich). It has been widely demanded by the gemstone industry that the experts of the gemological community make a special effort to end the “andesine controversy” or so-called “andesine fiasco”. It will be a test and a statement of the gemological community that new treatments will not remain unanswered, and we have pledged to play a role in it.

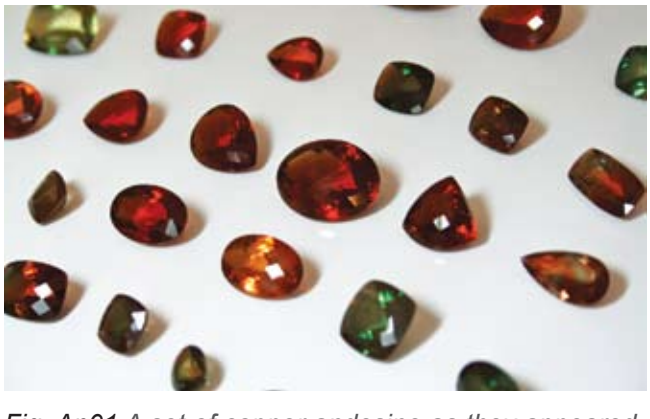

Fig. An01 A set of copper-andesine as they appeared on the gem market in 2011 under the trade name Tibetanite. Largest faceted gem is 35ct. They are all claimed to be untreated and from Tibet.

Fig. An02A

Fig. An02B

Fig. An02A-B View from one of the palaces roofs in Lhasa of the surrounding 6000m high mountains that have to be crossed to reach the claimed location of the red andesine occurrences in Tibet (see inserted map). A large number of stunning beautiful copper-bearing andesine appeared in the market and the following questions were asked (See for example Lit. An7, 15, 24-26, 30, 32, 33, 35, 38 and 40): Are these stones found in Tibet or elsewhere? Are they of natural color or is their color produced by a treatment?

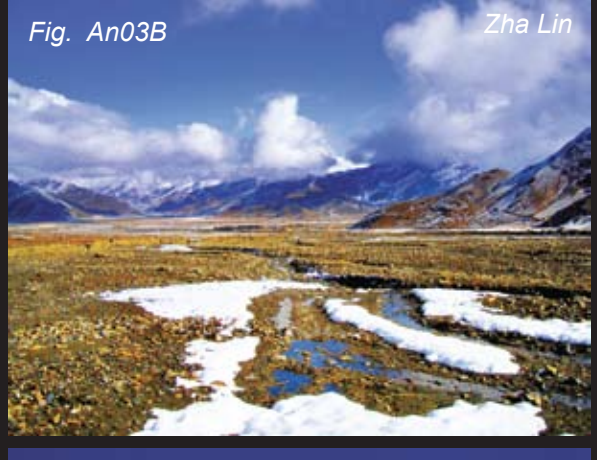

Fig. An03A, B, C Scenery of the location where the new mines in Tibet (Zha Lin and Yu Lin Gu) are found geologically in Flysch and near Ophiolites (Lit. An07 and An17). Coordinates see inserted box. Pictures courtesy Litto Gems.

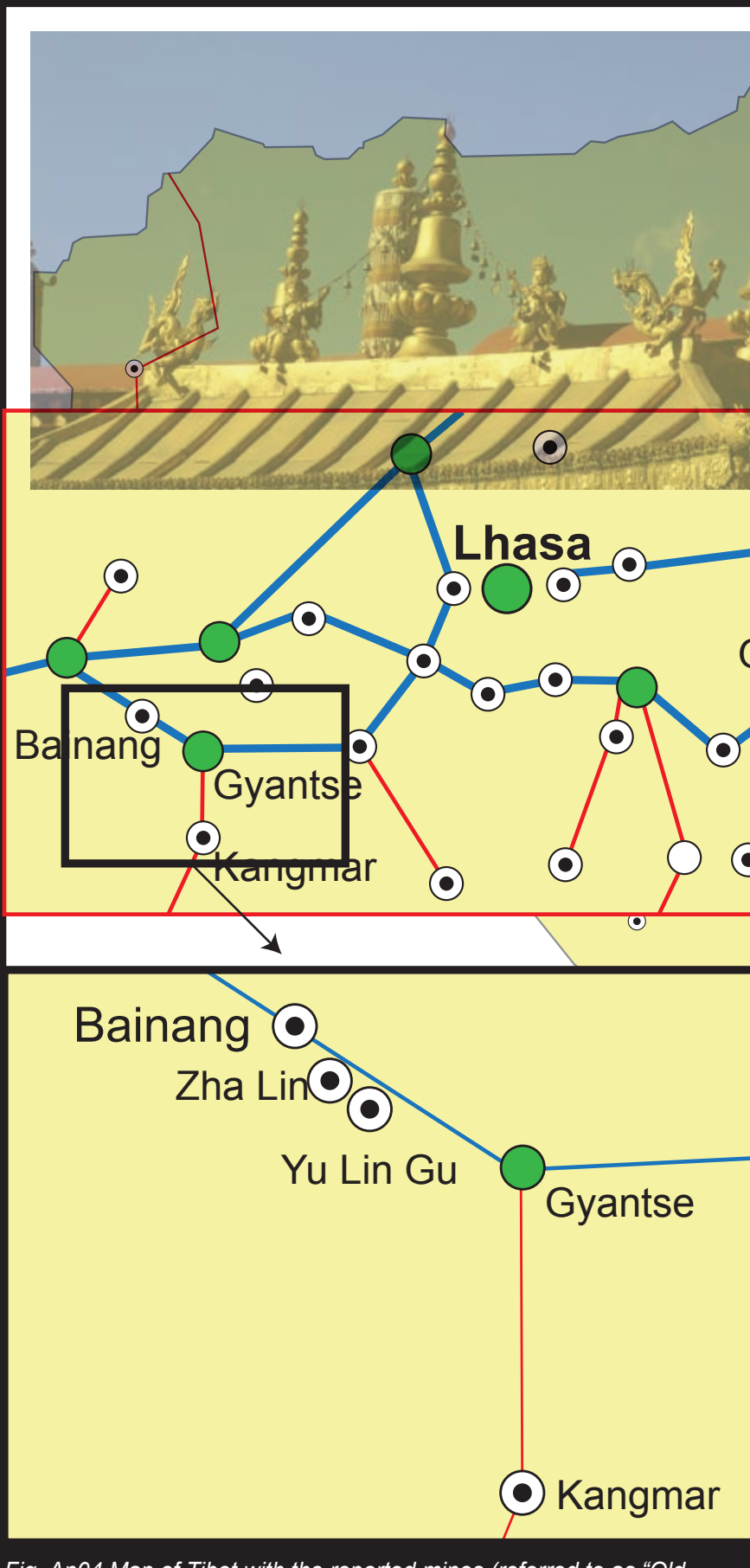

Fig. An04 Map of Tibet with the reported mines (referred to as "Old Mine") and the new mines reported in 2010 (referred to as "New Mines"). The new mine at Gyaca (See also Fig. An08) is interpreted as being "salted" with materials from the other mines that is found 400 miles to the West.

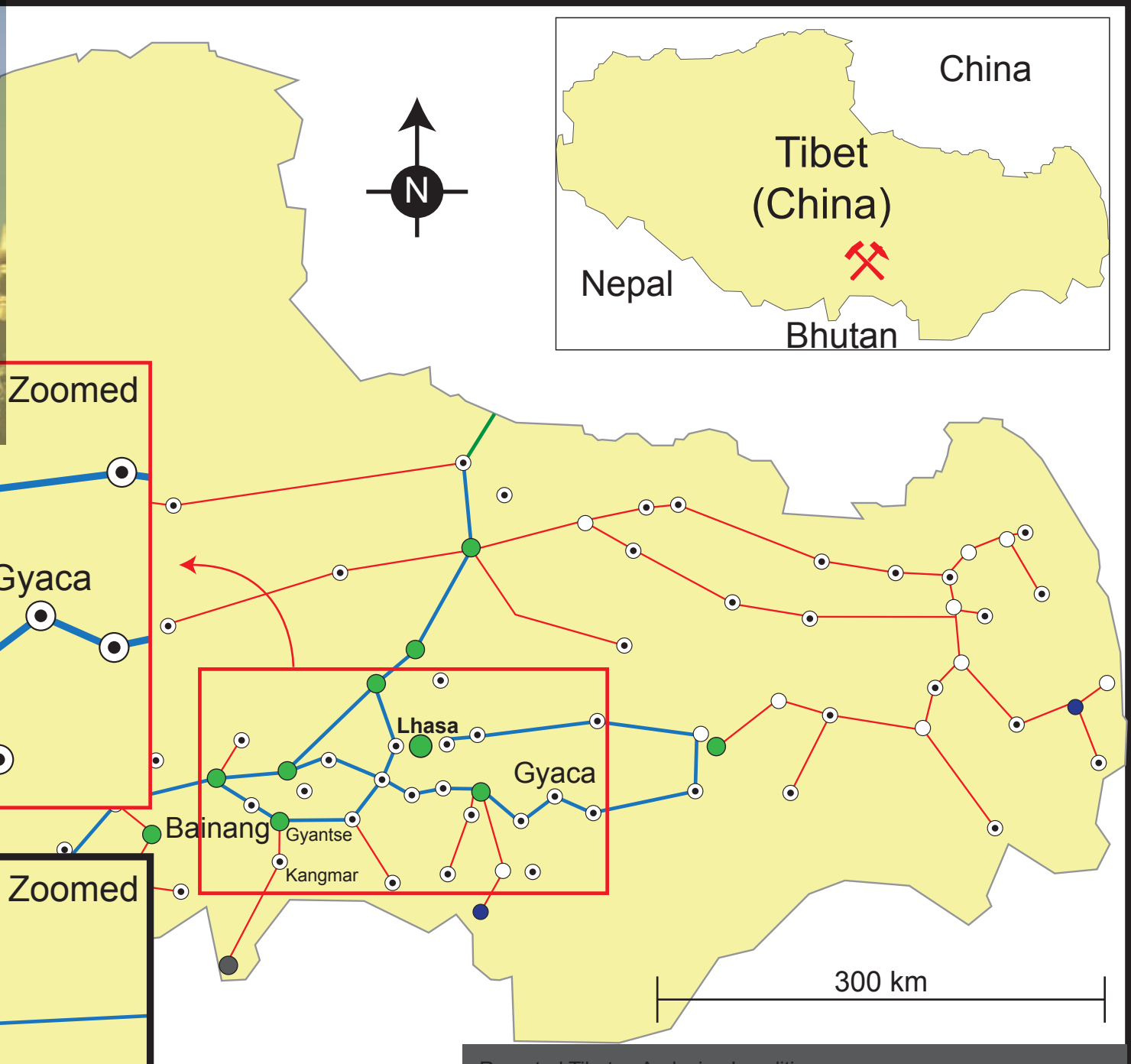

Reported Tibetan Andesine Localities

Location	GPS coordinates	Elevation
Old Mine		
Bainang	29°02.57'N, 89°22.17'E (south mine) 29°02.71'N, 89°22.18'E (north mine)	4,072 m 4,049 m
New Mines		
Zha Lin	29°03.95'N, 89°20.88'E	3,929 m
Yu Lin Gu	29°03.08'N, 89°20.76'E	4,102 m
Gyaca	29°08.3.74'N, 92°35.56.77”E	3,253 m

GPS coordinates of Bainang, Zha Lin and Yu Lin Gu are from literature (Lit. An47) and by the authors (Gyaca). See also forthcoming article (Lit. An07).

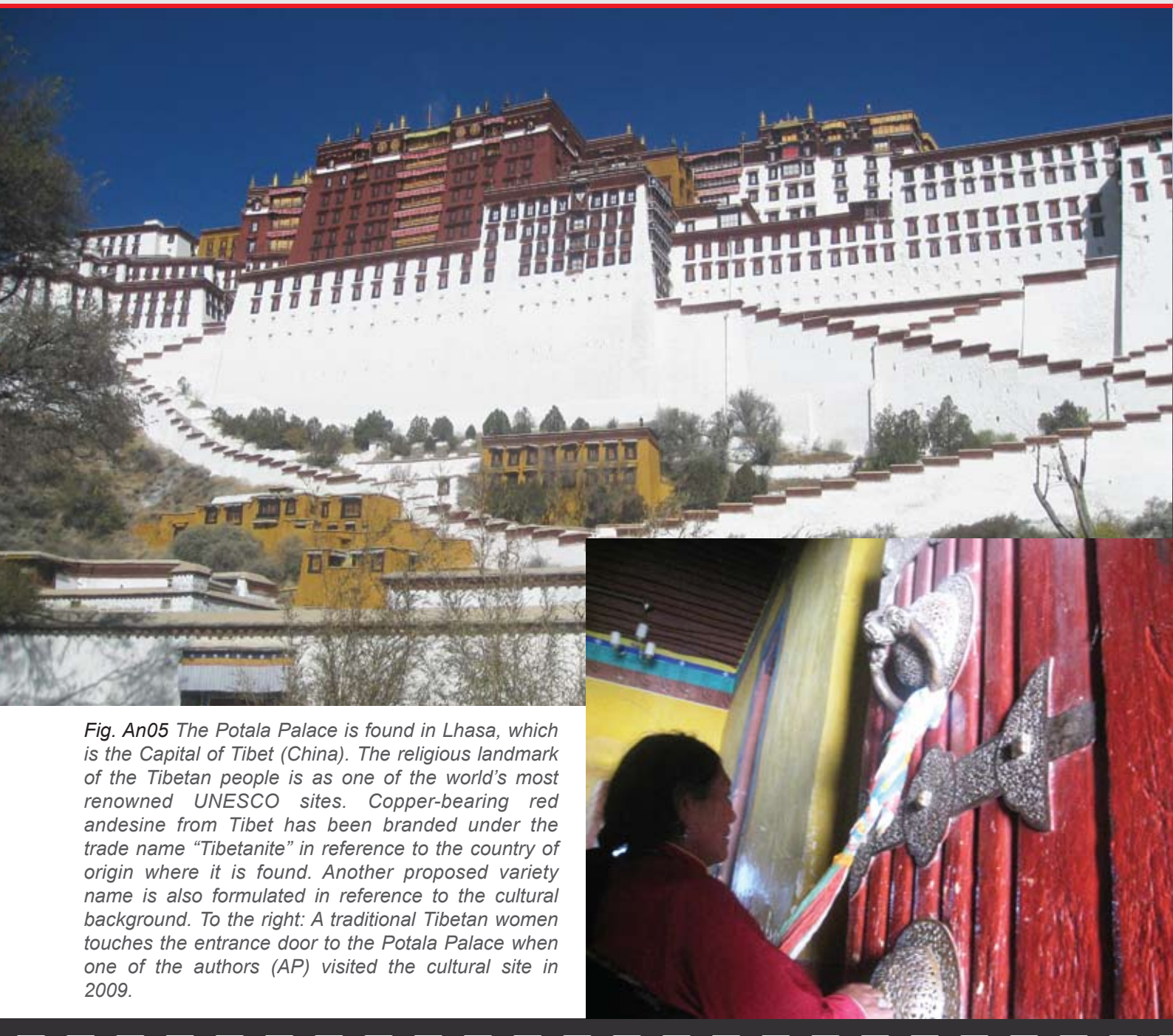

Fig. An05 The Potala Palace is found in Lhasa, which is the Capital of Tibet (China). The religious landmark of the Tibetan people is as one of the world's most renowned UNESCO sites. Copper-bearing red andesine from Tibet has been branded under the trade name "Tibetanite" in reference to the country of origin where it is found. Another proposed variety name is also formulated in reference to the cultural background. To the right: A traditional Tibetan women touches the entrance door to the Potala Palace when one of the authors (AP) visited the cultural site in 2009.

Fig. An06 Experiencing traditional religious rituals of the pilgrims in front of one of the Palaces in Lhasa in November 2009 (snap shot from the GRS Expedition DVD).

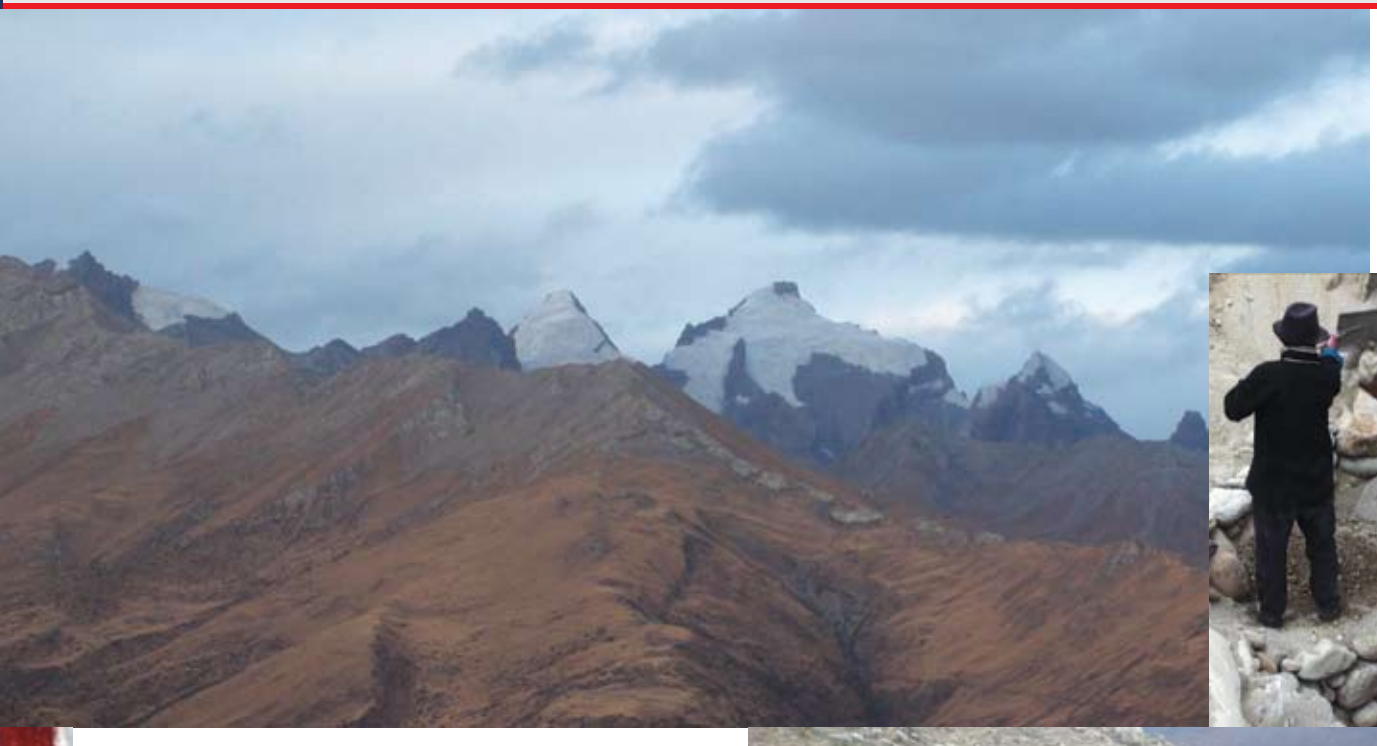

Fig. An07 The way to the mine leads from Lhasa over the high pass Budrangla (4910m) down to Gyaca where a group of miners lined-up with one of the authors (AP) during an expedition in November 2009. The picture below shows the unpaved road to the mine and a snap shot from the pick-and-shovel mining operation at Gyaca is shown above to the right.

Expedition of GRS to a collection point of copper-andesine in Tibet (Gyaca). Clips are from the movie shown in Tucson at the GILC meeting in January 2011 (Fig. An08)

Over a 5500m high pass down to the mining area of Gyaca

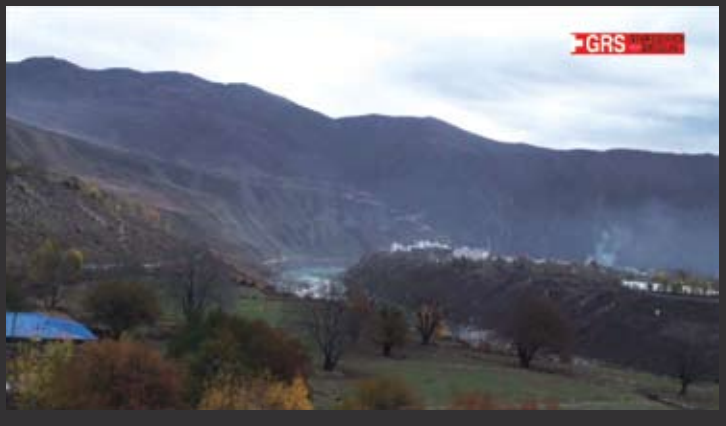

The tent at the mine entrance

Carrying food and GRS lab equipment to the mine site

Collecting and carefully labeling copper-bearing andesine samples

Mine entrance at Gyaca with a Tibetan gospel

Investigating the alleged occurrence of copper-andesine associated to large boulders in an alluvial sand and gravel deposit at the level of disturbed gravel layers

Studying undisturbed sedimentary layers with no findings of copper-bearing andesine

Copper-bearing andesine was found in disturbed layers only

No copper-bearing andesine was found in undisturbed sedimentary layers

Extremely small samples of copper-bearing andesine was found in the loose gravels

A small sorting platform was present with some very limited small-scale mining activities at 4-5 small open pits of max 3 m depth.

Hundreds of copper-bearing andesine emerged from a very small volume of gravels

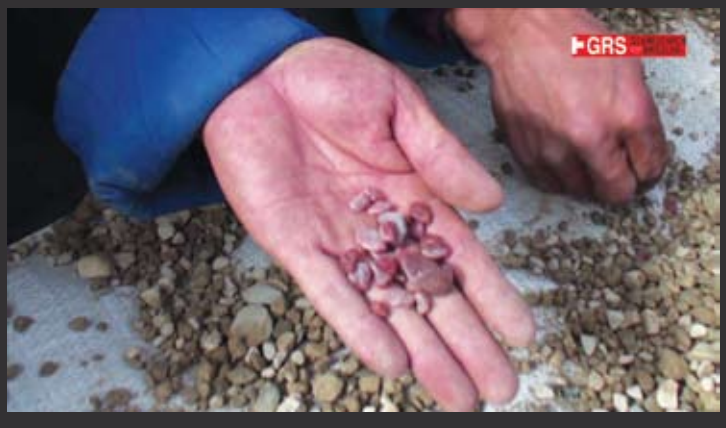

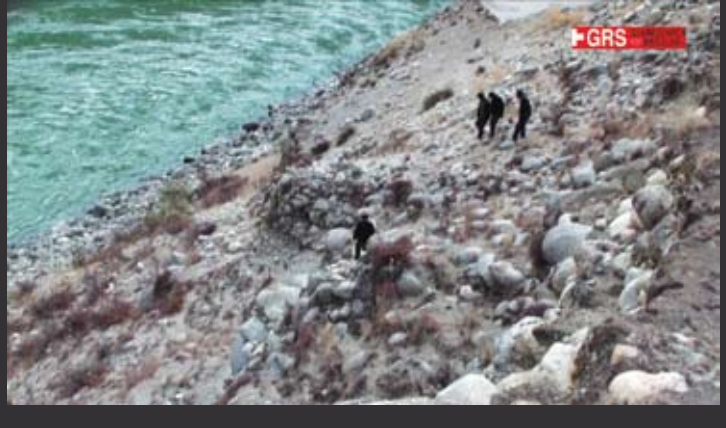

An erosion cliff towards the river was inspected

A group of miners was sent as an advance-team during a critical inspection

Copper-bearing andesine findings at the Gyaca mine site

One of the authors noticed that the area was actively salted with copper-bearing andesine by the advance-team.

A black marble rock was presented to one of the authors containing red mineral inclusions, presumably copper-bearing andesine.

One of the authors was cooking food for the mining crew with his own portable kitchen and food brought from Switzerland

Testing of the rock with the alleged copper-bearing andesine with the help of a portable microscope and with hardness testing revealed that the red mineral was not copper-bearing andesine but a red carbonate.

An inspection of the mining camp revealed that it was obviously only used for a limited amount of days.

Fig. An09 The first mining spot of Tibet near Bainang revealed the occurrence of Tibetan andesine in a sedimentary deposit (picture provided by Marco Cheung). This expedition in 2008 was summarized in a report that described the deposit as derived from Quaternary-Tertiary volcano-sediments related to Jurassic-Cretaceous volcanic rocks (further details See Lit. An01). A short tunnel is shown that apparently produced copper-bearing andesine (See rough materials presented on the hand). Access to the mine was not permitted in subsequent expeditions that tried to re-investigate the authenticity of the occurrence (Lit. An07 and An47). Coordinates see Fig. An04.

Fig. An10 “Walk in for fee digging, all welcomed” at the Dust Devil Mining near Plush (Oregon). Other than at this mining site, visitors are welcomed on invitation by the mine owners only. The exact coordinates of the mines are known to a certain extend to the authors. They are not disclosed here and must be requested from the mine owners directly. Walk-in is not recommended. Picture M.P.

THE SUNSTONE MINES IN OREGON

“Sunstone” (copper-bearing labradorite) is the official State Gemstone of Oregon. It is advertised as the “All-American Gemstone” and as an untreated pristine gem. Different mining areas can be differentiated. The mining in the public area includes pick-and-shovel operations and in addition, highly mechanized mining operations are used in commercial mining areas (Example See Dust Devil Mining Fig. An14). The localities of the sunstone occurrences are shown in Fig. An11.

The location of a new mine operation (PAN) cannot be disclosed but material from that mine has been received and investigated along with the other materials.

Two major highly mechanized sunstone mines are found today in Oregon: Dust Devil Mining Company (DDMC) in Lake County and Ponderosa in Herney County (Fig. An11 and see also Lit. An29 and An35-37). At present, the Ponderosa mine (Desert Sun Mining Co.) produces the highest yield according to the personal communication of gemologist and consultant Mariana Photiou (See acknowledgments) and is owned by 9 partners. The Ponderosa Mine is more than 100 miles to the north of the Plush area. Details of the mining operation at the DDMC has been portrayed in Fig. An14-16 and faceted gems are presented in Fig. 17A from the Plush mining area. Research on both major mines and a further not yet published mine are shown in Fig. An36, 50-53, 92-93, and Tab. An02, 05, 12).

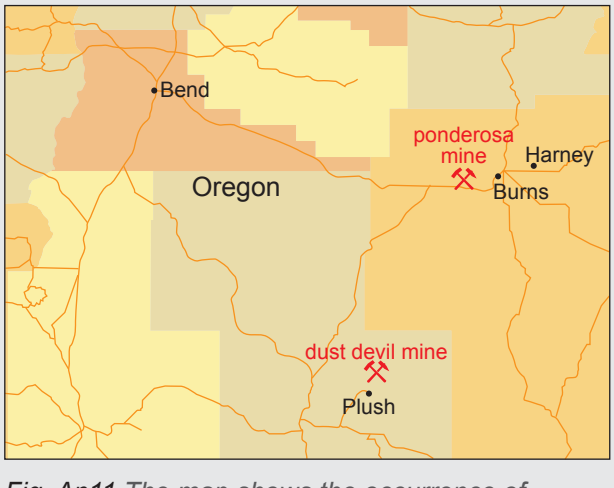

Fig. An11 The map shows the occurrence of sunstone in the State of Oregon (USA). The location of the Ponderosa mine in northwestern Harney County (Desert Sun Mining Co.) and the Dust Devil mine near Plush is shown.

SUNSTONE OCCURRENCES:

Sunstone at Plush was formed in basalts from typical shield volcanoes in Miocene Age stretching over square miles (Lit. An29). The age of the Oregon sunstone has been determined for one example with K-Ar dating (See Tab. An05) that confirmed this age within the margin of error. In a cross section, several layers of basalt typically lay on the top of each other, separated by red ashes and tuffs (Fig. An12). The labradorite phenocrysts were originally formed in a magma chamber and were transported by the magma to the surface. According to field observations, sunstone may be enriched at the bottom of an erupted basalt layer, while yellow feldspar is found on the upper part of the flow but the field relations may also be more complicated (Lit. An37, Fig. An15A-C). The formation of sunstone from Oregon needs an additional source of copper and a mechanism to incorporate the copper into the feldspar. According to information from the miners, the type of rough is different depending on the mines (pers. com. M.P.):
The Ponderosa rough possesses a hard cinder coating, mostly, translucent whitish clear feldspar, deep red and vivid green (higher yield of red and green). The DDMC Plush produces with transparent champagne, yellowish and clear feldspar (no coating) with lighter colors, clear red and lighter greens (higher yield of stones displaying Schiller effect). PANA has the coating, and the vivid colors' of the Ponderosas with the clarity, and transparency of the DDMC. From the new mine, no sufficient data is available at the present time.

PRODUCTION

Only highly mechanized mining at a large scale such as at Dust Devil Mining produce the volume mentioned below in the year 2000 (Lit. An36):
120'000 ct per day split up into 15'000 ct gem quality orange to red and other color shades, 15'000 ct "Schiller" stone, the rest yellows.
The total production of the Ponderosa area was estimated in the past as 250'000 ct per year (Lit. An29). It must have increased dramatically since.

Fig. An12 Oregon sunstone occurs in soils composed of multiple basaltic lava flows, ashes and sedimentary rocks. The picture portraits proud mine owners of the Faceters Folly mine in the Plush area (State of Oregon, USA) showing their latest findings in front of their mine. Picture M.P.

Box An01 Sunstone from Oregon

As described in the literature, different types of sunstone qualities are known (Lit. An29 and An37):
Dichroitic Sunstone: Appear red when viewed from one direction, and green when turned in another direction
Trichroitic Sunstone: Red, green and yellow depending on the viewing direction
Sunstone with Schiller: Adularescence due to small platelets such as native copper is called "Schiller". Two-sided "Schiller" is a specialty when the "Schiller"-effect can be seen from opposite sides.
The following gem quality categories can be distinguished: Sunstones with intense red "Schiller", color-changing in different light sources, intense red colored without "Schiller", trichroitic (red, green, yellow) or dichroitic colors (red, green), watermelons (red core, green rim), different color varieties including bi-colored, orange, pink, green, salmon, peach and yellow colored sunstones (most valued were mentioned first).
Sizes (Lit. An37): Up to max. 300ct, gem sizes of 3-60ct, average top sizes 15-30ct (spectacular award-wining carvings are possible from larger sizes).
Origin of color (Lit. An23):
-Yellow color by Fe^{3+}
-Red color by copper colloids
-Green color and anisotropy by intervalence interaction of Cu+ and Cu
-Schiller by lath of copper metal

Fig. An13 Rough Sunstone from the Ponderosa mine. This untreated copper-bearing feldspar showed a red color in the center and color-less rim. Cross-section is 13mm. Picture M.P.

Intense red sunstone from DDMC

Fig. An14A Annual artist dig event at the Dust Devil Mining in Oregon by invitation only. Pictures M.P.

Fig. An14B The washing plant at the Dust Devil Mining in Oregon (USA) is shown. Only water is utilized and environmental standards are cared for.

Fig. An15A-B The stratigraphic profile of the basaltic layers and sediments at the DDMC mine. Pictures by Amber Clark

Fig. An15C A different type of rock formation can be found in other mining sites such as in this outcrop (side wall) from the new PANA mine in Plush (Oregon). Detailed geological fieldwork is necessary to understand the differences in sunstone formation between the different mines. Picture by Lisa Pike.

Fig. An15C A set of Oregon sunstones roughs produced from the DDMC.

Fig. An15D A sunstone presents himself in the original basaltic matrix (originating from the PANA mine).

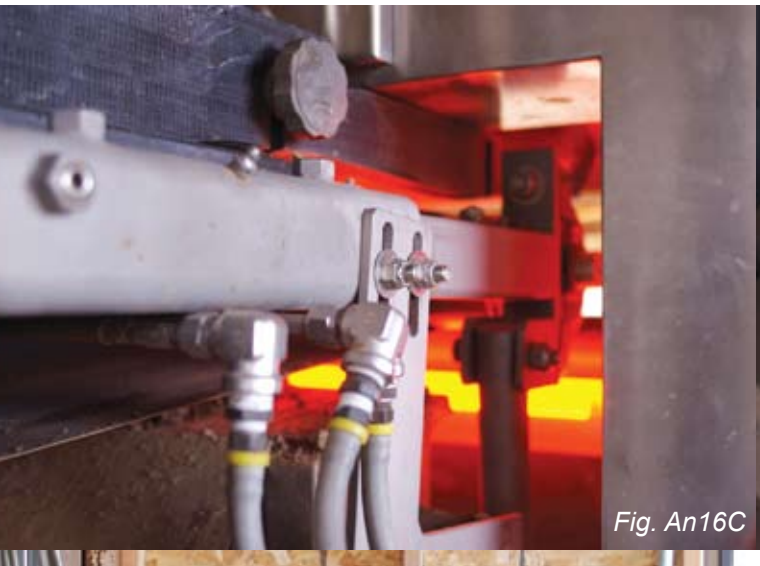

Fig. An16C

Fig. An16A

Fig. An16B

Fig. An16D Gemologist and mining consultant Mariana Photiou (M.P.) holds a fine discovery of an Oregon sunstone.

Fig. An16A-C
Mining operations at the Dust Devil Mining: One of the owners Don Buford (DDMC) and Mariana Photiou setting up the sorter on a cold winter day in Oregon (Fig. An16A). The mining engineer (Craig Andes) is waiting in the collection area (Fig. An16B) and the sorter is shown in operation (Fig. An16C). Pictures M.P.

COMPARISON OF THE TWO REPORTED MINING OPERATION IN TIBET AND OREGON

The mining in Tibet was studied during various expeditions (Lit. An07) and the only mining practice found was a primitive picks-and-shovels operation. Such a mining strategy does not produce enough material for the sunstone gem industry. In Oregon, different levels of the lava flow must be mined to reach the gem-bearing level of a particular horizon (Lit. An37). For this purpose, deeper pits have to be made with the use of heavy machinery (See Fig. An14B and An15A) and the removal of large amounts of overburden (See Fig. An12). It has to be seen, whether the primitive mining practices used in Tibet can explain the large productions of high-quality andesine that are claimed to come from the different localities. The reports in the literature have convinced us, that the mining in Oregon is authentic and the quantity of mined gemstones is well understood and investigated (See for example Lit. An29 and An36-37). The mine operation at Gyaca in Tibet, for example, was found according to our own fieldwork, to be unrealistic and the operations appeared staged (See Fig. An08. pages 7-13). Other mining operations in Tibet were reported as authentic by other field researchers but the potential of the mines remains unknown (For example Lit. An06 and Lit. An24).

Fig. An17A
A sunstone collection from Bob Fittro (miner and artist) from one of the mines in Plush (Faceters Folly), (Picture M.P.). Sunstone sizes range from 5-7ct, 2 stones are over 20ct, the largest is over 24ct.

Fig. An17B
A set of Oregon sunstones with various red and tricolor varieties from the Ponderosa mine average 5-7ct largest sunstone above 9ct in size (Picture M.P.).

Expeditions	Bainang (Naissa)		Gyaca		Zha Lin	
	Sample No.	ct	Sample No.	ct	Sample No.	ct
Before 2008 (not specified)	Ref-8025 Ref-8026	9.638				
August 2008 Abduriyim	 2010-111234 2010-111236 2010-111237	3.287 2.73 5.803 2.227				
Sept, 2009 Peretti			10810-1 10810-2 10808 10797 10856 10979-1 10856)	1.236 1.462		
Sept, 2010 Hughes						
Sept, 2010 Abduriyim					2010-111242 2010-111243	1.344 3.979

Source	Diffusion-treated					
	Xian		Shenzhen		Others	
	Sample No.	ct	Sample No.	ct	Sample No.	ct
China, Abduriyim	AA-Xian1 AA-Xian2	25.785 32.1	AA-Shenzen1 AA-Shenzen2	6.989 10.532		
Columbia Gem House, Eric Braunwart					17402477	
GRS Collection					2010-112727	3.019

Box An02 Definition of Sample Groups

Old Mine	A2
New Mines	A3, A4, A5, B, C2
Market Stones	D, E, E1, E2
Diffusion-Treated Stones	G, G1, G2, K
Yellow-Colored Andesine from Inner Mongolia	H

Interpretation (based on non-destructive tests)	
Market stones	Undeterminable or diffusion-treated
New Mine	Yu Lin Gu mines can be identified as natural (not diffusion-treated)
	Bainang (old mines) and Zha Lin mine (new mine) are mostly undeterminable.
Oregon Mines	Can be identified as natural (not diffusion-treated)

Tab. An01 (continued)

Yu Lin Gu		Yu Lin Gu	
Sample No.	ct	Sample No.	ct
2010-HughesA	1.314		
2010-HughesB	2.749		
Upper Yu Lin Gu	1.318		
Yu-LinGu Hughes Sept2010	2.749		
		2010-112728	4.18
2010-111239	2.489	A-Large (fragment 1)	0.521
2010-111238	5.623	"	0.826
2010-111240	3.855	"	0.943
2010-111241	6.998	A-Small	2.258
		B-Large	1.976
		B-Large (fragment)	0.172
		B-Large (fragment)	0.168
		B-Large (fragment)	3.161

Sample Categories Explanation

Old mines in Tibet

(A) Rough andesine samples obtained from the mine in Tibet explored by Abduriyim [14] and provided to GRS by Litto Gems and/or ETH Zurich (See Lit. An30)
A(2) Additional samples collected in the 2008 expedition were directly sent by Abduriyim to GRS

New mines in Tibet

A(3) Samples from the new mine in Yu Lin Gu were obtained from 2 sources, R. W. Hughes and A. Abduriyim (Lit. An07), expedition November 2010
A(4) Zha Lin.
A(5) Sample from Yu Lin Gu Expedition 2010, indirectly received from Litto Gems.
(B) Approximately 1 kg of rough sample collected by A. Peretti during an expedition in 2009 from the new mine in Gyaca.

(C2) Fifty samples claimed as being natural rough copper–andesine from Tibet (indicated as not diffusion-treated) were supplied by a company from Shenzhen (China). The material was indicated to originate from the waste area of the Tibet from different new mining spots (See Lit. An13)

Sample Categories Explanation (continued)

Market stones

(D) Three faceted gem-quality andesines that are claimed to come from the DR Congo (See Lit. An31), were acquired at the Tucson Show in 2006 (See Lit. An13).

(E) Three faceted gem-quality samples claimed to be diffusion-treated copper–andesines from Tibet were acquired at the Hong Kong Jewellery Show in September 2009 (See Lit. An13)

(E1) Faceted red and green andesine from Tibet were provided to GRS during ICA Gem-Show 2008 in Dubai (See Lit. An13)

(E2) Fifty faceted samples of top gem quality and large size were obtained from a specialized dealer in 2011. Stones are disclosed as untreated andesine from Tibet.

Samples from Oregon

(F) Faceted gem-quality labradorite (sunstone) were indicated as being produced from Oregon and were acquired from the jewelry show 2008 in Bangkok (market stones) (See Lit. An13)

(F2) Desert Sun Mining (Ponderosa) rough materials were acquired at the Tucson show in 2011.

(F3) Dust Devil Mining, Plush. Rough materials were selected from large lots from the miner's production at the Tucson show in 2011.

(F4) Ponderosa mine materials directly obtained from mining consulting Mariana Photiou in Tucson in 2011. New fine material was included, from the Pana mine (owned by Randy Reinikka and David Weathley)

Diffusion-treated samples

(G) Rough samples of Asian origin were claimed as diffusion-treated and were obtained from traders in September 2009 (See Lit. An13)

G(1) Diffusion-treated from Xian University were obtained from Abduriyim (See Acknowledgments)

G(2) Diffusion-treated Shenzhen laboratory were obtained from Abduriyim (See Acknowledgments)

(K) Inner Mongolia andesine were experimentally diffusion-treated by J. Emmett on samples from GRS (See Lit. An13)

Fig. An18 The samples of group A(2) (See Tab.An01) are shown. Samples appeared water-worn or tumbled. Cracks and cavities were filled with minerals and glassy residues. These fissures and cavities were analyzed in more details (See Fig. An90, An94-95, An97, Tab. An02, Tab. An04, Tab. An07).

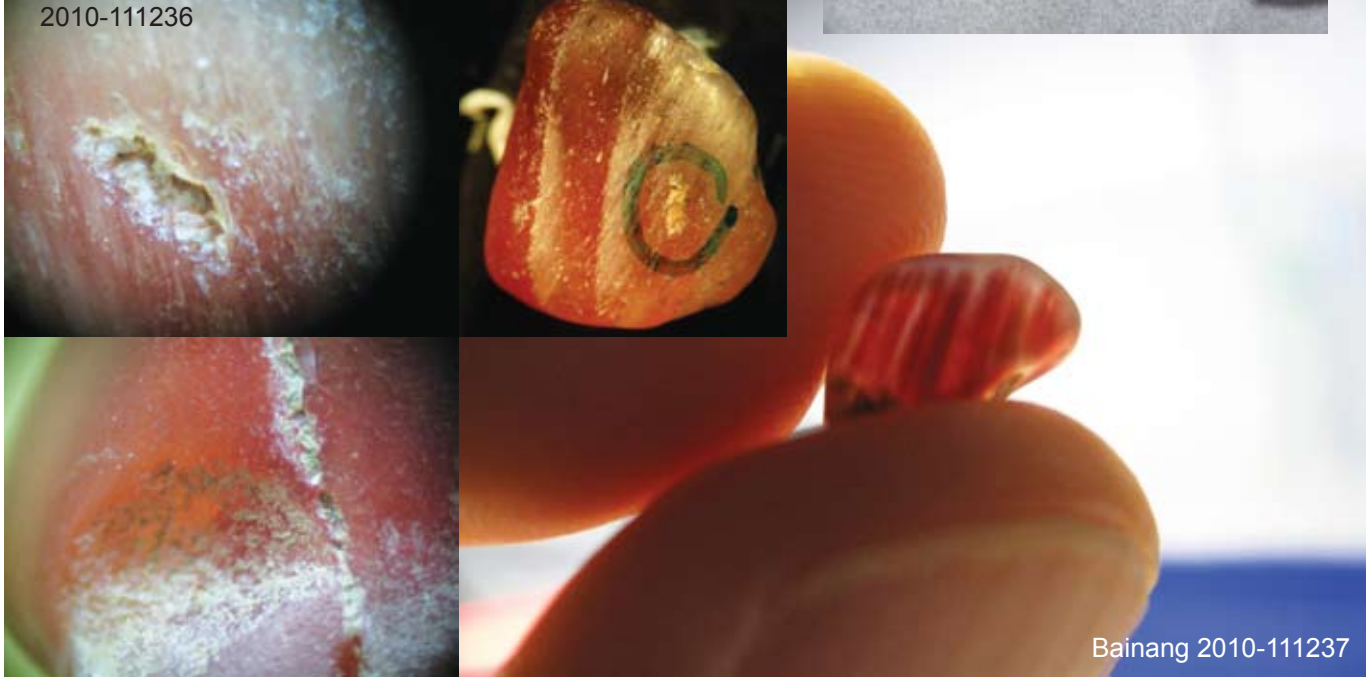

Fig. An19 *These samples from the new mines collected during the expedition in 2010 were received from one of the expedition members in late 2010 (Abduriyim) and included samples from Yu Lin Gu and Zha Lin. Original labeling of samples is shown with collection date. Samples ranged in color from pastel partially colored to medium red translucent andesines.*

2010-HughesA and B-YuLinGu

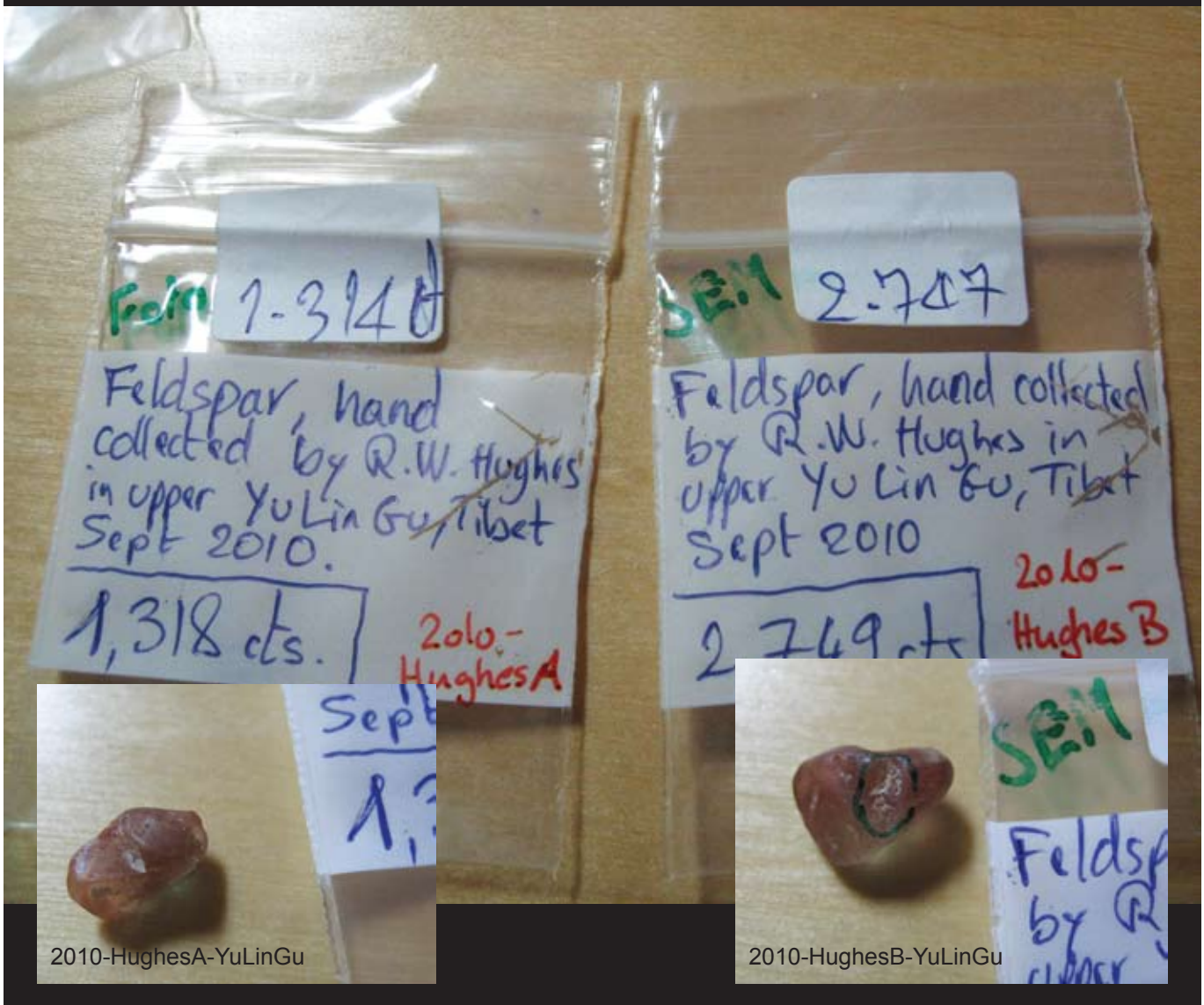

2010-HughesA-YuLinGu

2010-HughesB-YuLinGu

Hughes 2010

Fig. An20 These samples from the new mines were collected during the expedition in 2010 from Yu Lin Gu and were received from one of the expedition members in 2011 (RWH). Original labeling of samples by the collector is shown including the collection date (29th and 30th September 2010).

Yu Lin Gu

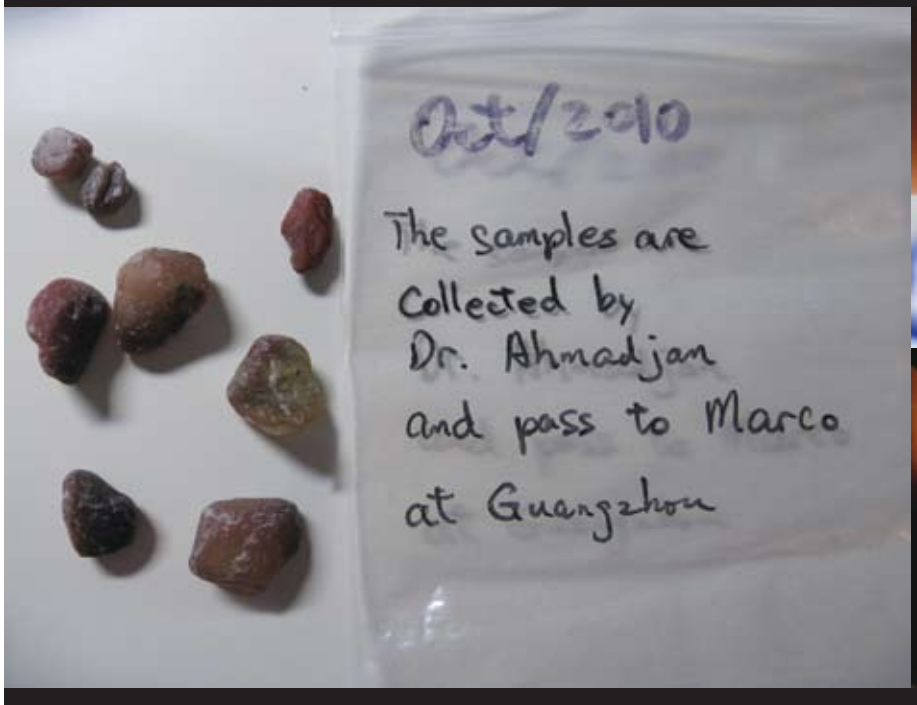

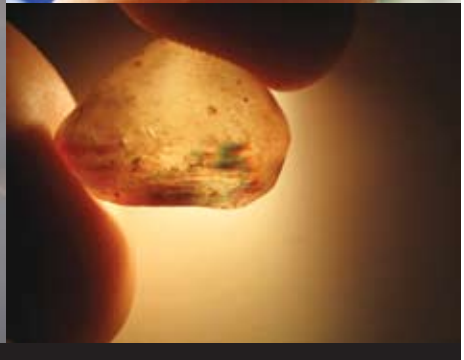

A-small-Tibet

A-large-Tibet

B-small-Tibet

B-large-Tibet

Fig. An21 These samples were obtained in 2010 from Marco Cheung who received them from one of the expedition members (Abduriyim) in Guangzhou, when the expedition members returned from Tibet. Note: Range of colors from almost colorless to green. One sample was intense red and translucent. There were no gem quality samples in this lot.

Fig. An22 The upper picture shows the different sizes found in the alluvial deposit with silt and sand sizes collected from layers with sedimentary structures. No copper-bearing andesine was found in these lots. Large amount of 5-20mm sized copper-bearing andesine samples were collected and sorted according to the spot of findings. Hand-collected samples are in the bags on the lower left. Other samples were taken from the mined lots that were present in a container at the production site (Expedition details See page 06-13).

Fig. An23 These samples were collected from 4 mining spots all in disturbed layers at the bottom of several meter deep open pits. From these materials we polished a set of samples that are shown. These included materials with concentric color zoning (green core and red rim, with red color zoning and with alternating red and green color zoning). Further analyses of this material confirmed the field observation that the mine was salted. The materials were found to be natural untreated materials from other collection points in Tibet. Further samples See Fig. An24-27.

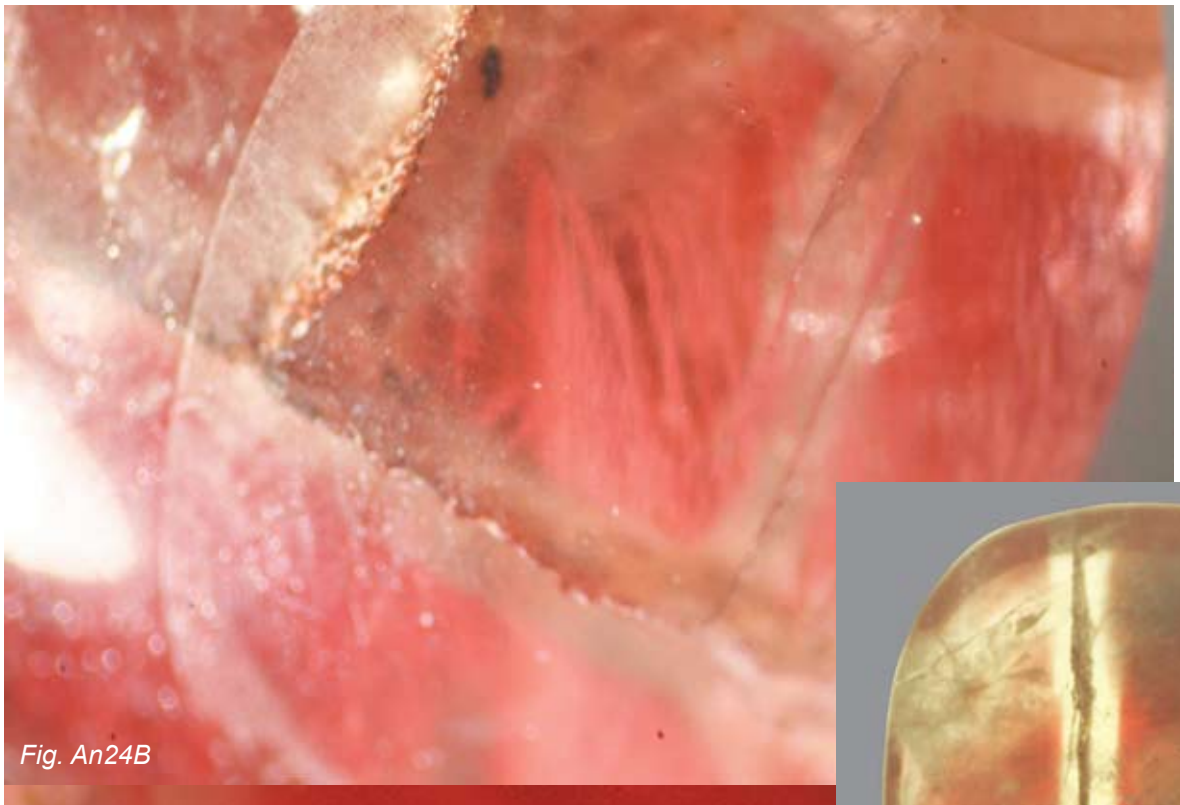
Fig. An24B

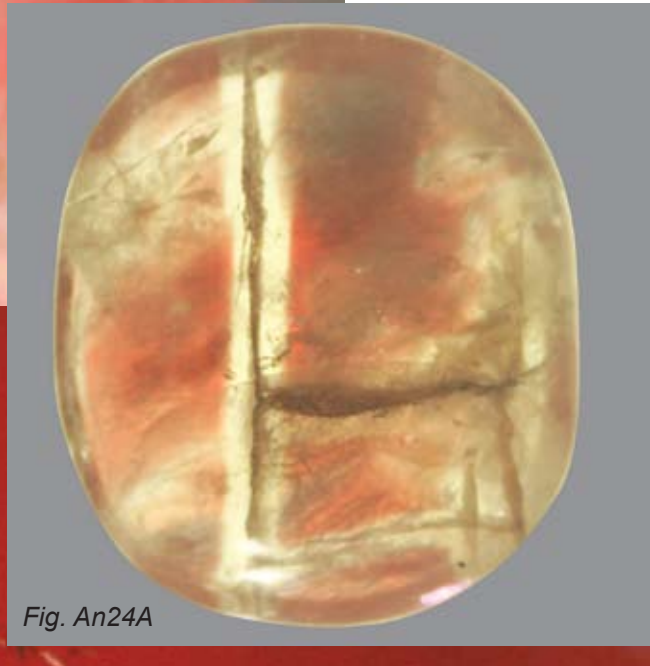
Fig. An24A

Fig. An24C

Fig. An24A-C This copper-bearing andesine was hand-collected from the Gyaca mine in Tibet and was polished by GRS in-house. The sample showed various generations of intersecting fluid inclusion trails. A white rim has been established adjacent to each fluid inclusion trail and created a blocky network of red colored areas in the andesine (Fig. An24A-B). A portion of the fluid-trail is enlarged and shows a interconnecting negative tube system. These tubes are partially filled with opaque daughter minerals and trapped original ore-forming fluids (Fig. An24C).

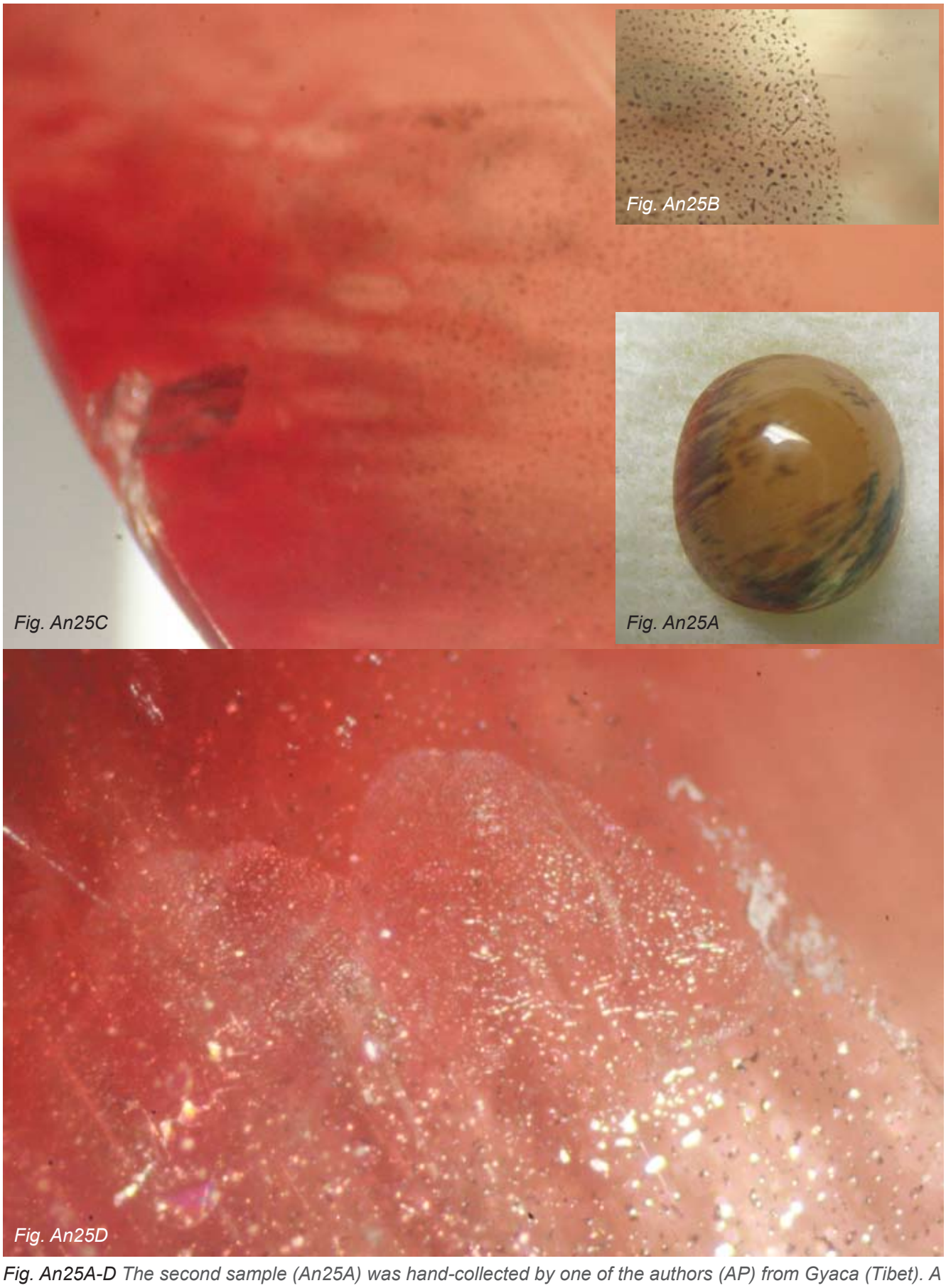

Fig. An25A-D *The second sample (An25A) was hand-collected by one of the authors (AP) from Gyaca (Tibet). A fluid inclusion trail formed in this copper-bearing andesine with isolated fluid inclusion tubes (An25B).The fluid inclusion entered the sample from a cavity on the surface with glassy residues (An25C). A series of secondary fluid inclusion trails emerged from the main trail and black daughter minerals are present (See right lower corner of Fig. An25D). Fluid inclusion analysis of this sample see Fig. An54-56.*

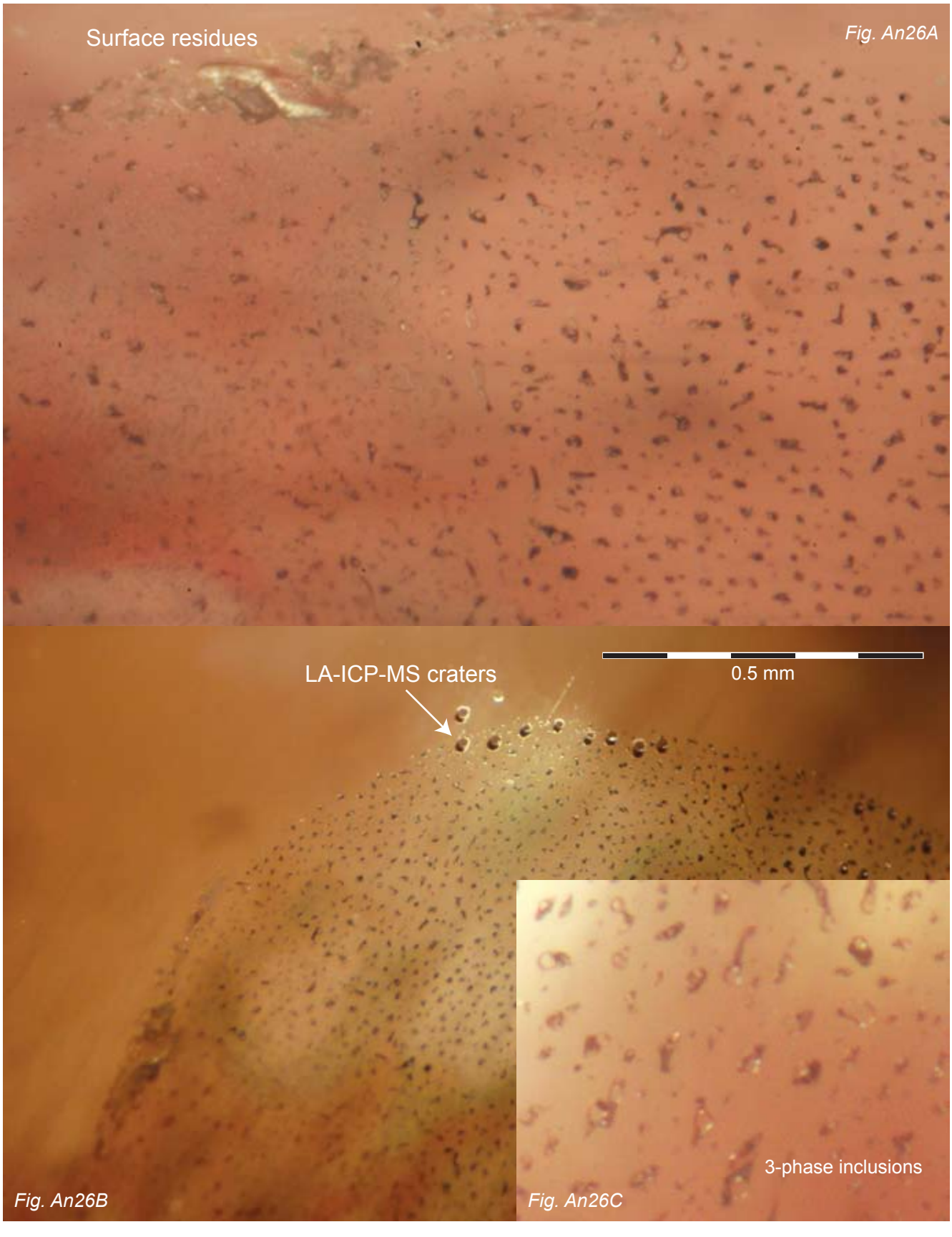

Fig. An26A-C The fluid inclusion trail of Fig. An25 has been enlarged in the microscope to show some important details. The glassy entry point of the fluid inclusions into a copper-bearing andesine from Tibet is shown (Fig. An26A) and the position of the LA-ICP-MS measuring points (Fig. An26B). Fluid inclusion analysis of this sample see Fig. An54-56. The area next to the entry point is void of black daughter minerals. In another portion of the trail, almost every negative crystal contains 3-phase inclusions with black daughter minerals and transparent solids. In a larger magnification, it is visible that large vapour bubbles are present and, together with the black daughter mineral, they fill up the entire fluid inclusion voids (Fig. An26C).

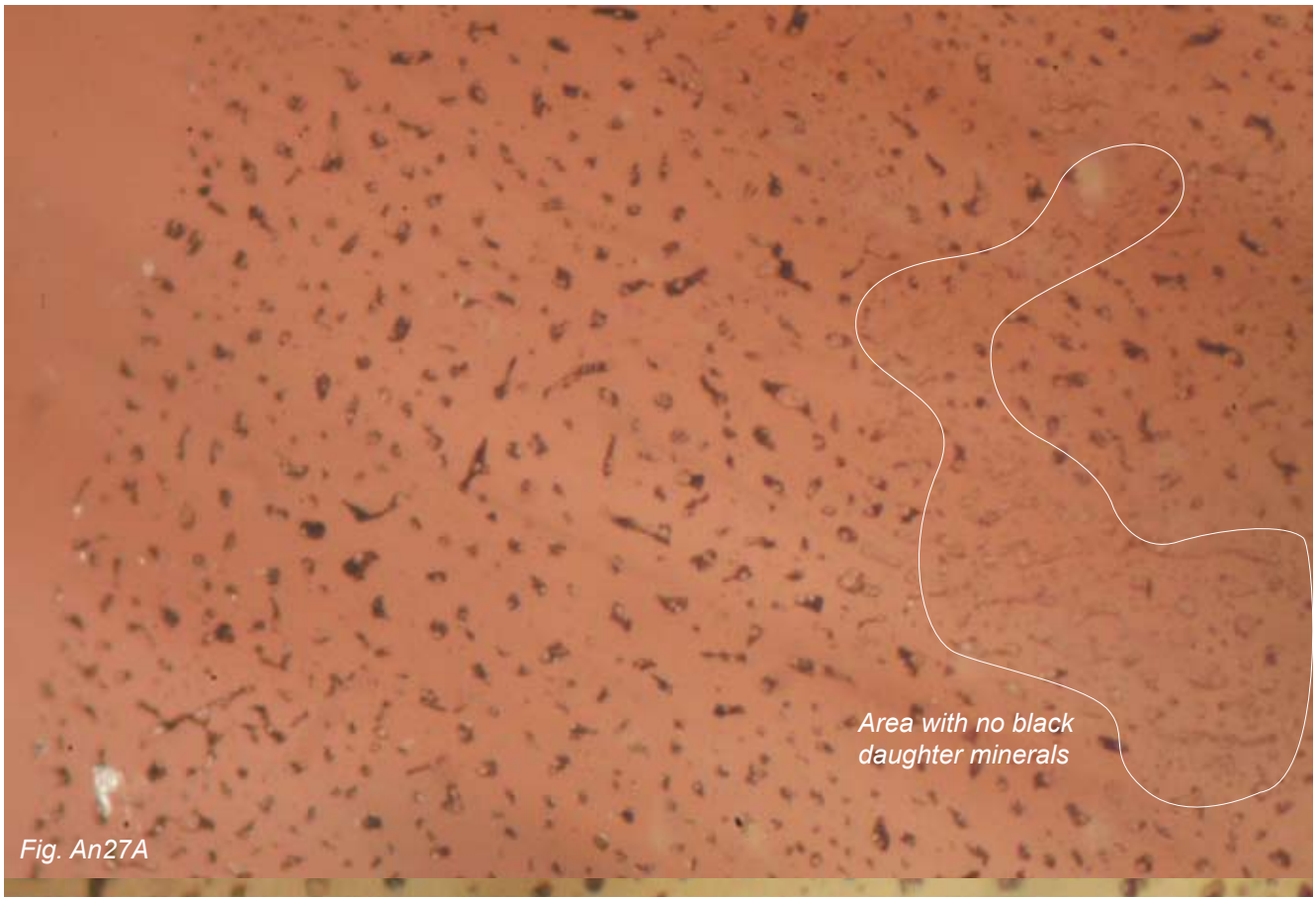

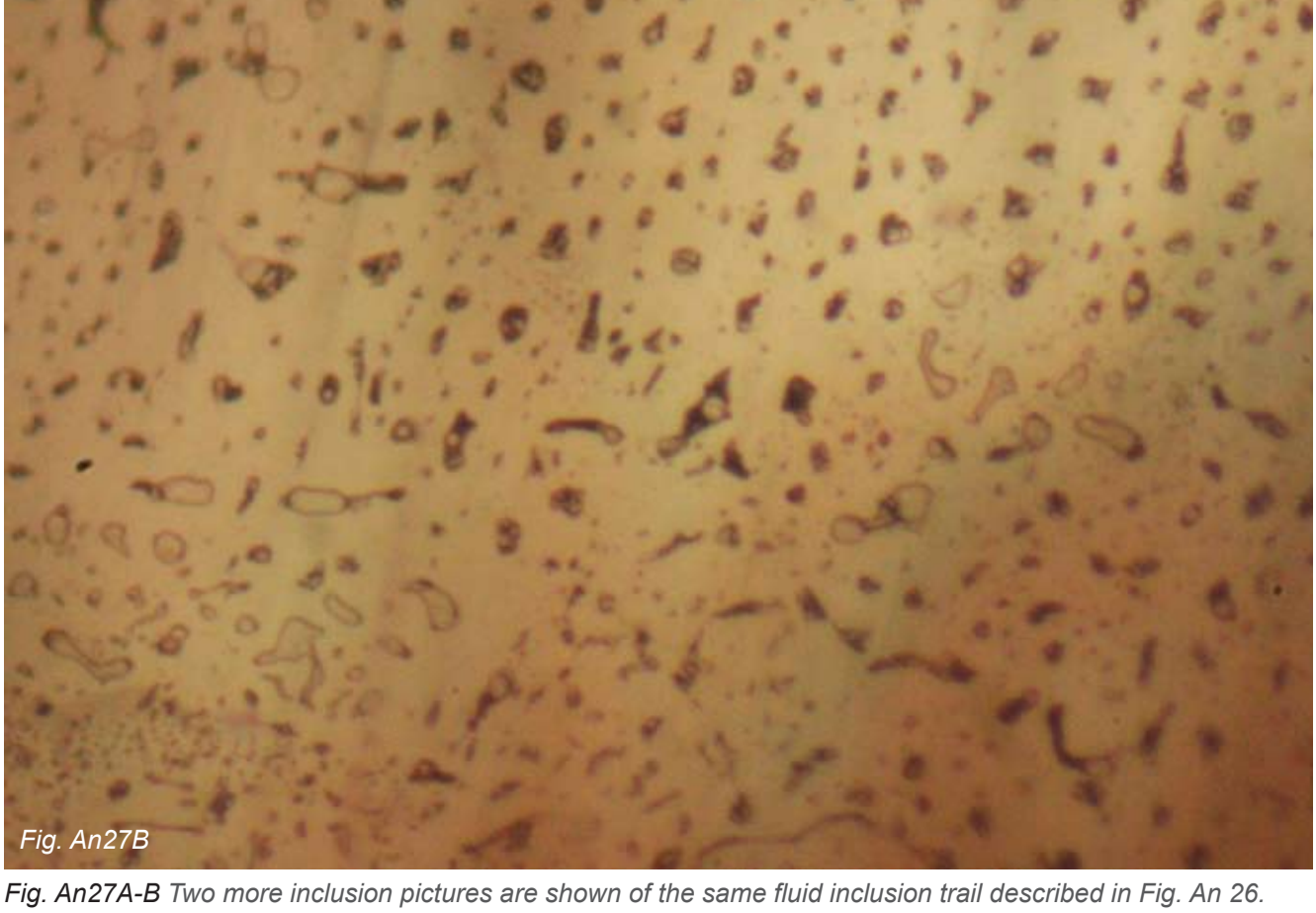

Fig. An27A-B Two more inclusion pictures are shown of the same fluid inclusion trail described in Fig. An 26. The separation of areas with and without black daughter minerals is highlighted and the shape of tubes, without decrepitating, documents that the sample was not heat-treated after the fluid inclusion trails were formed.

Fig. An28A

Fig. An28B

Fig. An28C

Fig. An28A-F This copper-bearing andesine from Upper Yu Lin Gu (Tibet) shows a particular isolated color zone. It is a symmetrical color zoning of red and green bands that is found associated with a fluid inclusion trail (Fig. An28A). In a particular crystallographic direction of the andesine, red stripes are found in angle of about 30 degrees to the direction of the fluid inclusion trail (Fig. An28C). Along this zones, copper naturally diffused into the andesine directly emerging from the fluid inclusion trail (See also Fig. An37 and An39-41). A symmetrical color zoning with red and green stripes was created in this way. The red color is located more close to the fluid inclusion trail and it is bordered by on outer zone of green color (Fig. An28F). The fluid inclusion trails emerged

Fig. An28D

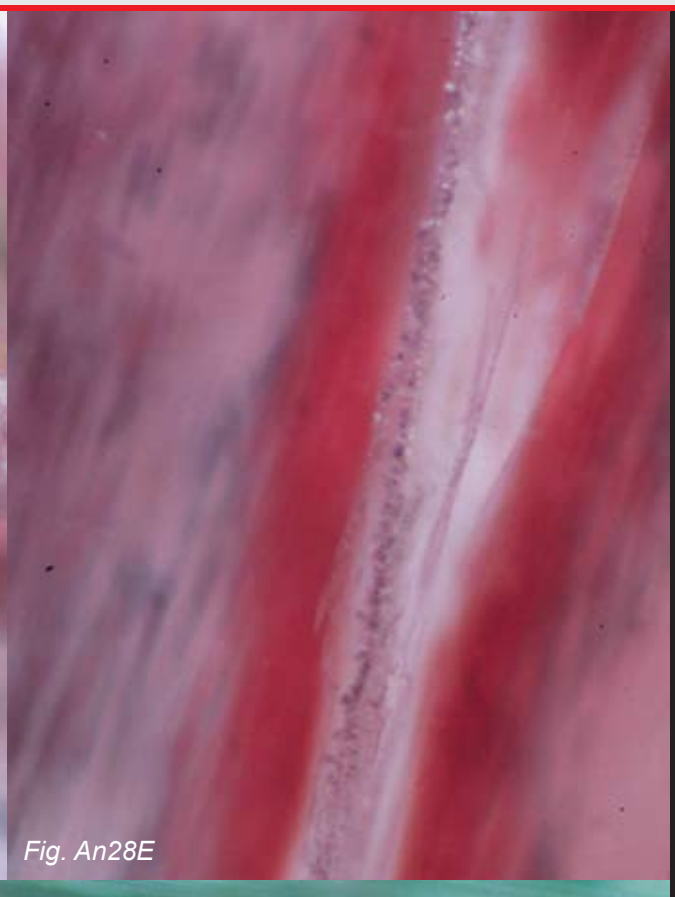

Fig. An28E

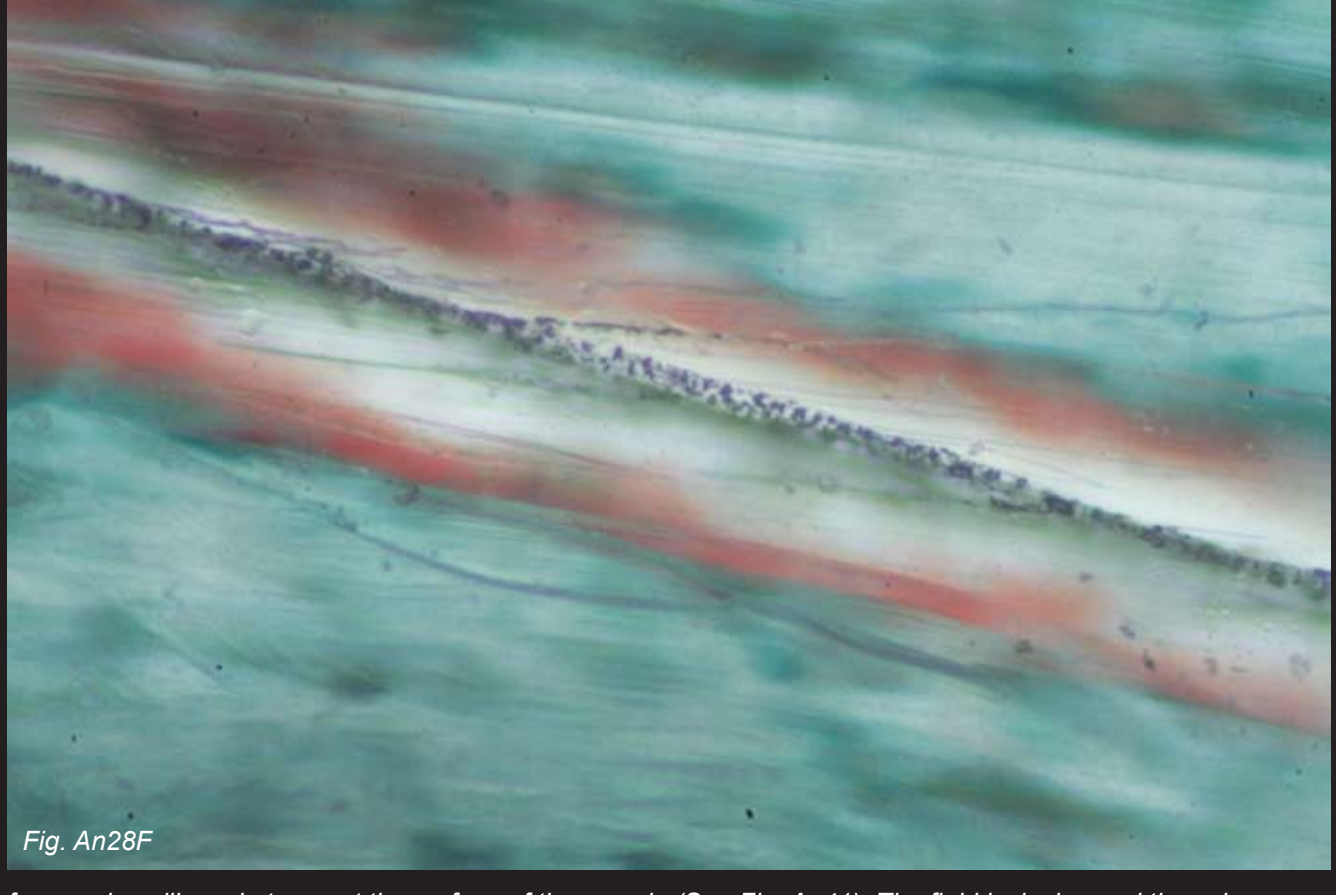

Fig. An28F

from a glass-like substance at the surface of the sample (See Fig. An41). The fluid inclusion and the color-zoning in the stone is formed after the formation of the feldspar itself and is clearly linked to the entry point containing glass-like materials and a hydrothermal alteration event (Fig. An28C). This event is younger than the formation of the andesine itself (see also Argon-dating and analysis of this sample, Tab. An05, Sample Upper Yu Lin Gu, Hughes 2010). Details of the fluid inclusion formation (healed secondary trails emerging from a central trail and no decrepitating of the tubes) indicated that the sample was not heated after the fluid inclusion trail was formed (Fig. An28D and An28E).

EXPERIMENTAL

Single-crystal X-ray studies were carried out on a natural plagioclase of gem quality (ca. 0.2 mm in maximum dimension, source A, Tab. An01) using a Bruker APEX II SMART diffractometer (MoKα, λ = 0.71073 Å). Diffraction data were collected with ω scans at different φ settings (φ-ω scan) (Lit. An09). Data (9562 reflections up to θ = 30.5°) were processed using SAINT (Lit. An09). An empirical absorption correction using SADABS (Lit. An41) was applied yielding Rint = 2.83% and Rσ = 2.00%. The structure was solved by direct methods with subsequent analyses of difference-Fourier maps. The plagioclase structure was refined in primitive triclinic setting (a = 7.1071(1), b = 7.6057(1), c = 7.6406 Å, α = 115.192(1), β = 100.671(1), γ = 106.729(1)°, V = 334.61 Å3) using the program SHELX97 (Lit. An42) to R1 = 2.3%. The refinement [130 parameters, including anisotropic atom displacement parameters, 1998 Fo > 4σ (Fo)] has been carried out with neutral atom scattering factors. Due to the strongly disordered nature of tetrahedral Si and Al, all tetrahedral sites were refined with Si scattering factors. Extra framework sites were refined with Na and Ca scattering factors, allowing variation of the corresponding ratio with the additional constraint that the extra framework sites are fully occupied by (Na+Ca). As the K content was unknown, the refined Ca occupancy contains also minor K due to similar numbers of scattering electrons (Ca: 20, K: 19).

RESULTS

Extra framework sites are smeared out and were refined on two partially occupied adjacent positions, ca. 0.75 Å apart. Their average occupancy is 0.51(2) Ca and 0.49(1) Na. Based on this ratio the calculated composition of the plagioclase is assumed to be $Ca_{0.51}Na_{0.49}(Si_{2.49}Al_{1.51})O_8$. There are four symmetry independent tetrahedral sites T1-T4, showing following average T-O distances: 1.654, 1.676, 1.654, and 1.655 Å. If we assume that a Si-O distance in feldspar is ca. 1.62 Å and the corresponding Al-O distance is ca. 1.75 Å, strong Si-Al disorder is evident. T1, T3, and T4 are enriched in Si whereas T2 has about Si/Al = 1:1. The structural data did not provide any indication of twinning, incommensurate behavior, diffuse scattering or additional exsolutions. The results are very similar to those of an An0.48 plagioclase (Lit. An12). The structure represent a strongly disordered plagioclase with a composition close to the “andesine-labradorite” boundary.

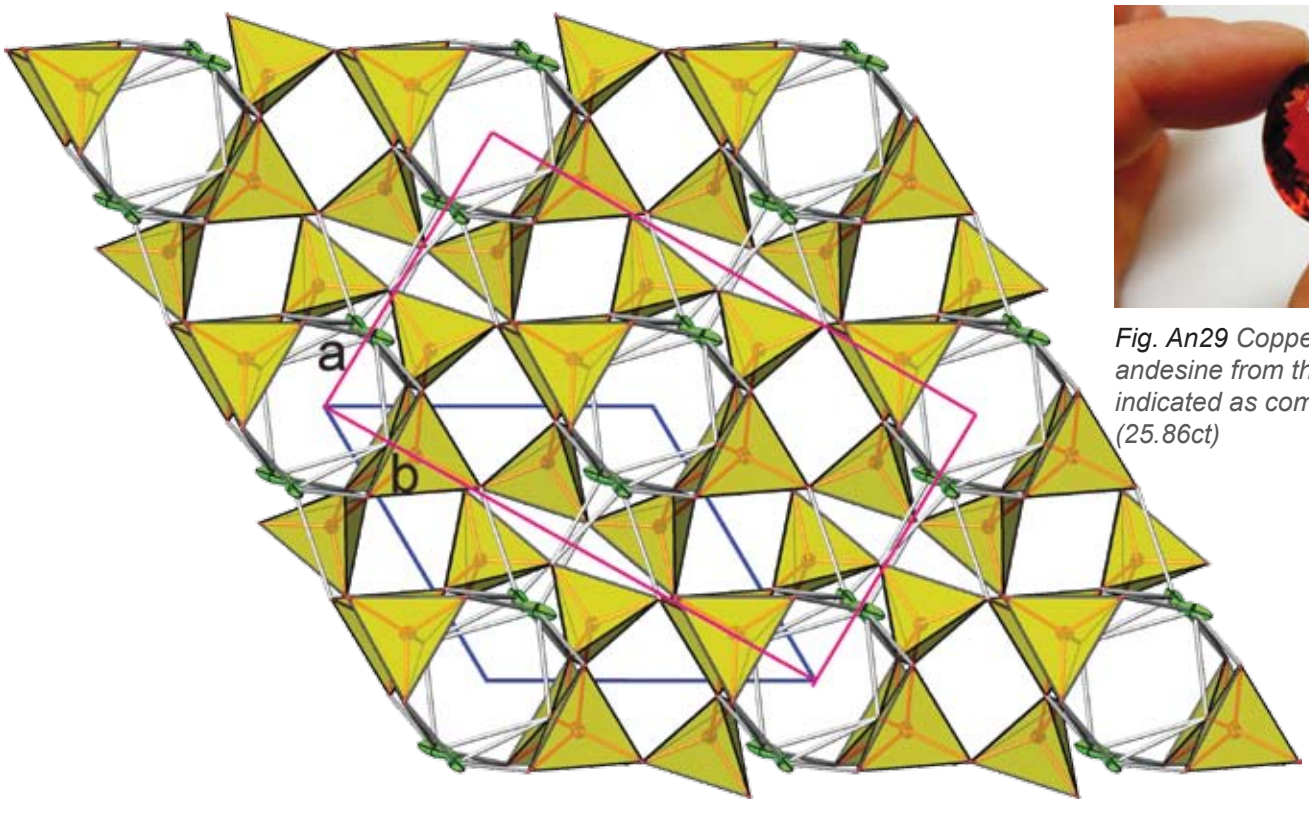

Fig. An29 Copper-bearing andesine from the market indicated as coming from Tibet (25.86ct)

Fig. An30 Stick and ball -polyeder model of the andesine-labradorite structure. Dark blue lines show the triclinic unit cell in primitive setting whereas the red lines (with labels) correspond to the C-centered setting chosen for unit cell refinement. Green probability ellipsoids indicate disordered Na, Ca sites bonded to the tetrahedral framework. Yellow tetrahedral characterize (Si,Al)O4 tetrahedral with disordered Si and Al distribution
Recalculated for C-centered setting, the lattice parameters are:
a = 8.1703(2), b = 12.8723(2), c = 7.1071(1) A, alpha 86.551(1)°, beta = 116.175(1)°, gamma = 89.710(1)°, V = 669.22(5) (errors of a,b and c are probably underestimated and for direct comparison with data in Tab.An02, above errors should be multiplied by 5).

LATTICE PARAMETER DETERMINATIONS

One crystal ((0.2-0.4 mm in dimension) of each sample was glued on a glass needle.
Using an Enraf Nonius CAD4 single-crystal diffractometer (MoKα radiation) equipped with a scintillation counter, a preliminary orientation matrix including cell dimensions was determined on the basis of 25 centered reflections. The originally primitive lattice was transformed into a face-centered setting.
For more precise cell dimensions, not influenced by Kα1-Kα2 splitting, relatively strong high θ reflections were selected between 25 and 30° θ (e.g.: 10 0 0, 0 16 0, 0 0 9, 9 5 -5, 8 12 -4, 10 6 -5, -5 -13 2, 6 12 -3, 10 4 -4, 10 6 -4 including the symmetry equivalent reflections). Using these Kα1 centered reflections another set of preliminary cell dimensions was refined.
In order to reduce experimental errors such as non-ideal crystal centering and diffractometer misalignment, each reflection was re-centered on four diffracting positions ("front-side", "back-side", positive θ, negative θ). Averages of such measurements were taken to refine the final cell dimensions. For a direct comparison of all cell-parameter measurements, all crystals were measured according to the same strategy and on the basis of the same set of centered reflections. We assume that the refined values for each crystal are reproducible within 3 esd's.

RESULTS

Corresponding results are summarized in Tab. An02 and plotted in Fig. An31-32. 5 different groups have been made:
1.) Old mine andesine (A2-Banaing)
2.) New mines (A3-Yu Lin Gu. A4-Zha Lin and B-Gyaca)
3.) Oregon Sunstone (Ponderosa mine)
4.) 2 types of diffusion-treated andesine (G1-Xian, G2-Shenzhen)
5.) Inner Mongolia

Six of the samples correspond to those that were measured with K-Ar-dating (See Tab. An05) and all of the

Tab An02 Lattice Parameters of Feldspar

	A2	A3	A3	A3	A3	A3
	Bainang Naisa 2010-111237 2.227ct Ar-Tested	Yu Lin Gu 2010-111241 6.998ct	Yu Lin Gu 2010-111238 5.623ct	Yu Lin Gu Hughes Ar-Tested	Yu Lin Gu 2010 Hughes 2.749ct Ar-Tested	Yu Lin Gu Abduriyim 2010-111239 2.489ct Ar-Tested
a Å	8.1757(4)	8.1747(7)	8.1735(8)	8.1794(6)	8.1757(10)	8.1771(9)
b Å	12.8755(9)	12.8793(13)	12.8784(9)	12.8818(18)	12.8762(12)	12.8771(13)
c Å	7.1065(13)	7.1097(9)	7.1095(10)	7.1109(8)	7.1101(10)	7.1088(11)
α °	86.557(9)	86.578(9)	86.588(8)	86.635(10)	86.576(9)	86.569(10)
b °	116.168(10)	116.166(8)	116.179(10)	116.166(7)	116.195(10)	116.180(10)
γ °	89.702(5)	89.700(8)	89.722(7)	89.694(8)	89.746(9)	89.721(8)
V Å^3	669.77(15)	670.22(13)	670.00(14)	670.89(13)	670.03(15)	670.14(15)

	A4	B	F3	G1	G2	H
	Zha Lin 2010-111243 3.979ct Ar-Tested	Gyaca Ref10808 5.193ct	Oregon Ponderosa	AA-Xian Diffusion-treated	AA-Shenzhen 2.374ct Ar-Tested	Inner Mongolia
a Å	8.1744(10)	8.1745(6)	8.1742(7)	8.1740(4)	8.1753(6)	8.1744(8)
b Å	12.8813(17)	12.8782(16)	12.872(2)	12.8753(17)	12.8776(12)	12.8763(14)
c Å	7.1116(7)	7.1117(9)	7.1011(11)	7.1080(10)	7.1087(6)	7.1117(12)
α °	86.582(9)	86.570(10)	86.545(13)	86.595(11)	86.568(7)	86.555(11)
b °	116.196(9)	116.171(9)	116.052(9)	116.156(6)	116.161(6)	116.203(9)
γ °	89.750(10)	89.707(9)	89.408(10)	89.674(7)	89.683(7)	89.818(8)
V Å^3	670.32(15)	670.30(14)	669.47(17)	669.85(14)	670.10(10)	670.04(16)

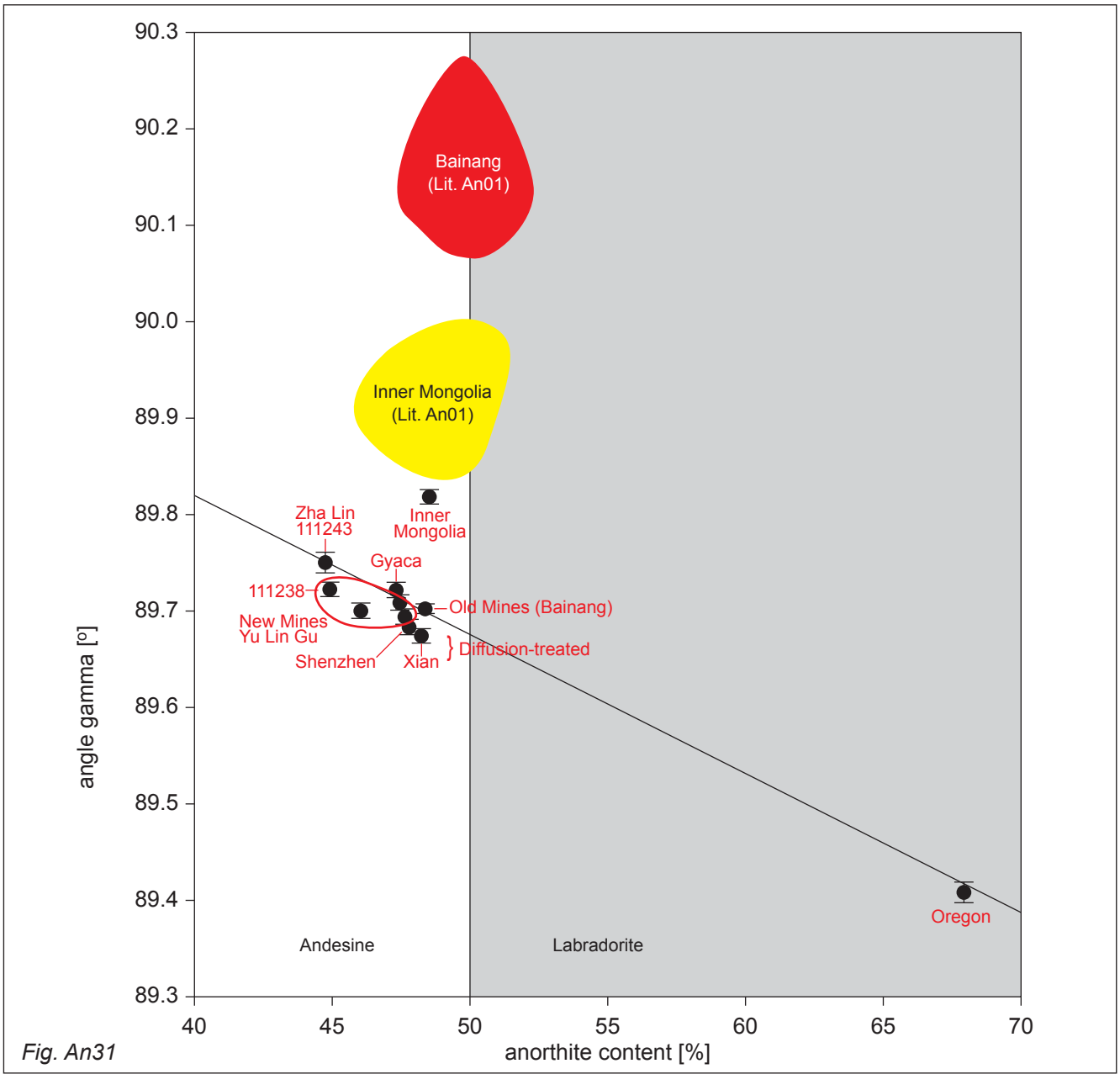

Fig. An31

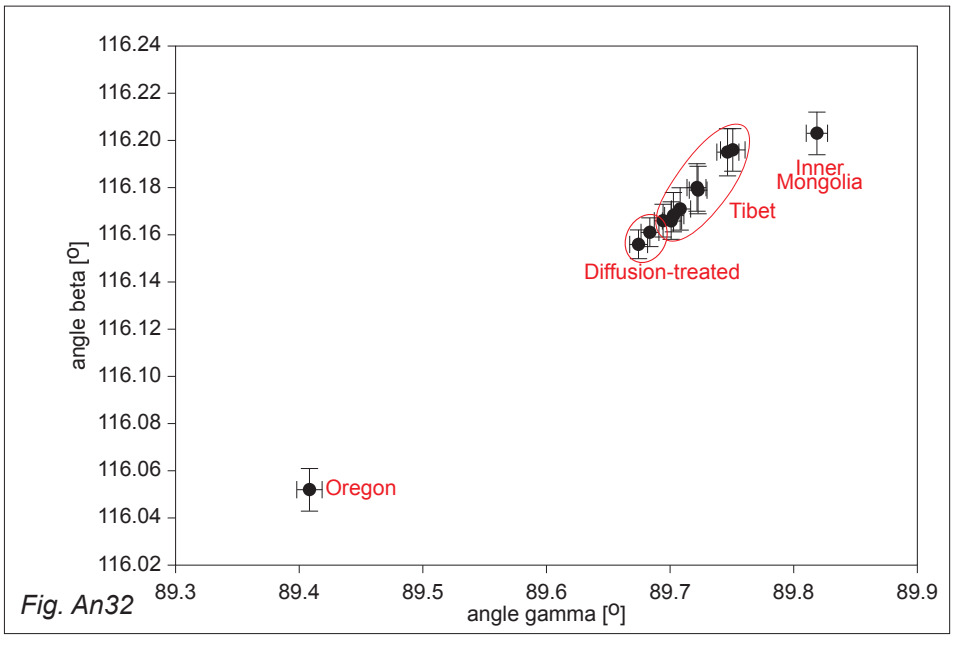

Fig. An32

Fig. An31-32 Gamma angle versus anorthite-concentration diagram (Fig. An31) and the gamma versus beta angles diagram (Fig. An32) for feldspars of different origin. Note differences between Oregon and Tibetan feldspars and the overlap of lattice parameters of diffusion-treated with copper-andesine from Tibet. Inner Mongolia values are differently as they do not fit in the general trend of the other feldspars.
Note that the gamma angles for Tibetan andesine from Bainang (Lit. An01) is considerable higher than our values for the same origin.

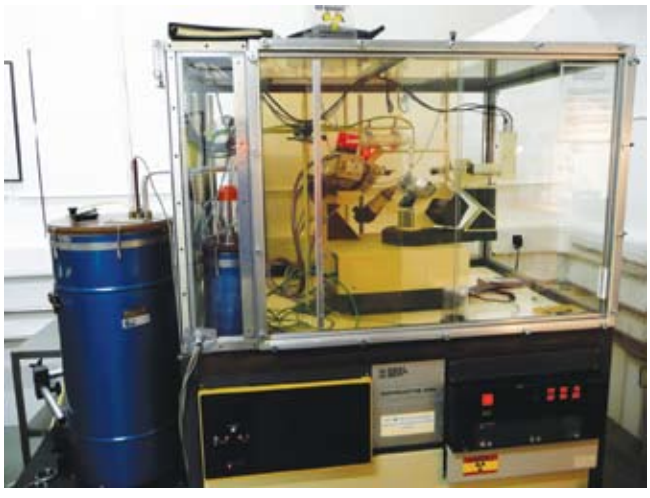

Fig. An33 Enraf Nonius CAD4 single-crystal X-ray diffractometer, equipped with a point detector (scintillation counter), which was used for measurement of precise cell dimensions at high diffraction angles.

samples were measured by LA-ICP-MS (Tab. An06 to 13) and four of the samples were measured by fs-La-MC-ICP-MS (Fig. An103 and Fig. An106-108). Based on the high accuracy of the measurements, significant variations were found in different cell parameters. The variations in the gamma angle of Tibetan andesine (old mine) and Mongolian counterparts has been already published and used to reconstruct the formation conditions of Tibet andesine and to differentiate it from andesine from Inner Mongolia (Lit. An01). The interpretation in the literature makes reference among others to the variations of the gamma values (at given chemical composition) and makes suggestions for formation conditions that lead to the growth of andesine in Tibet (e.g. volcanic against plutonic and metamorphic). It is based on temperature-related ordering of Al/Si-distribution in the four $(Al/Si)O_4$ tetrahedral sites of the andesine as a function of temperature. First, it is necessary to discuss the variations in our measured gamma values, compare chemical compositions of the samples and then compare them with the findings in the literature. As shown in Tab. An02 and Fig. An31, it is evident that the Oregon labradorite has the lowest and the sample from Inner Mongolia has the highest gamma-angle. The old and new mines Tibetan andesine have very similar lattice parameters (See Fig. An31 and Fig. An32). The gamma angles of the diffusion-treated samples are almost matching with those of all Tibetan andesines (group 1 and 2). Diffusion-treated samples were, however, different to the Inner Mongolia sample.

Together with the variations in the cell parameters, we have to take into considerations the variations of the chemical compositions. Only the Oregon feldspar is of significant different chemical composition (Labradorite) and all other samples are of very similar with almost matching anorthite-content (See Fig. An31) at the border of labradorite to andesine.

Regarding other lattice parameters (Fig. An32), again the sample from Oregon was found to be different and some slight variations is found again between the different samples from Yu Lin Gu (A3, Tab. An02). This shows that the formation history of Oregon feldspar is different than those of the Tibetan feldspars.

In comparison to the work published previously on Tibetan andesine (Lit. An01), our gamma values are one order of magnitude more accurately measured (pers. com. Th. Armbruster). Furthermore and in contrast to the previously published work, our data are reported with errors on angles. Therefore, a direct comparison is rather difficult. If we ignore this obstacle, in a first approximation, the gamma values of our andesine from Bainang (old mine material from Tibet, Tab. An02) are lower than those reported in the literature for the same material (See Lit An0) and more similar to Inner Mongolia values (Fig. An31). We can follow their interpretation that the andesine from Tibet correspond to those of typical volcanic andesine of low ordering. The lattice parameters of Tibetan andesine from the new mines are not reported yet and therefore, they will be interpreted here for the first time. As shown in Fig. An31-32 and Tab. An02, old and new mine material are almost completely matching. We can therefore apply the same genetic interpretation as for the old mine material, namely that the new mine materials from Tibet represent typical volcanic feldspars formed at high temperature with low degree of ordering.

Some differences in the cell parameters of the other groups are also important to note. The gamma angle of the Inner Mongolia is higher than those of samples originating from the old mines (Bainang). The opposite trend, however, was reported in the above mentioned work (Lit. An01 and Fig. An31). In this respect, our investigation does not confirm the previously published data and also we cannot confirm their conclusion that the Inner Mongolia andesine have lower degree of ordering than the Tibetan andesine.

The similarity of lattice-parameters of untreated samples from Tibet and the diffusion-treated samples is very striking. It would allow us to put forward the suggestion, that Tibetan material may be used as basic materials for diffusion-treatment and not only those from Inner Mongolia as suggested in the literature (Lit. An01). This is very well possible since a good portion of the andesine from Tibet have insufficient coloration (See page 25-26).


Fig. AN34A

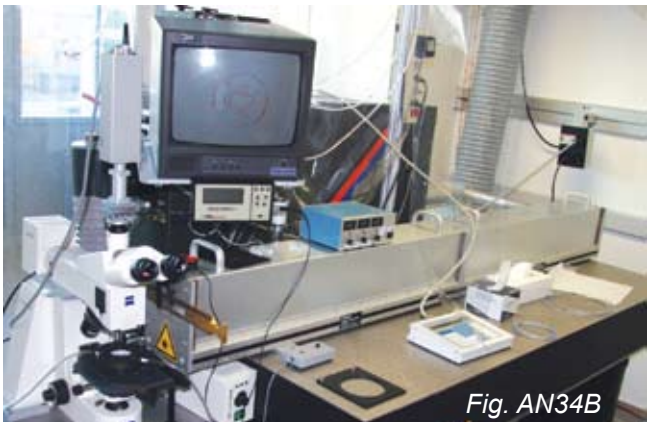
Fig. AN34B


Fig. AN34C

Fig. An34A-C As reported earlier (Lit. An13), a 193-nm ArF excimer ablation system (Lambda Physik, Gottingen, Germany) coupled to an ICPMS (Elan 6100 DRC, Perkin Elmer, Norwalk, CT, USA) was used for elemental analyses. In addition to the analysis of elements in the previous report (Li, Be, B, N, Mg, Al, Si, K, Ca, Sc, Ti, V, Cr, Mn, Fe, Co, Ni, Cu, Zn, Ga, Ge, Rb, Sr, Y, Zr, Nb, Sn, Cs, Ba, La, Ce, Pr, Nd, Sm, Eu, Gd, Tb, Dy, Ho, Tm, Hf, Pb, Bi, Th and U), the element Ag was added to the element menu. For quantitative analysis, NIST 610 was used as external calibration material and Al served as internal standard. During the first initial study the entire mass spectrum was collected and based on significant appearance of peaks reduced to 50 elements. Since the first test samples did not contain detectable Ag (pers. com. G. Fontaine), this element and other precious metals were not measured. However during this study, few samples showed significant concentrations of Ag. Therefore, after having detected this element in the new samples, we re-analyzed samples representative of the different groups of the previous analyzed material (Lit. An13), see Tab. An01 and Tab. An06-13. All samples were measured 2 to 3 times on the girdle of faceted (Fig. An35A) and polished samples and randomly on the surface of rough samples. Furthermore, series of profiles were generated on samples that were first cut half and polished. Each sample was ablated for minimum 40s at a repetition rate of 10Hz, using a crater diameter of 80-micrometers in single spot ablation mode (Fig. An39, An42A, An43A, An47-50 and An52). Larger diameters were used only when fluid inclusions and bulk were targeted (See Fig. An55B).

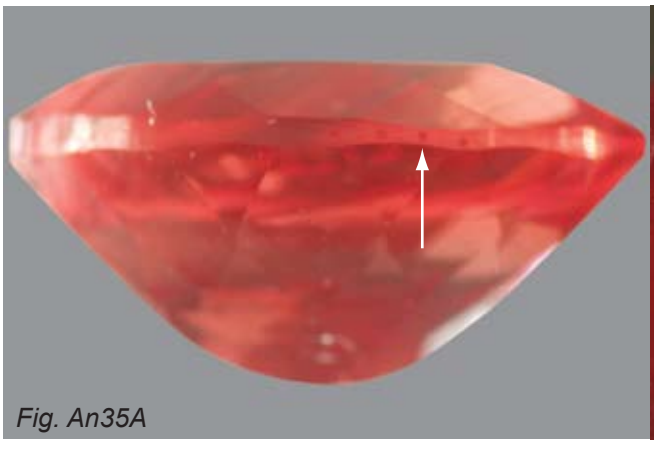
Fig. An35A

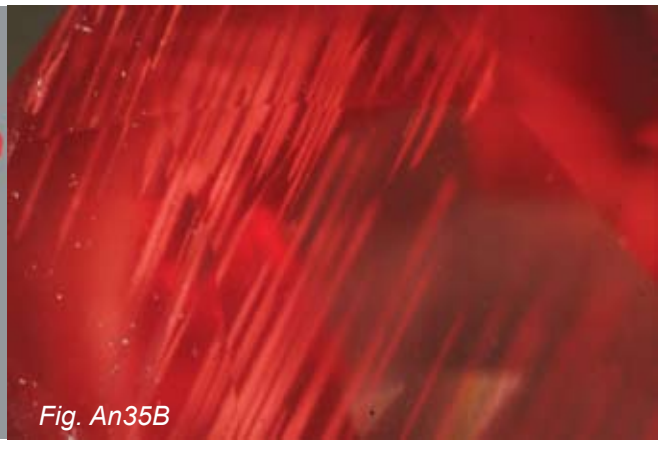
Fig. An35B

Fig. An35A-B shows one of the "Tibetan Andesine" that appeared in the market and Fig. An35B shows heterogeneous copper stripes visualized in the same gemstone in certain directions in the feldspar crystal.

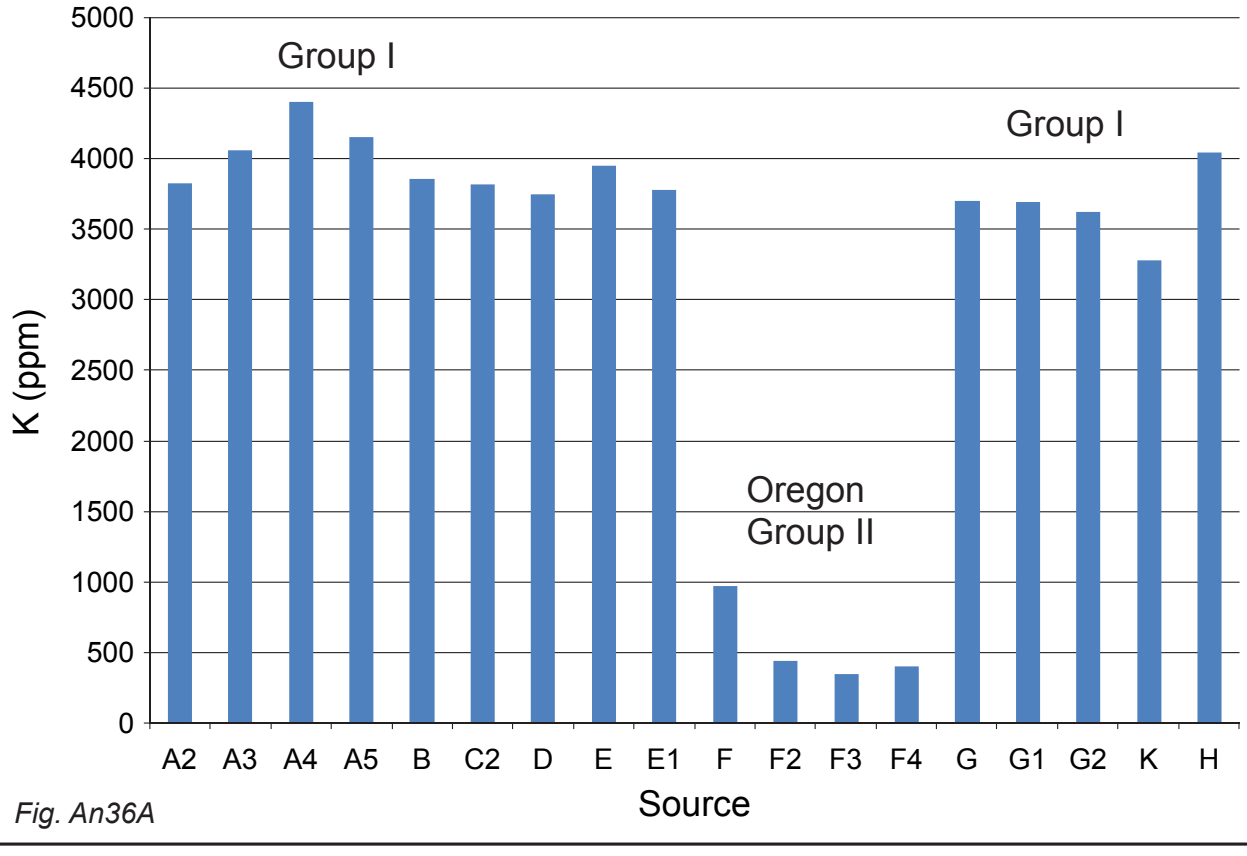

Fig. An36A

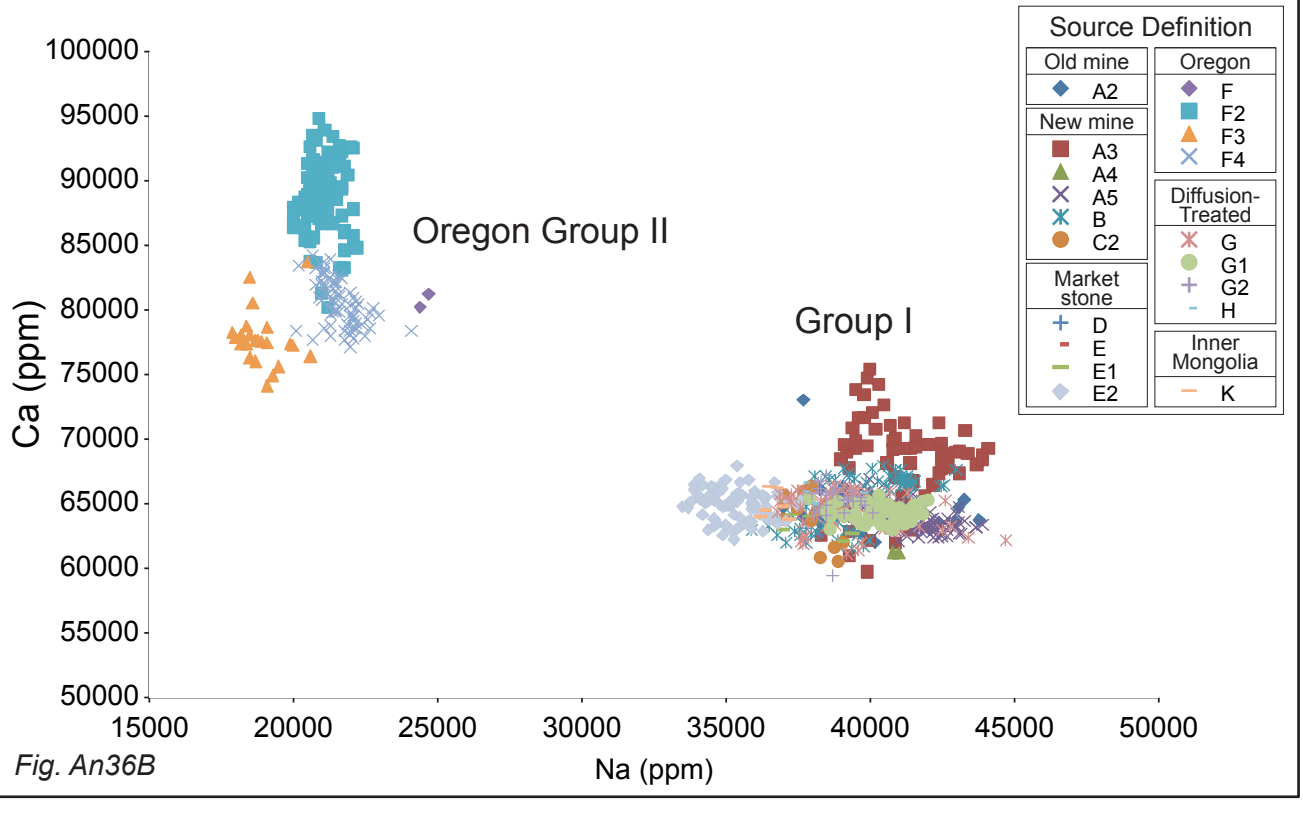

Fig. An36B

Fig. An36A-B Concentrations of elements Ca, K and Na (in µg/g (ppm), determined by LA-ICP-MS) in feldspar of different provenances (K-concentrations are averaged values, accuracy with a relative error of 10%).Two different groups were distinguished: Group I includes gems from Old Mine (Bainang), New Mines (Zha Lin and Yu Lin Gu, "Gyaca"), Market Stones (Tucson, Dubai and Hong Kong), Diffusion-treated feldspars (Xian University and Shenzhen, Emmett experiments) and untreated Inner Mongolia feldspar. Group II includes the different mines from Oregon. Group I corresponds to transitional compositions from labradorite to andesine and group II to chemical composition of labradorite (Fig. An31).

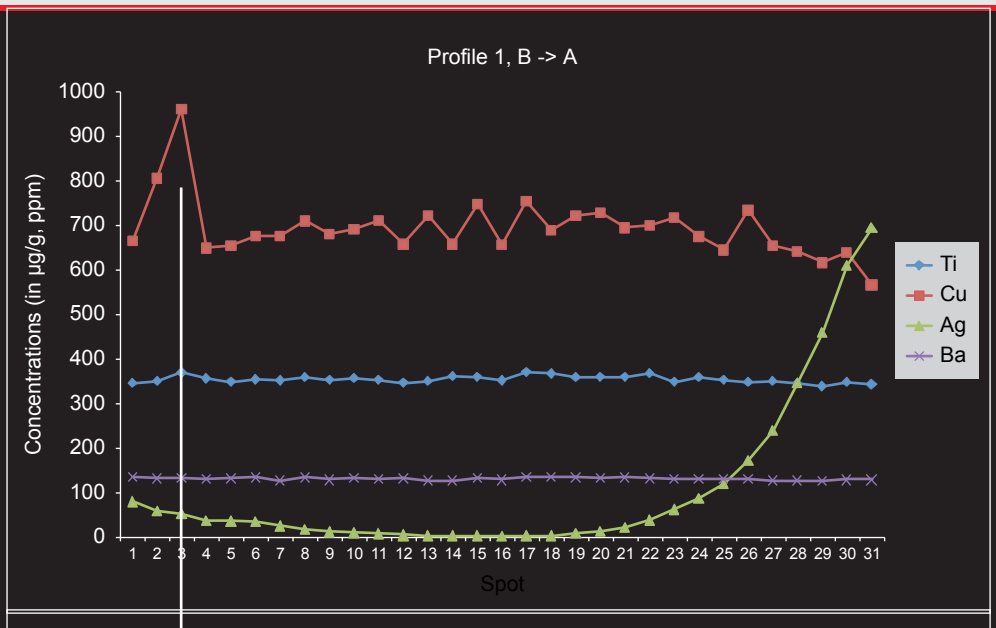

Fig. An37A

Fig. An37B

Fig. An37C

Fig. An37A-C Concentration profile across an upper Yu Lin Gu copper-bearing andesine perpendicular a fluid inclusion trail (See also Fig. An39). Part of the lower left corner was taken off and used for further argon-testing (Tab. An04) and copper-isotope testing (Fig. An108A). The two chemical profiles show a pronounced increase of Cu in the area of the fluid inclusions, but an increase in the Ag concentration towards the rim of the natural surface of the crystal. Fig. An37C shows the measured sample.

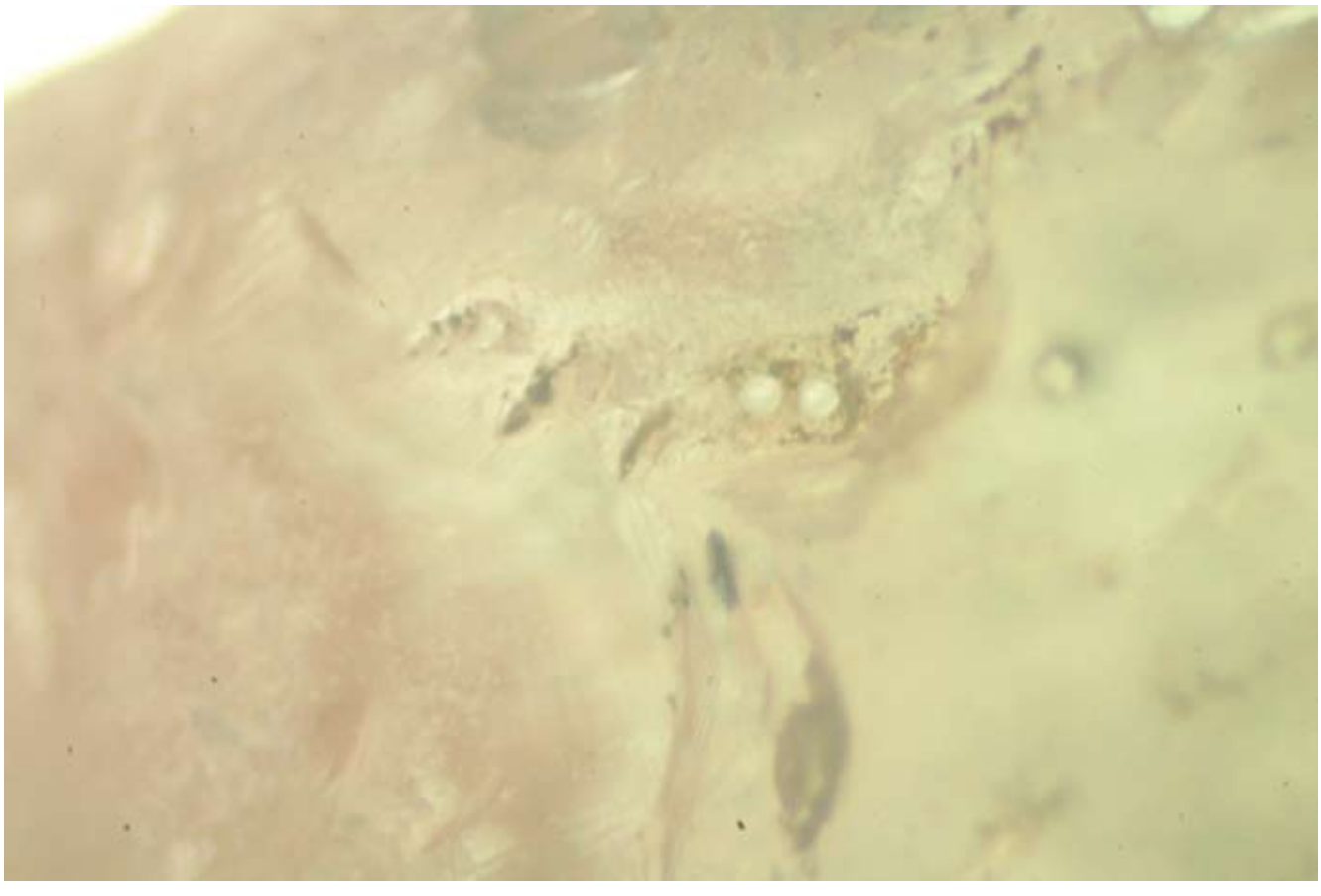

Fig. An38 Surface glass areas were found on the entry point of the fluid inclusion trail in this copper-bearing andesine from Tibet, Yu Lin Gu. These glassy residues were analyzed by LA-ICP-MS (See Tab. An03).

Tab An03 LA-ICP-MS Chemical analysis of glassy residues in comparison to the matrix

	Shenzhen diffusion-treated			2010_Hughes Yu Lin Gu	
	surface glass		andesine matrix	andesine plus surface glass	
	avg(3)	stdev		avg(2)	stdev
Li	79.8	6.6	17.9	8.38	0.46
Na	40951	1652	38700	37950	212
Mg	524	19	448	495	74
Al	85428	-	147000	147000	-
Si	326469	10167	285900	279400	1273
K	22335	736	3380	4815	969
Ca	35179	436	59400	59100	1556
Sc	0.293	0.031	0.253	0.247	0.018
Ti	227	2	356	444	134
V	55.5	2.1	1.49	4.33	3.83
Mn	275	4	22.6	32.1	8.8
Fe	3084	202	2870	3660	905
Co	8.02	0.41	0.358	0.637	0.223
Ni	19.2	1.5	0.396	33.3	21.6
Cu	23323	1454	634	610	0
Zn	183	6	3.44	6.73	1.70
Ga	9.32	0.09	17.1	15.4	0.1
Ge	0.984	0.227	0.920	0.847	0.443
Rb	30.2	0.4	0.653	2.94	2.40
Sr	606	7	1030	1050	0
Y	0.125	0.023	0.141	0.158	0.011
Zr	0.406	0.045	bd	0.174	0.189
Ag	0.720	0.923	bd	382	4
Ba	80.2	2.7	118	131	7
Pb	37.8	8.8	0.509	1.01	0.76
U	20.4	0.8	bd	0.034	0.020

Tab An03 Concentrations (in µg/g, ppm) of residues in comparison to the matrix determined by LA-ICP-MS. Differences in Al-, Si- and K-concentrations as major elements (for simplifications both analyses are normalized to the same Al-concentrations; the Al-concentration in the Shenzhen sample was determined by SEM-EDX) and differences in V, Mn, Zn, Ni, Co, Ag, Cu, Zr, Pb and U were determined and indicate that the glasses are enriched in these element concentrations.

Concentration profile of an Upper Yu Lin Gu (Sample R. W. Hughes) copper-bearing andesine determined by LA-ICP-MS

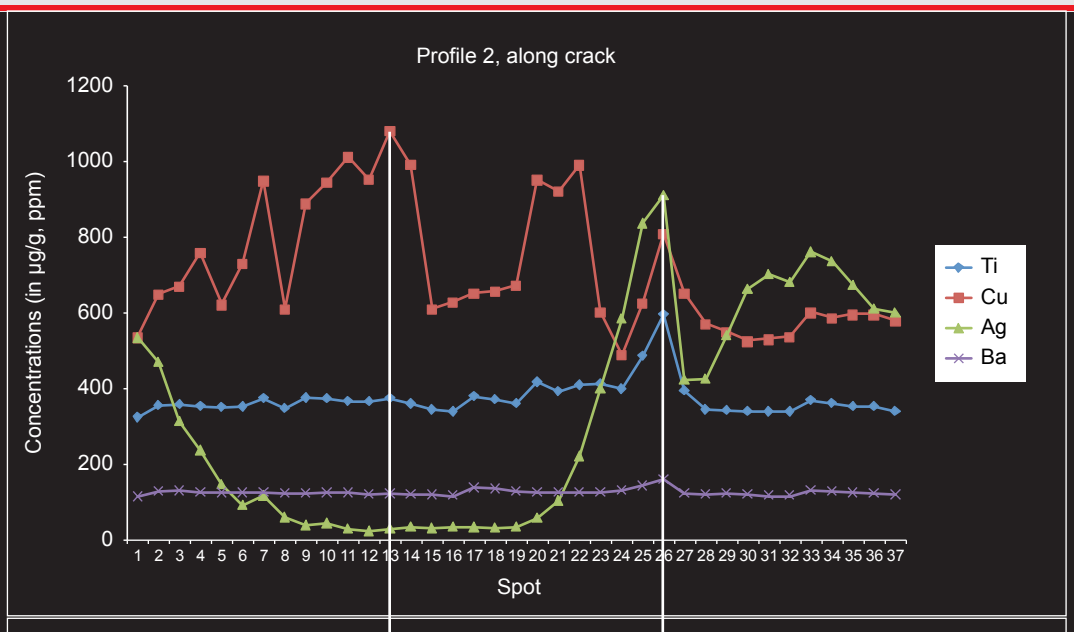

Fig. An39A

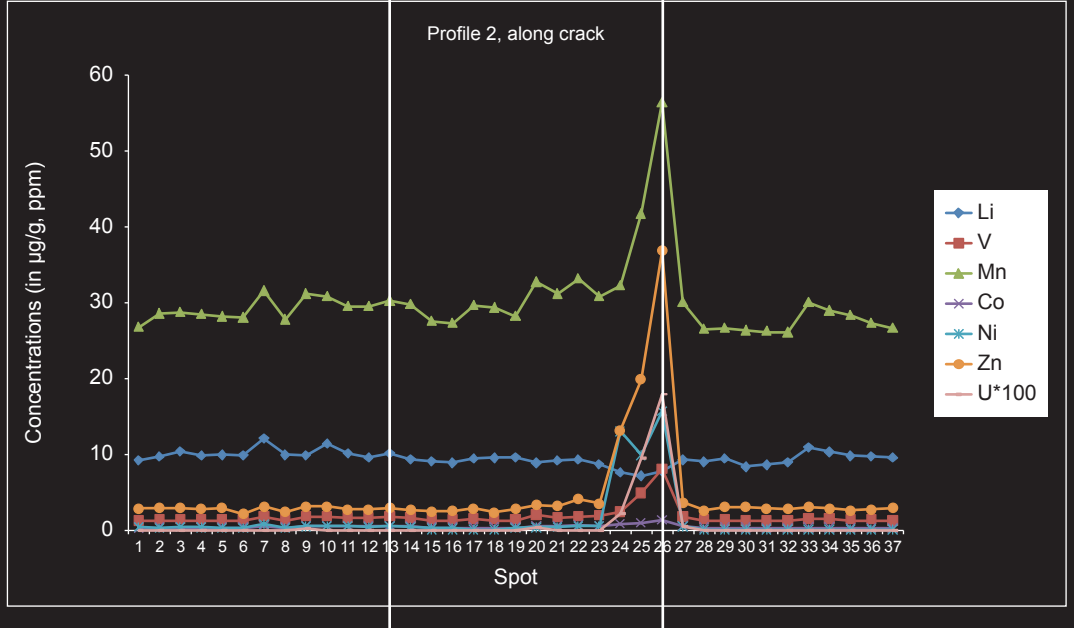

Fig. An39B

Fig. An39C

Fig. An39A-C Concentration profile of an Upper Yu Lin Gu copper-bearing andesine which was acquired parallel to a fluid inclusion trail (See also Fig. An37). Note that at point 13, a fluid inclusion was opened and provided the highest Cu-concentrations. At the same spot no significant Ag concentration was detected and no further enrichment of elements relative to the matrix was found. At point 26 we measured the glassy residues, which contained enriched concentrations of Ag, Ti, Ba, Mn, Zn, V, Co and U. Li did not show any concentration enrichment at both points (13 and 26). Detailed fluid analyses See Fig. An54-56.

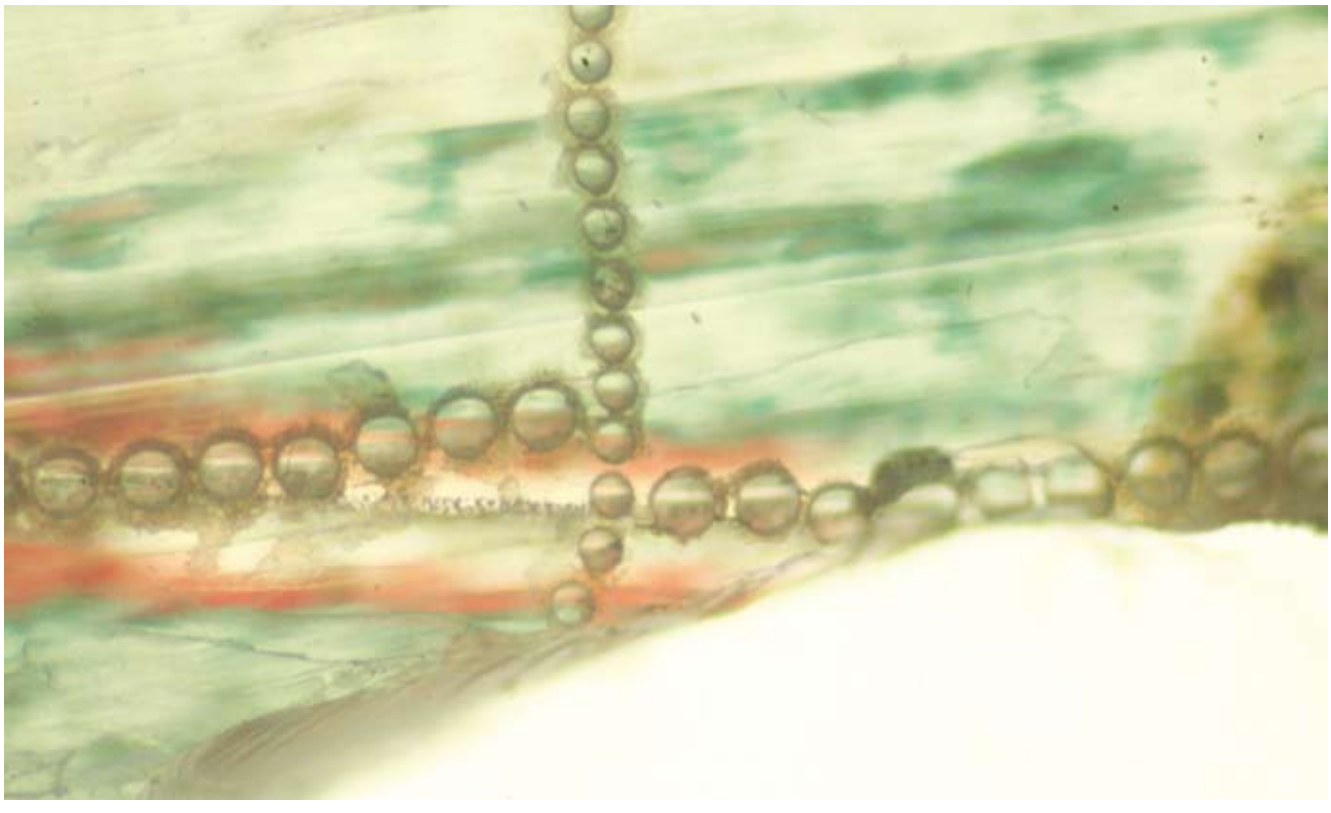

Fig. An40 shows the adjacent color zonation, the sampling positions for LA-ICP-MS and the under laying fluid inclusion trail. Position 13 represents a mixture of fluid, daughter minerals and matrix (See Fig. An39C). Enrichments in Co, Cu, Zn, Ni, Rb, Zr, Pb and other elements were found.

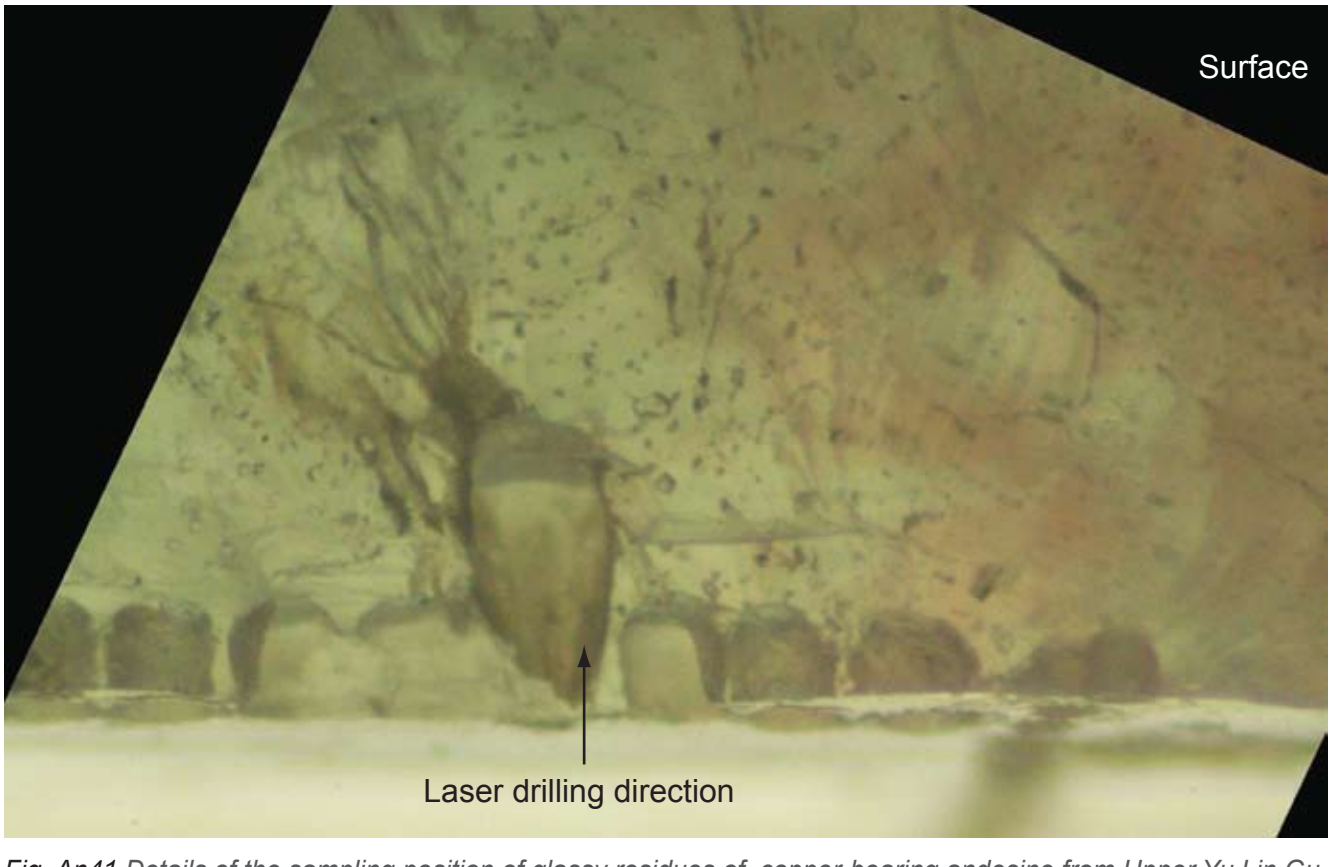

Fig. An41 Details of the sampling position of glassy residues of copper-bearing andesine from Upper Yu Lin Gu (sample No. Yu Lin Gu 2010, See Fig. 39C).
Note that the area of glassy residues is found to be enriched in the following elements: Ag, Cu, Ni, Mn, Zn, V, Co, Rb, Zr, Pb, Th, and U (other elements See Tab. An03).

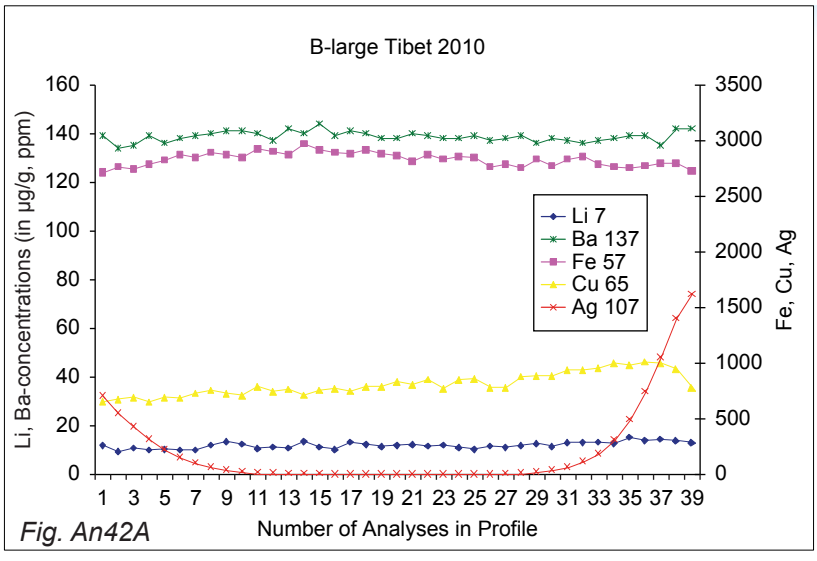

Fig. An42A

Fig. An42B

Fig. An42A-B Concentration profiles of copper-bearing andesines collected from Gyaca An42B shows a picture of the sample with a pronounced white rim and the laser craters used for analysis. Note that a pronounced Ag increase at the rim is accompanied by a decrease in the Cu-concentration. Close to the intersection of the white rim, the Ag- and Cu-concentrations are equal and in the outer zone the Ag/Cu-ratio is greater than 1. No such pronounced trends were found in other element concentrations, such as Fe, Ba or Li.

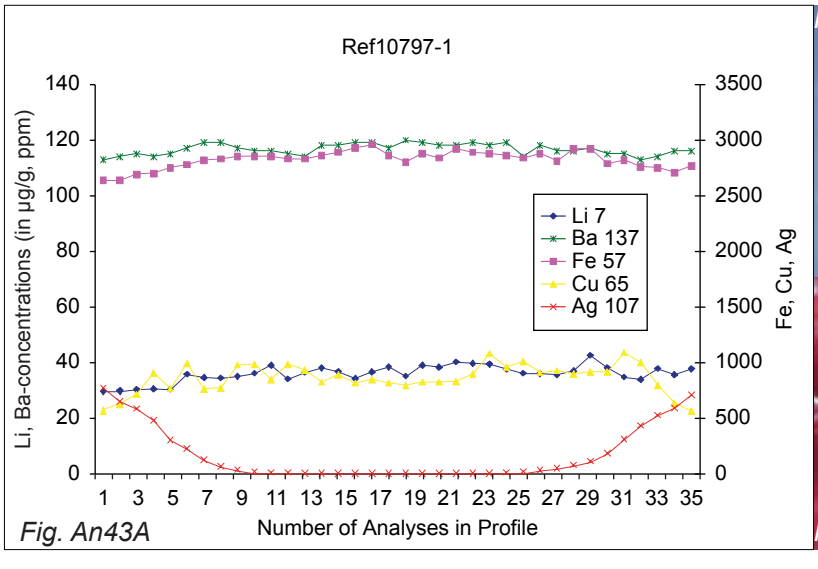

Fig. An43A

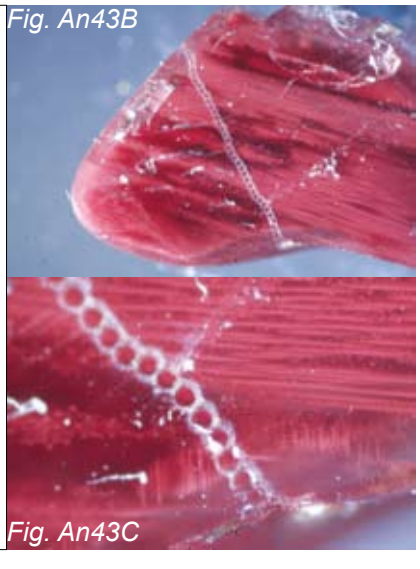

Fig. An43B

Fig. An43C

Fig. An43A-C Concentration profiles of copper-bearing andesines collected from Yu Ling Gu.
Fig. An43B shows a picture of the sample with a pronounced white rim and the laser craters used for analysis (see a zoom in Fig. An43C). Similar to Gyaca (Fig. An42A-B) a pronounced Ag increase at the rim accompanied by a decrease in the Cu-concentration occurs. Close to the intersection of the white rim, the Ag- and Cu-concentrations are equal and in the outer zone the Ag/Cu-ratio is greater than 1. Here also, no pronounced trends were found in the other element concentrations.

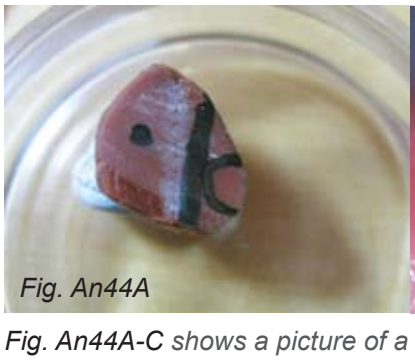

Fig. An44A

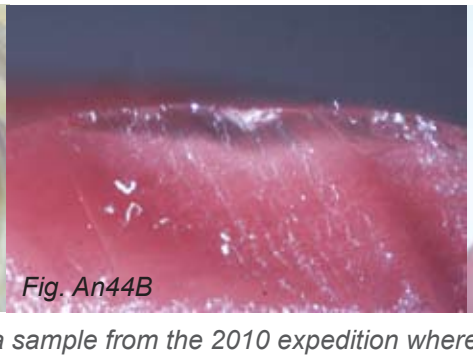

Fig. An44B

Fig. An44C

Fig. An44A-C shows a picture of a sample from the 2010 expedition where the white rim (Fig. An44B) was analyzed extensively. An44C shows a profile close to the rim of the sample, where higher Ag- than Cu-concentrations were determined in comparison to the sampling positions towards the sample center (circle like structure) (data See Tab. An05, Sample 2010 Hughes A).

Diffusion Treated Xian University

AA-Xian1 Diffusion-treated

Shenzhen diffusion-treated

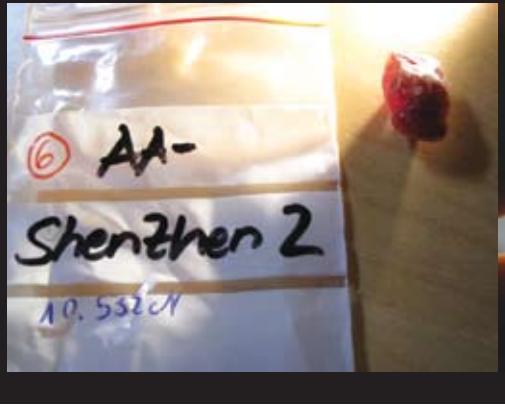

Fig. An45B

Fig. An45C

Fig. An45A-C These different types of diffusion-treated materials were supplied for examination (Original bag descriptions, See also acknowledgements).

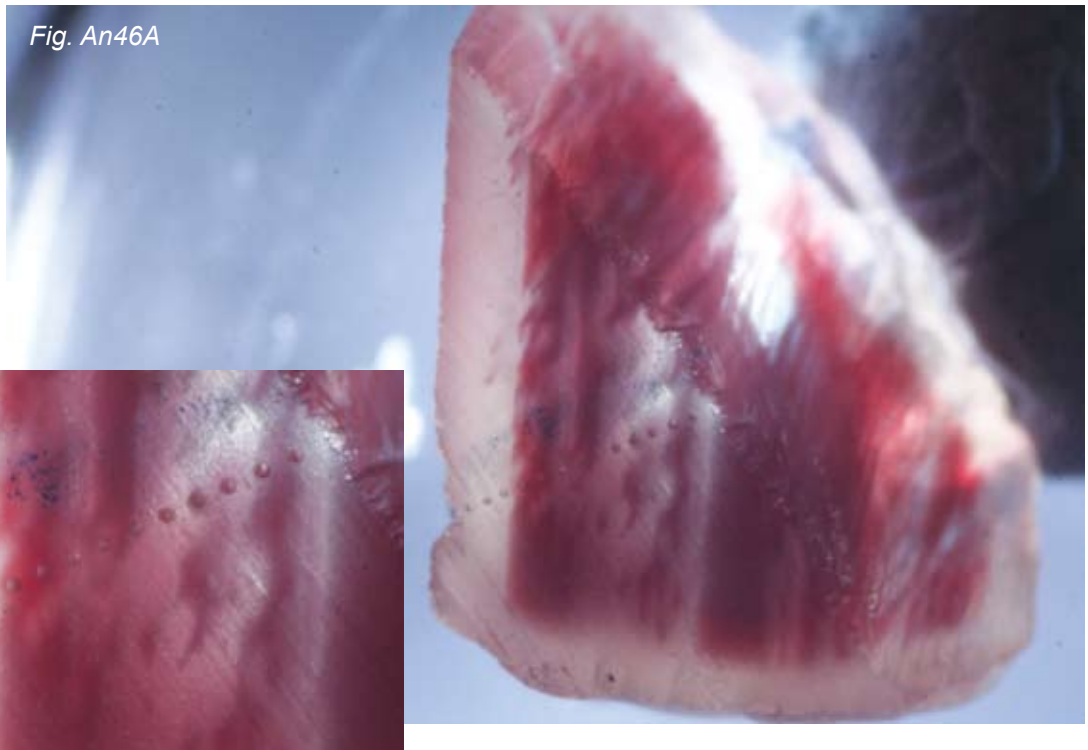

Fig. An46A-B Cross-section of a diffusion-treated copper-bearing andesine with a white rim and the craters produced by LA-ICP-MS. The chemical profiles are shown on page 47.

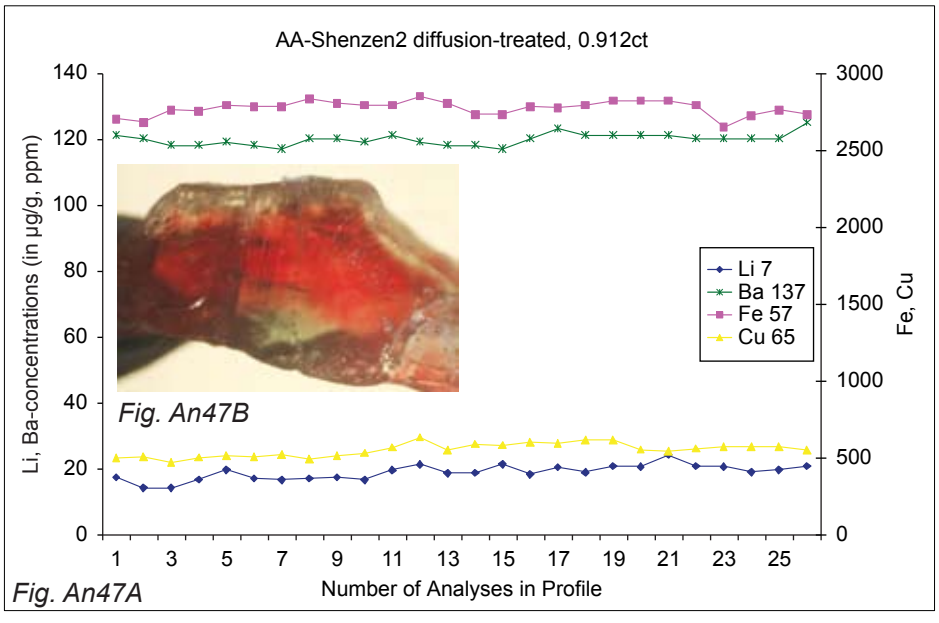

Fig. An47B

Fig. An47A

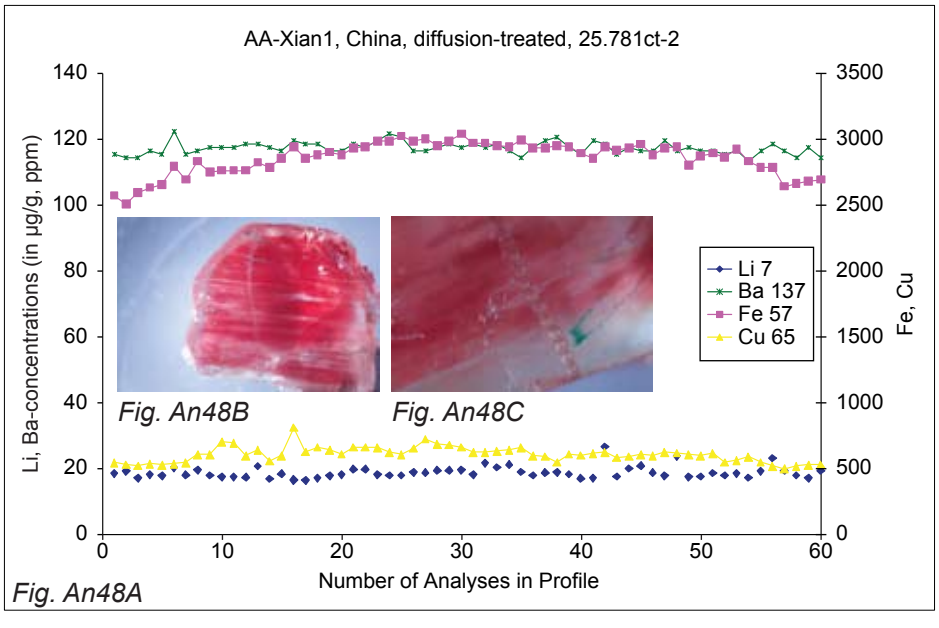

Fig. An48B

Fig. An48C

Fig. An48A

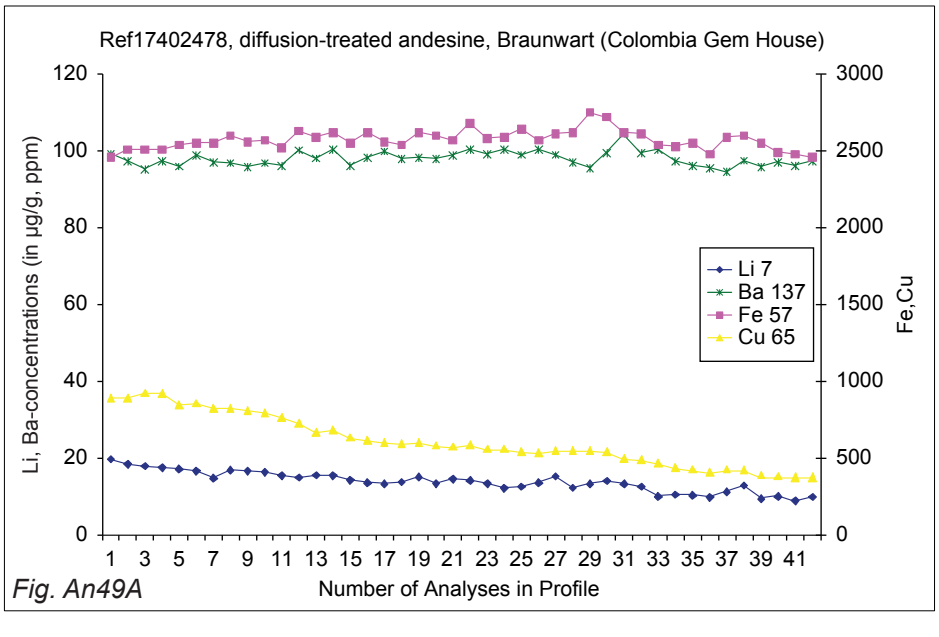

Fig. An49A

Fig. An47A-B to Fig. An49A-B
Concentration profiles of 3 samples from different sources and their accompanying pictures (Fig. An47B and An48B). Two samples were obtained from Abduriyim in September 2010 (Shenzhen factory and Xian University) and one sample from Braunwart (Columbia Gems) earlier. The first two samples displayed a white rim (See inserted photos of the samples). Samples were cut in half and the sampling positions indicate that the profile is passing through the white rim. In contrast to the natural andesines (see Fig. An42A-B and An43A-B) it can be seen that no particular and abrupt decrease of Cu was found in the rim zone. However, the Cu-concentration in sample 3 (Braunwart, Columbia Gem House) increases towards the rim (point 1-10) and this increase is well correlated with an increase in the Li-concentration, which has been reported earlier (Lit. An13).

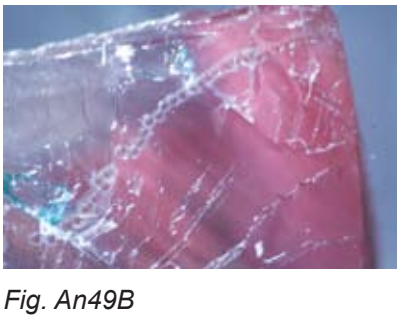

Fig. An49B

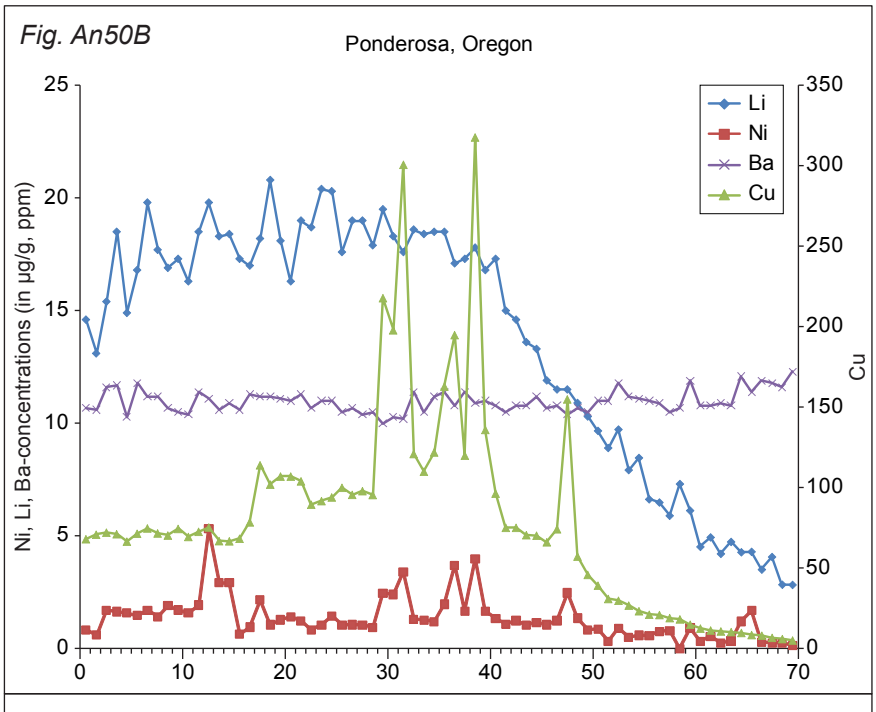

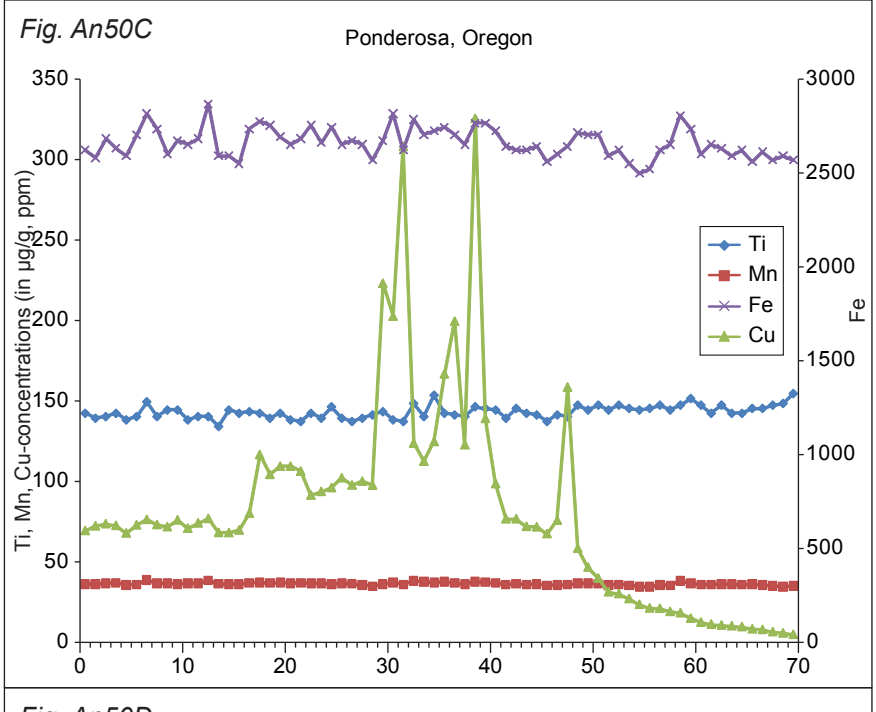

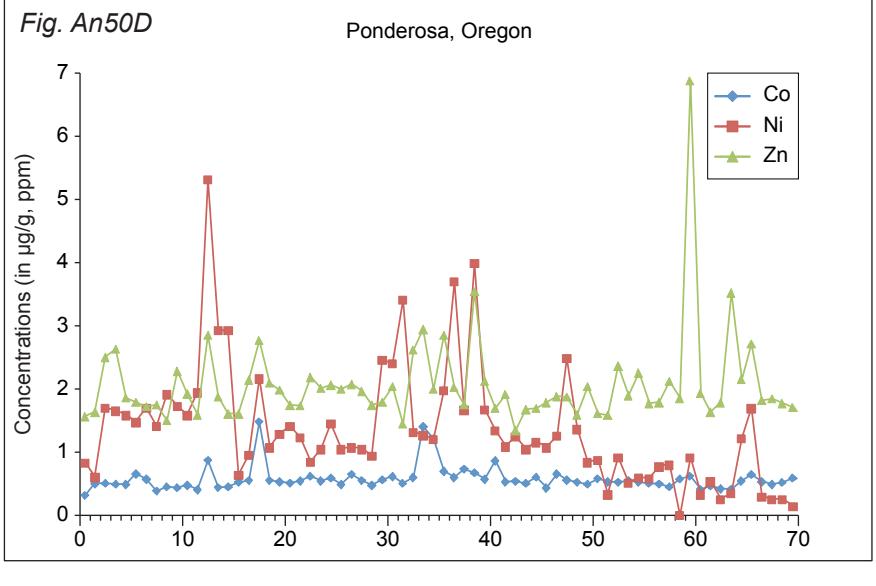

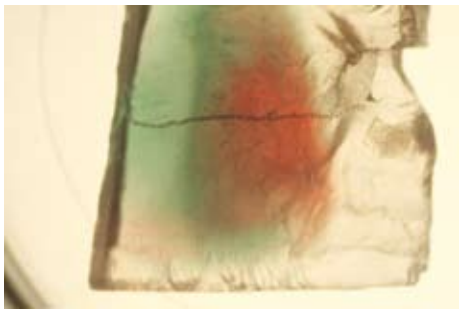

Fig. An50A

Fig. An50A-D Three concentration profiles of different concentrated elements of a cross section through the interior of a copper-bearing labradorite (sunstone) from Oregon. The first graph shows that the highest concentrations of Cu are found in the red core of the sample accompanied with irregular increased Ni-, Co- and Zn-concentrations. The pronounced Cu peaks indicate the ablation of copper-platelets. Ag-concentrations were below the limits of detection. The increasing Li-concentrations show a similar trend to the Cu-concentrations. Ti, Ba, and Fe concentrations were homogenously distributed throughout the analyzed area. Exactly the same results were obtained on a different sample (data not plotted).

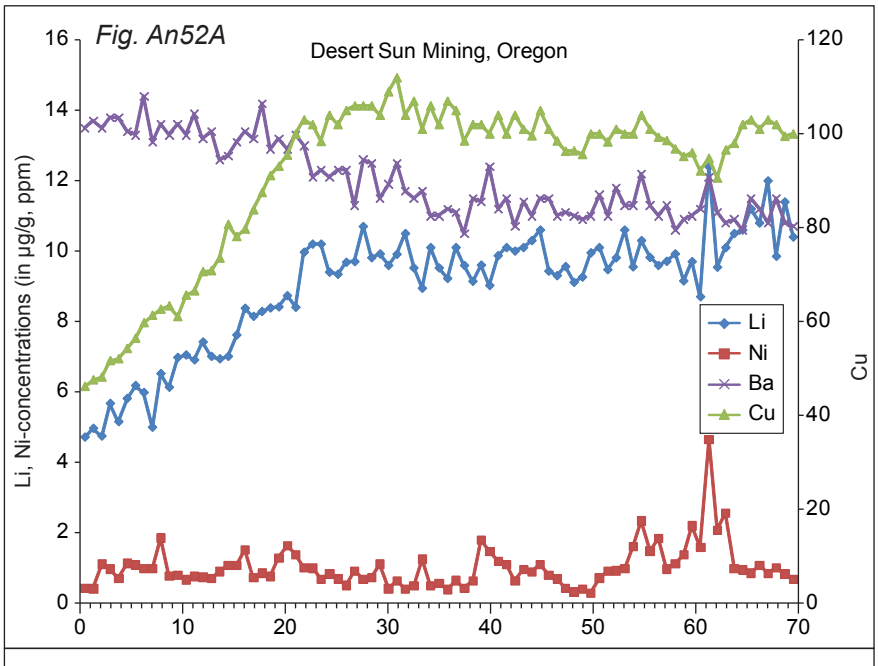

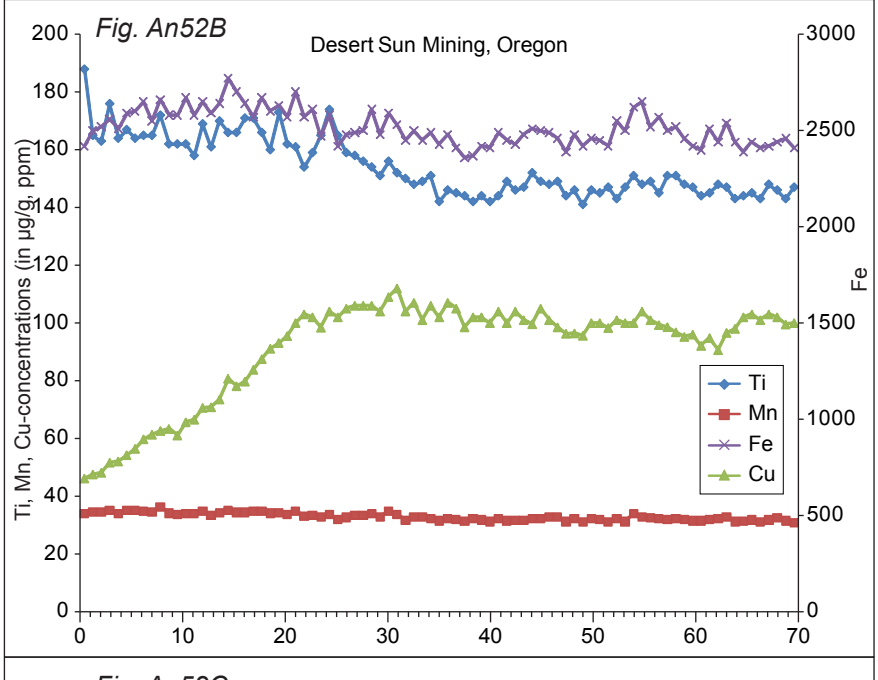

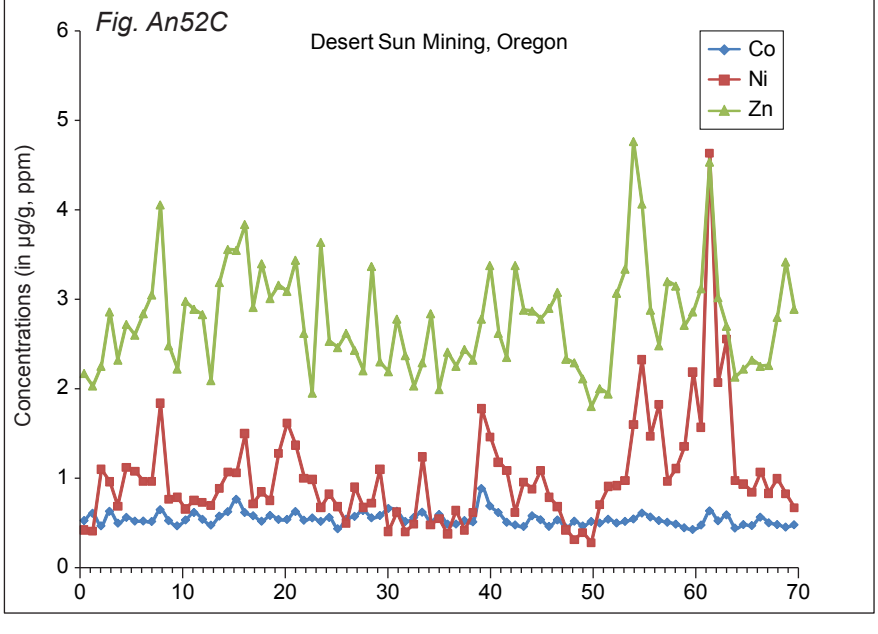

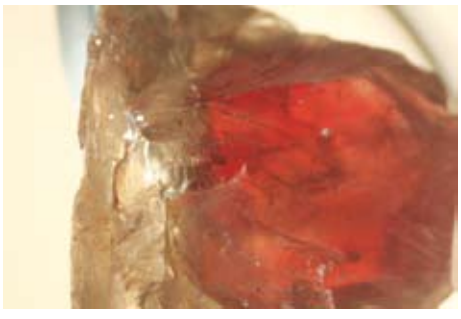

Fig. An51

Fig. An51 Picture of a copper-bearing labradorite (sunstone) from Ponderosa, Oregon (Desert Sun Mining)

Fig. An52A-C Three concentration profiles of different concentrated elements of a cross section through this sample. The Cu concentration measured from the rim to the red center increases the red core (approx. from 50 to 100 µg/g Cu). Li concentrations are correlated to the increase in Cu. Ti shows an opposite trend and is more enriched in the colorless rim. The irregular concentrations of Ni and Co are most likely due to contributions from micro inclusions (See Fig. An93A).

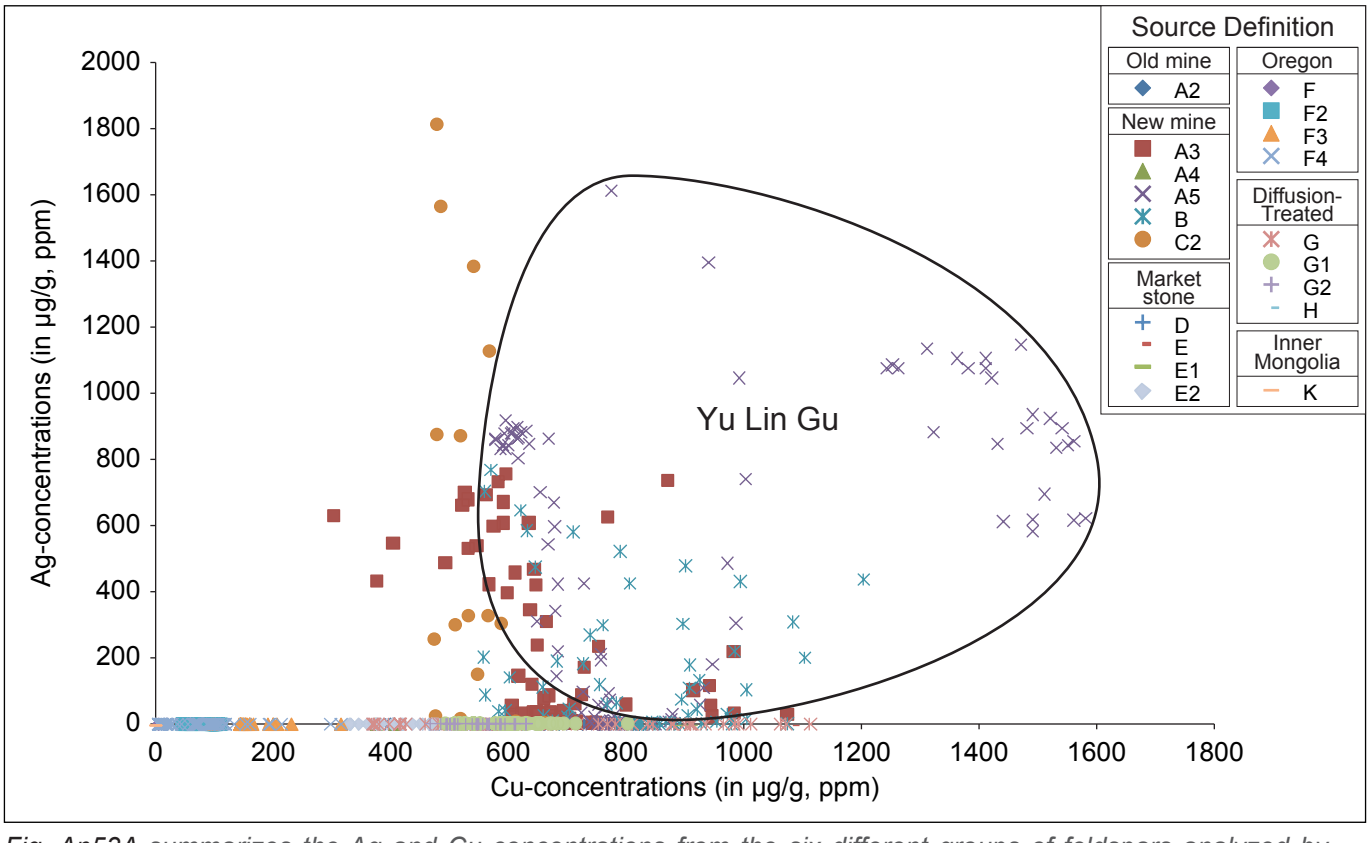

Fig. An53A summarizes the Ag and Cu concentrations from the six different groups of feldspars analyzed by LA-ICP-MS. Only the new mine provides Ag/Cu ratios which allow unambiguous discrimination from the other groups. The circle represents the sampling location Yu Ling Gu.

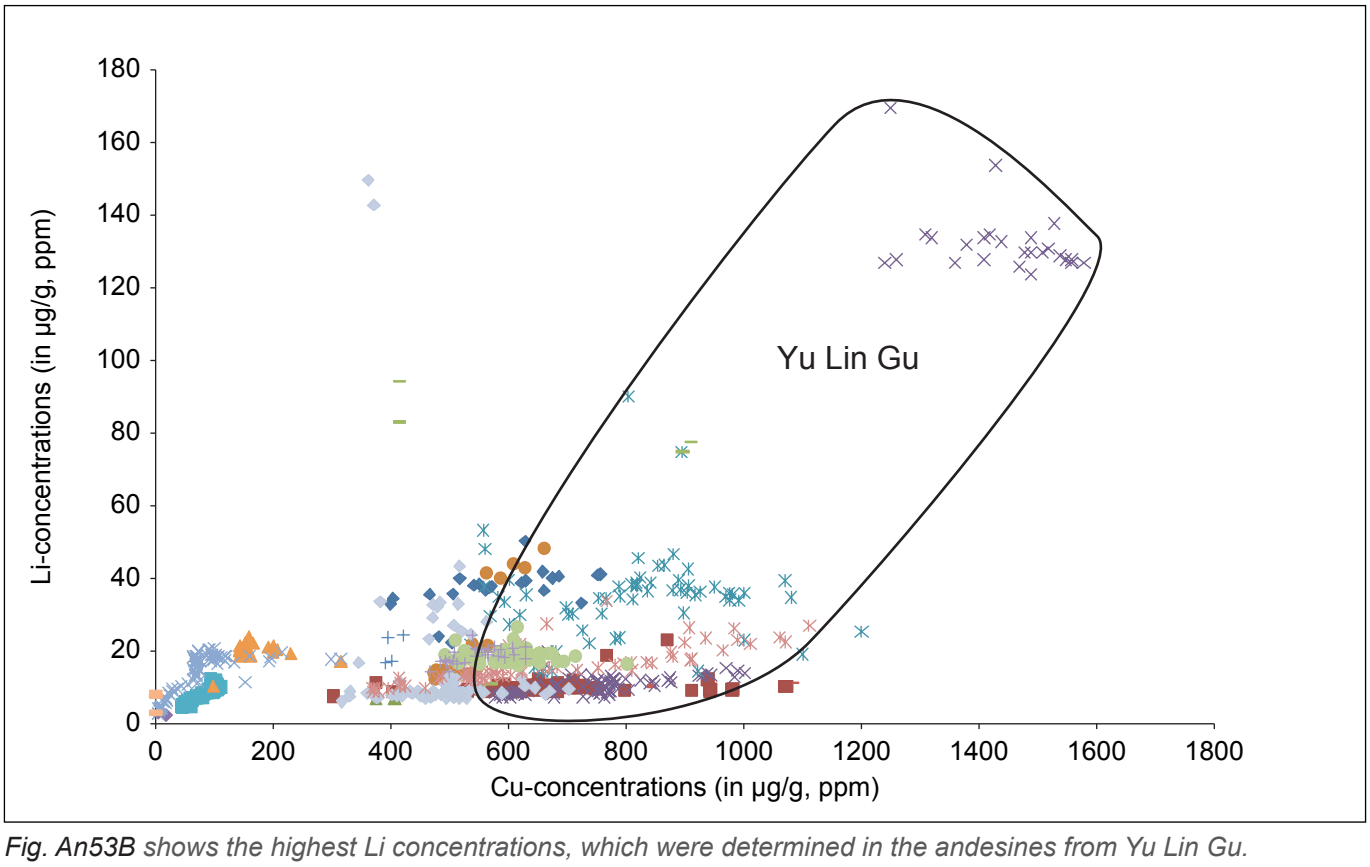

Fig. An53B shows the highest Li concentrations, which were determined in the andesines from Yu Lin Gu.

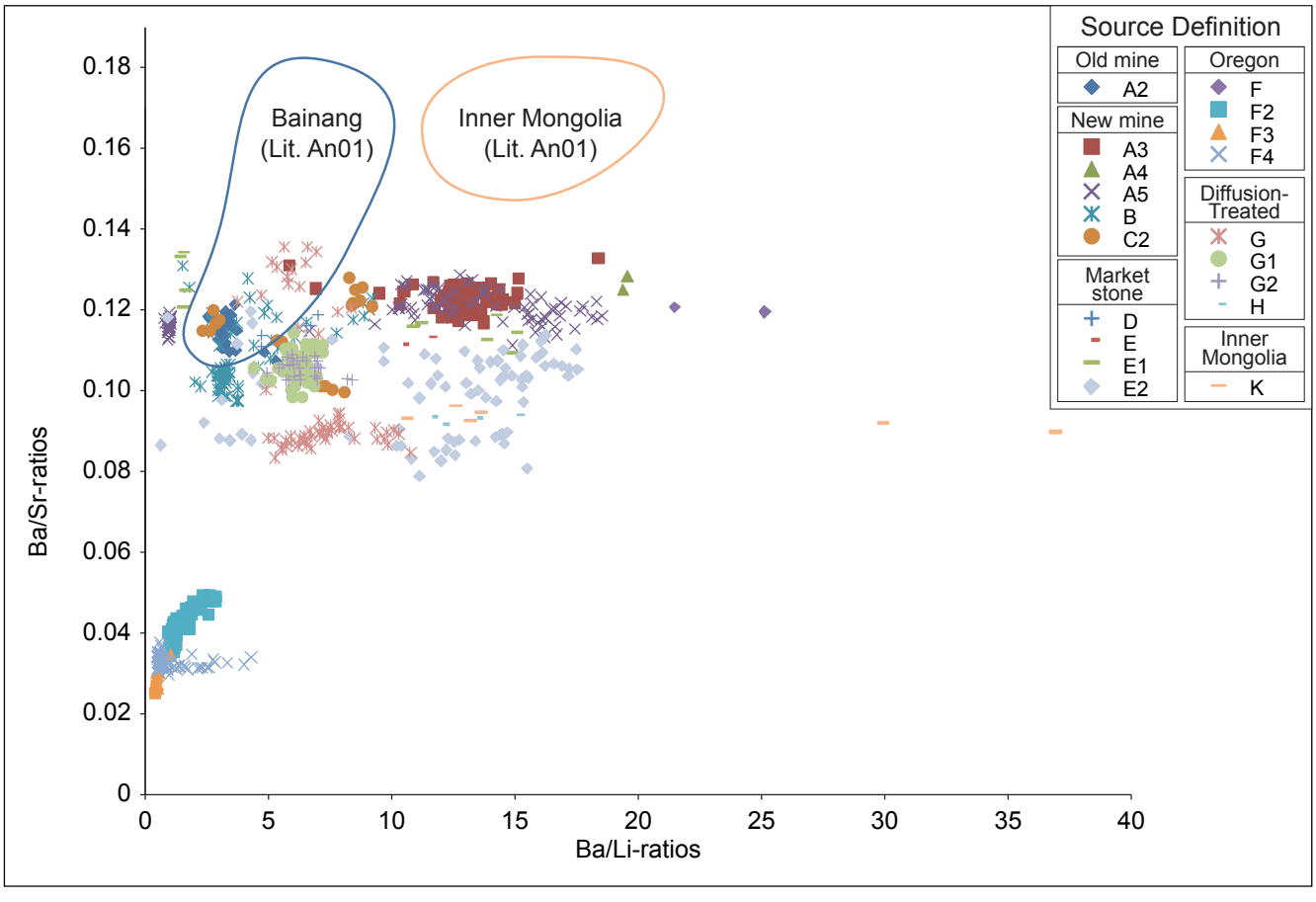

Fig. An53C shows the Ba/Sr versus Li/Ba discrimination (concentrations in µg/g, ppm). Old mines and diffusion-treated samples are indistinguishable (See also Lit. An13). In contrast to the previous observations, the new mines and particular the element ratios of the Yu Ling Gu mines can be separated from the diffusion treated counterparts. The ratios that are published in the literature (Lit. An01) from Inner Mongolia and the old mine (Bainang) are inserted. Our Inner Mongolia ratios are outside the field published in the literature (Lit. An01).

CONCLUSION LA-ICP-MS

The results presented in page 40-50 indicate that the natural Tibetan andesines from the new mine (Gyaca and Yu Ling Gu) can be distinguished by the presence of high concentrations of Ag, which is accompanied by decrease in the Cu concentration (See Fig. An37, An39, An42 and An43). The Yu Ling Gu mine shows the highest discrimination level due to high Cu/Ag-ratios, Ba/Sr- versus Ba/Li-ratios (See Fig. An53A-C).

In contrast, none of the different types of diffusion-treated samples contained Ag above the limits of detection (µg/g, ppm). However, the absence of Ag does not imply a diffusion treatment, since none of the Sunstone from different mines in Oregon, as well as some of the mines from Tibet (Bainang and Zha Lin), contained Ag above the limits of detection. Regarding other elements-concentration, the Cu-concentrations in Oregon samples decrease towards the rim and are significantly lower than all other counterparts. Furthermore, the distinct heterogeneous Cu and irregular trace element distribution are characteristic for the sunstones from Oregon. In contrast, the Cu-concentrations in diffusion-treated samples may increase towards the white rim (Fig. An49A). Furthermore, none of these samples contained irregular peaks of trace elements (Fig. An47A-An49A).

Given the facts above it must be concluded that Ag can only be used as discriminator for two mines (Gyaca and Yu Ling Gu). However, Gyaca is a salted mine, and it might well be that the materials comes from Yu Lin Gu. Polishing off the white rim will not remove the entire Ag-concentration, since the penetration depth is between 1 and 2 mm. All other information about the element variation within the gems can only be acquired from cross-section analysis, which makes it difficult for application to faceted gems without destruction.

FLUID INCLUSIONS ANALYSIS BY LA-ICP-MS

The fluid inclusions shown in Fig. 26 and 27 were analyzed with LA-ICP-MS and the results are given in Fig. An54-56 and Tab. An04).

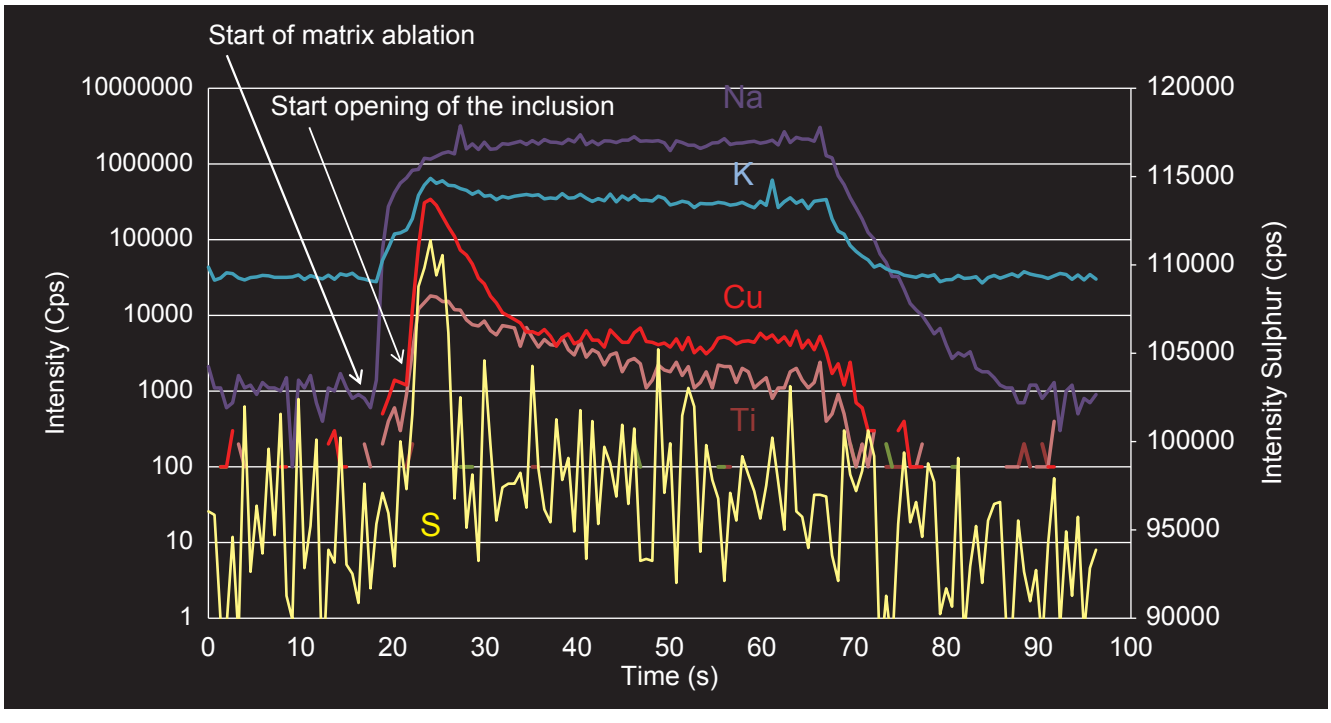

Fig. An54 shows the transient signals of Na as one matrix element and the elements Cu, Ti, K, and S detected in the liquid or vapor containing phase of the inclusion. The Na signal intensity provides no increase at the position of the inclusion and represents the matrix only. This can also be seen by comparing Na to the signal structure of Al as shown in An55C.

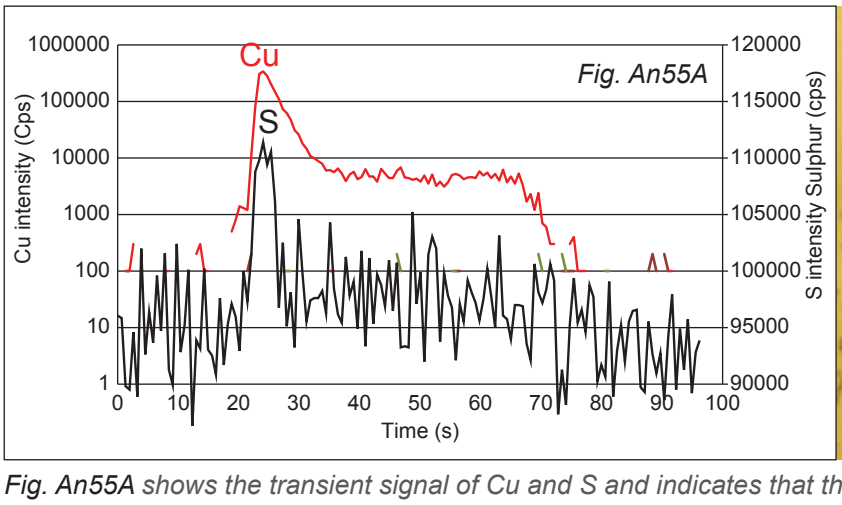

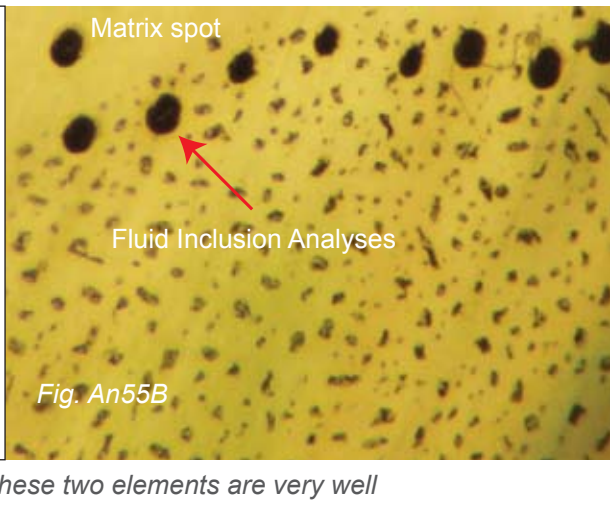

Fig. An55A shows the transient signal of Cu and S and indicates that these two elements are very well correlated. The detection of S is most interesting and its concentration must be very high, since the overall sensitivity of sulfur in ICP-MS is rather low when compared to other elements (Lit. An16).
Fig. An55B shows the fluid inclusion trail measured and the measuring points.

RESULTS

13 fluid inclusions analyzed in one copper-bearing andesine sample provided information about a large number of elements contained in such multiphase inclusions (Fluid inclusion images See Fig. An26-27 and An55B). The intensities of the detected signals were significantly above those of the andesine matrix, which was measured next to the inclusions for comparison. The chemical compositions (in ppm) of the fluids have been calculated (See Tab. An03) based on the internal standard of the matrix. Therefore, these concentrations represent relative values only, since the quantification procedure described in the literature (Lit. An20) was not applicable in this preliminary study. This was mainly due to the fact that the required Na intensity (used commonly as internal standard for fluid inclusion analyses and determined prior to LA-ICP-MS analysis by micro thermometry) was not detectable above the

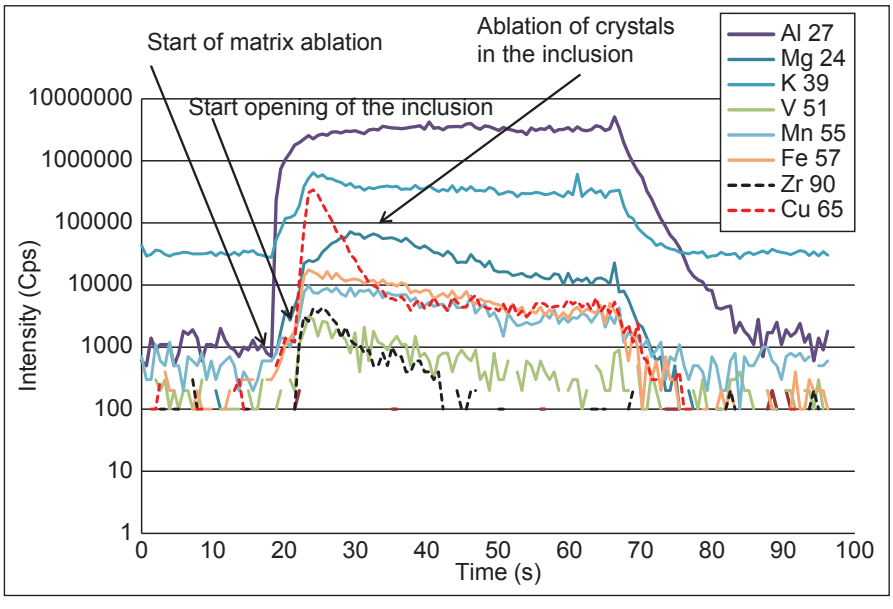

Fig. An55C summarizes a selection of transient signals for the ablation into a multiphase fluid inclusion. The Al signal intensity represents the matrix of the andesine. The dashed element Cu, Zr and K are indicators for the fluid or vapor phase of the fluid inclusion. The transient signals of e.g. Fe, Mn, and Co represent the ablation of the solid crystals contained in the inclusion. It can be seen that the signals of these elements increase slower as the liquid or vapor phase containing elements, which is due to the different ablation process. The different elements (e.g. Fe, Mn) indicate that the fluid contained different elements at high concentration, which are preserved as crystals in the inclusion. K is shown as indicator for the andesine matrix. However, it is also present in the fluid, which can be seen as the increase in signal intensity at approx. 25 s. Details about the analysis of fluid inclusions can be found in Lit. An08, An20 and An43. The steep and fast increase of the Cu signal is typical for Cu in a none-solid phase form, which vaporizes faster than the solid minerals.

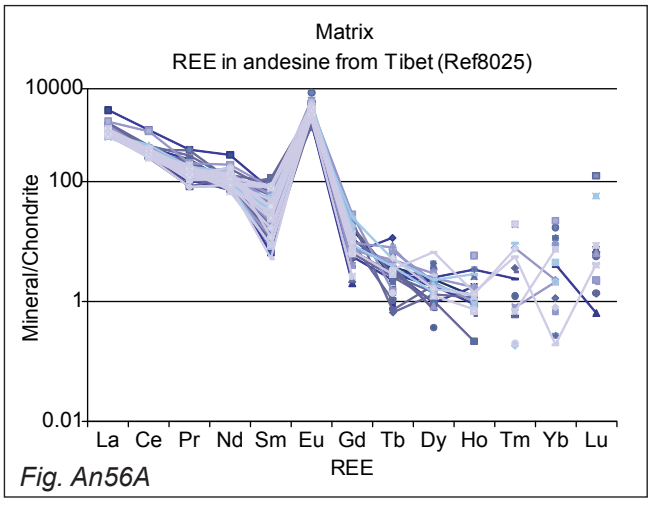

Fig. An56A

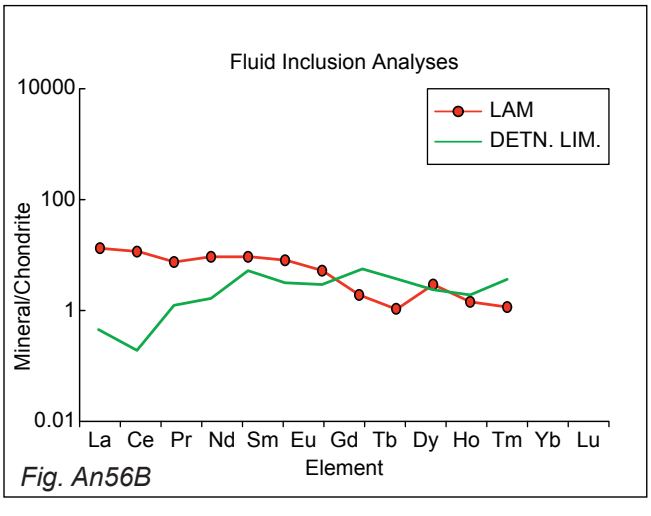

Fig. An56B

Fig. An56A-B The relative concentration determined within the fluid inclusion (Fig. An56B) indicate that the fluid contained light REE's as indicated in the Mineral/Chondrite plot. Significant concentrations above the limits of detection were found for La, Ce, Pr, Nd and Sm. The other REE element concentrations are represented by the limits of detection. Comparing host (Fig. An56A from another comparable sample) and fluid inclusion compositions it is evident that they have similar REE fingerprints (LREE concentrations and similar slope) with the exception of Eu-concentrations (positive Eu-anomaly in the copper-bearing matrix). It cannot be determined, however, whether the Eu-concentration is caused by Ba interferences (See Ba-concentrations in the copper-bearing andesine, Tab. An08 and 09) and therefore the Eu-concentrations must be treated with care.

content of Na in the natural andesine matrix. However, the elements K, Cu and Ti were good indicators for the opening of the fluid inclusions. Furthermore, Fe, Mn, Mg and other elements were indicators for the remaining mineral phases (daughter minerals) within the inclusions (See also Fig. An27A-B). The composition of these fluids proved the authenticity of the host andesine sample. Furthermore, the detection of sulfur together with Cu in such inclusions is a first indication for a very specific type of geological process that was involved in the formation of the copper-bearing andesine (See Lit. An08). However, only further detailed studies on these fluid inclusions (including heating and freezing experiments) will unravel more details on the exact geological formation history of the Tibetan copper-bearing andesine. This requires an extensive sampling and is beyond the scope of this book.

Tab. An04 Chemical concentrations within individual fluid inclusions in relation to the andesine matrix, Sample No. GRS-Ref10687-2, Gyaca (Tibet)

Inclusion 1

Isotopic mass			Li	Na	Mg			K	Ti	V	Mn	Fe	Co	Cu
			7	23	25			39	49	51	55	57	59	65
			ppm	ppm	ppm			ppm	ppm	ppm	ppm	ppm	ppm	ppm
			Li 7	Na 23	Mg 25			K 39	Ti 49	V 51	Mn 55	Fe 57	Co 59	Cu 65
ju09a04	04	Fluid	6.1	40823	2544			4703	1010	12	89	7974	3	2135
ju09a05	05	Fluid	5.3	39553	2742			4657	1193	15	100	9012	4	2780
ju09a06	06	Fluid	12.7	40319	2702			4842	1183	15	100	9101	4	3236
ju09a07	07	Matrix	11.6	40466	516			3763	344	3	32	2936	0.4	566
ju09a08	08	Matrix	6.7	40643	507			3699	374	1	28	2825	0.4	502

Isotopic mass			Zn	Sr	Y	Zr	Nb	Ag	Ba	La	Ce	Tb	Tm	U
			66	88	89	90	93	107	137	139	140	159	169	238
			ppm	ppm	ppm	ppm	ppm	ppm	ppm	ppm	ppm	ppm	ppm	ppm
			Zn 66	Sr 88	Y 89	Zr 90	Nb 93	Ag 107	Ba 137	La 139	Ce 140	Tb 159	Tm 169	U 238
ju09a04	04	Fluid	13	925	1.5	12.7	1.4	-0.2	122.4	2.3	4.4	0.2	0.0	-0.1
ju09a05	05	Fluid	16	945	1.4	12.1	1.6	-0.7	123.4	2.4	4.7	-0.1	0.1	0.048
ju09a06	06	Fluid	-4	955	1.1	9.4	1.4	0.2	125.1	2.0	4.2	0.1	0.1	0.030
ju09a07	07	Matrix	0	929	0.3	0.4	0.3	-0.1	117.1	1.1	1.9	0.1	0.1	-0.005
ju09a08	08	Matrix	17	962	-0.04	0.3	0.2	0.5	115.2	1.0	1.9	0.0	-0.3	-0.1

* all negative values represent LOD

Inclusion 2

Isotopic mass			Li	Na	Mg	S	Cl	K	Ti	V	Mn	Fe	Co	Cu
			7	23	24	32	35	39	49	51	55	57	59	65
			ppm	ppm	ppm	ppm	ppm	ppm	ppm	ppm	ppm	ppm	ppm	ppm
Chondrite			2.4	7245	143000	NA	NA	854	654	85	2940	278000	764	168
Run detection limit			1.48	1.22	0.51	45.19	70.17	3.92	3.42	0.34	0.72	18.68	0.27	1.06
ju09b03	03	Fluid	10	42196	1562	370	329	4384	1175	13	82	7685	2	2975
ju09b04	04	Fluid	8	40550	2967	263	195	4360	1276	15	98	10367	4	2342
ju09b05	05	Fluid	10	40261	4862	380	313	5041	1528	17	149	13227	6	5629
ju09b06	06	Fluid	7	38791	1797	325	335	4176	884	9	77	7067	3	2920
ju09b07	07	Fluid	10	40428	1559	236	341	4203	918	9	73	6884	2	2443
ju09b08	08	Fluid	8	42409	1557	298	286	4208	910	9	75	6816	3	3536
ju09b09	09	Fluid	10	39261	2562	259	298	4612	1197	13	100	8859	3	3160
ju09b10	10	Fluid	9	39518	1702	209	293	4217	919	9	72	6909	2	1766
ju09b11	11	Matrix	12	38463	435	233	381	3460	333	1.3	30	2828	0.5	462
ju09b12	12	Matrix	8	40390	462	236	397	3558	345	1.7	32	2824	0.7	458

Isotopic mass			Zn	Sr	Y	Zr	Nb	Ag	Ba	La	Ce	Tb	Tm	Pb	U
			66	88	89	90	93	107	137	139	140	159	169	208	238
			ppm	ppm	ppm	ppm	ppm	ppm	ppm	ppm	ppm	ppm	ppm	ppm	ppm
Chondrite			462	11.9	2.25	5.54	0.375	0.33	3.41	0.367	0.957	0.058	0.036	3.65	0.012
Run detection limit			3.19	0.10	0.10	0.22	0.12	0.34	0.59	0.10	0.09	0.09	0.09	0.17	0.08
ju09b03	03	Fluid	2	967	1.9	14.9	1.4	0.9	137	2.7	5.3	0.11	-0.15	0.70	0.12
ju09b04	04	Fluid	10	946	1.9	13.5	1.1	-0.3	132	2.8	5.4	0.15	-0.11	0.49	-0.04
ju09b05	05	Fluid	14	1013	2.7	18.4	2.1	-0.2	146	3.0	6.9	0.04	0.04	0.60	0.08
ju09b06	06	Fluid	15	1043	1.2	8.3	1.1	0.0	127	1.9	4.1	0.06	0.08	0.91	-0.03
ju09b07	07	Fluid	5	1021	1.1	8.2	1.0	0.1	126	2.2	4.3	0.01	-0.03	0.69	0.02
ju09b08	08	Fluid	8	998	1.2	8.4	1.0	0.3	143	2.1	4.3	0.04	0.18	0.45	0.04
ju09b09	09	Fluid	10	997	1.7	12.5	1.3	0.2	135	2.6	5.3	0.02	0.06	0.52	0.03
ju09b10	10	Fluid	7	1048	1.1	7.1	0.8	0.2	135	1.8	3.4	0.02	-0.06	0.57	-0.06
ju09b11	11	Matrix	-0.3	1050	0.2	-0.2	-0.001	0.01	122	1.1	1.8	-0.05	0.03	0.31	-0.01
ju09b12	12	Matrix	-0.3	1046	0.2	0.0	0.12	0.12	124	1.1	2.1	0.07	0.09	0.33	0.00

* all negative values represent LOD

Tab. An04 Relative comparison of increased concentrations within individual inclusions and the andesine matrix. The andesine matrix was integrated over the entire ablation sequence (approx.60 s) and all concentrations reported were calculated based on Al as internal standard and NIST610 as external standard (See Lit. An20). The commonly used Na concentration (typically derived from microthermometry) could not be determined due to the fact that no signal intensity above the matrix could be measured. Therefore, only relative changes in the concentration can be given. Furthermore it is well possible, that the presence of low K intensity could be an indication that only vapor was trapped in the inclusions. Further evidence for this is the absence of Cl, which is difficult to measure due to the high ionization potential. However, in most of the high salinity inclusions (See Lit. An20) it has been detected previously in other research projects and for inclusion sizes similar as in this study (10-20 µm). However, it has not been found in vapor inclusions.

SEM-EDX ANALYSIS

Method: Scanning Electron Microscopy (SEM) and Energy Dispersive X-ray Spectroscopy (EDX)

METHODS

For a better electric conductivity, the samples were mounted with a conductive adhesive carbon paste on sample holders and were covered with a 40 nm carbon layer. Secondary and backscattered electron images as well as semi-quantitative chemical analyses were obtained with a FEI XL30 Sirion FEG scanning electron microscope (10-30 KV/Spot 3-5) equipped with an EDAX Energy Dispersive X-ray Spectrometer. Secondary electron images (SE) provide a good morphological contrast and backscattered electron images (BSE) a better material contrast. Chemical compositions were calculated from measured EDX net intensities after correction for matrix, absorption and fluorescence effects (ZAF corrections) using the EDAX Genesis software.

SAMPLE DESCRIPTION

Representative samples from the old and new mines of Tibet, diffusion-treated Chinese andesine, as well as Oregon sunstone (copper-bearing labradorite) were investigated (Fig. An57).

RESULTS

The results include SEM-SE, SEM-BSE images of residues and particles found on feldspar surfaces (Fig. An59-93) as well as semi-quantitative chemical analyses. Solid particles included quartz that was found embedded in glassy residues of both diffusion-treated (Fig. An60B) as well as non-diffusion-treated samples. It was identified in both cases as alpha-quartz by Raman analyses (Fig. An95A). The chemical compositions of the glass residues were found to be K-rich in comparison to the feldspar matrix (See Fig. 81A and Tab. An03). Opaque particles included copper and copper-oxides in the form of various types of aggregates and dendrites. Fe-oxide particles were found only on the surface of diffusion-treated andesine, both on the glass surface as well as on the entire surface of the andesine. In addition, some needle-like Ca-Al-silicates were present (Fig. An63A, An66, An71 and An74). Particles found on diffusion-treated and non-diffusion-treated samples were very similar but the crystallization patterns and distribution were different (e.g. compare Fig. An66 and An74). Copper particles were present on the entire surface of diffusion-treated samples (Fig. An62B), whereas in the Tibetan samples they were restricted to the glassy areas only (Fig. An83). A dendrite growth of copper (Fig. An59) is exclusively found on the surface of diffusion-treated sample. In samples collected from one of the mines in Tibet, we identified Fe-Ni-Cu-sulfide particles (Fig. An78), Fe-Ti-oxides (Fig. An86) and a native silver platelet (Fig. An90). These particles were not found on the surface of the diffusion-treated samples. The well-crystallized Fe-oxide crystals on the other hand, were only found on diffusion-treated andesine (Fig. An68).
No such particles were found on any of the Oregon samples although samples collected from 4 different mines were included in the research. In contrast, Ni-rich particles (Fig. An93) as well as Fe-oxide and Fe-hydroxide crusts were found.

INTERPRETATION

Particles on the surface of Tibetan andesine were found only in areas where they were protected from natural erosion processes (or from tumbling). In diffusion-treated samples, the particles were distributed on the entire surface as no erosion process had destroyed them. The presence of many isolated delicate dendrites without the presence of glassy residues indicates that the diffusion-treatment was not using a Flux method. Melted residues on the surface of diffusion-treated samples were found only as isolated droplets. They are interpreted as contaminations present on the original andesine surfaces that were mobilized during the high-temperature treatment process. The discovery of a silver-platelet on the surface of a Tibetan sample (Fig. An90A) is consistent with the presence of silver concentrations in the glassy residues (Fig. An42-An43 and Tab. An03). It is interpreted as a natural formation.
Surface crusts on samples from Oregon are identified as products of weathering and no particles typically found on the surface of the Tibetan andesine are present. It suggests that Oregon sunstone (labradorite-feldspar) and Tibetan copper-bearing andesine are formed by different geological process.

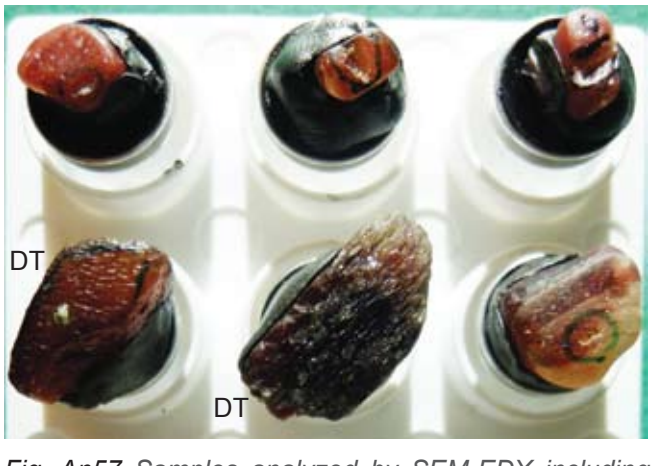

Fig. An57 Samples analyzed by SEM-EDX including natural copper-bearing Tibetan andesine and 2 diffusion-treated counterparts (marked with DT)

Fig. An58 Portrait of the laboratory (Group: Prof. B. Grobéty) of the University of Fribourg equipped with a FEI XL30 Sirion FEG scanning electron microscope. The working scene shows one of the author's (MM) discovery of the delicate copper-bearing dendrites on the surface of a diffusion-treated andesine with a SE detector used for highly detailed and resolved images (See also Fig. An59).

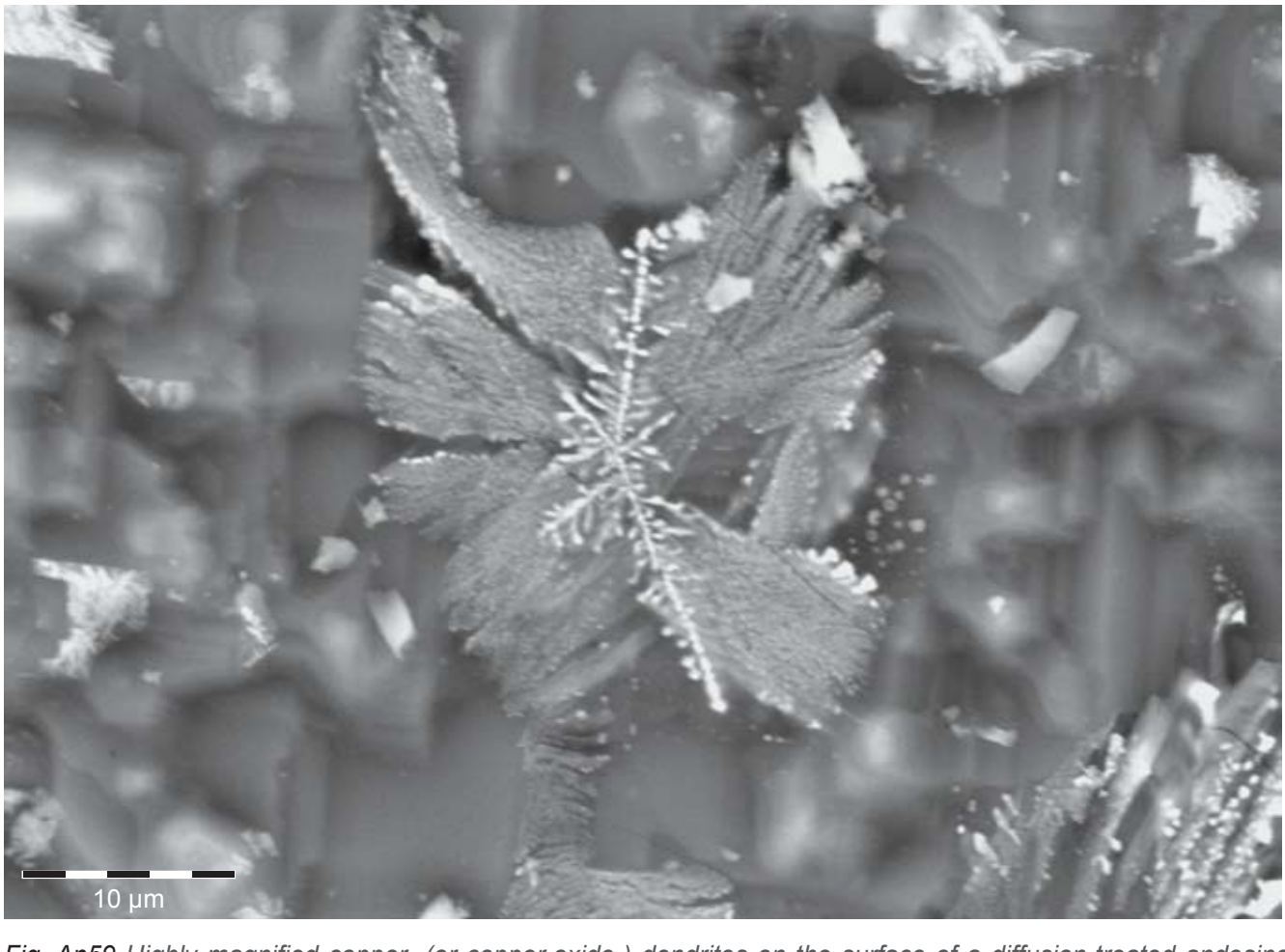

Fig. An59 Highly magnified copper- (or copper-oxide-) dendrites on the surface of a diffusion-treated andesine (Sample Ref AA-Shenzhen 1). Diameter of dendrite is 15 microns. The particle proves that no Fluxes were used during the diffusion-process as it is found directly on the andesine surface without further Flux present. The sample from Abduriyim (See acknowledgments).

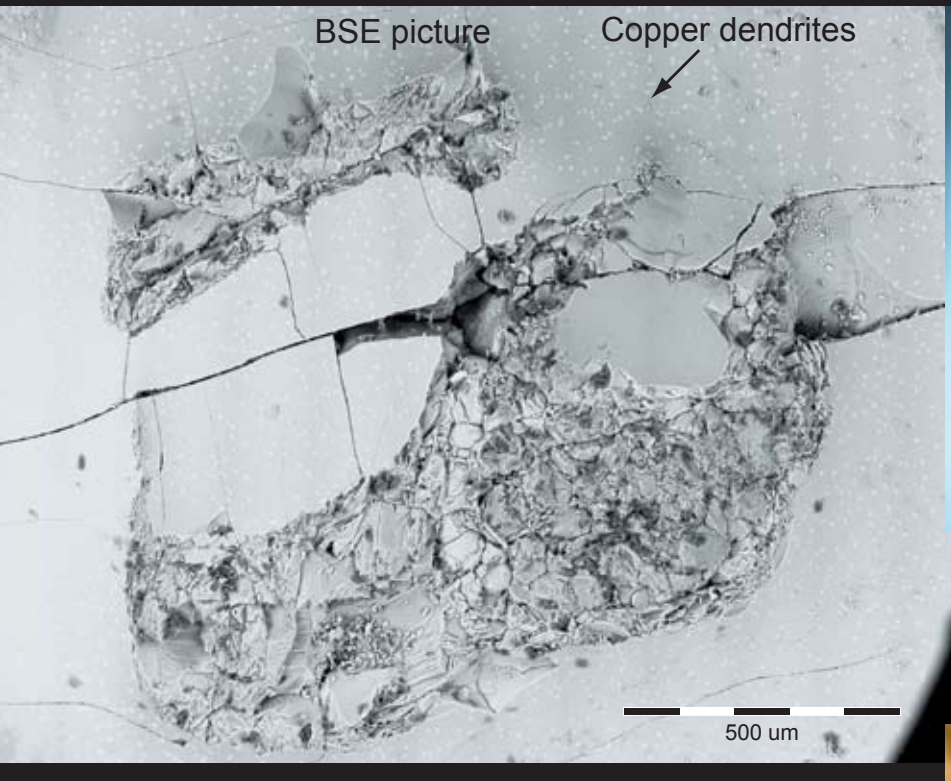

Fig. An60C SEM-BSE image of the green glass and surrounding matrix. Note the myriads of small copper-bearing particles are scattered over the entire area, both on top and extensively on the andesine surface.

Fig. An60A Diffusion-treated andesine from Shenzhen with a glassy residue on its surface. Length of crystal is 15mm.

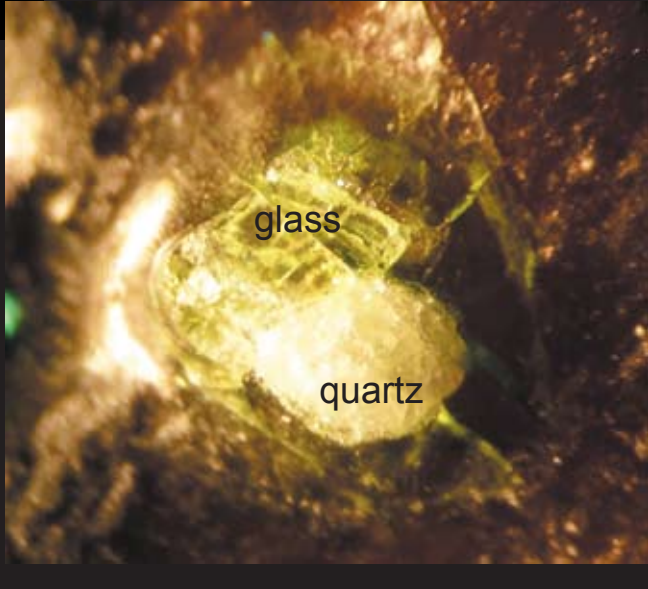

Fig. An60B Magnification of the glassy residue found on the diffusion-treated andesine reportedly treated in Shenzhen, China (Fig. An60A). Note the presence of a quartz grain that is surrounded by greenish-colored glass. The glass composition showed lower Al-concentrations and higher Si-concentrations in comparison to the andesine host mineral (approx. 14.5 % Al_2O_3, 66.5 % SiO_2, 3.1 % K_2O, 5.8 % CaO and 2.6 wt.-% Na_2O). Further chemical compositions see Tab. An03. Note: The green glass also contained traces of uranium.

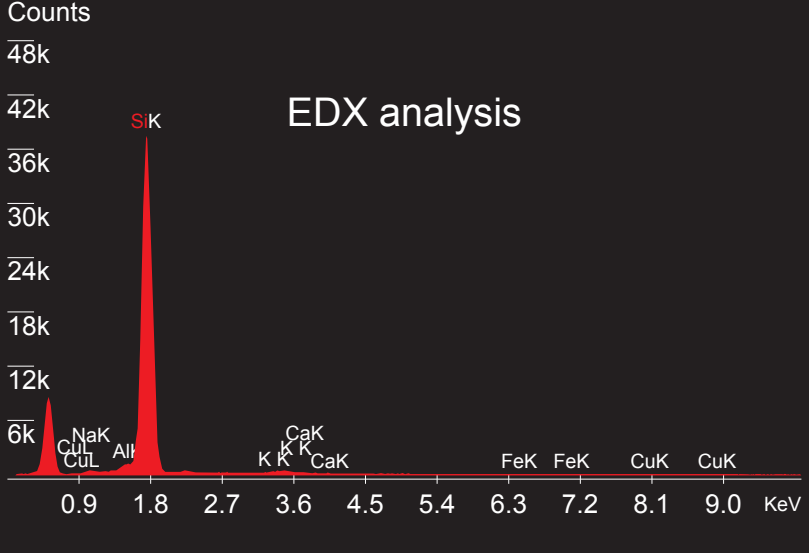

Fig. An60D EDX spectrum of the quartz crystal (Raman spectrum see Fig. An95A).

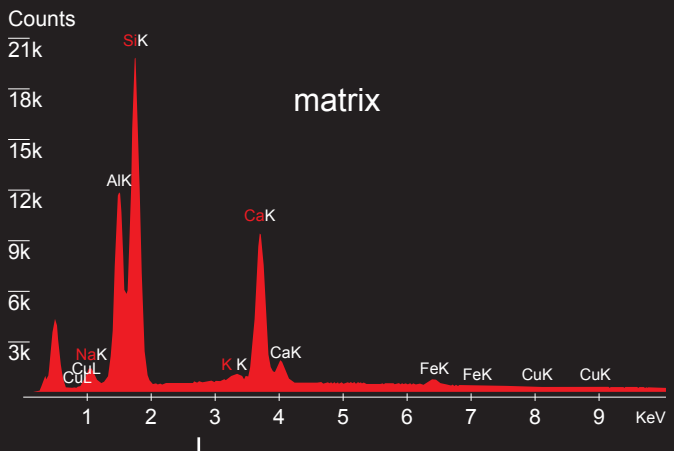

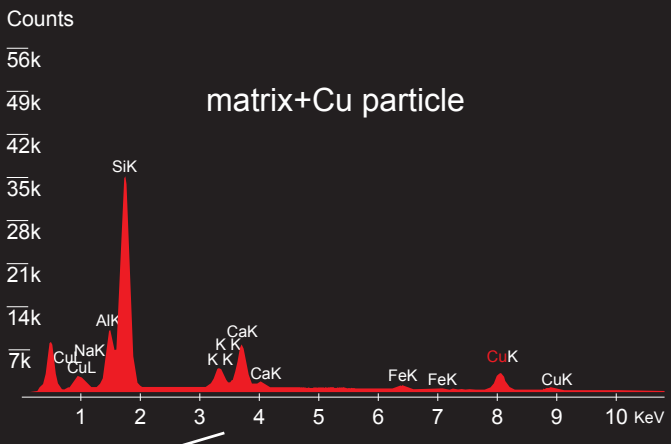

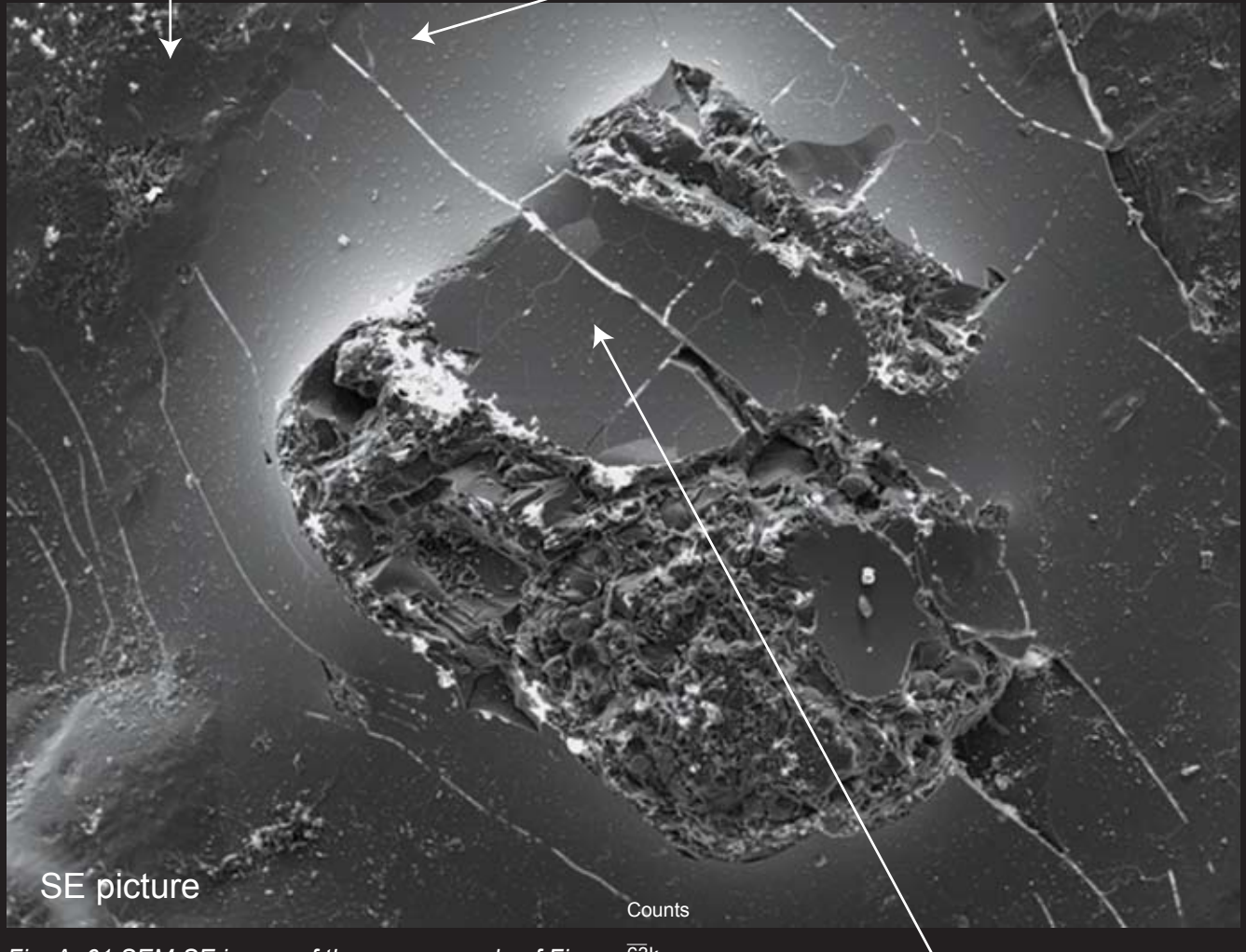

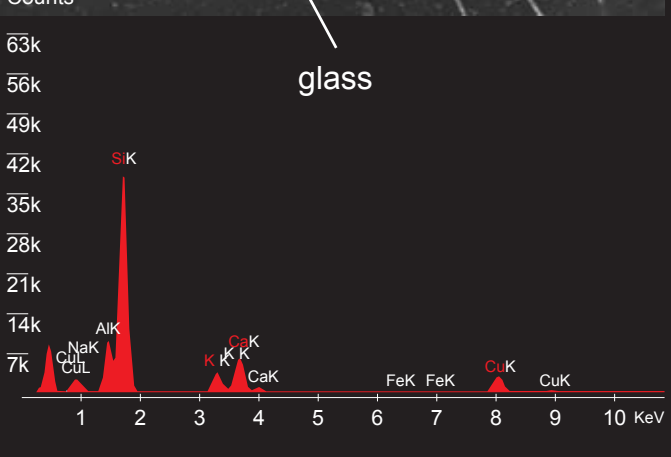

Fig. An61 SEM-SE image of the same sample of Fig. An60B. It is seen that the green glass is filling a well-contained cavity together with quartz. EDX spectra of andsine matrix, particles and glass are included (acceleration voltage 30kV).

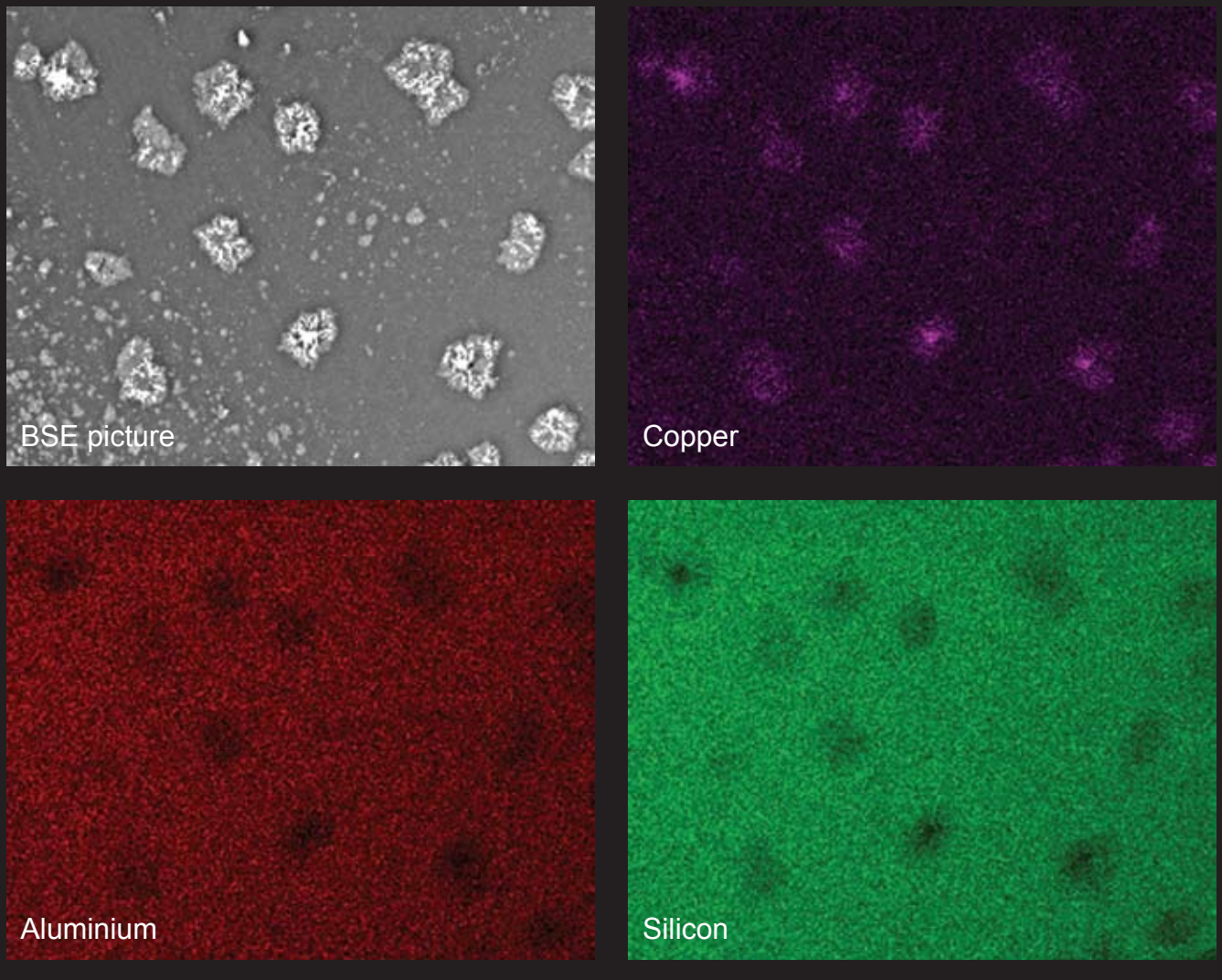

Fig. An62B Element map of the surface of a diffusion-treated andesine obtained with EDX. Note 10 µm sized cooper-bearing particle aggregates do occur regularly over the entire area. Chemical mapping shows lower concentrations of Al and Si in the dark areas. Increased concentrations of Cu appear as lighter violet tones. A BSE image shows the aggregated copper particles of the same area.

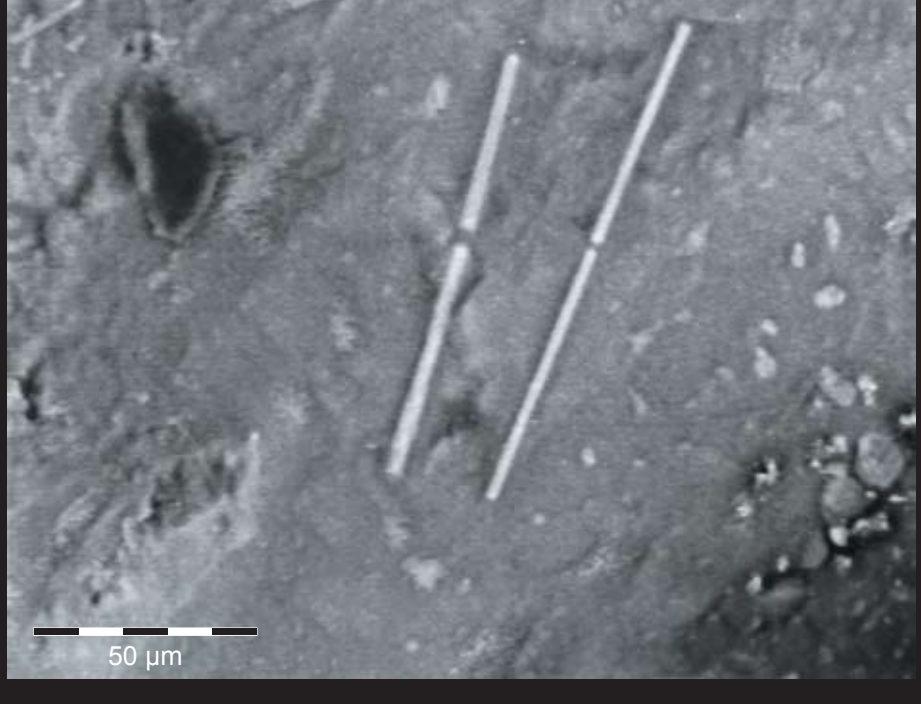

Fig. An63A Elongated needles of 100 µm in length are found on the surface with chemical compositions corresponding to a non-identified Ca-Al-Silicate.

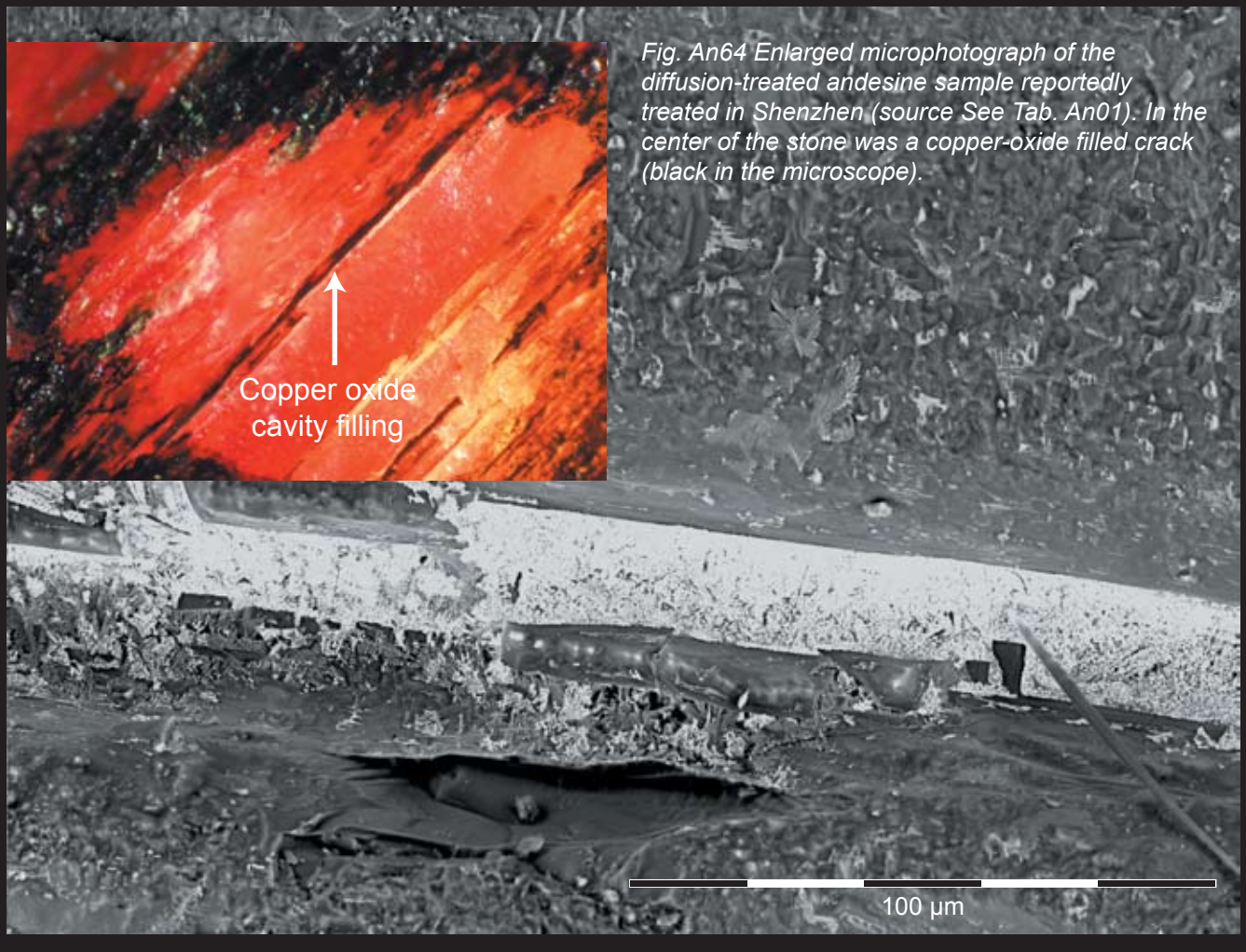

Fig. An64 Enlarged microphotograph of the diffusion-treated andesine sample reportedly treated in Shenzhen (source See Tab. An01). In the center of the stone was a copper-oxide filled crack (black in the microscope).

Fig. An65A BSE image of the filled crack (Acceleration voltage: 30kV). The copper-oxide filled crack appears brighter in contrast to the andesine background (EDX spectrum not show).

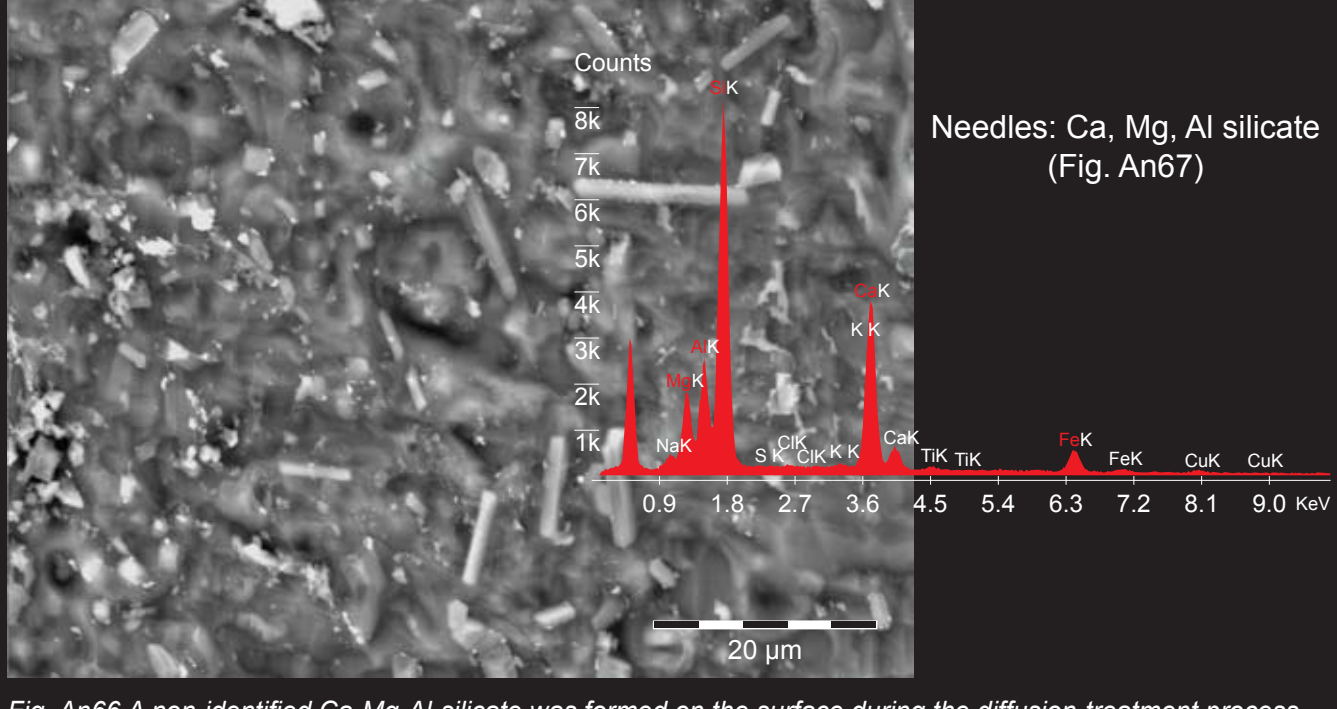

Fig. An66 A non-identified Ca-Mg-Al-silicate was formed on the surface during the diffusion-treatment process, See SEM-BSE Image (Fig. An67) and corresponding SEM-EDX spectrum (Acceleration voltage 30 kV).

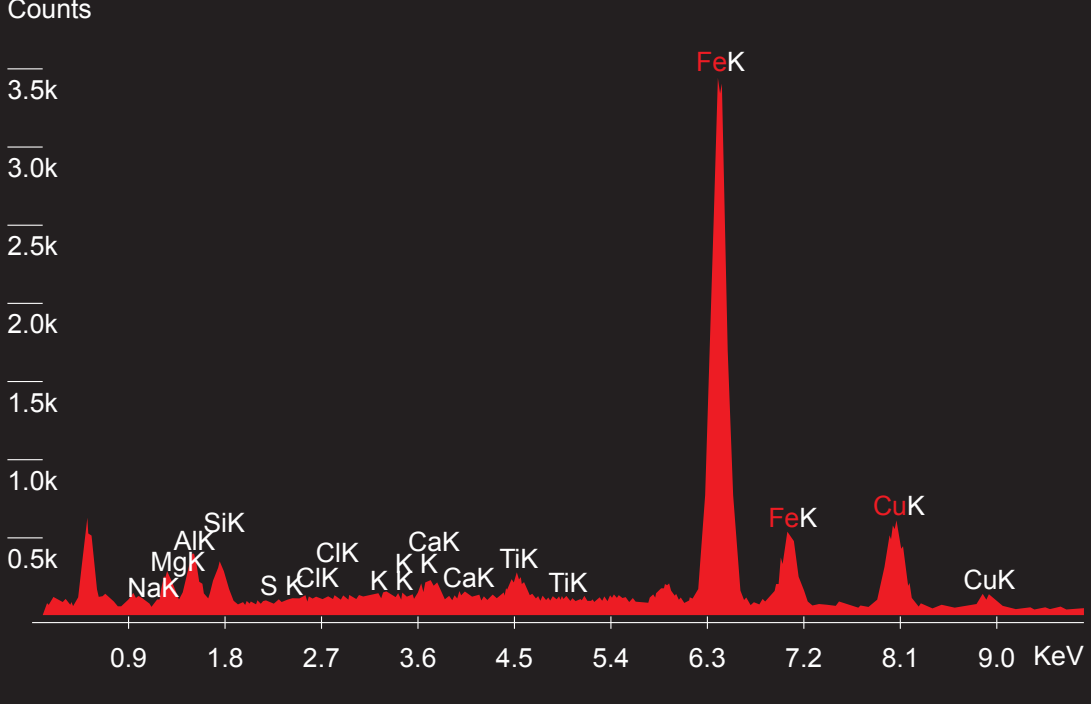

Fig. An68 BSE image of synthetic Fe-oxide crystals formed during the diffusion-process on the surface of the andesine. It is found next to the particles described in Fig. An66 scattered over the entire surface of the sample. Corresponding EDX spectra of the particles see below (elements other than Fe and Cu from matrix).

Fig. An69A

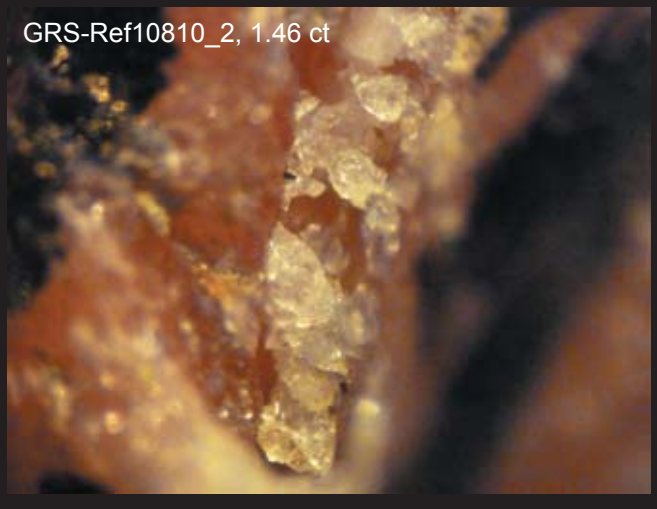

Fig. An69B

Fig. An69A-B Rough crystal of a natural copper-bearing andesine, hand-collected by one of the authors (AP) from the new mines in Tibet (Gyaca). Enlarged picture is from an area containing glassy residues from another sample (Fig. An69B).

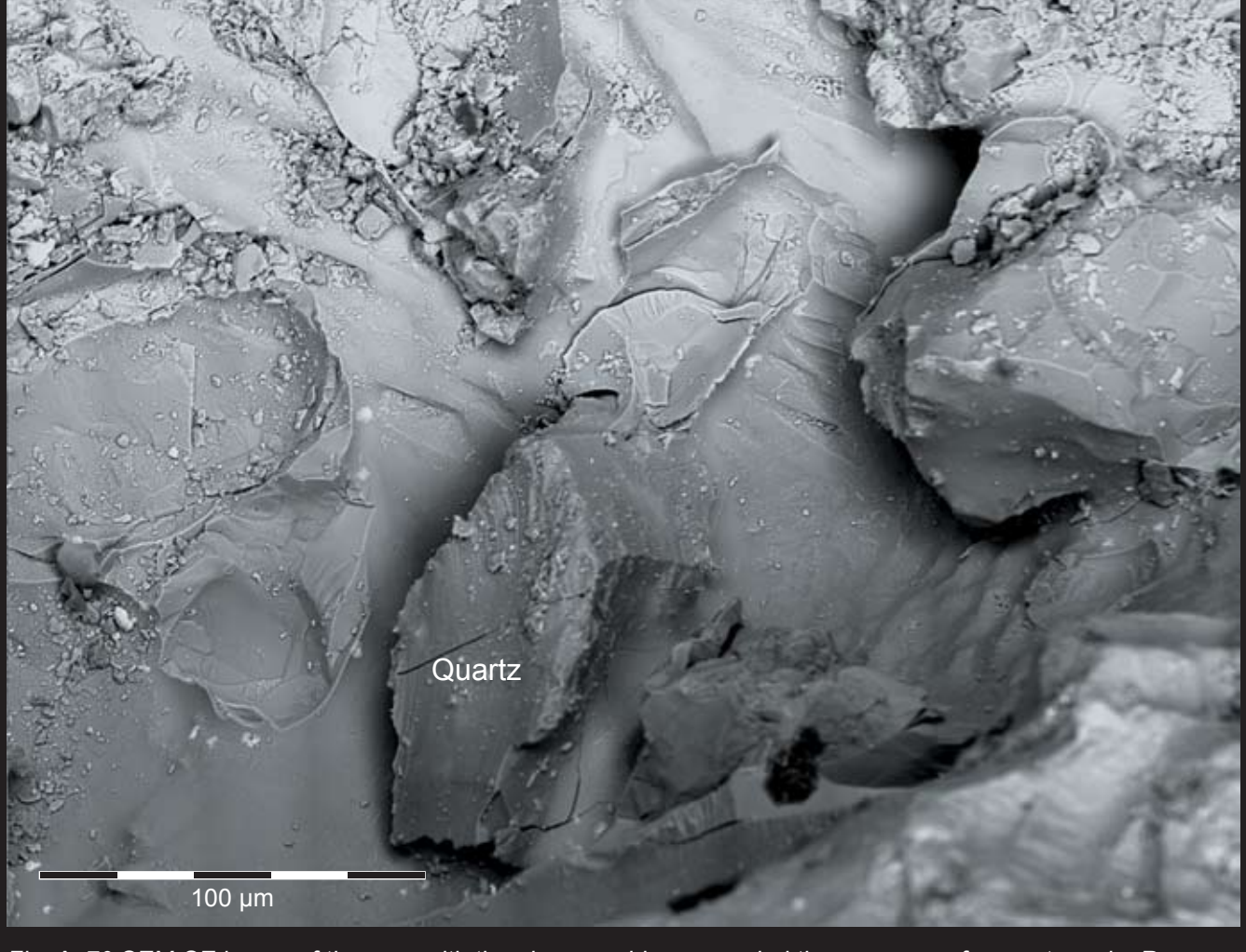

Fig. An70 SEM-SE image of the area with the glassy residues revealed the presence of a quartz grain. Raman analysis confirmed alpha-quartz.

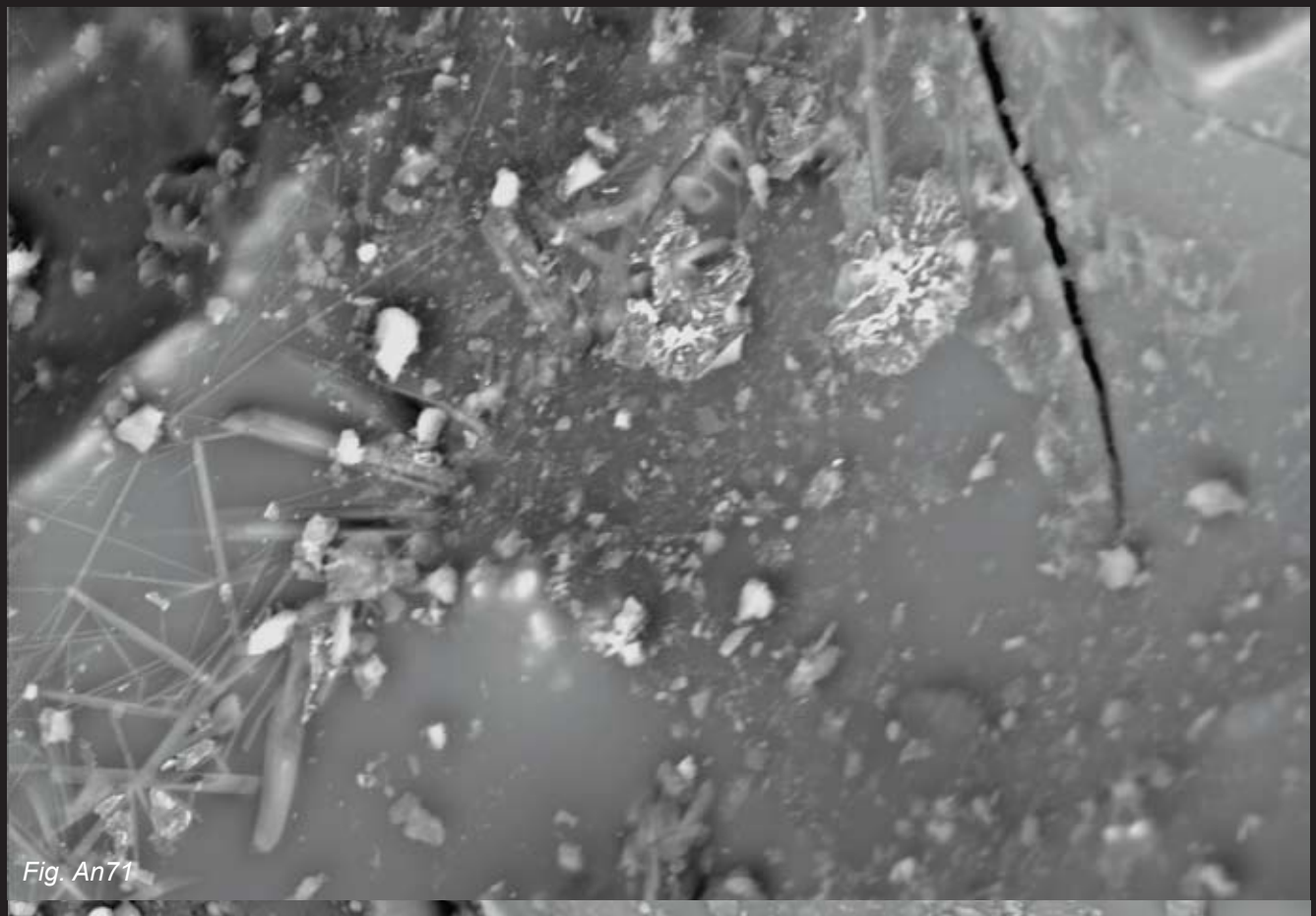

Fig. An71

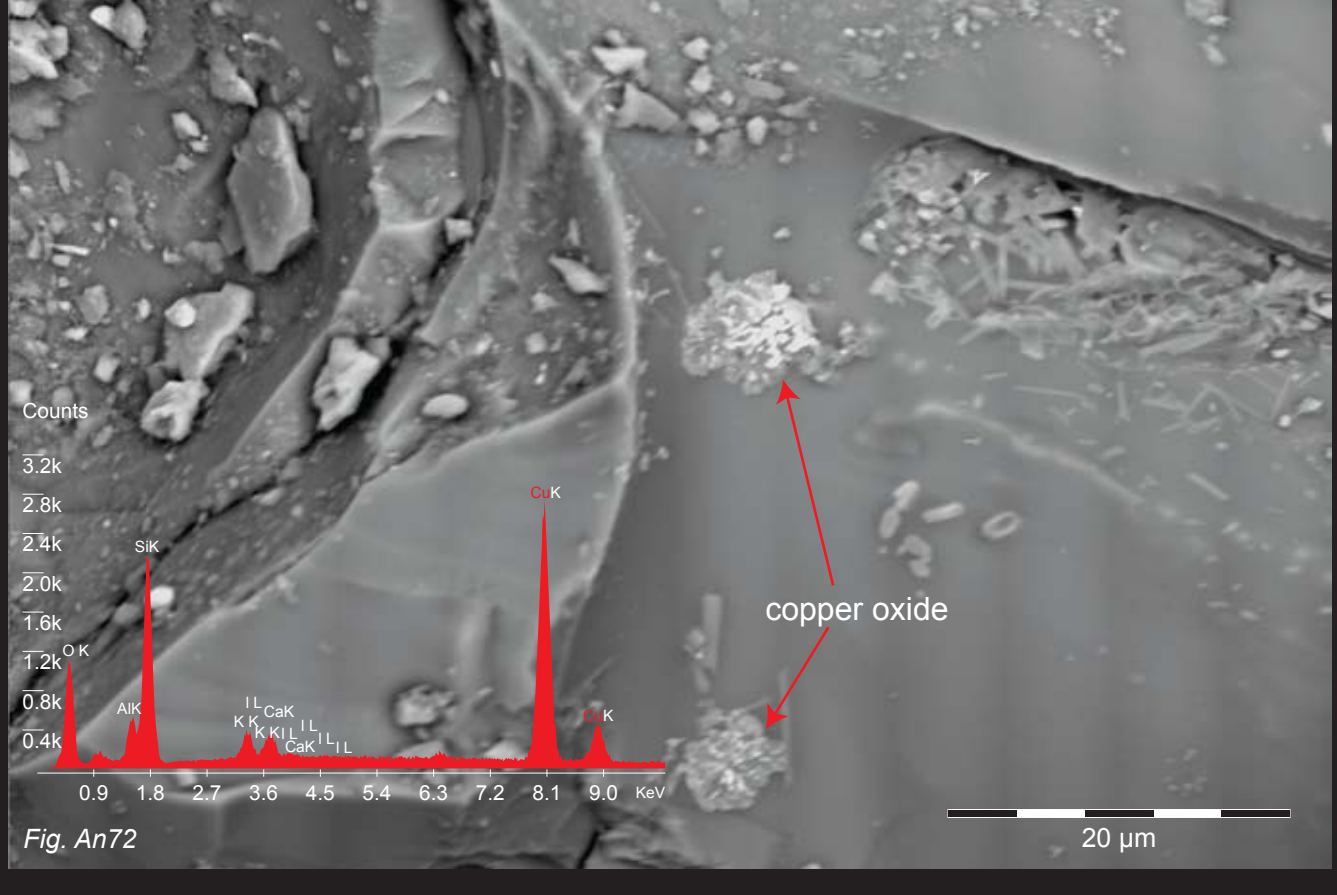

Fig. An72

Fig. An71-74 SEM-SE image of the surface of a natural Tibetan andesine revealed copper-oxide particle clusters (Fig. An72) and silicate needles to be confined to the glassy areas (Fig. An71), a copper-oxide particle (Fig. An72), patchy copper-dendrite in an enlarged image (Fig. An73) and needle-like minerals of a non-identified Na-Ca-Mg-Al-Silicate (Fig. An74, See also included SEM-EDX spectrum).

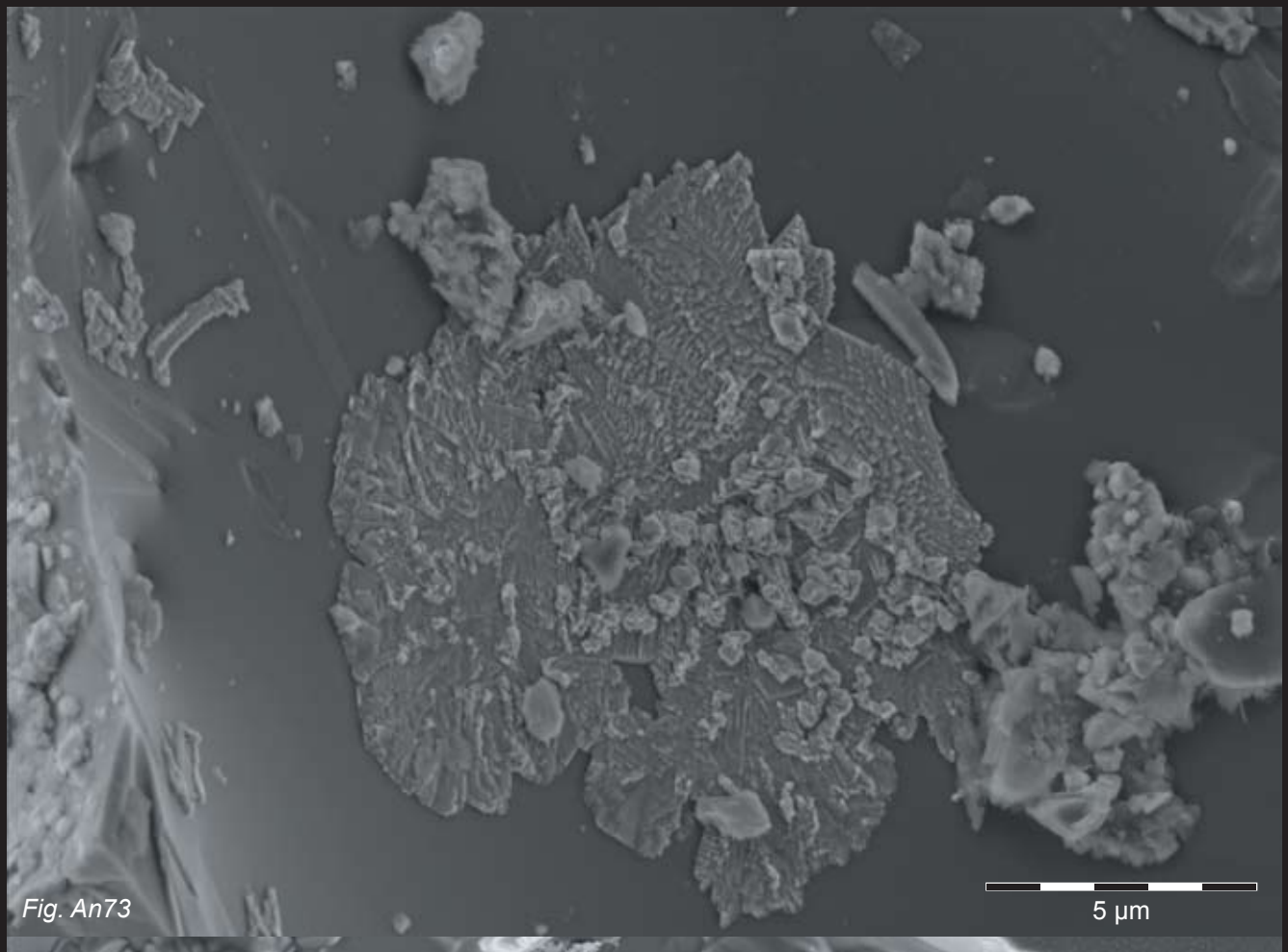

Fig. An73

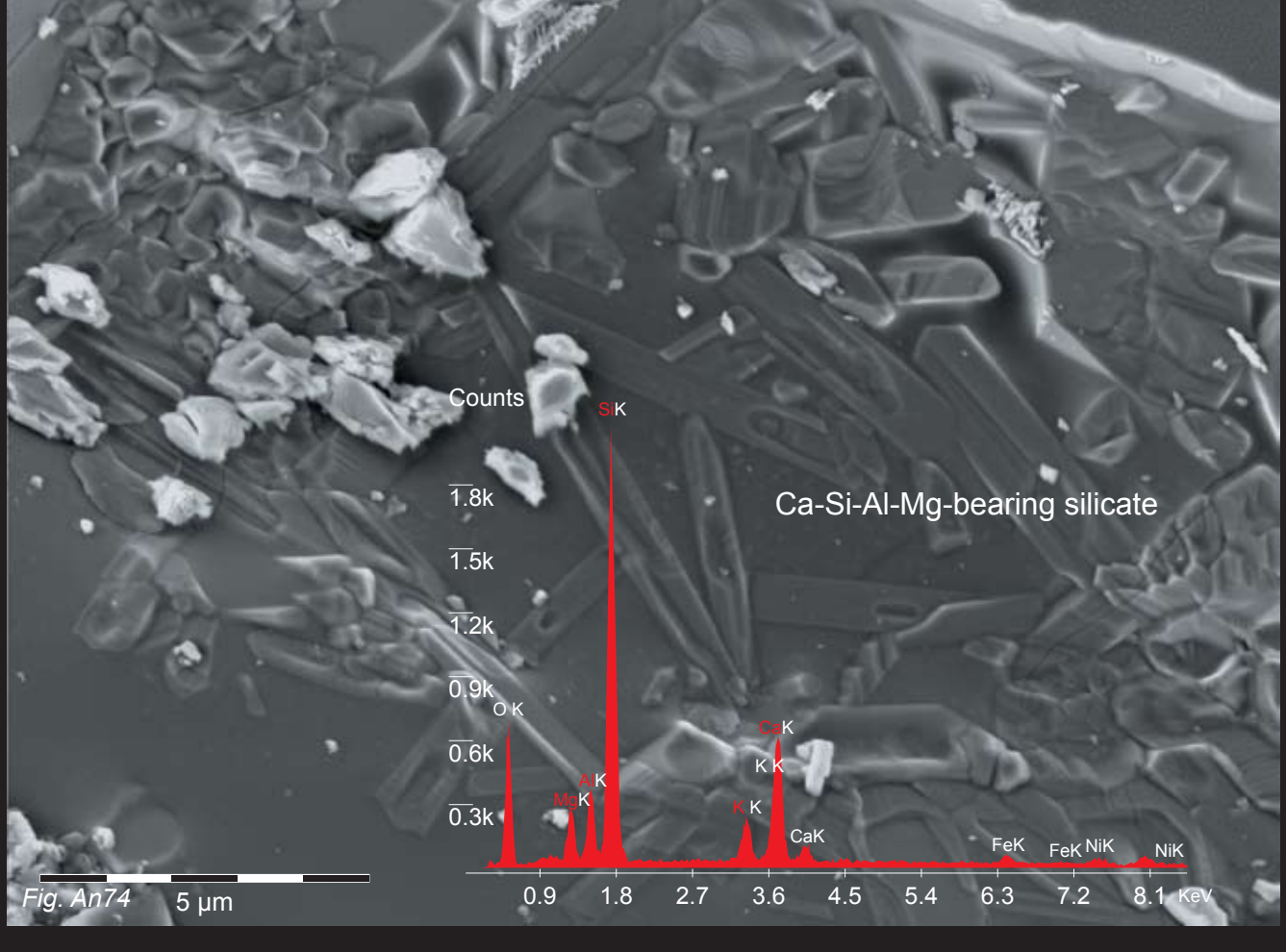

Fig. An74

Fig. An75 Image of the copper-bearing andesine analyzed with SEM-EDX containing glassy residues in cavities.

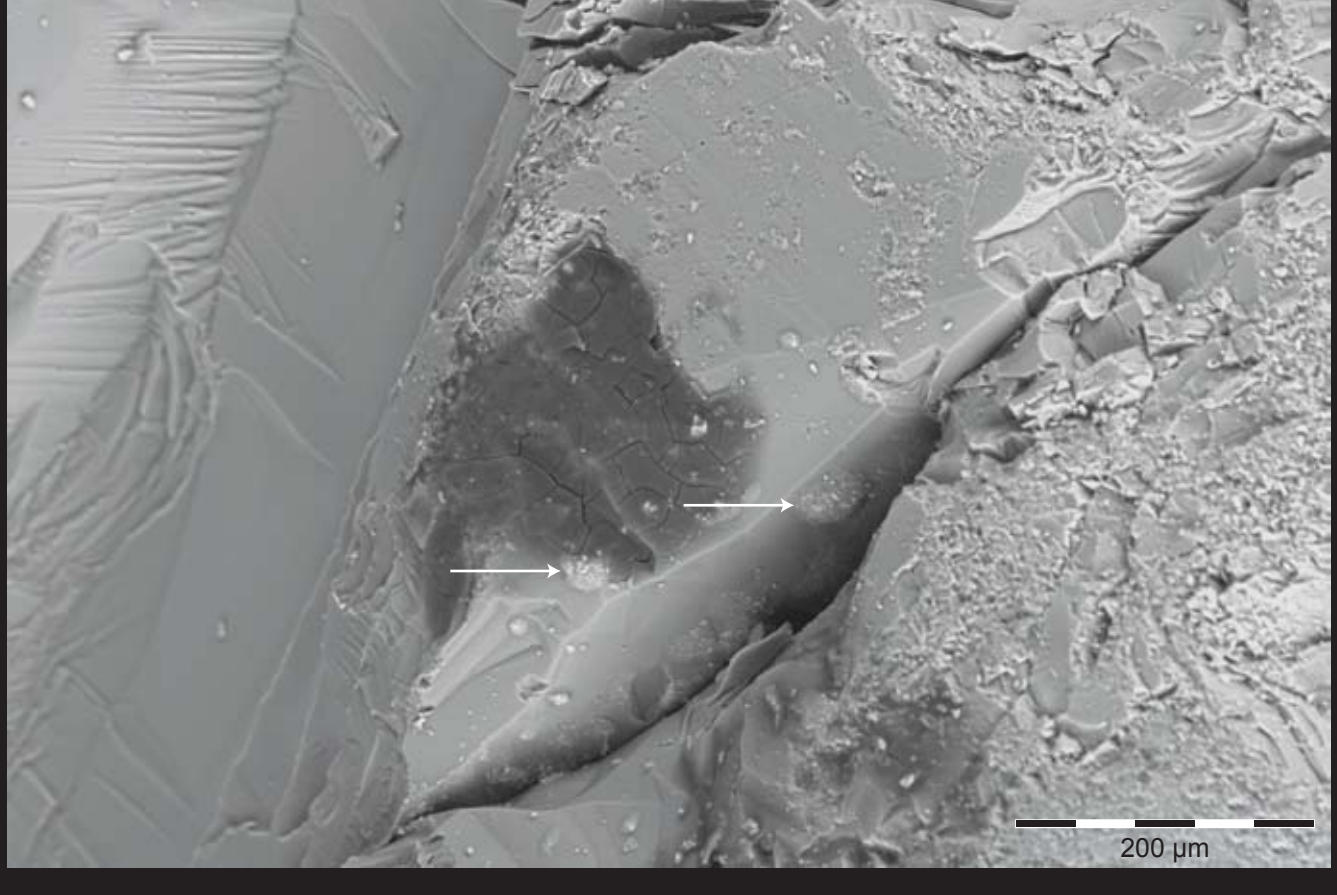

Fig. An76 SEM image showing the appearance of patches of copper-particles (see arrows) in areas protected from abrasion.

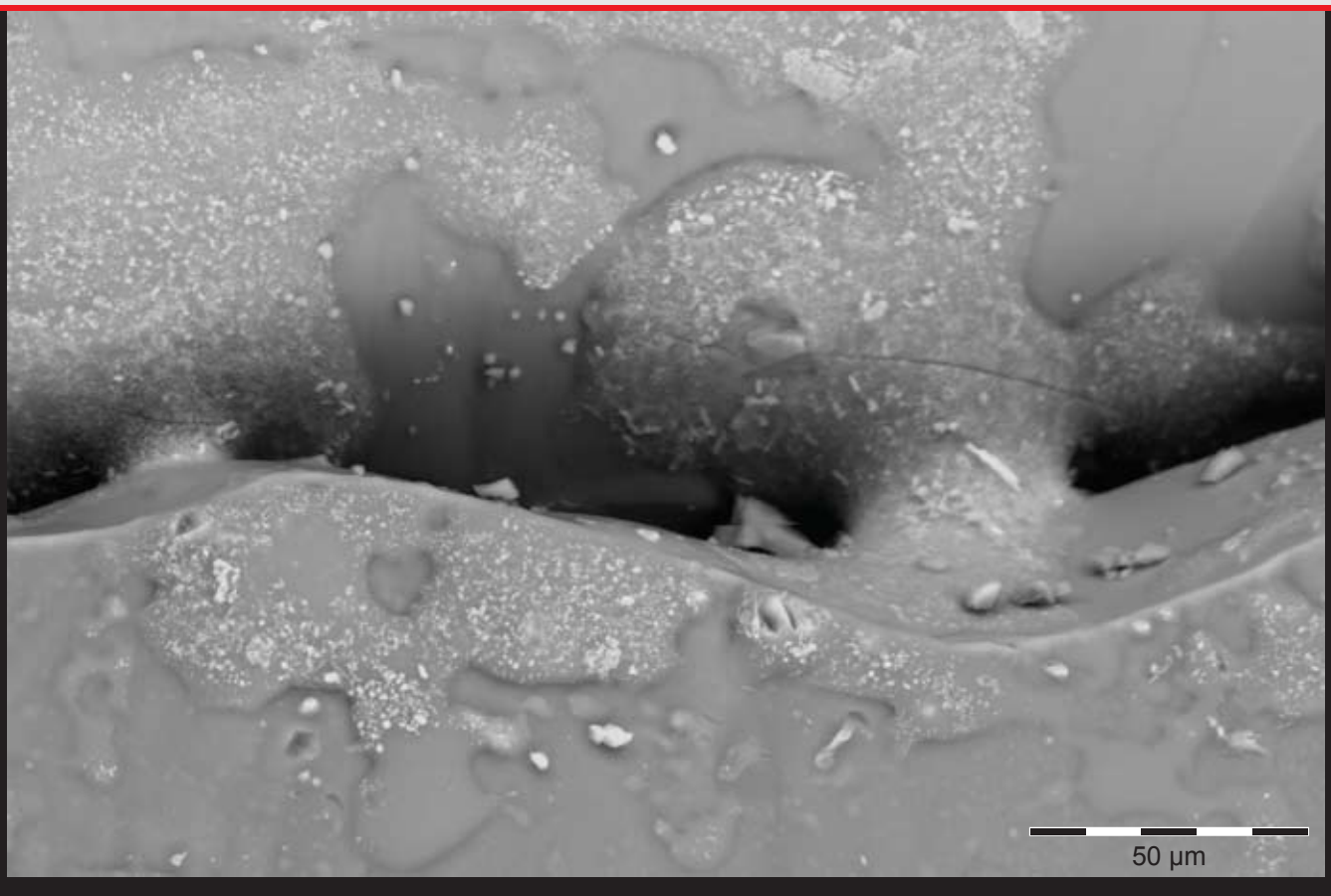

Fig. An77 SEM image from the melted residues on the surface of a copper-bearing Tibetan andesine.

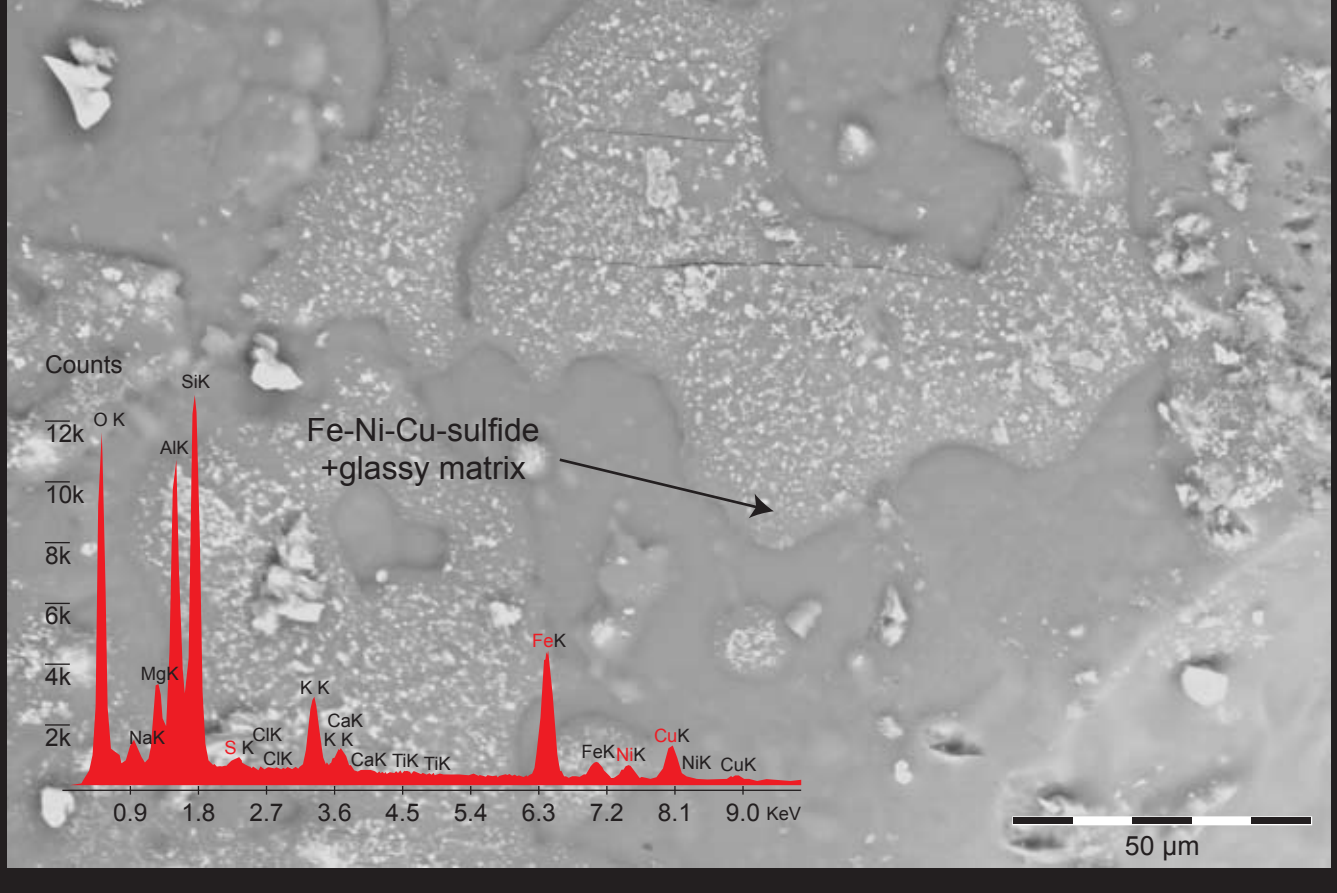

Fig. An78 SEM-SE images of melted residues from the surface in the concave portion of the andesine. The residues are spotted with numerous particles of 5-10 µm in size containing Fe, Cu, Ni and S. This indicates the presence of sulfides (See SEM-EDX spectrum, obtained at 30kV. Elemental signal from sulfide in red).

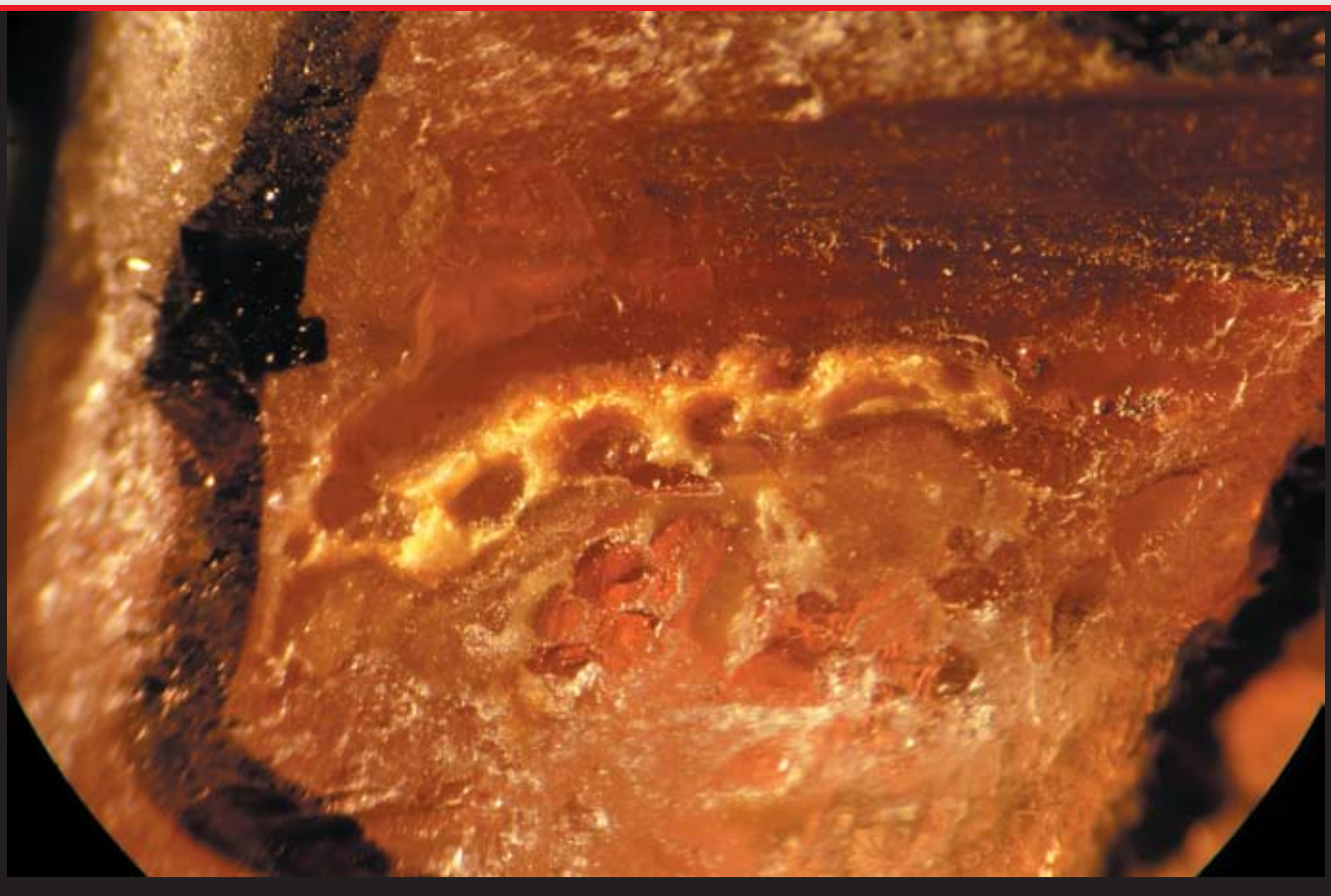

Fig. An79 Enlarged area containing glass residues

Fig. An80 Image of a sample from the old mine in Tibet (Expedition 2008, Bainang) with measuring positions and enlarged (See Fig. An79). Areas studied in detail by SEM-EDX are indicated.

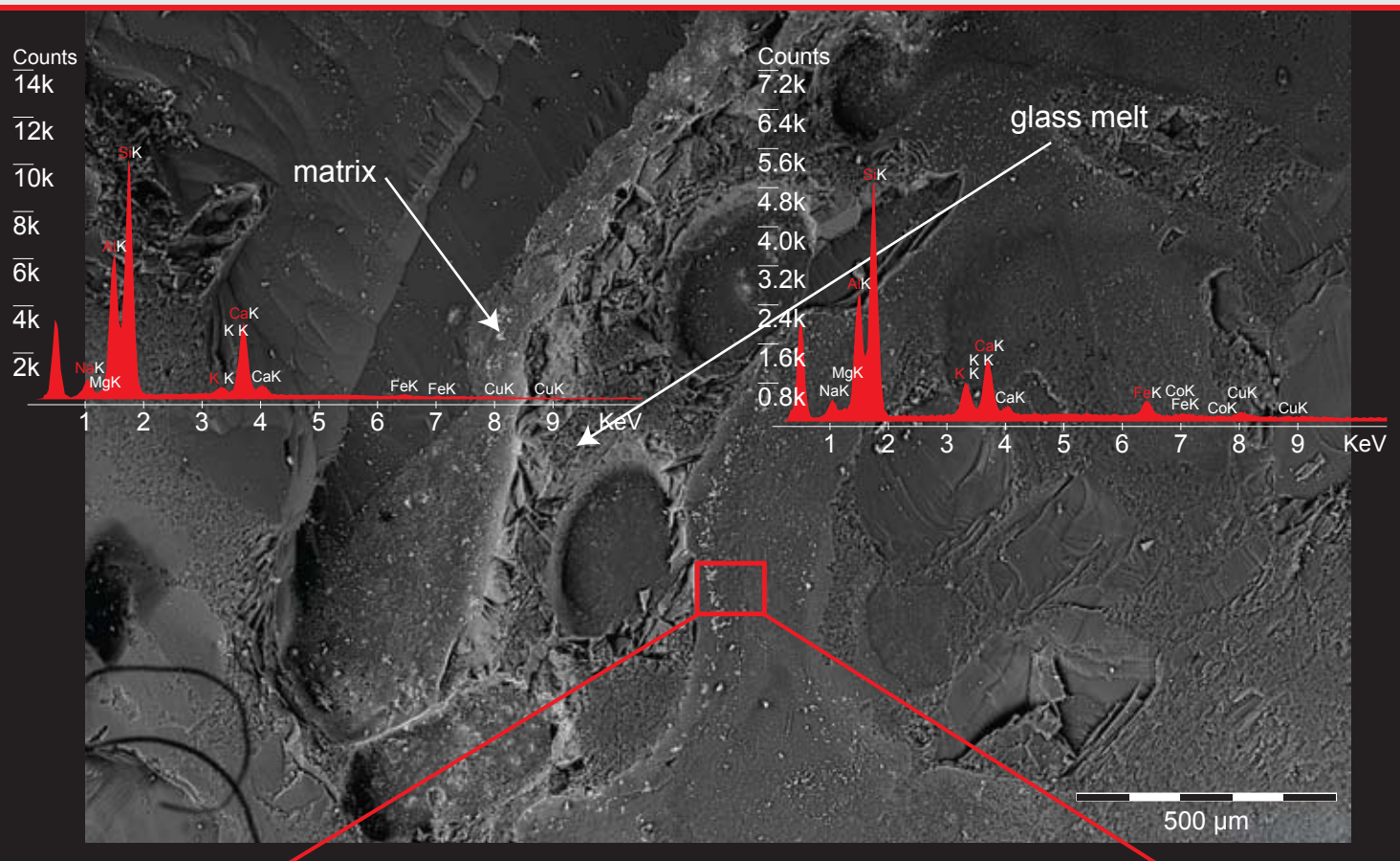

Fig. An81A SEM-SE-image of the surface of an andesine containing residues (SEM-EDX analysis inserted). The zoomed area below shows the size of the copper/copper-oxide-particles.

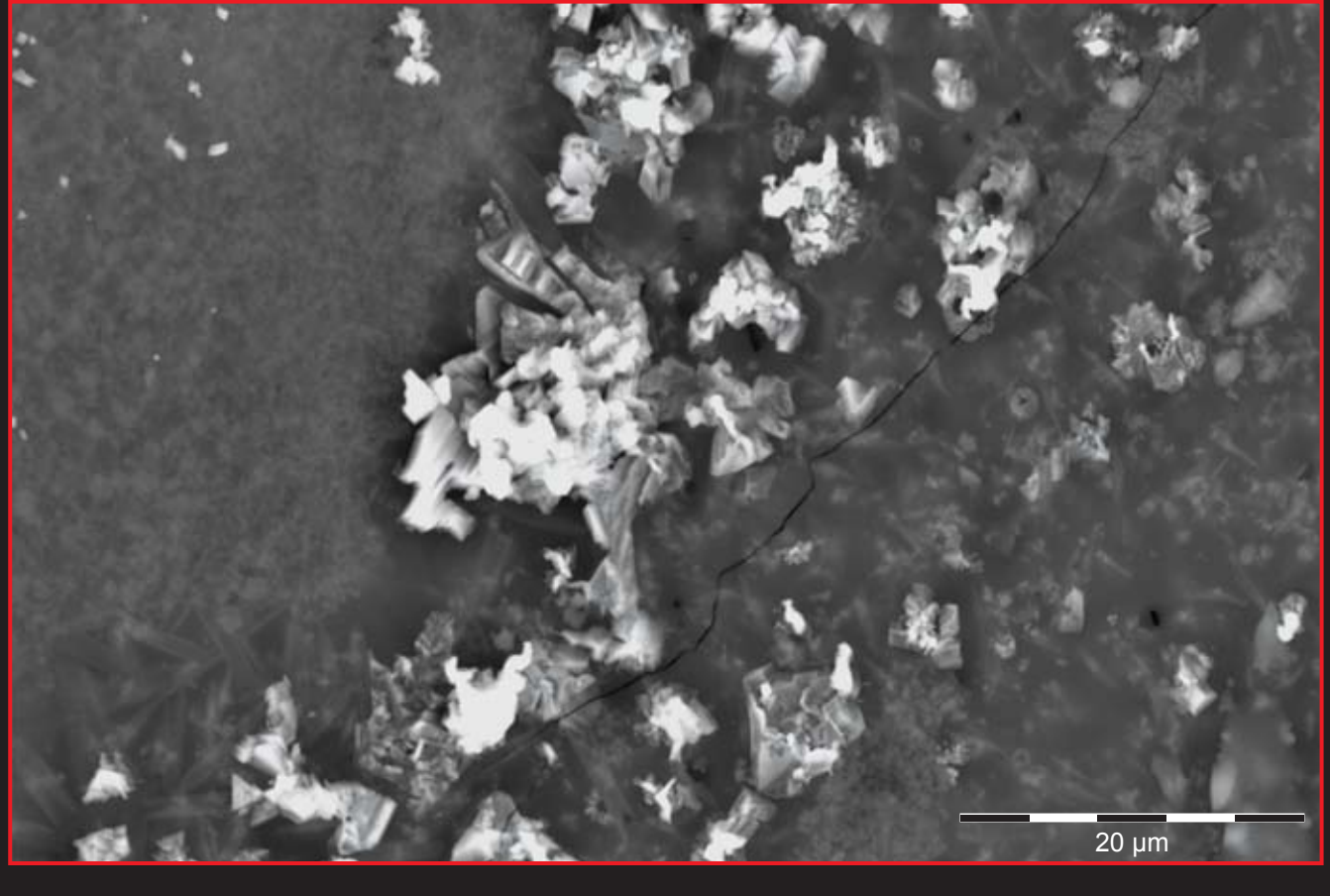

Fig. An81B SEM-SE image of copper particles (5-10 µm in size).

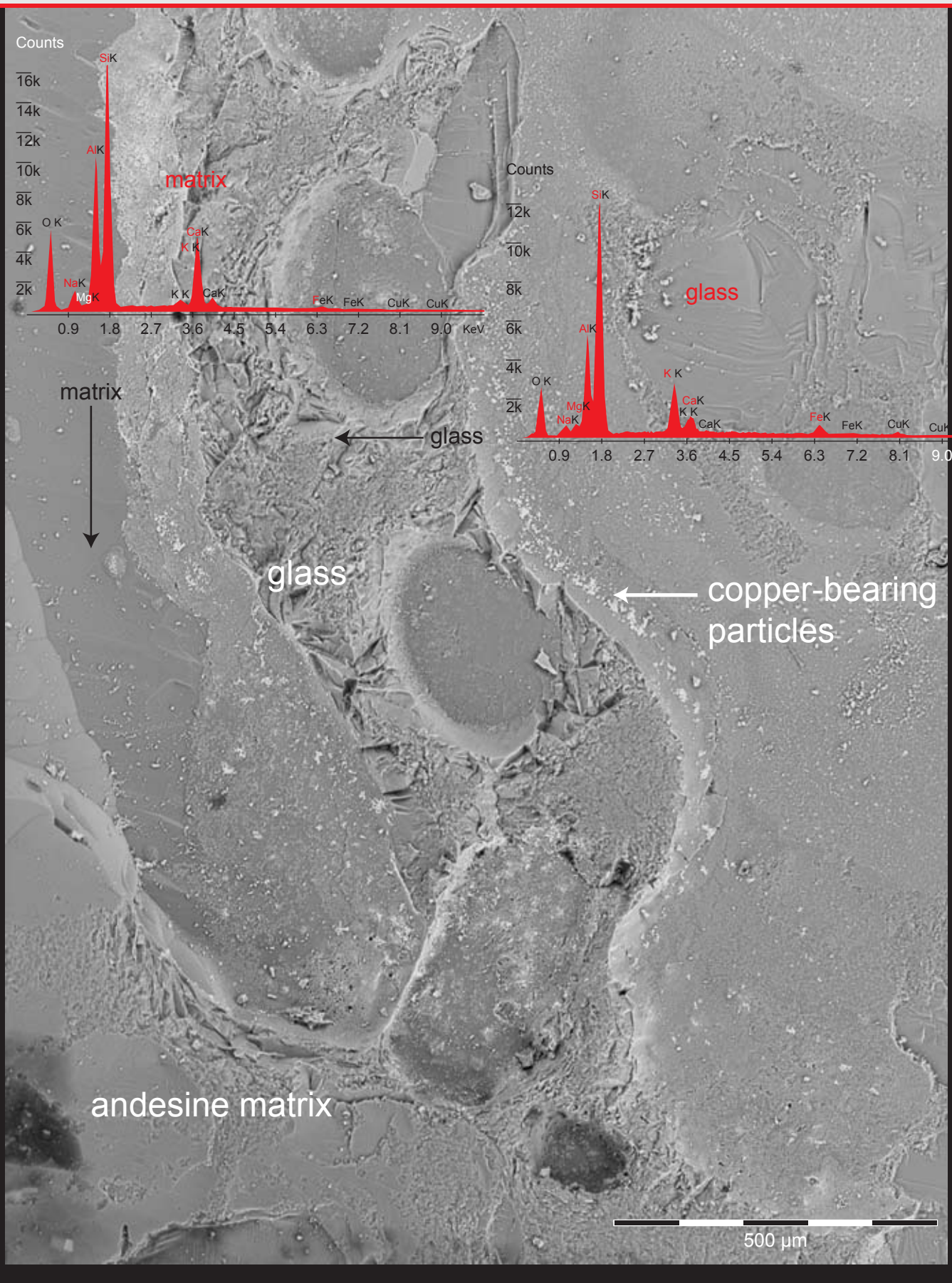

Fig. An82-84 SEM-SE-image of the entire area of a residue found on the surface of a Tibetan andesine from the old mines (Bainang). The entire films of the melted areas are covered with myriads of Cu-bearing particles. Further images with higher magnifications are included (Fig. An83-84). It is clearly seen that the glassy residues are formed in a second stage on the surface of the andesine and have not been produced by melting of the andesine (Fig. An84).

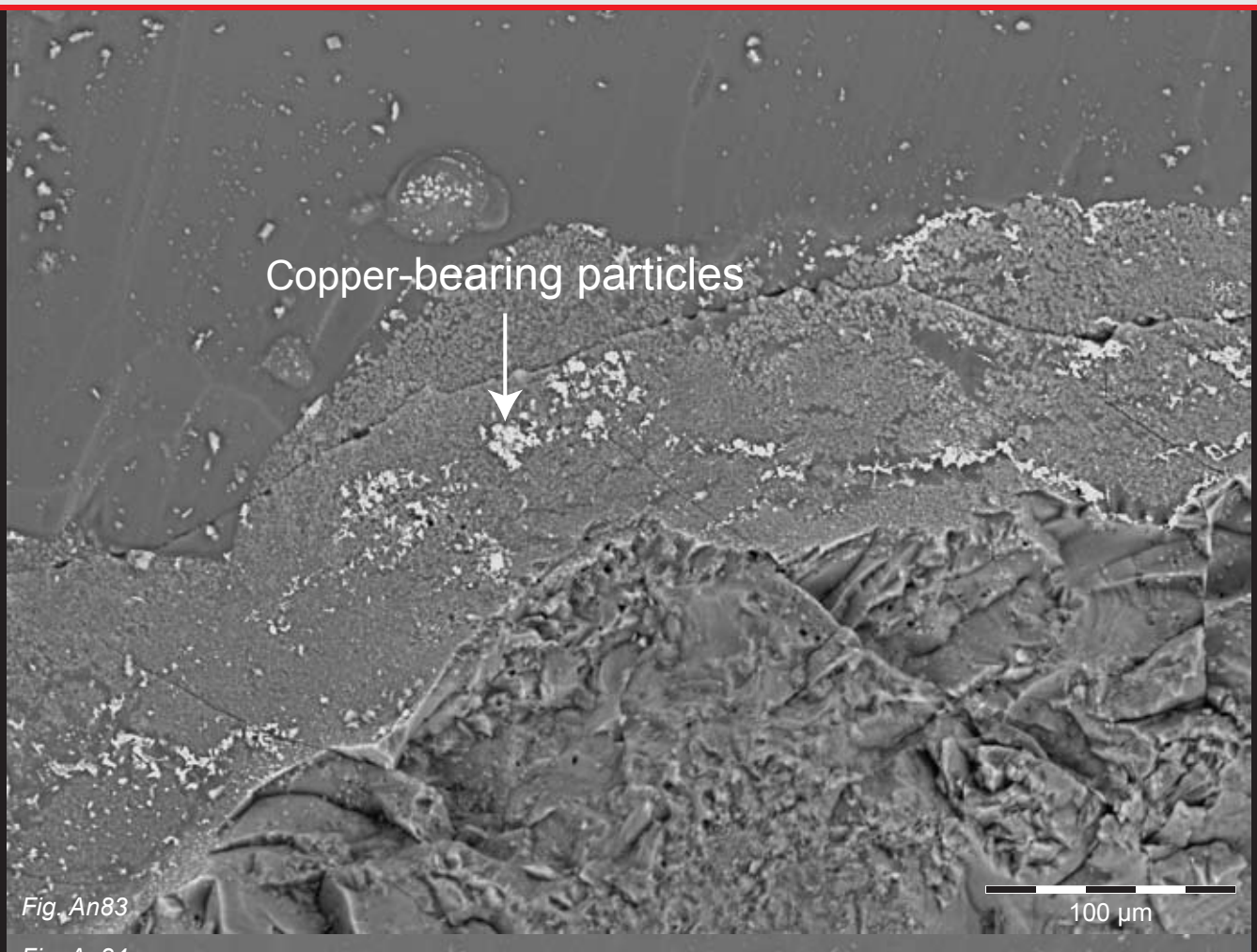

Fig. An83

Fig. An84

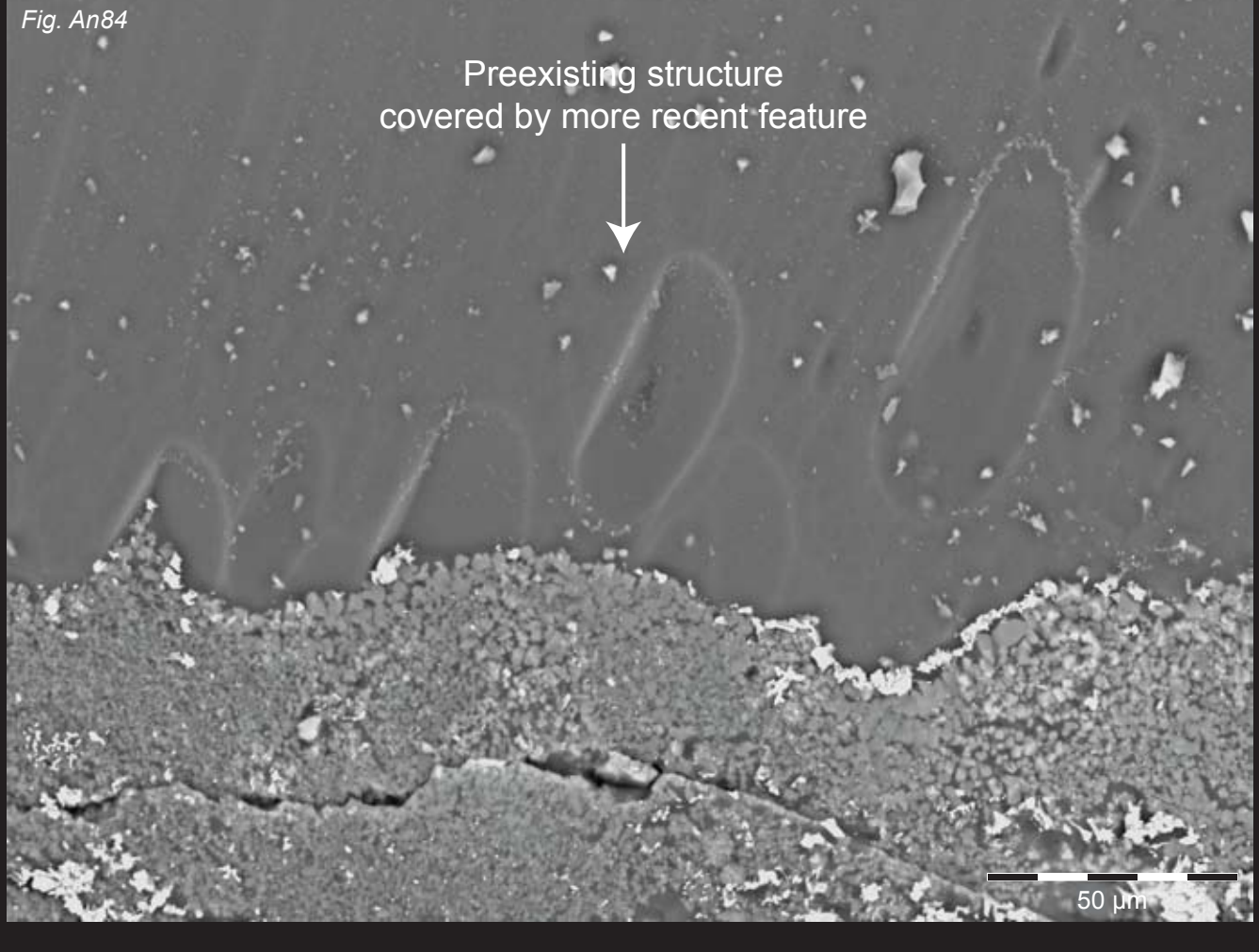

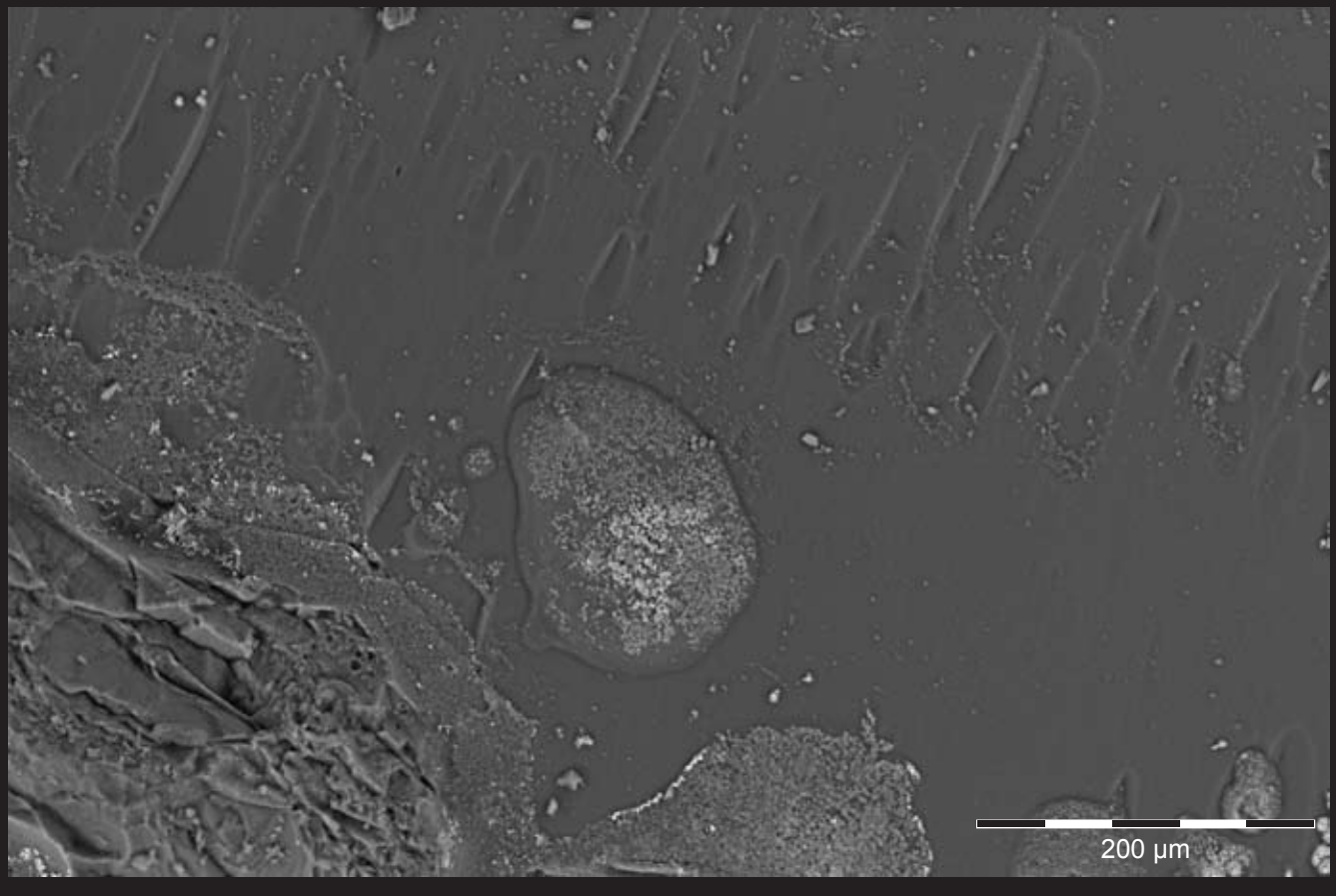

Fig. An85 SEM-SE-image of residues found on the surface of Tibetan andesine.

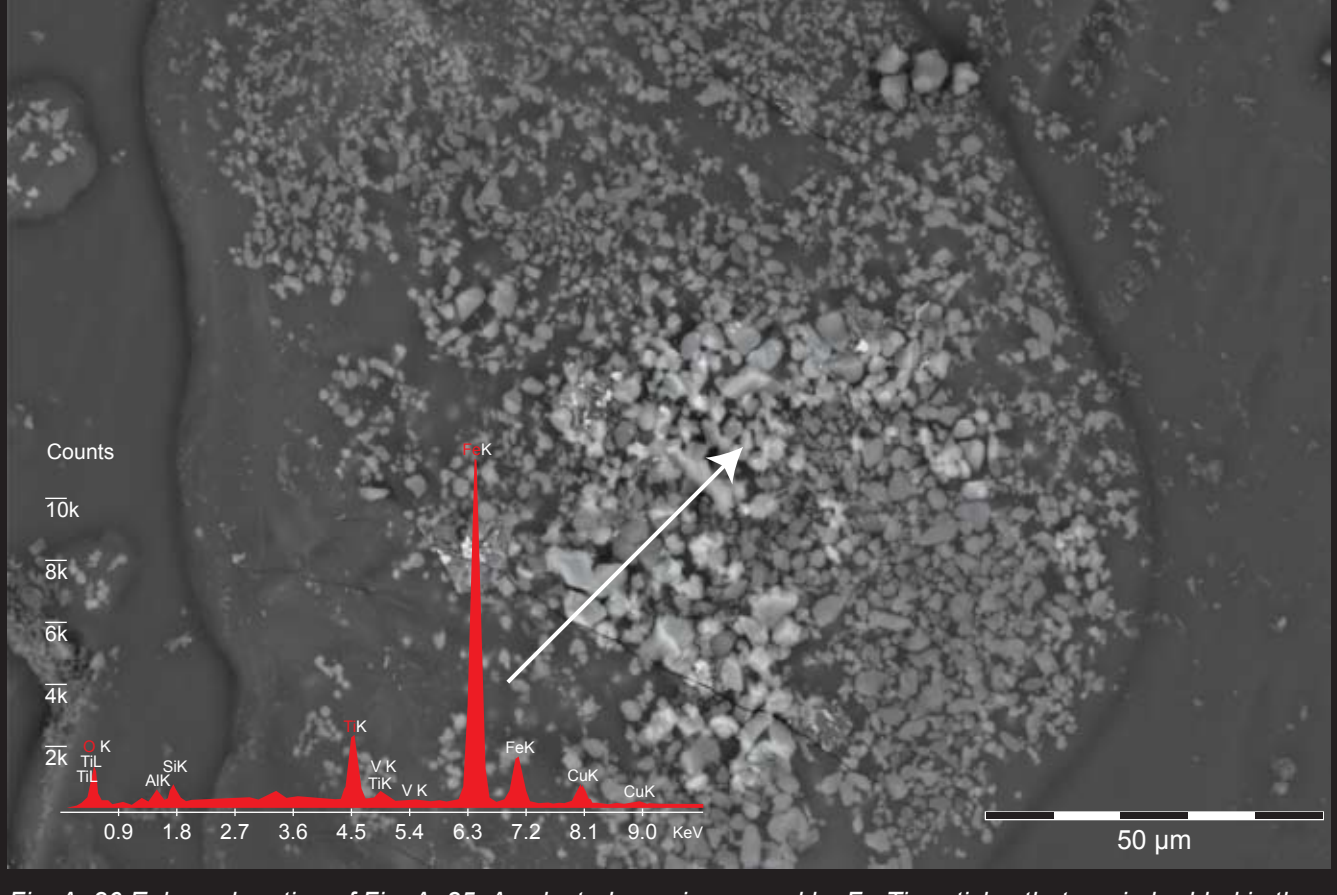

Fig. An86 Enlarged portion of Fig. An85. A selected area is covered by Fe-Ti-particles that are imbedded in the glassy residue.

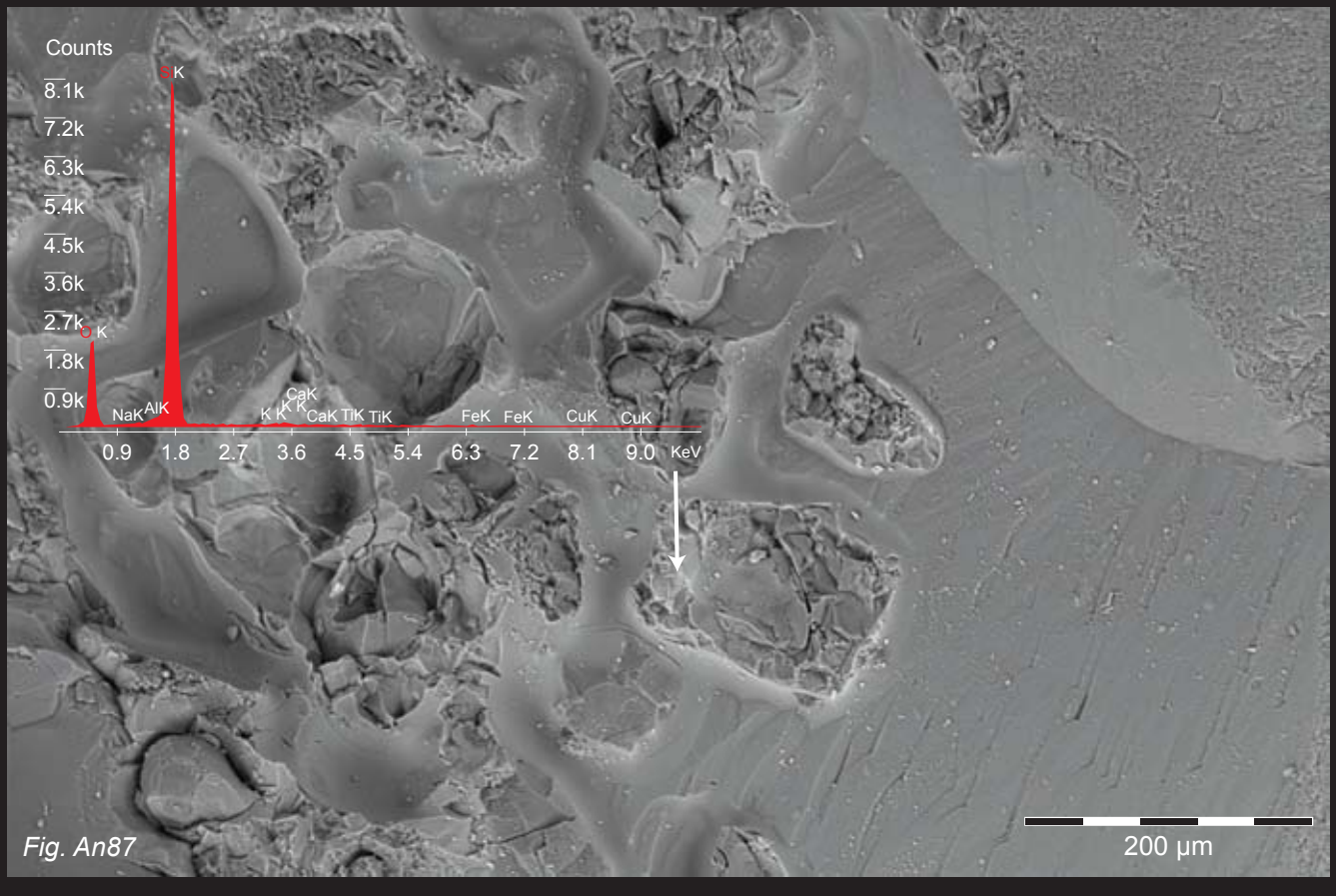

Fig. An87

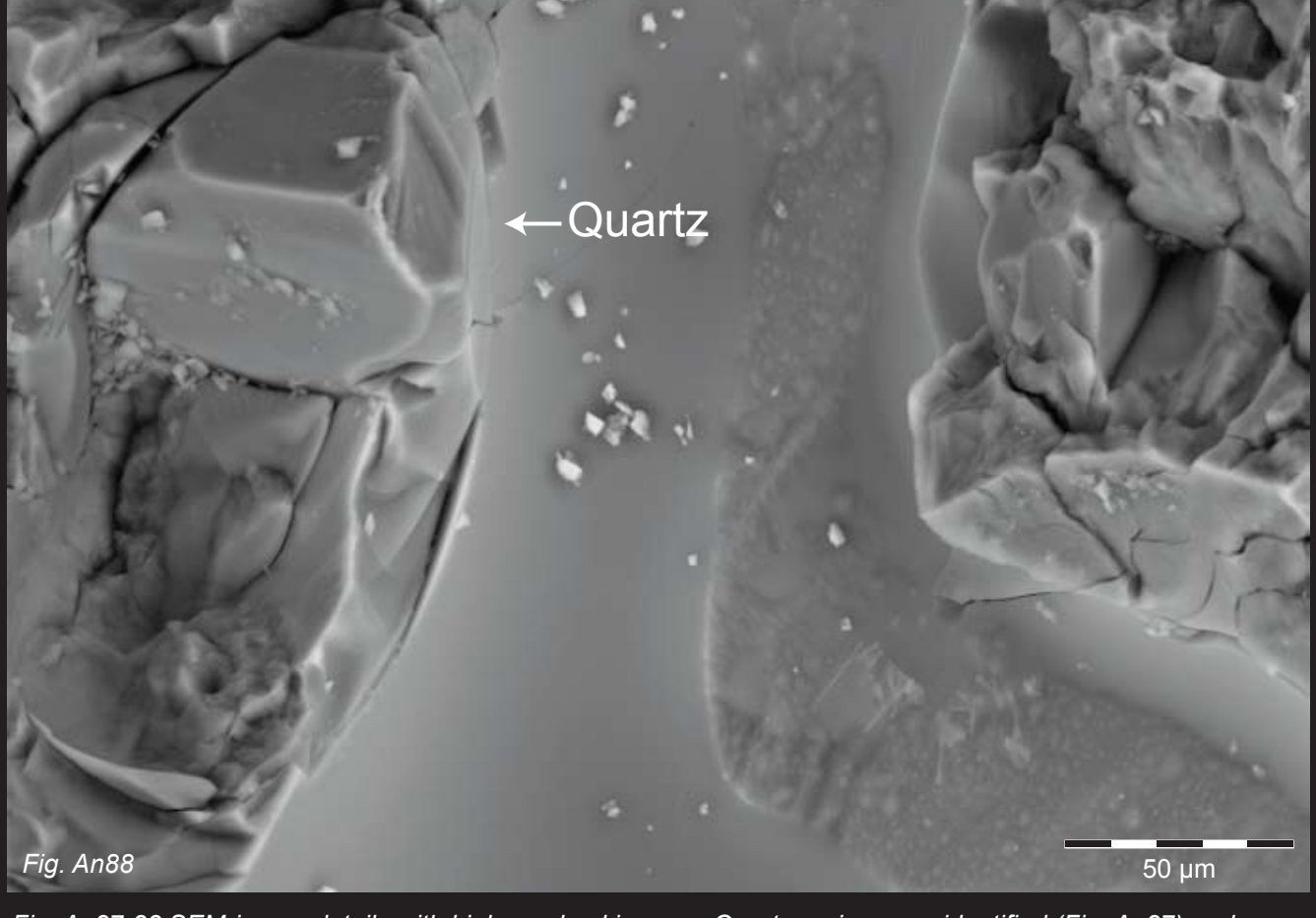

Fig. An88

Fig. An87-88 SEM-image details with high resolved images. Quartz grains were identified (Fig. An87) and several µm small copper-bearing particles were present (Fig. An88) as evidenced by EDX analysis (not shown).

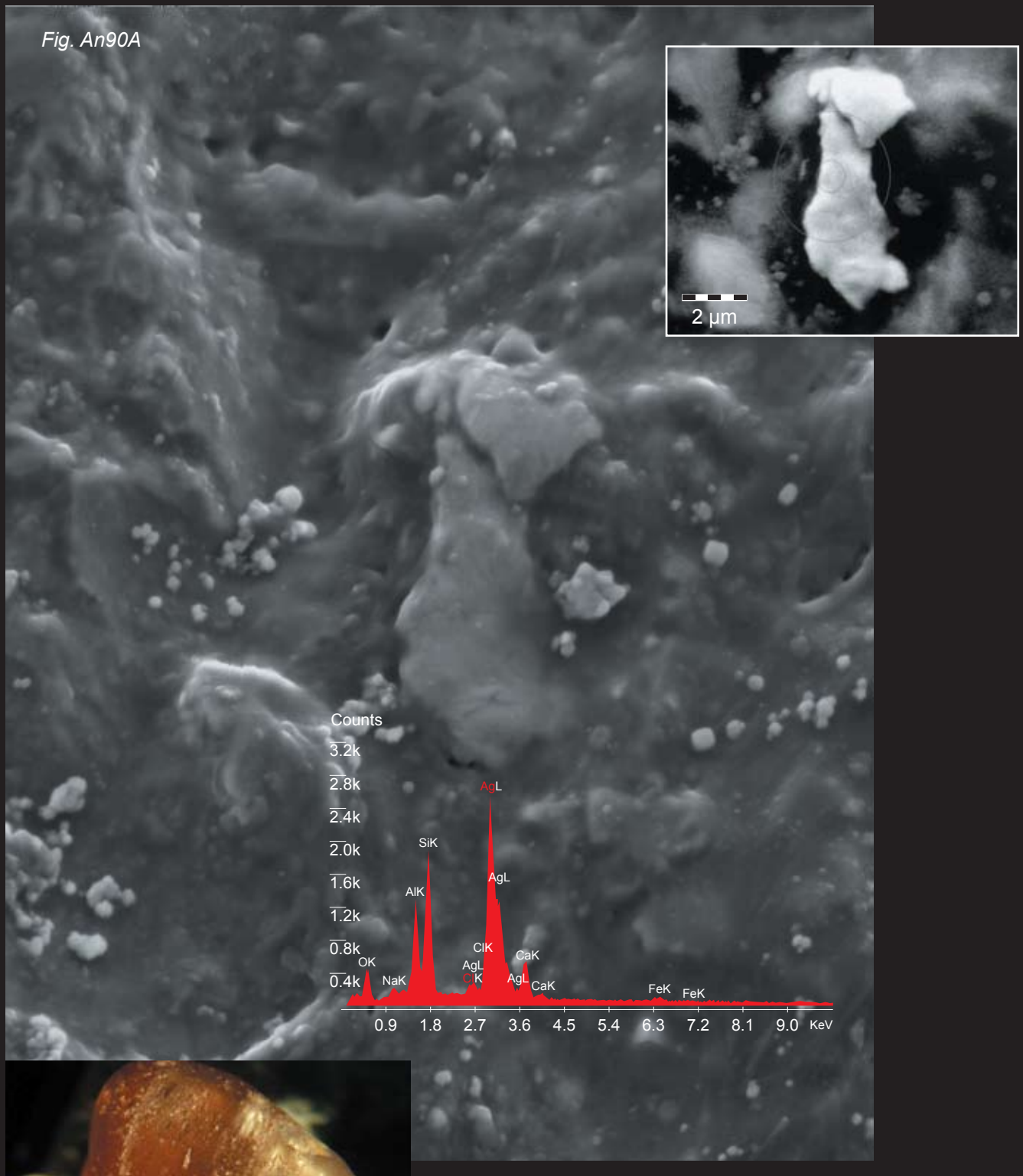

Fig. An90A-B A 5 µm large silver platelet was found on the surface of this Tibetan andesine (Fig. An91) from the expedition in 2008 (Lit. An01). The samples were hand-collected from the mine and supplied to GRS in 2011 (Ref-No. 2011-111236, Fig. An18). BSE-image is inserted (Fig. An90B) and EDX spectrum of the particle identifies it as native silver (measurement includes matrix).

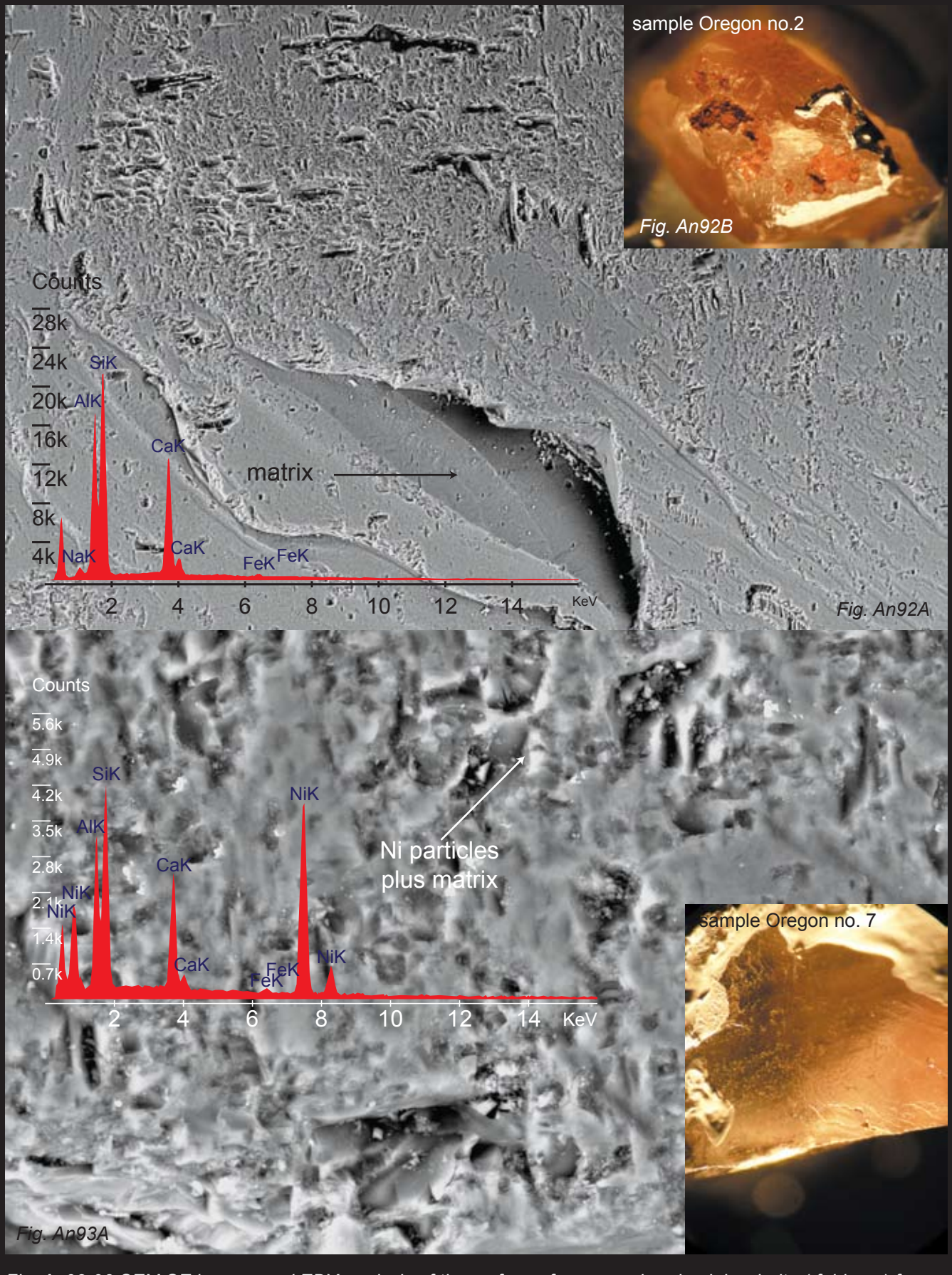

Fig. An92-93 SEM SE images and EDX analysis of the surface of a copper-bearing labradorite (-feldspar) from Oregon. The labradorite did not show any of the glassy residues found in the copper-bearing andesine from Tibet. No copper platelets were present but Ni-rich opaque inclusions were detected (See SEM-EDX spectrum, mixed matrix-particle is analyzed). Most of the samples contained Fe-oxide or Fe-hydroxide coatings without the presence of any glass (Fig. An92). Sample pictures are inserted.

RAMAN ANALYSIS

Raman spectroscopy was carried out using a Jobin Yvon LabRAM-HR800 instrument with an integrated Raman microprobe consisting of an Olympus BX41 microscope confocally coupled to an 800 mm focal-length spectrograph. A frequency-doubled Nd-YAG continuous-wave laser with an excitation wavelength of 532.12 nm (green) and a sample power of about 19 mW was focused on the sample surface and the Raman signal was collected in backscattered mode. The sampled volume was a few µm3 using a 100X objective. The spectra were recorded with the software Labspec™ v. 4.14.

MATERIALS TESTED

Representative samples of the group of diffusion-treated, old mine material and new mine were tested and the results are shown in Fig. An94-An95.

SURFACE RESIDUES AND PARTICLES

The following particles have been identified:
Alpha-quartz is found in melted residues on the surface of two samples, belonging to diffusion-treated and new mines material (Fig An95A). No tridymite (the high temperature-low pressure-modification of SiO_2) was found.
Most surprising was the finding of silica-carbide (Fig. An94B) on the surface of one of the samples. This sample was specifically indicated as being collected personally during the 2008 expedition. The silica carbide particle was found hardly pressed in a crack and was approx. 30 microns in size.

INTERPRETATION

The presence of alpha-quartz in glassy residues is interpreted as contaminations not related to the diffusion process. The presence of these quartz crystals in the melts on the surface of diffusion-treated samples indicates that the diffusion process must have used temperatures within the stability field of alpha-quartz. The presence of calcite and anatase proves that the sample is natural and has not been heat-treated to high temperatures.

The finding of silica-carbide as contaminations in the cracks is very interesting as it is used in the tumbling and polishing industry but almost never occurs in nature. It indicates that this sample was tumbled and, as it was hand-collected from the mine, it must have been salted into the mines of Bainang after polishing. Further confirmation of this interpretation has been provided by the realities on the ground reported by another expedition to Tibet (See Lit. An47).

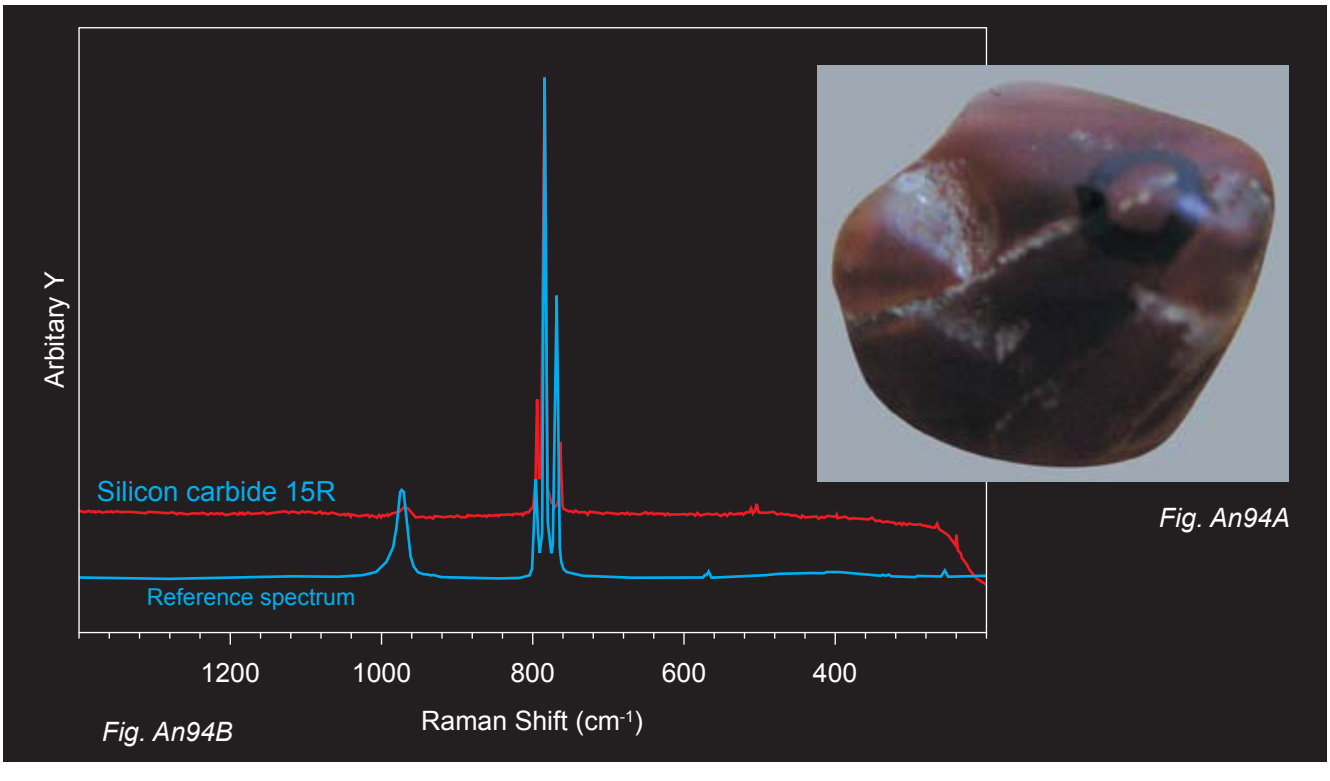

Fig. An94A-B This copper-bearing andesine was hand-collected directly from the mines in Tibet (Bainang) by one of the expedition members and than supplied to GRS. Note that the sample is rounded and contains a white vain with different mineral inclusions (See Fig. 95A-D). A black grain inside the fissure was identified as silica carbide (Fig. A94B). In red is the signal from the sample.

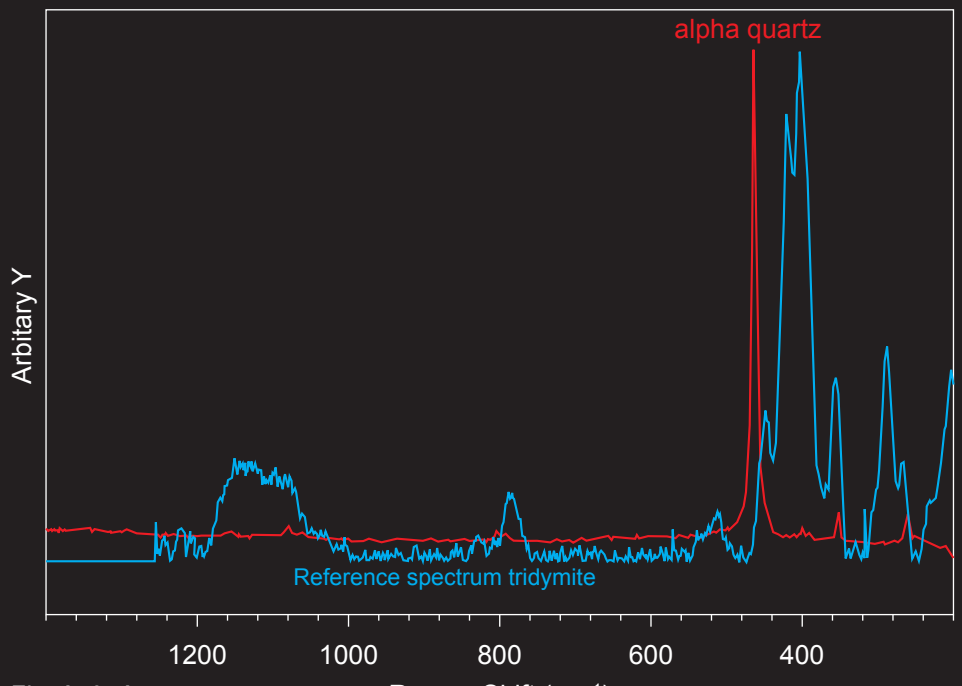

Fig. An95A

Fig. An95A-D Raman spectra of included minerals exposed to the surface of an Tibetan andesine (Bainang mine). Red signals are from sample and the reference spectra in blue are shown for comparison. Analyses by Glenn Lambrecht (See Acknowledgments).
The following minerals were identified:
Alpha quartz (Fig. An95A), anatase (Fig. An95B) and calcite (Fig. An95C).

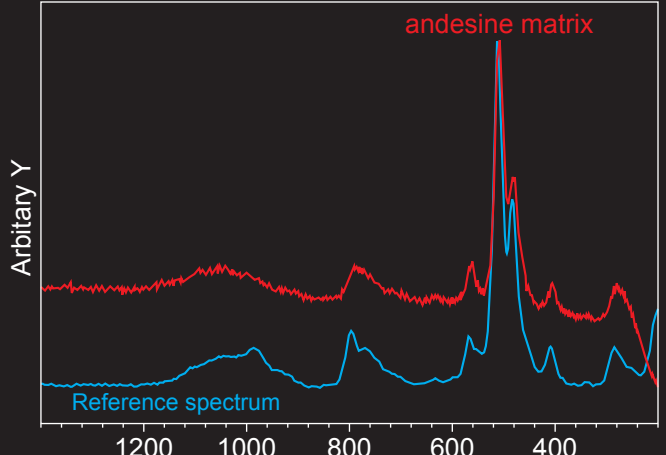

Fig. An95B

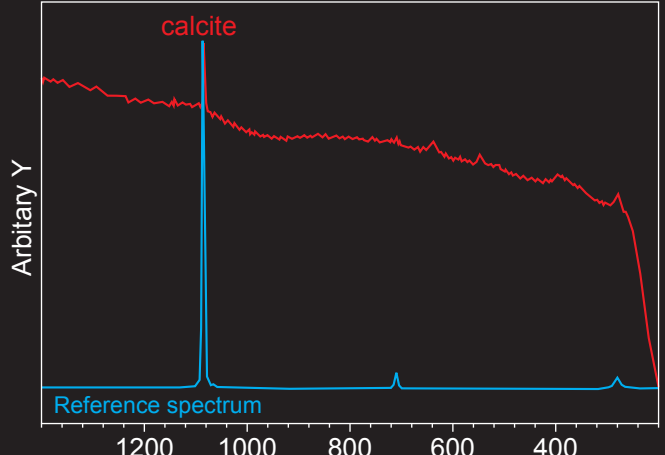

Fig. An95C

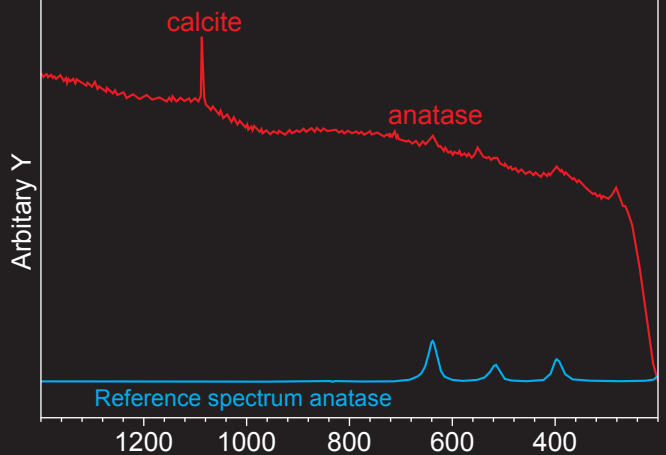

Fig. An95D

Fig. An96 A second copper-bearing andesine from the Bainang mine in Tibet with the occurrence of mineral inclusions such as found in the sample Fig. An94A.

RADIOGENIC ARGON ANALYSIS: ANALYTICAL TECHNICS

The andesine samples were loaded in the vacuum extraction system connected to the MAP 215-50B rare gas mass spectrometer at the Institute of Geology, University of Berne. The system has been described elsewhere (Lit. An45); the analytical approach followed here is a modification of the standard step heating protocol used for 39Ar-40Ar dating. It is based on the property of pristine feldspars to release Ar over a fairly broad temperature interval (Lit. An46). We chose three temperature steps, viz. 990 °C, 1250 °C and 1400 °C, because they reflect different degassing regimes from the andesine (See Tab. An05). The first step combines the initial (subordinate) degassing of the andesine structure with possible surface adsorbed/implanted Ar. The second step is above the nominal melting temperature of andesine and should contain a substantial proportion of the radiogenic gas. The third step corresponds to completely molten andesine, which being less viscous than in step 2 is expected to have undergone complete degassing. The sum of all three steps is the total radiogenic 40Ar (Ar*). The K-Ar age is then simply calculated from the total Ar* and the K concentration determined on a dry aliquot of the same crystal used for the Ar analysis.

By the stepwise heating we obtained not just the bulk K-Ar age but also first-order information on the release characteristics of each sample. While the detailed release patterns are expected to differ, in broad terms all should share the characteristic behavior of pristine feldspars, whereby the three steps have all the same order of magnitude (i.e. are within a factor 10 from each other). Indeed, samples that we are certain are pristine do conform to this prediction, and repeat analyses of samples from the same mine (one could call them "geological aliquots") have very similar degassing patterns (See Fig. An97A-B).

Tab An05 Argon Experiments

Sample	Temperatures	Percent of Ar*total	Ar*total (ml/g)	K (g/g) ± 1 sigma	Alter (Ma)	$^{40}Ar/^{36}Ar$
Zha Lin 2010-111243 3.979ct	990 °C 1250 °C 1400 °C	0.23 0 99.77	7.10821E-07	0.0051 ± 0.0005	35.7 ± 3.7	294.16 244.51 1422.87 481.45
Yu Lin Gu 2010 Hughes 2.749ct	990 °C 1250 °C 1400 °C	65.92 34.08 0	2.52108E-07	0.0043 ± 0.0004	15.1 ± 1.7	610.55 523.01 292.15 458.02
Yu Lin Gu 2010-111239 2.489ct	990 °C 1250 °C 1400 °C	28.82 27.68 43.51	6.30926E-08	0.0041 ± 0.0004	3.9 ± 0.8	381.1 713.41 2900.54 537.14
Upper Yu Lin Gu Hughes, Sept. 2010	990 °C 1250 °C 1400 °C	0 48.32 51.68	5.48165E-08	0.0043 ± 0.0004	3.2 ± 1.3	248.38 368.69 370.2 327.62
Bainang Naisa 2010-111237 2.227ct	990 °C 1250 °C 1400 °C	34.16 32.23 33.61	1.09641E-07	0.0045 ± 0.0004	6.2 ± 0.8	368.37 376.39 435.12 385.92
PANA mine Oregon	990 °C 1250 °C 1400 °C	35.29 2.79 61.92	5.7912E-08	0.0009 ± 0.0001	15.4 ± 5.5	334.16 299.29 470.78 353.65
AA-Shenzhen diffusion-treated 2.347ct	990 °C 1250 °C 1400 °C	100 0 0	5.52343E-08	0.0036 ± 0.0004	3.9 ± 0.6	455.29 287.24 256.15 336.45

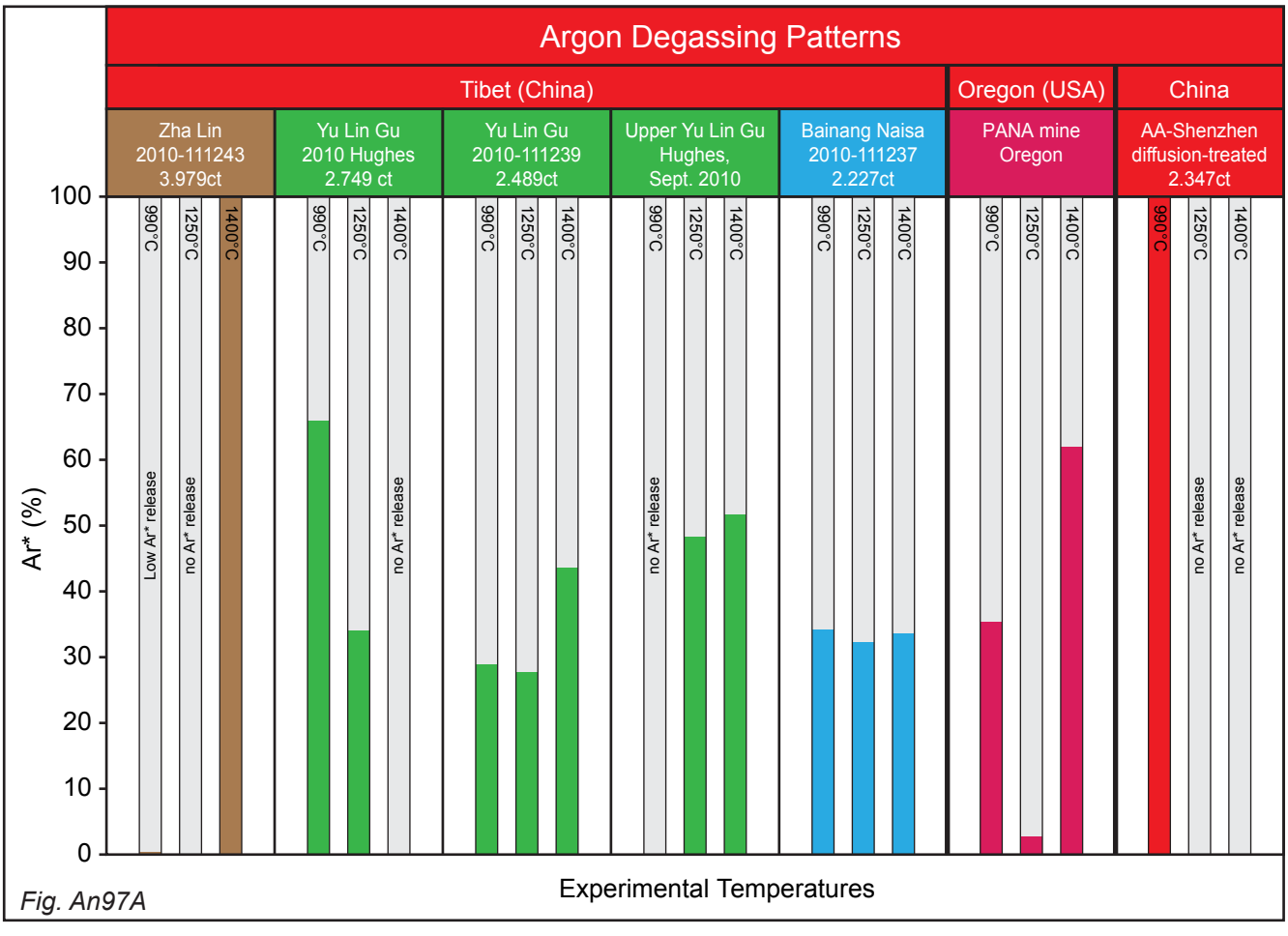

Fig. An97A

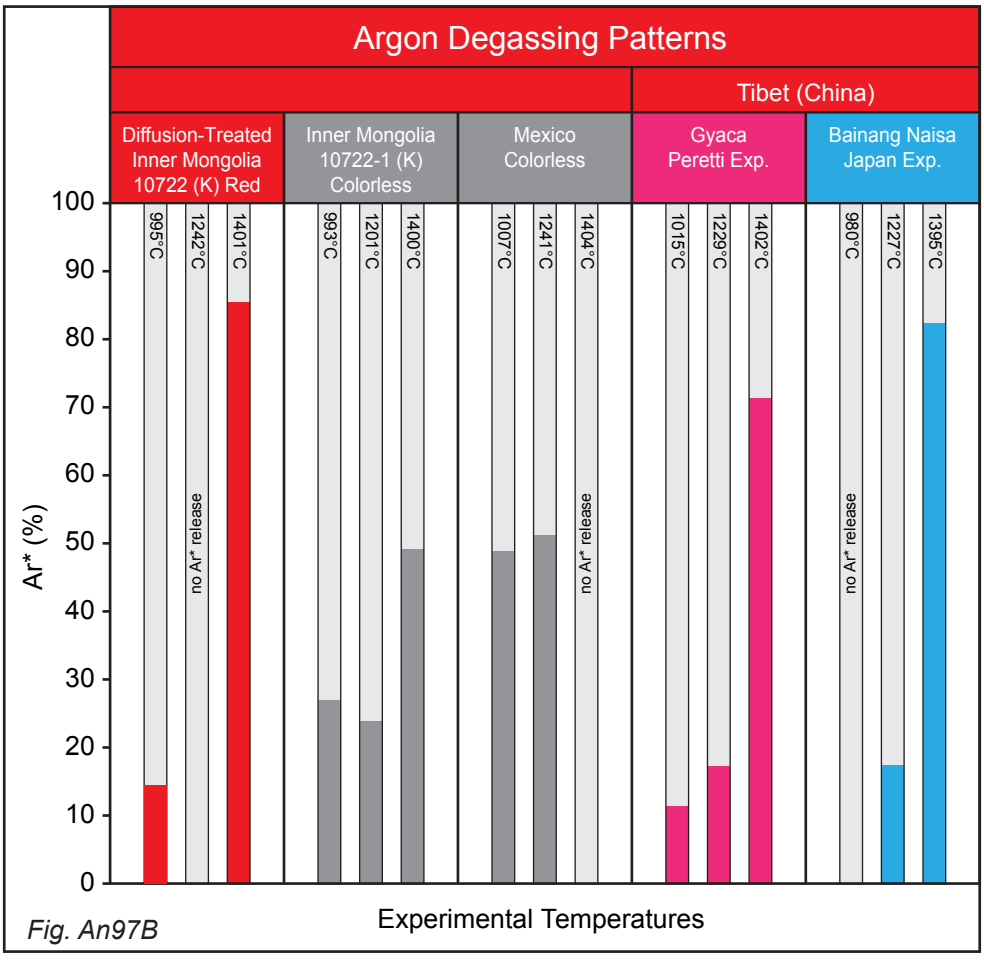

Fig. An97B

Fig. An97A-B Radiogenic 40Ar (Ar) concentrations in copper-bearing andesine from various localities in Tibet, Oregon, andesine from Inner Mongolia (China) and diffusion-treated counterparts. Colored bars show the proportion of the total Ar* released at each oven temperature and add up to 100 %. The release of Ar* from the different samples is shown for various temperatures. Uncolored bars denote no significant release of Ar*. This presentation is more informative than the bulk analysis. Results shown in Fig. An97B are already published data (Lit. An13).*

Fig. An98 Mass spectrometer used for the determination of Ar concentrations in natural and diffusion-treated Copper-bearing andesine*

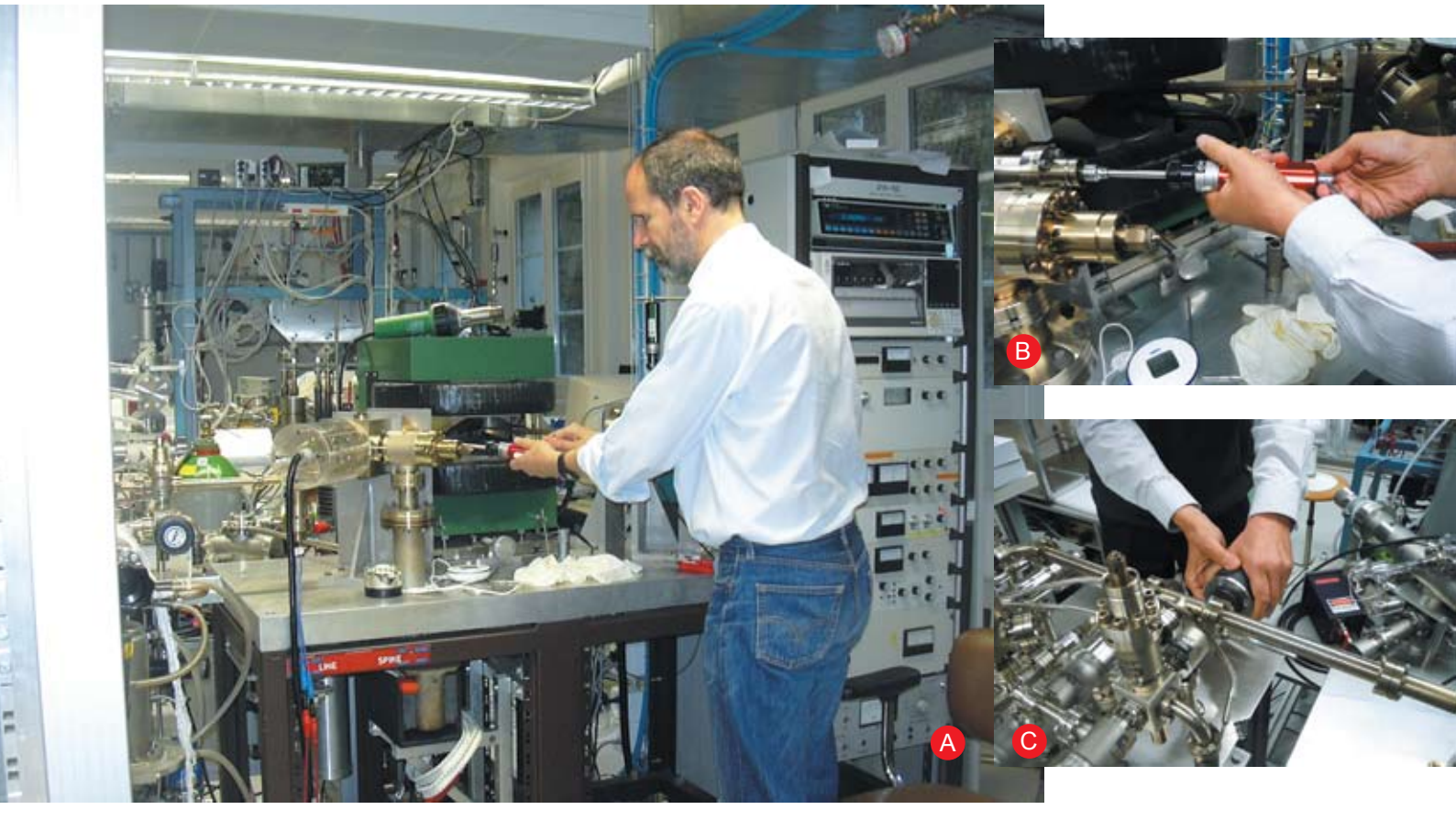

Fig. An99 Extraction system used for the determination of Ar concentrations in natural and diffusion-treated copper-bearing andesine.*

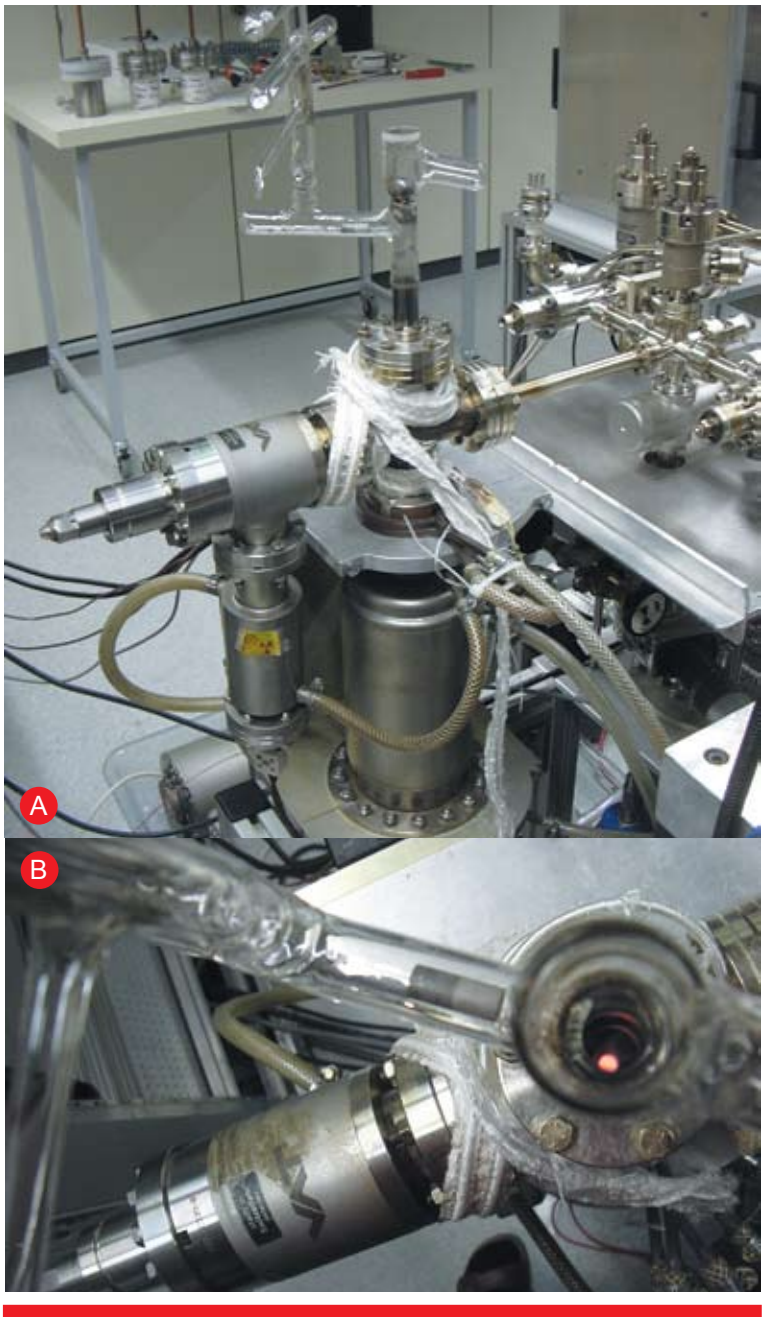

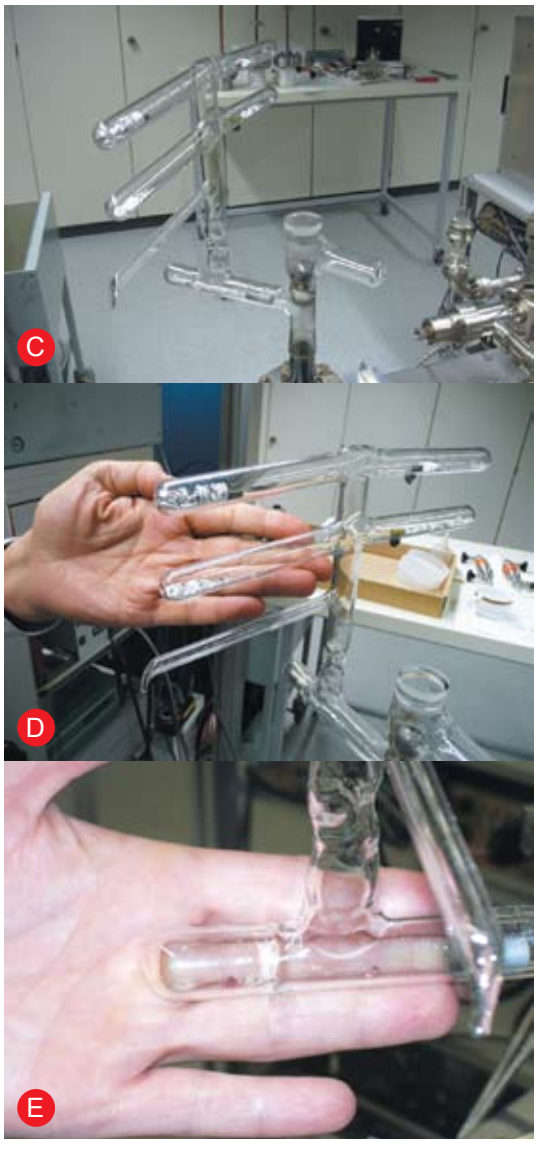

Fig. An100A-E Andesine samples are kept in an evacuated vacuum chamber (A, D, E) and than moved by magnets (C, E) into the oven which heats them up to 1500°C (B). Argon is degassed from the samples heated in the oven, purified from reactive gases, and transported into the mass spectrometer where the Ar is ionized. The magnetic field deflects the Ar isotopes, which are measured by a Faraday cup having a known sensitivity. The Ar isotopic ratios are displayed in Tab. AN05 as a function of the degassing temperature, providing the fingerprint for the heating history of the andesine samples.

Box An03 The principle of K-Ar age determinations

The decay of the radioactive isotope 40K, with a half-life of 1.25 Ga, produces the radiogenic isotope 40Ar.
To determine the K-Ar age of a sample, the daughter/parent ratio, 40Ar/40K, must be determined after correction for the Ar acquired when samples are exposed to the atmosphere. In addition to 40Ar, which accounts for about 99.6% of the total Ar, the Earth's atmosphere contains two minor isotopes, 36Ar and 38Ar, which are not radiogenic. These isotopes are used to detect, and correct for, atmospheric contamination. Andesines contain a few 100 to 1000 ppm K, which ensures that over geological times their radiogenic 40Ar concentration will increase detectably. However, when an andesine is heated to a sufficiently high temperature for a sufficiently long time, the Ar it contains will be out gassed. This is a desirable feature of the protocol used for the age determination. It is also an unwanted by-product of artificial heating to induce Cu diffusion in treated andesines, which can be detected by the out gassing pattern during our laboratory analyses.

RESULTS

The results are shown in Tab. An05 and Fig. An97A-B and Fig. An101A-B. Of special interest is the temperature-dependent degassing patterns, which will be discussed individually for every sample.

DEGASSING BEHAVIOR OF ANALYZED FELDSPARS

PANA mine (Oregon, USA)

The Ponderosa sample is clearly identified as natural and not diffusion-treated. Its degassing pattern is characterized by the highest Ar* degassing at 1400 °C.

AA Shenzhen (China)

The diffusion-treated sample AA Shenzhen released no Ar* in temperature steps 2 and 3.

Yu Lin Gu (Tibet, China)

Two of the three Yu Lin Gu samples have a similar Ar* degassing behavior (differences at 990 °C are considered of lesser importance). The Yu Lin Gu Hughes 2010 sample (Upper Yu Lin Gu) is different from the other two: it has a very different K-Ar age and released no Ar* at 1400 °C.

Bainang (Tibet, China)

The Bainang sample directly obtained from Ahduriyim for this publication released similar Ar* concentrations in all three temperature steps. It shows a very a different degassing behavior and K-Ar age compared to the Bainang sample analyzed earlier (Lit. An13) that had been attributed to the same mine.

INTERPRETATION

Untreated samples, such as the “Ponderosa” sample and the untreated Inner Mongolia sample reported earlier (Lit. An13), show the highest Ar* release at 1400 °C. Conversely, treated samples clearly demonstrate the loss of Ar* as an effect of artificial treatment, both in terms of a lower K-Ar age and of a modified degassing pattern. As an example, two already published samples (Lit. An13), sample 10722-1 (untreated Mongolia) and sample 10722 (half of sample 10722-1 experimentally treated by Emmett) demonstrate this behavior (Fig. An97B and An101B).

In this work, the diffusion-treated sample AA Shenzhen shows no release of Ar in the 1250 °C and 1400 °C steps. We attribute this pattern to the Cu doping treatment and suggest that the duration of the artificial treatment was sufficiently long to degas the Ar* from the sample. The Ar* release at low temperature could be interpreted as the result of a backwards-diffusion of argon from the closed oven during the Cu doping.

Zha Lin

The Zha Lin sample only released Ar* at the highest temperature and is different from all other samples. Because its K-Ar age is much higher than that of the Mongolian andesine, its provenance cannot be Mongolia, whether or not it has been artificially treated. It is possible that this sample has either been diffusion-treated for a short time, or has another crystal structure more retentive of Ar*, or underwent a metamorphic-metasomatic event after its formation. We determined cell parameters of all samples analyzed for K-Ar (Tab. An02). While the cell parameters allow a discrimination of the Ponderosa labradorite from the andesines, they show no significant difference amongst andesines that had the largest differences in their Ar* release pattern. The only sample significantly different is the Yu Lin Gu 2010 sample, which also has a different K-Ar age (see below). We conclude that the marked differences in the Ar* degassing pattern are not a primary feature of the crystal structure but are a secondary feature that depends on the thermal and hydrothermal-metasomatic history of each sample.

Upper Yu Lin Gu

Two samples are very similar and are likely to have the same origin. We consider them as untreated.

Yu Lin Gu (Hughes 2010 sample 2.49ct)

The K-Ar age of this sample is much higher than the other two Yu Lin Gu samples. One possible explanation is that this sample is not from the same mine. An artificial Cu doping treatment could then explain the degassing pattern of this sample. However, this is not a proven hypothesis and natural (geological) causes can also be envisaged. Since natural Ag-Cu-bearing fluid inclusions have been observed in some Yu Lin Gu samples, it is possible that the fluid circulation event (and attending Ar* loss) affected the two sampling areas to a different degree. In this case the different degassing pattern and the different K-Ar age are an effect of the location-specific geological history.

Bainang

The uniform degassing behavior of this sample suggests that it is probably untreated. On the contrary, the K-Ar age and the degassing pattern of the other sample allegedly from this mine (Lit. An13) are incompatible with a common origin. Because the two “geological aliquots” are in mutual contrast, we conclude that at least one of them is treated and at most one of them could be natural.

INTERPRETATION OF THE AGE (See Fig. An101A-B)

A K-Ar age calculation on bulk argon concentrations without taking into account the degassing pattern as a function of temperature steps during Ar isotope analysis would be not conclusive and rather misguiding. The K-Ar age is useful only when the age of samples from the same deposit and that are known with certainty to be untreated, is independently known. For example, if the suggestion (Lit. An13) that samples collected in Tibet ultimately derive from Mongolia were true, then all ages < 17 Ma on Tibetan samples would be the result of artificial treatment.

Experimental heat-treatment of an aliquot of sample 10722 (Lit. An13), and comparison with the untreated aliquot, demonstrates that heat-treatment does lower the age, and at the same time heavily modifies the Ar* release pattern (Fig. An101B). While it is clear that heat treatment causes a lowered K-Ar age of old samples, the logical inversion is not true: a young K-Ar sample can just as well reflect the young geological age of an untreated sample.

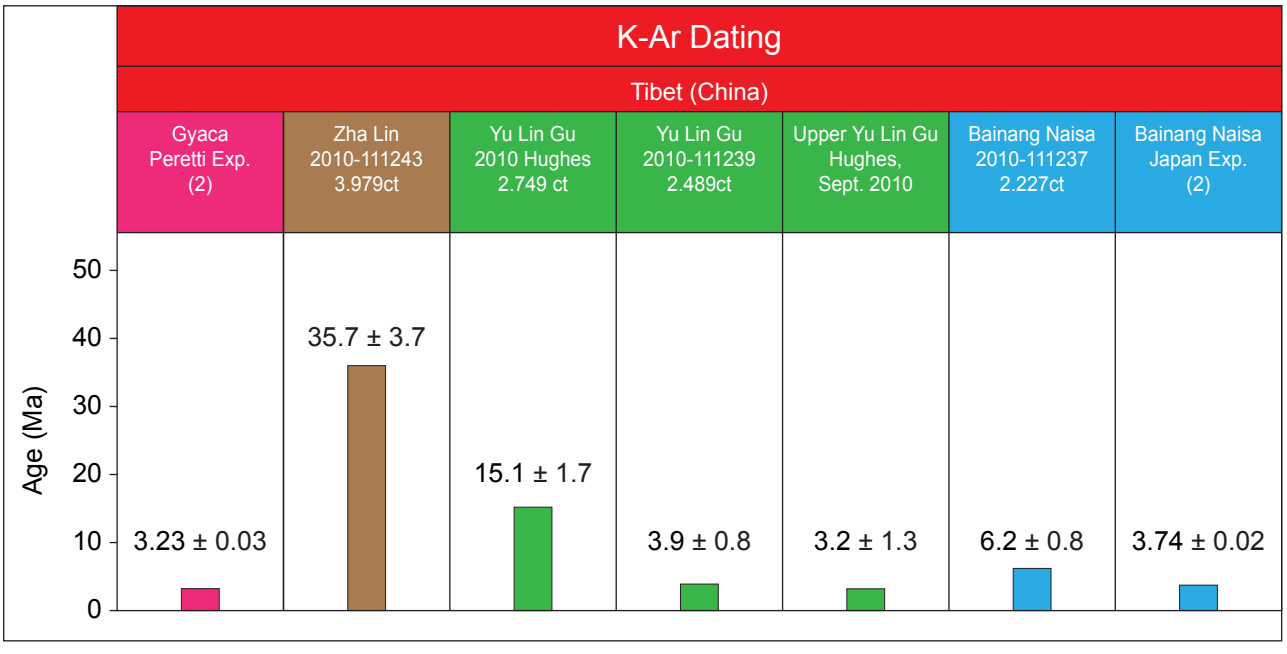

Fig. An101A

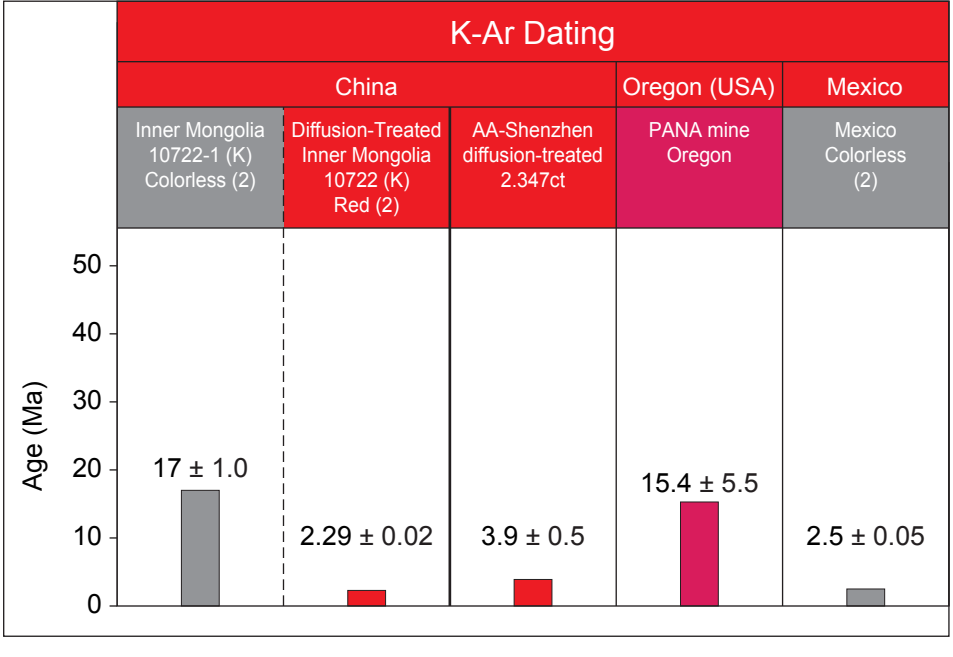

Fig. An101B

Fig. An101A-B K-Ar ages of copper-bearing andesine crystals: (A) this work; (B) from Lit. An13. Highest ages were found for Zha Lin, Yu Lin Gu (Tibet) and Oregon. Low ages, however, could also be primary young geological ages and do not necessarily indicate artificial treatment, if the effects of the treatment are not confirmed by an anomalous pattern of the temperature release of Ar.*

The bulk 40Ar/36Ar ratios are also less informative than the fingerprinting provided by the temperature-dependent degassing pattern. For example, the diffusion-treated sample AA Shenzhen gives a 40Ar/36Ar ratio as high as that of the untreated samples, and would therefore be identified as untreated. Conversely, the Bainang sample would be identified as treated if only the bulk K-Ar ages are considered (in the assumption that its geochemical and trace element pattern identifies its provenance as Inner Mongolia). However, the nearly uniform Ar* release at different temperatures is an indication that the sample is not diffusion-treated.

Finally, high K-Ar ages are also not a guarantee that the sample is not diffusion-treated. As an example, sample Zha Lin shows a suspicious degassing pattern, which leads us to suggest that it might be artificially treated. The possibility that Ar* loss occurred naturally must also be taken into account by an integrated study of fluid inclusions.

The age of the Oregon sample is coincident (at the 1 sigma level) with the geological constraints in the literature (mid-Miocene, Lit. An29) for a volcanic field. However, the age of the measured Oregon sample has to be considered with caution as a younger age could be invoked: (a) the out gassing of K-feldspar is sometimes incomplete at 1400 °C (Lit. An34); this effect could be more relevant for the Ponderosa sample, which degassed two thirds of its Ar* above 1250 °C; (b) the Cu-bearing stones attest to a hydrothermal circulation, which is very likely to have induced Ar* loss (Lit. An46).

IR-UV-fs-MC-ICP-MS Instrumentation at the Research Group for "Trace Element and Micro Analysis" at the Department of Chemistry and Applied Biosciences, ETH Zurich, Switzerland

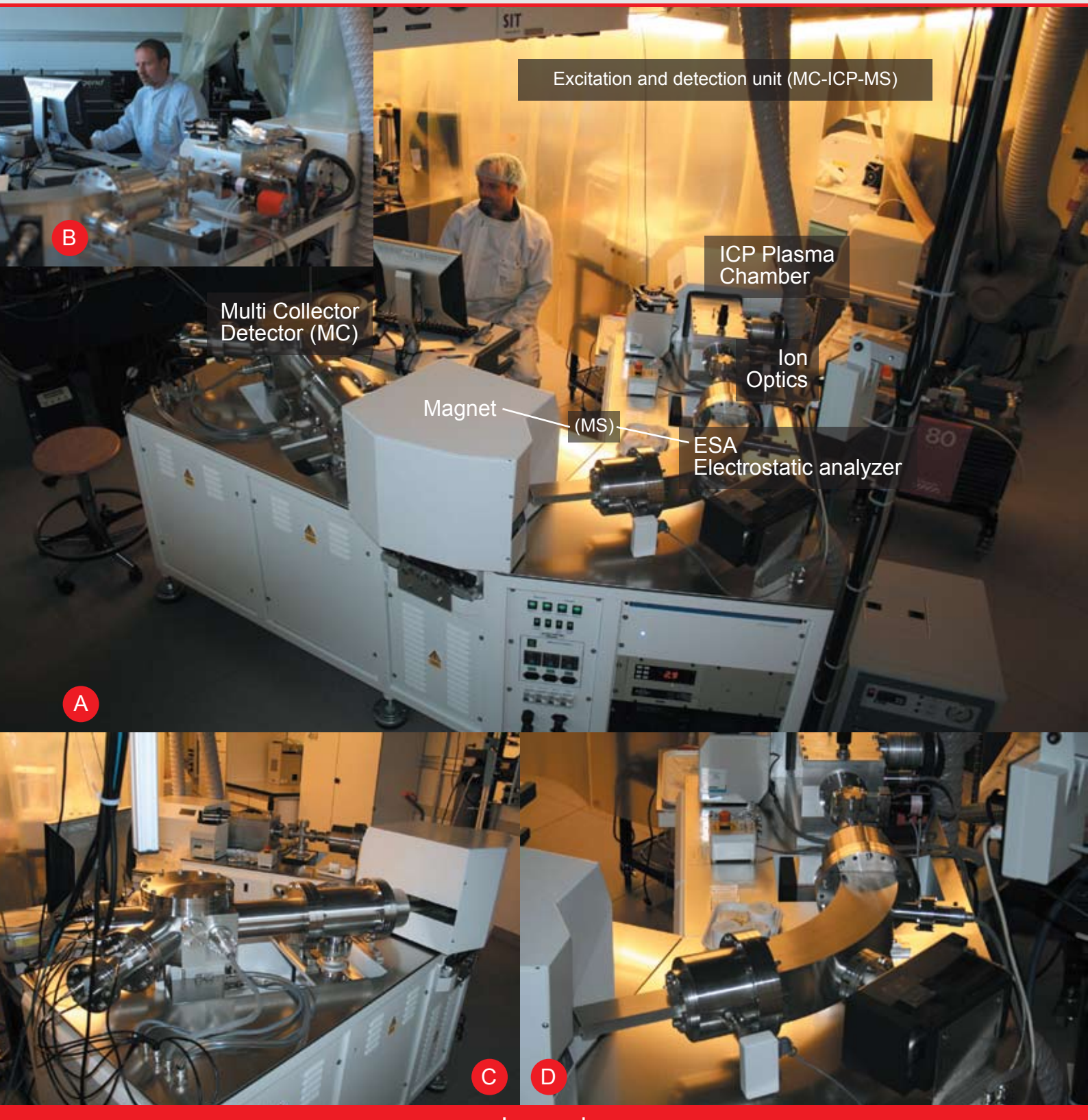

Legend

A) Overview of the multicollector inductively coupled plasma mass spectrometer (MC-ICP-MS, Nu Instruments, UK), which is used for high precision isotope ratio determinations (e.g. Cu isotope ratio measurements)
B) Side view of the MC-ICP-MS with the data acquisition computer
C) Detector block (Faraday detectors) for measuring multiple isotopes simultaneously
D) Blow up of the electrostatic analyzer (ESA)
E) Overview of the entire femtosecond laser ablation system (solid state Ti-sapphire, Coherent, USA), which can be operated at 760-820 nm, 380-410 nm, 265 nm and 200 nm at various energy levels)
F/G) Different views into the same amplifier for generating the short pulses

Multi component laser system for generation of ultra short pulses (femtoseconds) in infrared, visible and ultraviolet wavelength

METHODS

The UV femtosecond laser was used in our study as sampling tool. The material from the sample is ablated without considerable production of heat, which is one of the most important prerequisites for stochiometric sampling (sample remained compositionally unchanged). The gems material is directly transformed into very small particles (Nano-aerosol", approx. 1/10 000 millimeter or even smaller) that are carried by helium into an inductively coupled plasma mass spectrometer. Within the argon plasma (ICP) the particles are vaporized, atomized and ionized, separated by mass/charge ratios and finally detected. Microscope optics for sample viewing and the airtight ablation chamber for hosting the samples for analysis (laser beam interaction with the gemstone leads to production of nanoparticles which are transported in a highly-pure helium gas flow towards the ICP) are pre-requisits of this technique. Only few ng of material are required for analysis and the crater sizes are commonly within 10 to 50 micrometers in diameter and 5 micrometers in depth. The sample required for analysis cannot be measured by the conventional scale used in the gem industry (<0.000 000 5 ct). Therefore, this technique is considered to be quasi non-destructive. However, low concentrations of Cu require longer sampling periods (scanning mode) for precise Cu isotope ratio determinations. The degree of destruction of the sample is higher than for elemental analysis by LA-ICP-MS since stable isotope ratios require an analysis in scanning mode.

FEMTOSECOND LASER: EXPLANATION

One femtosecond (0.000,000,000,000,001 s) is an unimaginably short time. While light travels around the Earth more than seven times in one second, it only travels one-hundredth of the thickness of a hair in a femtosecond (fs). For some time now, ultra-fast lasers have been on the market with a stream of extremely short, high intensity light pulses, each lasting for only a few femtosecond. Such lasers break records: the output during the short pulse is equal to that of 100 atomic power stations, and its light intensity can be compared to the intensity of the sunlight falling on Earth bundled in the tip of a pencil. (From http://www.fascination-of-light.net)

Cu-bearing gemstones including Cu-bearing Plagioclase (andesine) from the new mines in Tibet and Cu-diffused andesine counterparts were analyzed for trace elements using LA-ICP-MS and isotope ratios using femtosecond-LA-MC-ICP-MS. Natural Cu-andesines from Tibet and diffusion-treated andesines were analyzed by fs-LA-MC-ICP-MS (Fig. An103) and the isotope ratios were acquired by standard sample bracketing using NIST610 glass as standard. The composition of the andesine, especially the Cu concentration, was very similar to that of NIST610. The results indicate that treated samples provide a similar or negative ∂65Cu/63Cu value (see equation 1) compared to NIST610, whereas the untreated samples from Tibet were found to have a positive bias.

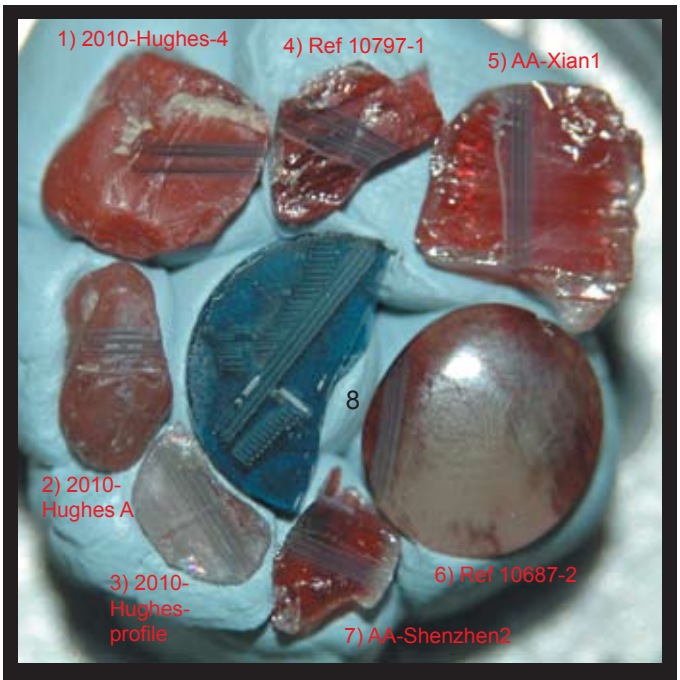

Fig. An103 The samples shown in the figure were analyzed by fs-LA-MC-ICP-MS in scanning mode. The integration time was 30 seconds, which corresponds to 600 µm sections on the sample. In the plots, the open symbols are for the different sections of the 3 runs. The averages in the plots (closed squares) correspond to the average over the 3 runs for the same section.

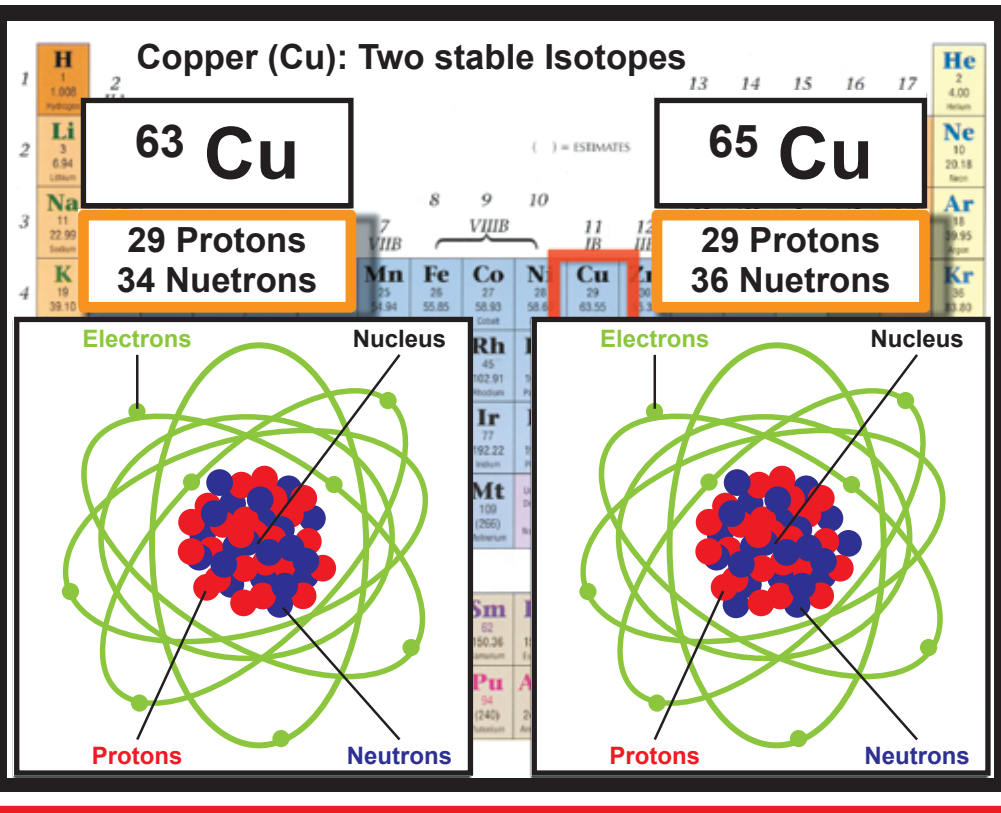

Fig. An104 The two Cu isotopes measured with fs-LA-MC-ICP-MS. A simplified atomic model is shown for the explanation of the difference between the two different isotopes.

Box An04 Definition of "Delta"-value

The delta is calculated as in equation 1:

$$\text{"Delta"} = 1000 \times \left(\frac{2 \times \left(\frac{^{65}Cu}{^{63}Cu}\right)_{sample}}{\left(\frac{^{65}Cu}{^{63}Cu}\right)_{NIST,} + \left(\frac{^{65}Cu}{^{63}Cu}\right)_{NIST,2}} - 1 \right)$$

and indicates the relative changes of the Cu isotope ratio for andesine in comparison to NIST610. The average of the brackets before and after the samples is taken as reference value for the delta calculation.

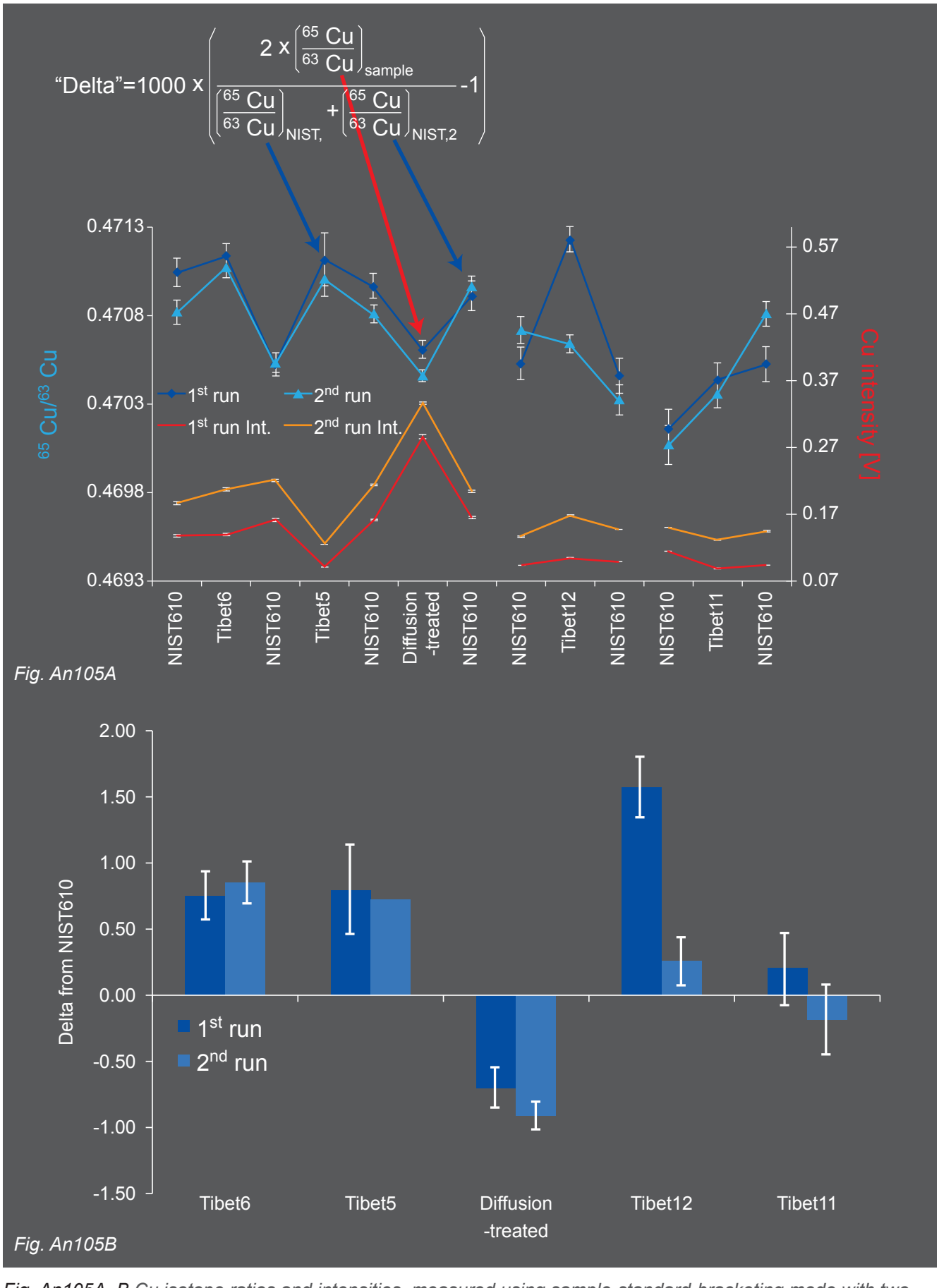

Fig. An105A, B Cu isotope ratios and intensities, measured using sample-standard-bracketing mode with two replicates per sample. The measurement cycle contained 4 samples from Tibet (two rough and two faceted samples) and one sample labeled as diffusion treated (presented in a seminar at the Hong Kong show, September 2009, Lit. An28). The diffusion treated sample shows a negative Cu-isotope ratio in comparison to NIST610, whereas the Tibet samples are in the positive region.

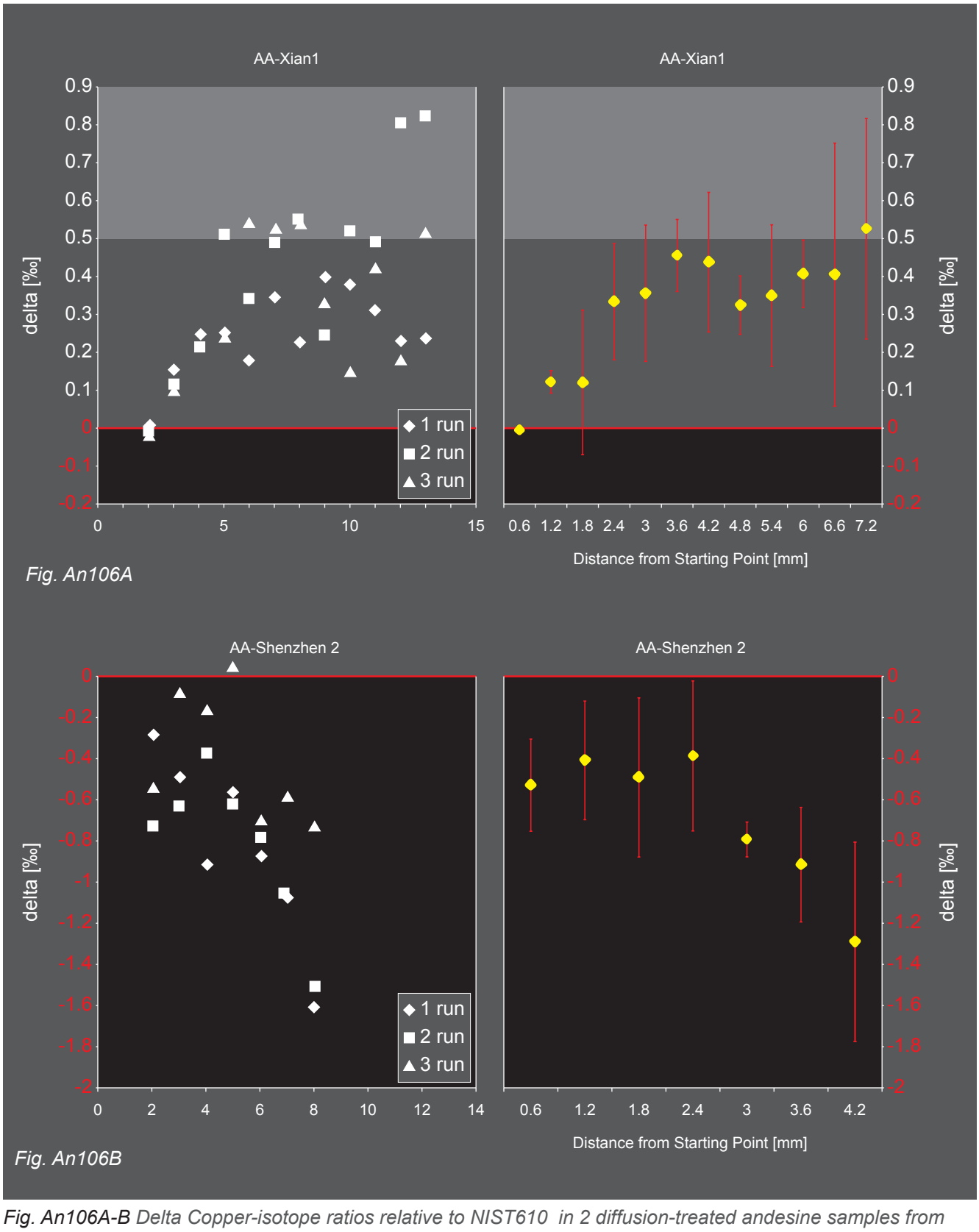

Fig. An106A-B Delta Copper-isotope ratios relative to NIST610 in 2 diffusion-treated andesine samples from (A) the University of Xian (China) and in a diffusion-treated andesine from (B) an undisclosed laboratory in Shenzhen (China). The delta values are shown for each run individually and the averages of each section for the 3 runs is shown on the right (distance from surface in x-axis). On the left side, the x-axis represents the number of the section integrated for the single run (1 = first 600 um, 2 = the second 600 and so forth). Points are measured across a profile into the interior of the sample (in mm). The delta values show high variability and are ranging from 0 to 0.5 (Fig. An106A). Similar to Xian, the Cu isotopes in Shenzhen (Fig. An106B) vary also over a broader range (-0.4 to -1.4). However, their delta values are shifted into negative values when compared to NIST610.

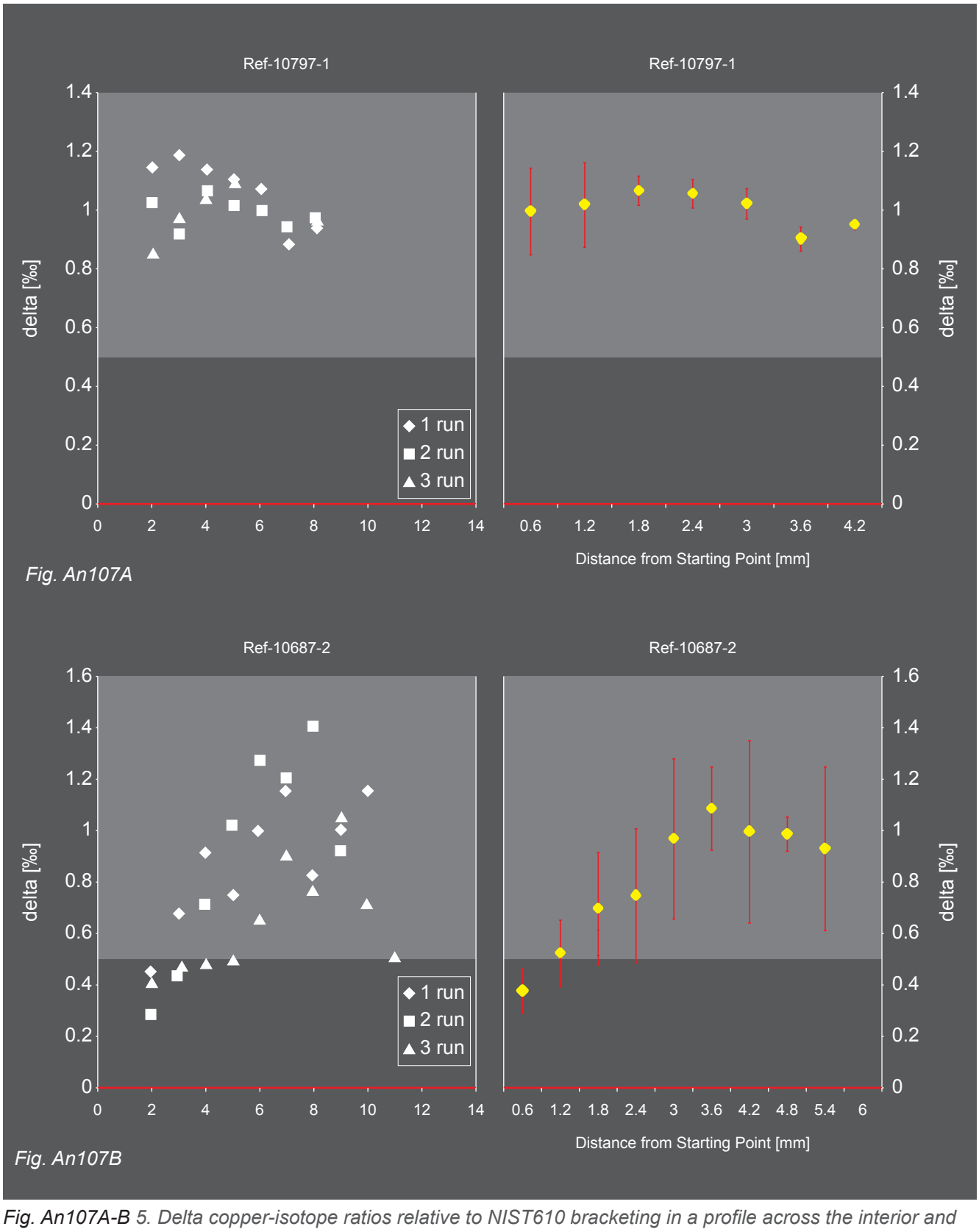

Fig. An107A-B 5. Delta copper-isotope ratios relative to NIST610 bracketing in a profile across the interior and on the surface of two natural copper-andesine from Tibet. The values for the profile show very little variation and provide positive values only (approx. 1). Considerable variations were found along the profile in sample B, which was measured on the sample surface. However, the values are also positive (0.4-1). Explanation of x-axis See Fig. An106.

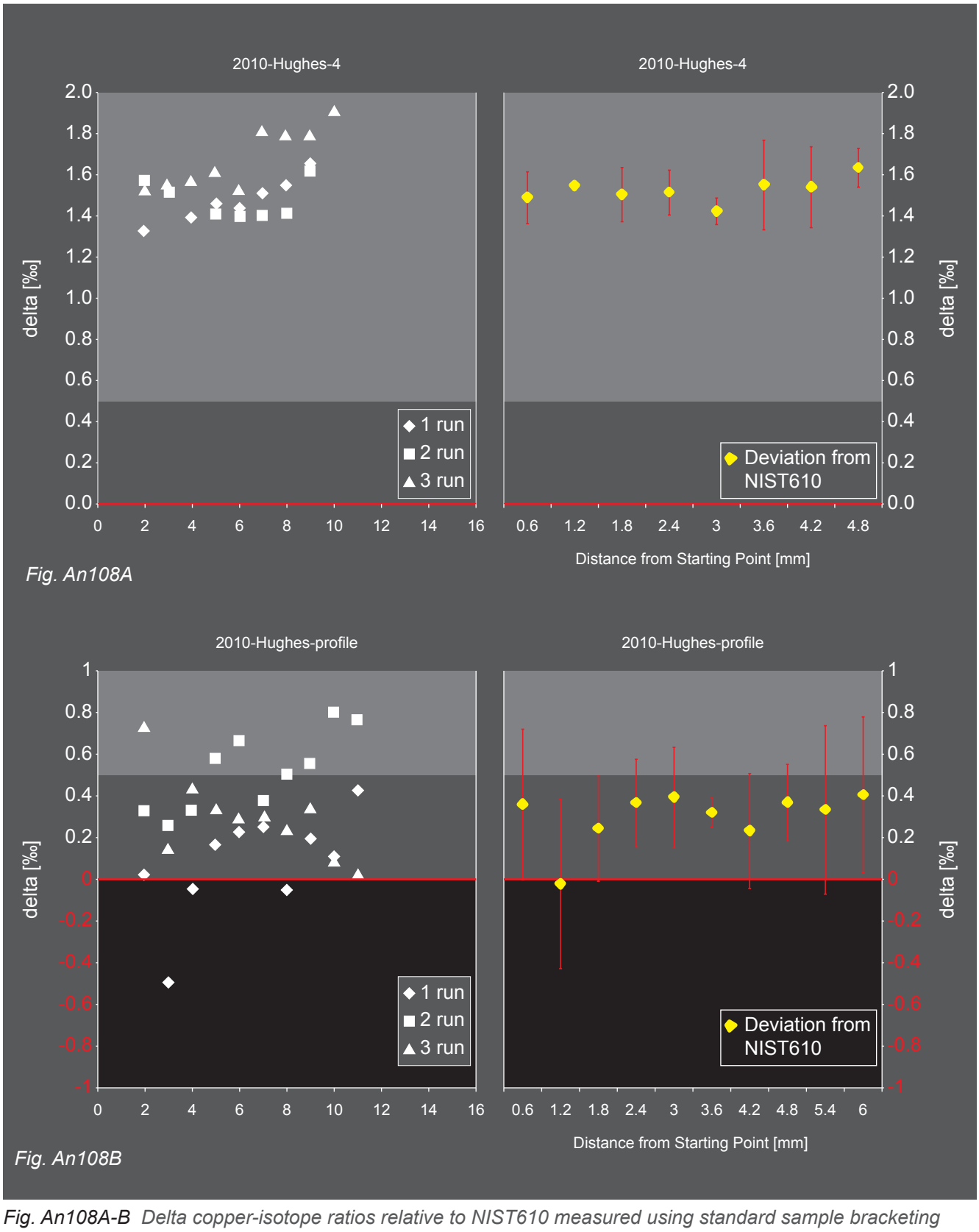

Fig. An108A

Fig. An108B

Fig. An108A-B Delta copper-isotope ratios relative to NIST610 measured using standard sample bracketing (and signal deviations) on a cleavage surface (corresponding to a profile) across the interior (Fig. An108A) and on a profile (See Fig An39A). Both samples are natural copper-andesine from Tibet (Yu Lin Gu). The values are high in the positive with all the measured points above 1.3 (for A) and above 0-0.4 (Fig. An108B). No variation is seen across the cleavage surface profile. However, large differences were found in the delta values for sample (Fig. An108B). Explanation of x-axis See Fig. An106. Due to the restricted amounts of data points on samples 2010-Hughes A (4), due to large uncertainties the data could not be interpreted due to large uncertainties (-0.4 to 0.3) and are not shown in a profile plot.

CONCLUSIONS COPPER ISOTOPE RATIO MEASUREMENTS

Natural copper andesine from the so-called new mines (Gyaca, Yu Lin Gu) can be separated from diffusion-treated samples (Xian University and Shenzhen), when measuring isotope ratio profiles from the rim to the core of the samples. The delta copper-isotope ratios in the natural sample are dominantly positive when compared to NIST610. The isotope ratio reproducibility on the natural samples is more stable across the entire sample than in the diffusion treated samples, which provide low or negative delta copper isotope ratio values in comparison to NIST610. These additional isotope ratio measurements confirm our earlier findings that natural samples have a positive delta value when compared to the diffusion treated samples. However, measurements on the sample surface are less indicative and show higher variations (See also Lit. An13) and Fig. An107B. Combining all detailed observations on the different stones analyzed within this study, it is well possible that isotope fractionation and differences (negative and positive values between the diffusion treated samples and natural counterparts) occurred. Since these measurements require longer signal acquisition, resulting in longer sampling periods on the sample surface in profile mode, the method cannot be called “non-destructive” when applied to faceted gems. Therefore, only selected and representative stones allowed to suffer minor damages can be tested.

PHOTO-INDUCED COLOR-CHANGES IN COPPER-BEARING ANDESINE

Further observations were made in the course of the visual re-investigation of all the samples from our previous work (Lit. An13). We noticed that the use of the femtosecond laser with a very high irradiation (See Fig. An102) initiated a color change within the samples in the vicinity of the profiles (line scans, see Fig. An109A-D). Green turned into red (sample Kongo-2289-ETH-No.2) or lightened the color from orange-red to a lighter color of the same shade or to light green (Ref-10808, Bainang mine). It seems therefore most likely, that copper-andesine can also be treated by NIR (760-820 nm) heating. Since we are unable to determine the temperature of the laser radiation precisely, this new observation needs to be studied in more detail, e.g. heat treatment experiments.

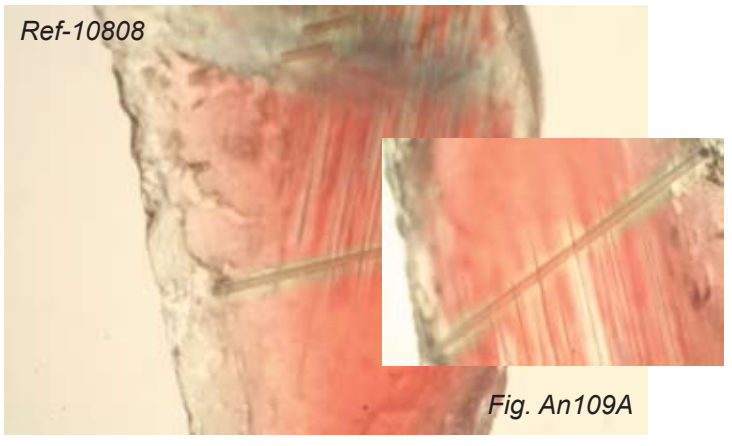

Fig. An109A

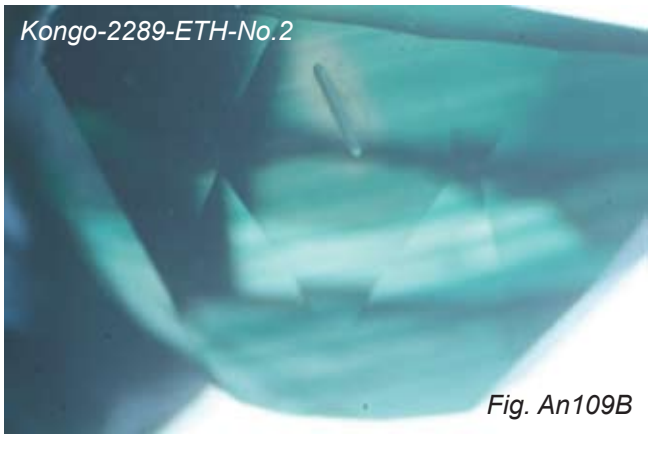

Fig. An109B

Fig. An109C

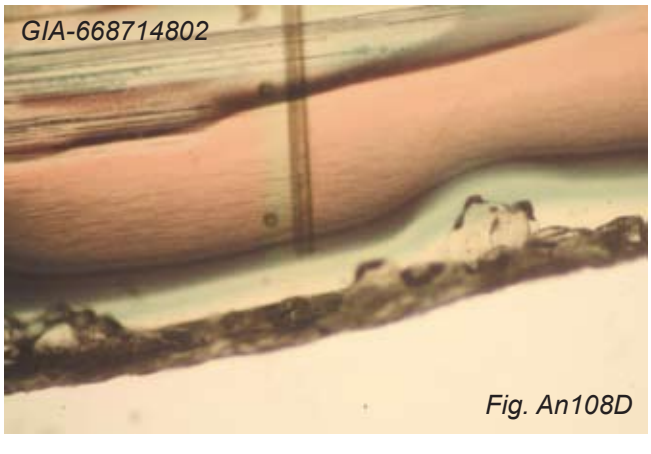

Fig. An108D

INTERPRETATION OF AUTHENTICITY OF TIBETAN RED ANDESINE

Natural copper andesine can be confirmed from 3 different mines of Tibet. These Tibetan andesines underwent a natural diffusion process associated with hydrothermal fluids. LA-ICP-MS analyses of fluid inclusions analyses indicated that the solutions contain copper and sulfur and they were of low salinity. Silver concentrations were determined in few inclusions only but it diffused into the surface of the copper-bearing andesine only, indicating that it was present in the system.

Fractionation of metals such as copper and silver is known from ore deposits of magmatic-hydrothermal origin and has been reported elsewhere (Lit. An08). Such fractionation has been described in a case study as following: First hydrous silicate magmas are produced, followed by their crystallization, then volatile-rich fluids are separated from these magmas. It has been shown in detail that magmatic brine-vapor separation can cause selective metal transport and the chemical reactions (and other physical processes) leading to mineral precipitation. Based on detailed fluid inclusion analysis including LA-ICP-MS on a case study of an ore deposit around the large Mole Granite in eastern Australia (again Lit. An08), it was found that ground water mixed with hot brines originating from magmas. During this process certain elements, such as Cu and B were enriched in a vapor-phase, while Ag (among others) remained concentrated in the brines. It was suggested that copper disulfide complexes stabilized Cu in the S-enriched vapor phase, while in contrast most other metals were held in the brine by stable chlorine-complexes. Different geological models may be responsible for such a partitioning between Ag and Cu (e.g. fluid mixing, fluid-rock reactions or vapor separation). Therefore, only an extensive expansion of our preliminary fluid-inclusion study will allow revealing the exact details of the geological history of the ore-forming processes in Tibet. However, the fluid compositions found in fluid inclusions of Tibet andesine provided first indications for a similar process.

Low K-Ar ages (Lit. An40) are not necessarily proof of lab-induced diffusion-treatment. A hydro-thermal process would also cause Ar loss due to dissolution/reprecipitation during alteration. The temperature-controlled argon-release experiments helped to differentiate between natural and lab-induced diffusion processes.

The presence of uranium in melts found on laboratory diffusion-treated andesine from Shenzhen (Tab. An03) together with the presence of increased uranium-concentrations on the surface of Tibetan andesine (Fig. An39B) and in the fluid inclusions (Tab. An04) can be interpreted as following. We consider uranium a natural contamination product in the surface residues and fluids of natural Tibetan andesine. During the diffusion-treatment at relatively high temperature, the U traces that are found on the surface of natural copper-andesine melted and became mobilized into droplets (See Fig. An60A). Using Uranium as a natural tracer, it was concluded that natural Tibetan andesine was used in the diffusion-treatment (improving color of copper-bearing andesine from Tibet by additional diffusion-treatment). The crystal lattice parameter analyses and the complete match of diffusion-treated andesine and Tibetan counterparts confirmed this.

Only the combination of argon-testing, multi-element analysis and copper isotope analysis can separate natural from diffusion-treated Tibetan andesine and other counterparts. Testing in the last three weeks of over 41 faceted copper-andesine gem quality faceted stones circulating in the market, we were not able to identify one single example where we were confident about their authenticity and none of them had any traces of silver. Market stones tested previously (Lit . An13) and in this work also did not contain traces of silver (See Tab. An10 and Tab. An11). It must be feared that natural gem quality samples are of great rarity and we are of the opinion that most of the gem quality material in the market is actually

diffusion-treated or indeterminable. Unfortunately, copper-isotope measurements and argon-testing are not strictly non-destructive (See conclusions page 90). Currently, the most important proxy that can be tested in a non-destructive mode (as reported for all other gems) is the presence of silver (See Tab. An05-12).

On this basis, most of the copper-andesine from the new mines (See group A2, A3 and C2, Tab. An01 and Fig. An04) can be identified as 'natural.' The stones from old mines (Bainang) and the new mine Zha Lin may be found natural or indeterminable, depending on the presence of Ag. The most critical test for this analysis is LA-ICP-MS. The gem-quality stones collected to date from the open market (group D and E, Fig. An01), with the exception of Oregon samples, turned out as either indeterminable or possibly diffusion-treated. However, many of them we could not test for copper-isotope ratios, as it would have created minor damages. The fact that a certain portion of the Bainang material (A) completely overlaps with the properties of the diffusion-treated Inner Mongolia andesine provides the miners theoretically a loop-hole to mix diffusion-treated materials into the lots. If the materials are tumbled (See Fig. An94) it would be difficult to identify and analyze rough surfaces and recognize them with common gemological instrumentation.

The unusually large number of gem quality copper-bearing andesine samples in the market seems to be in contrast to the quality and color of copper-andesine collected from the mines by gemologists needs to be further investigated. Random testing of faceted andesine using destructive tests will be the only possibility to understand the true ratio of diffusion-treated versus natural copper-bearing andesine in the market.

Fig. An111 Gem quality copper-bearing andesine of different colors as they appear on the market. They were disclosed as untreated and from the origin of Tibet but remained undeterminable after non-destructive testing.

Fig. An112A Red colored cracks are not observed in the untreated counterparts and are interpreted as proof for diffusion-treatment.

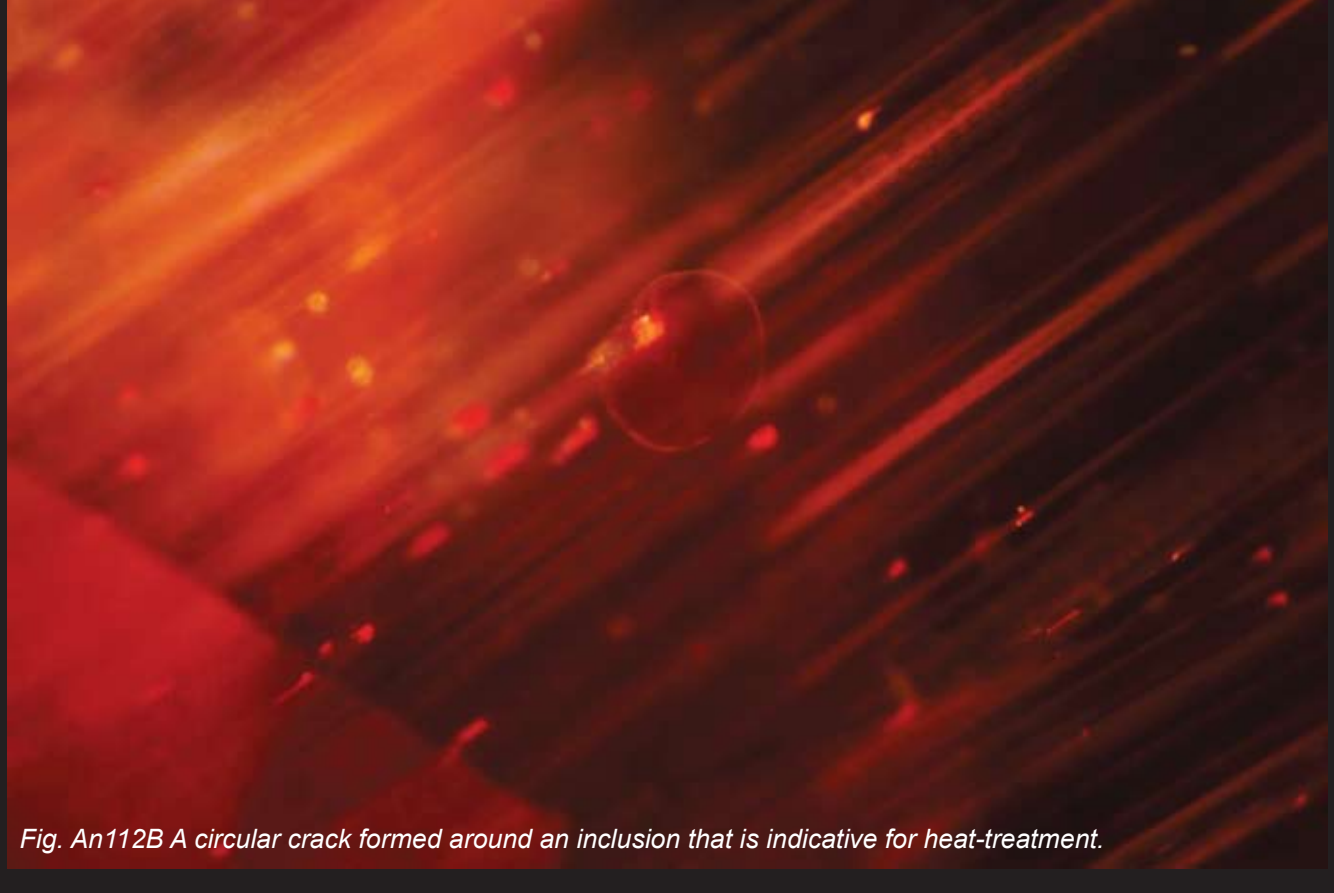

Fig. An112B A circular crack formed around an inclusion that is indicative for heat-treatment.

Note: These inclusion pictures were taken from a faceted copper-bearing andesine declared as untreated in the market. Applying non-destructive tests (LA-ICP-MS) the two samples were undeterminable from diffusion-treated andesine (proxy element Ag was not found). After microscopic examination, however, it was clearly visible that these faceted stones were treated (See Fig. An112A-B).

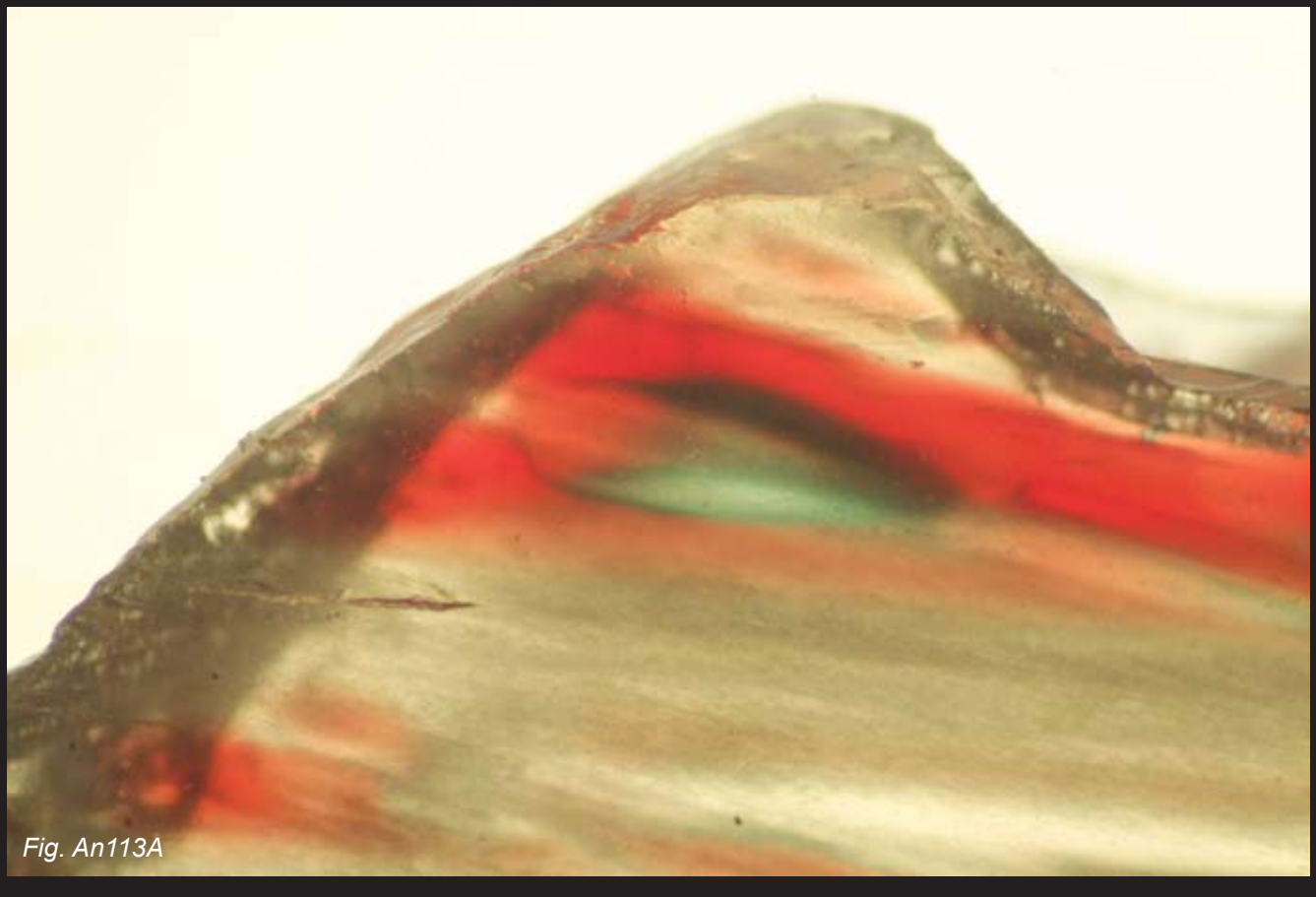

Fig. An113A

Fig. An113B

Fig. An113C

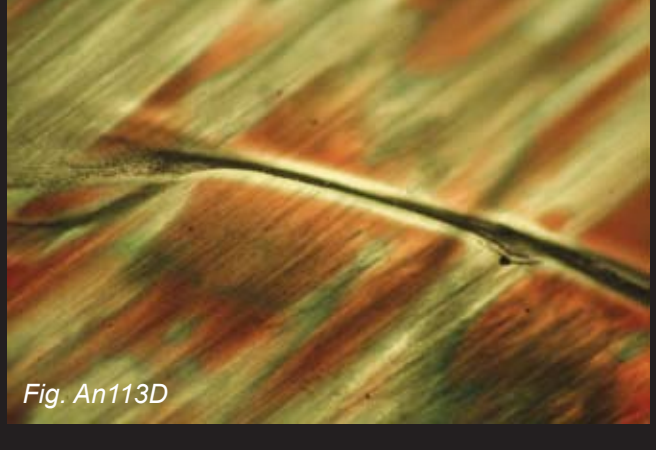

Fig. An113D

Fig. An113A-D Microphotograph of an experimentally diffusion-treated Inner Mongolia andesine (GIA-No 17401893, Emmett experiments) shows a typical red and green color zoning (Fig. An113A), red stripes (Fig. An113B) and white rim on both sides of the crack (Fig. An113C and An113D). Note that the particles trapped in the crack were opaque black solids without the presence of fluid-inclusions such as found in Tibetan samples. The formation of a white rim around the crack, however, is similar to the white rims formed adjacent fluid-inclusion trails (Fig. An24A and An28C) and rim-effects of other diffusion-treated samples obtained from other treatment laboratories (Fig. An46A and An46B).

		2010-112728_1		A-large				2010 Hughes A												
		Yu Lin Gu, Abduriyim		Yu Lin Gu, Sept. 2010				Yu Lin Gu, Sept 2010, 1.31ct												
		outer rim (white)	inner rim	outer rim		transition	inner rim	surface							core			outer rim			
Li	7	7.25	7.52	135	127	130	130	7.75	8.23	7.11	7.56	7.81	7.36	7.71	8.27	9.65	8.07	7.82	7.14	6.62	7.57
Na	23	40200	40900	39800	39100	40000	39800	40200	40500	39800	40800	41400	40600	40700	40300	40100	40200	39300	38100	38900	38600
Mg	24	481	488	486	475	486	479	467	451	448	476	490	489	499	493	498	482	459	442	465	466
Al*	27	147000	147000	147000	147000	147000	147000	147000	147000	147000	147000	147000	147000	147000	147000	147000	147000	147000	147000	147000	147000
Si	29	263800	281300	252800	251200	261000	259500	261500	265500	263000	264400	266900	259500	260300	255900	254100	256600	254700	252900	256200	249700
K	39	4150	4290	4020	3920	4090	4100	4350	4990	5490	4360	4220	4180	4230	4090	4060	4110	4350	4600	4590	4270
Ca	42	65000	65000	63400	63900	65500	65400	65600	65700	65700	65700	64900	65000	65800	65000	65100	65700	66700	66500	66500	65700
Sc	45	0.196	0.222	0.228	0.270	0.240	0.270	0.295	0.290	0.224	0.224	0.264	0.260	0.243	0.252	0.326	0.214	0.222	bd	bd	bd
Ti	49	356	364	369	356	360	363	367	362	363	364	354	364	368	358	393	369	366	351	354	351
V	51	1.51	1.57	1.38	1.53	1.49	1.51	1.43	1.68	1.65	1.49	1.52	1.61	1.55	1.33	1.48	1.38	1.42	1.39	1.52	1.45
Mn	55	29.1	30.0	29.8	29.3	30.7	29.4	29.7	26.7	28.8	28.7	29.5	29.2	29.1	28.7	29.1	28.7	27.6	26.5	28.2	28.5
Fe	57	2770	2870	2710	2700	2820	2800	2740	2820	2880	2870	2820	2790	2770	2900	2810	2820	2840	2760	2870	2820
Co	59	0.448	0.522	0.395	0.497	0.478	0.491	0.374	0.365	0.506	0.533	0.482	0.425	0.453	0.430	0.470	0.495	0.447	0.433	0.526	0.340
Ni	60	0.598	0.439	0.787	1.25	bd	1.35	1.29	1.82	14.1	4.29	0.684	bd	bd	bd	bd	bd	0.862	2.29	1.18	1.01
Cu	65	583	733	1320	1370	1500	1520	574	597	628	636	697	685	659	816	806	795	536	499	528	530
Zn	66	3.28	2.87	2.70	4.28	3.21	3.48	3.56	2.58	4.24	2.57	3.74	2.90	2.66	3.37	3.33	3.75	2.36	1.89	2.82	3.39
Ga	71	17.0	16.9	17.3	17.0	16.6	16.7	17.2	16.5	17.6	16.8	16.5	17.2	17.2	16.8	16.0	16.6	17.3	16.5	16.5	17.0
Ge	72	0.914	0.697	0.970	1.120	0.993	0.782	0.748	0.696	0.881	bd	0.711	0.816	bd	bd	bd	0.589	0.848	bd	1.15	1.22
Rb	85	0.845	0.897	0.787	0.823	0.722	1.230	0.854	0.867	1.26	0.857	0.968	0.928	0.807	0.803	0.829	0.932	0.813	0.876	0.782	0.904
Sr	88	1140	1160	1130	1130	1130	1160	1160	1140	1140	1160	1160	1140	1130	1120	1100	1150	1140	1140	1110	1100
Y	89	0.167	0.158	0.146	0.170	0.176	0.146	0.144	0.163	0.175	0.151	0.165	0.151	0.164	0.108	0.159	0.144	0.138	0.180	0.131	0.133
Zr	90	bd	0.048	bd	bd	0.099	bd	0.070	0.073	0.097	bd	0.084	bd	bd	bd	bd	bd	bd	0.055	bd	bd
Ag	107	861	425	1140	1110	939	698	444	427	445	441	428	419	422	94.8	46.1	46.6	378	384	391	410
Ba	137	135	137	127	132	133	131	133	135	138	136	138	137	136	132	132	134	134	130	135	133
Pb	208	0.415	0.404	0.790	0.728	0.401	0.457	0.490	0.672	0.891	0.459	0.784	0.420	0.413	0.444	0.429	0.403	0.434	0.499	0.416	0.384
U	238	bd	bd	0.158	0.076	bd	bd	bd	bd	bd	bd	0.107	bd	bd	bd	bd	bd	bd	0.012	bd	bd
La	139	1.20	1.15	1.15	1.27	1.15	1.18	1.09	1.12	1.20	1.15	1.17	1.16	1.26	1.18	1.05	1.15	1.14	1.16	1.23	1.12
Ce	140	1.85	1.92	1.86	1.88	1.87	1.99	1.83	1.88	1.91	1.89	1.77	1.93	1.86	1.80	1.77	1.82	1.75	1.86	1.91	1.76
Pr	141	0.149	0.197	0.176	0.206	0.331	0.292	0.200	0.194	0.204	0.169	0.209	0.217	0.188	0.158	0.173	0.203	0.195	0.171	0.169	0.181
Nd	146	0.948	0.832	0.923	1.03	0.795	0.925	0.850	0.909	0.956	0.828	0.758	0.942	0.863	0.900	0.856	0.857	0.903	0.780	0.836	0.761
Sm	147	bd	0.217	bd	0.227	bd	bd	bd	0.206	bd	0.242	bd	bd	bd	0.178	bd	bd	bd	bd	bd	bd
Eu	151	0.428	0.386	0.411	0.346	0.433	0.377	0.458	0.367	0.440	0.390	0.427	0.381	0.367	0.402	0.399	0.438	0.405	0.410	0.417	0.424
Gd	157	0.206	bd	0.230	0.168	bd	bd	bd	bd	bd	bd	0.192	bd	bd	bd	0.236	0.152	bd	bd	bd	bd
Tb	159	bd	0.017	bd	bd	0.043	bd	bd	0.025	bd	0.019	0.022	bd	bd	0.039	bd	bd	0.023	bd	bd	bd
Dy	163	bd	bd	bd	bd	bd	bd	bd	bd	bd	bd	0.096	bd	0.139	bd	bd	bd	bd	bd	bd	bd
Ho	165	bd	bd	bd	bd	bd	bd	bd	bd	bd	bd	bd	bd	bd	bd	bd	bd	bd	bd	bd	bd
Tm	169	bd	bd	bd	bd	bd	bd	bd	bd	bd	bd	bd	bd	bd	bd	bd	bd	bd	bd	bd	bd

Tab An06 Chemical compositions of copper-bearing andesine from different mines in Tibet (in µg/g, non-averaged)

		2010-111239											2010-111242								
		Yu Lin Gu, Abduriyim, 2.489ct, Sept2010											Zhalin, Abduriyim, 1.619ct, Sept2010								
		surface											surface								
Li	7	9.33	9.41	7.90	8.12	7.47	7.85	8.56	8.66	8.68	7.38	7.10	10.9	8.08	7.91	7.24	8.02	7.61	6.95	8.62	6.08
Na	23	39800	39100	39800	39500	39600	39900	40400	40400	40000	39600	40000	41100	41100	40500	40900	38300	39900	39500	39900	39700
Mg	24	490	496	473	478	469	469	507	492	500	481	456	500	476	497	504	473	503	499	512	495
Al*	27	147000	147000	147000	147000	147000	147000	147000	147000	147000	147000	147000	147000	147000	147000	147000	147000	147000	147000	147000	147000
Si	29	261600	259000	272400	260800	260200	258100	254200	251800	257000	259100	249800	266000	263700	265400	239900	250500	247100	253900	248100	247200
K	39	3990	3960	4310	4170	4280	4250	4050	4050	3890	4010	4530	4040	3970	3880	4330	3570	3920	3850	3910	3860
Ca	42	65100	64300	66300	64900	64600	66200	65300	66400	65300	64900	64200	66600	65800	66600	66900	67700	64200	65400	64700	64600
Sc	45	0.185	0.364	0.296	0.335	bd	0.225	0.297	0.252	0.267	bd	bd	bd	bd	0.173	bd	0.226	0.326	0.224	bd	0.240
Ti	49	359	347	371	358	354	370	351	354	352	348	344	381	371	378	396	365	351	364	365	356
V	51	1.44	1.47	1.41	1.61	1.67	1.43	1.45	1.35	1.49	1.58	1.35	1.85	1.93	1.60	1.45	1.42	1.47	1.58	1.52	1.25
Mn	55	30.3	30.2	30.9	30.6	28.9	28.9	30.4	30.1	30.3	30.7	28.3	31.2	33.3	31.1	29.3	30.4	29.9	29.7	29.8	29.5
Fe	57	2750	2740	2810	2770	2730	2720	2770	2670	2740	2740	2690	2940	3030	2960	2700	2630	2750	2690	2690	2730
Co	59	0.537	0.485	0.439	0.385	0.501	0.358	0.512	0.547	0.442	0.445	0.433	0.419	0.422	0.589	0.385	0.439	0.429	0.430	0.481	0.378
Ni	60	bd	0.766	1.29	1.97	6.68	2.69	0.859	0.742	bd	bd	1.65	0.876	0.633	0.737	bd	bd	bd	bd	bd	bd
Cu	65	378	339	309	283	267	268	328	332	352	321	264	423	454	433	398	672	468	397	470	383
Zn	66	3.64	3.13	4.22	3.87	4.50	2.73	2.88	2.06	3.52	2.89	2.37	3.96	3.85	3.80	3.19	4.04	4.08	2.54	2.69	3.02
Ga	71	17.7	16.9	17.5	17.7	17.5	17.0	17.0	17.8	16.7	17.5	17.8	17.1	17.3	17.0	18.4	17.3	16.7	16.4	17.2	16.6
Ge	72	1.29	bd	0.885	0.697	0.883	1.12	0.915	bd	1.18	bd	1.42	bd	0.723	1.00	bd	0.855	1.200	bd	0.900	0.962
Rb	85	0.853	0.779	0.831	0.825	0.784	0.991	0.820	0.897	0.774	0.863	0.714	0.871	1.02	0.887	0.987	0.844	0.795	0.812	0.808	0.718
Sr	88	1130	1120	1120	1110	1090	1100	1100	1110	1110	1110	1060	1150	1150	1150	1140	1160	1100	1120	1100	1110
Y	89	0.149	0.118	0.157	0.187	0.208	0.122	0.205	0.133	0.161	0.166	0.144	0.136	0.137	0.128	0.184	0.176	0.144	0.186	0.157	0.161
Zr	90	bd	bd	bd	bd	bd	bd	bd	0.059	bd	bd	bd	1.400	0.460	bd	bd	bd	bd	bd	bd	bd
Ag	107	722	665	684	697	674	671	723	727	664	669	700	0.364	0.312	0.246	0.282	0.185	bd	bd	bd	bd
Ba	137	129	130	131	130	127	128	128	126	129	127	127	137	138	137	136	120	132	129	129	137
Pb	208	0.608	0.579	0.410	0.394	0.469	0.353	0.476	0.438	0.465	0.437	0.344	0.546	0.522	0.469	0.385	0.420	0.425	0.375	0.372	0.310
U	238	bd	bd	bd	bd	bd	0.019	0.220	bd	bd	0.017	bd	bd	bd	bd	0.037	bd	bd	bd	bd	0.062
La	139	1.14	1.10	1.11	1.12	1.12	1.06	1.11	1.12	1.12	1.07	1.06	1.28	1.23	1.16	1.23	1.22	1.18	1.13	1.17	1.27
Ce	140	1.89	1.98	1.88	1.87	1.85	1.79	1.89	1.80	1.80	1.80	1.75	1.96	2.03	1.96	2.03	1.96	1.93	1.96	1.87	1.95
Pr	141	0.442	0.196	0.230	0.189	0.209	0.261	0.196	0.196	0.214	0.164	0.195	0.210	0.205	0.225	0.188	0.194	0.183	0.198	0.152	0.183
Nd	146	1.01	0.804	1.00	1.00	0.759	0.748	0.849	0.850	0.762	0.902	0.995	0.940	1.07	0.942	0.820	0.935	1.02	1.05	0.925	1.06
Sm	147	bd	0.237	bd	0.341	0.256	0.235	bd	bd	bd	bd	bd	0.277	bd	bd	bd	0.279	0.277	0.246	bd	bd
Eu	151	0.356	0.371	0.521	0.378	0.432	0.373	0.396	0.430	0.420	0.366	0.414	0.459	0.393	0.449	0.420	0.485	0.417	0.495	0.424	0.444
Gd	157	bd	bd	bd	bd	0.304	bd	bd	bd	bd	bd	bd	bd	0.166	bd	bd	bd	bd	bd	bd	bd
Tb	159	bd	bd	0.055	bd	bd	bd	bd	bd	bd	bd	0.053	bd	bd	bd	bd	bd	bd	0.027	0.031	bd
Dy	163	bd	bd	0.124	bd	bd	bd	bd	bd	0.111	bd	bd	bd	bd	0.073	bd	bd	bd	bd	bd	bd
Ho	165	bd	0.194	bd	bd	bd	bd	bd	bd	bd	bd	bd	bd	bd	bd	bd	bd	bd	bd	bd	bd
Tm	169	bd	bd	bd	bd	0.029	bd	bd	bd	bd	bd	bd	bd	0.022	0.034	bd	bd	bd	bd	bd	bd

Tab An07 Chemical compositions of copper-bearing andesine from different mines in Tibet (in µg/g , non-averaged)

		A2		A2		A3		A3		A3		A3		A4		A5		A5		A5	
		2010-111235		2010-111237		2010_Hughes		2010_Hughes B		2010-111238		2010-111241		2010-111243		B-large		2010-112728		A-large	
		Bainang 2008, Abduriyim		Bainang 2008, Abduriyim		Hughes, Yu Lin Gu Sept. 30. 2010		Yu Lin Gu Hughes, 2.75ct		Yu Lin Gu, Abduriyim, 5.62ct		Yu Lin Gu, Abduriyim, 6.99ct		Zha Lin Mine, Sept. 2010		Yu Lin Gu, Abduriyim 2010		Yu Lin Gu, Abduriyim 2010		Yu Lin Gu, Abduriyim 2010	
		avg(20)	stdev	avg(2)	stdev	avg(60)	stdev	avg(2)	stdev	avg(2)	stdev	avg(2)	stdev	avg(2)	stdev	avg(39)	stdev	avg(36)	stdev	avg(24)	stdev
Li	7	38.4	3.8	23.1	1.1	9.79	0.80	8.13	0.93	20.9	3.2	12.6	2.1	6.93	0.01	11.8	1.4	8.61	2.09	133	10
Na	23	40430	1941	37350	495	41360	1390	39650	495	40400	707	38800	707	40900	141	42226	887	41242	760	39784	476
Mg	24	491	32	499	10	490	46	461	23	490	1	421	27	452	4	515	13	494	8	487	7
Al*	27	147000	-	147000	-	147000	-	147000	-	147000	-	147000	-	147000	-	147000	-	147000	-	147000	
Si	29	283320	10901	278450	1061	280853	8050	273800	1697	281250	7707	299200	1980	296100	849	284551	5638	276172	6644	259732	4778
K	39	3846	282	3610	14	4020	332	4250	28	4195	78	4740	0	4400	14	4121	125	4216	66	4088	65
Ca	42	64805	2291	64300	566	69215	2386	62450	495	60800	1556	61700	1131	61250	71	63067	505	64242	720	65256	782
Sc	45	0.351	0.087	0.317	0.002	0.237	0.034	0.259	0.057	0.336	0.002	0.321	0.023	0.423	0.029	0.343	0.054	0.263	0.051	0.258	0.056
Ti	49	384	76	357	5	358	18	355	3	359	11	365	7	356	1	373	7	364	6	364	5
V	51	1.44	0.08	1.40	0.02	1.41	0.17	1.35	0.03	1.33	0.10	1.36	0.11	1.42	0.04	1.60	0.20	1.48	0.09	1.52	0.12
Mn	55	29.9	2.1	30.6	0.1	27.4	1.9	28.1	0.8	27.0	0.8	28.0	0.3	25.9	0.9	29.7	0.7	29.5	0.6	30.1	0.5
Fe	57	2783	107	2710	14	2772	136	2870	57	2715	7	2910	28	2785	7	2827	62	2843	57	2779	53
Co	59	0.446	0.063	0.478	0.035	0.410	0.066	0.386	0.032	0.457	0.025	0.391	0.030	0.426	0.034	0.560	0.164	0.501	0.185	0.465	0.072
Ni	60	1.42	1.52	0.462	-	0.294	0.201	1.16	0.77	0.494	0.161	8.98	4.55	0.831	0.409	1.26	2.00	0.732	0.239	1.03	0.31
Cu	65	599	105	498	16	689	122	356	72	826	73	438	83	394	23	808	102	680	79	1450	102
Zn	66	3.78	1.64	3.13	0.21	2.53	0.51	4.02	0.54	3.46	0.06	3.41	0.42	2.85	0.06	3.38	0.43	3.24	0.39	3.18	0.46
Ga	71	17.4	1.0	15.7	0.1	15.4	0.9	16.7	0.1	16.3	0.0	16.4	0.1	16.3	0.0	17.7	0.5	17.3	0.5	17.2	0.4
Ge	72	0.805	0.212	0.718	0.033	0.702	0.092	0.763	0.064	0.510	0.045	0.701	0.219	0.820	0.129	0.877	0.413	0.801	0.139	0.935	0.201
Rb	85	0.766	0.047	0.670	0.050	0.793	0.082	0.809	0.057	0.805	0.002	0.873	0.008	0.873	0.026	0.934	0.160	0.854	0.057	0.888	0.186
Sr	88	1095	31	1085	35	1048	34	1045	7.1	1040	0	1090	0	1070	14	1131	24	1126	27	1143	13
Y	89	0.136	0.022	0.170	0.022	0.153	0.029	0.148	0.004	0.127	0.013	0.133	0.016	0.147	0.000	0.144	0.019	0.146	0.017	0.155	0.015
Zr	90	0.089	0.080	bd	-	0.151	0.242	0.039	-	bd	-	bd	-	0.049	-	0.061	0.016	0.059	0.014	0.084	0.014
Ag	107	0.135	0.016	bd	-	217	253	591	60	683	78	462	37	bd	-	220	393	535	388	907	190
Ba	137	126	4	118	2	128	5	136	3	133	4	133	3	136	1	139	2	133	2	133	2
Pb	208	0.478	0.128	0.403	0.031	0.373	0.037	0.557	0.025	0.497	0.023	0.413	0.035	0.502	0.074	0.530	0.132	0.445	0.047	0.484	0.106
U	238	0.022	0.018	bd	-	0.023	0.034	bd	-	bd	-	0.268	-	0.125	0.102	0.141	0.110	0.029	0.024	0.090	0.074
La	139	1.09	0.04	1.10	0.01	1.12	0.05	1.07	0.02	1.04	0.01	1.11	0.01	1.08	0.04	1.19	0.06	1.14	0.04	1.19	0.05
Ce	140	1.86	0.09	1.78	0.00	1.85	0.08	1.72	0.05	1.74	0.12	1.69	0.04	1.68	0.04	1.97	0.10	1.90	0.07	1.98	0.10
Pr	141	0.189	0.017	0.215	0.030	0.195	0.013	0.209	0.018	0.185	0.006	0.185	0.012	0.213	0.021	0.214	0.067	0.188	0.021	0.218	0.035
Nd	146	0.878	0.134	0.830	0.014	0.825	0.077	0.886	0.018	0.774	0.052	0.726	0.098	0.765	0.009	0.910	0.101	0.873	0.076	0.962	0.109
Sm	147	0.168	0.045	0.203	0.029	0.137	0.028	0.163	0.021	0.200	0.013	0.142	-	0.283	-	0.192	0.055	0.195	0.041	0.236	0.065
Eu	151	0.405	0.038	0.371	0.016	0.360	0.027	0.398	0.011	0.410	0.032	0.415	0.015	0.426	0.007	0.407	0.046	0.401	0.037	0.410	0.044
Gd	157	0.140	0.038	bd	-	0.091	0.019	0.094	-	0.140	0.023	bd	-	0.140	-	0.161	0.037	0.160	0.028	0.194	0.033
Tb	159	0.016	0.001	0.011	-	0.010	0.004	0.014	-	bd	-	0.016	-	0.017	0.000	0.027	0.015	0.025	0.010	0.032	0.008
Dy	163	0.092	0.011	bd	-	0.043	0.012	bd	-	bd	-	0.082	-	bd	-	0.092	0.015	0.088	0.015	0.149	0.060
Ho	165	0.015	0.004	bd	-	0.010	0.002	0.022	-	bd	-	bd	-	bd	-	0.024	0.007	0.020	0.005	0.029	0.011
Tm	169	0.021	0.001	bd	-	0.009	-	bd	-	bd	-	bd	-	bd	-	0.018	0.010	0.058	-	0.033	0.008

Tab An09 Chemical compositions of copper-bearing andesine from different mines in Tibet (in µ g/g, averaged)

		B		B		B		B		C2		C2		C2		C2		C2	
		Gyaca_Mine 2		Gyaca_Mine 2		Ref10808		Ref10797-1		Ref10694		Ref10696		Ref10698		Ref10695		Ref10697	
		Gyaca 2009 Expedition		Gyaca 2009 Expedition		Gyaca 2009 Expedition, 3.51ct		Gyaca 2009 Peretti Expedition		New Mine, Tibet, Litto		New Mine, Tibet, Litto		New Mine, Tibet, King Jewel 2009		Tibet, new mine, Litto		New Mine, Tibet, Litto	
		avg(14)	stdev	avg(12)	stdev	avg(2)	stdev	avg(36)	stdev	avg(2)	stdev	avg(2)	stdev	avg(4)	stdev	avg(5)	stdev	avg(2)	stdev
Li	7	42.8	21.4	22.8	5.2	24.5	3.8	35.9	3.1	14.2	0.7	21.8	0.4	14.2	0.6	43.3	3.1	13.1	1.2
Na	23	38643	947	38075	1186	37800	283	40644	1157	37250	354	38600	707	38775	340	37820	572	37500	707
Mg	24	484	6	470	16	491	4	501	13	476	7	476	-	472	4	486	2	479	7
Al*	27	147000	-	147000	-	147000	-	147000	-	147000	-	147000	-	147000	-	147000	-	147000	-
Si	29	279971	6538	282292	5936	290400	3253	280756	8187	264950	919	270300	2121	269800	1575	272680	1754	265150	1626
K	39	3976	170	3858	205	3675	21	3811	107	3710	14	3985	21	3848	41	3736	34	3730	71
Ca	42	63179	958	62675	839	62800	283	66850	516	64100	566	64150	71	61225	695	65200	644	65650	919
Sc	45	0.343	0.077	0.342	0.077	0.316	0.035	0.354	0.061	0.449	0.086	0.471	0.034	0.289	0.051	0.364	0.029	0.382	0.052
Ti	49	359	8	359	5	357	4	366	7	340	3	351	3	354	3	357	4	340	1
V	51	1.36	0.04	1.34	0.06	1.37	0.02	1.57	0.10	1.30	0.08	1.35	0.04	1.36	0.05	1.32	0.04	1.42	0.06
Mn	55	29.1	0.5	28.7	0.7	29.6	0.2	31.8	0.8	29.8	0.2	29.5	0.1	28.2	0.3	28.9	0.2	29.5	0.1
Fe	57	2730	51	2661	52	2745	7	2822	79	2515	21	2585	21	2690	32	2604	30	2440	0
Co	59	0.439	0.047	0.423	0.033	0.442	0.005	0.498	0.072	0.537	0.075	0.465	0.085	0.428	0.052	0.468	0.016	0.397	0.056
Ni	60	0.310	0.073	0.481	-	0.397	-	0.636	0.658	0.200	0.074	0.627	-	bd	-	bd	-	bd	-
Cu	65	721	132	839	183	573	47	858	129	543	10	558	19	507	17	615	37	479	2
Zn	66	3.01	0.44	2.65	0.28	3.32	0.11	2.94	0.44	2.96	0.18	3.05	0.04	2.92	0.44	2.83	0.34	2.50	0.15
Ga	71	16.2	0.5	15.7	0.4	16.1	0.3	17.1	0.5	15.7	0.2	16.2	0.4	16.2	0.3	16.0	0.5	14.8	0.1
Ge	72	0.677	0.127	0.677	0.200	0.680	0.024	0.910	0.484	0.675	0.120	0.688	0.059	0.735	0.130	0.686	0.112	0.700	0.020
Rb	85	0.711	0.047	0.690	0.060	0.697	0.043	0.766	0.072	0.663	0.001	0.695	0.032	0.704	0.006	0.683	0.050	0.754	0.032
Sr	88	1083	17	1053	11	1080	14	1141	20	1045	7	1065	7	1023	13	1021	18	1004	9
Y	89	0.141	0.018	0.143	0.015	0.123	0.002	0.151	0.022	0.144	0.007	0.132	0.013	0.120	0.003	0.141	0.008	0.147	0.024
Zr	90	0.047	0.008	0.046	0.013	0.041	0.002	0.063	0.020	0.030	-	0.035	0.002	0.043	-	0.052	0.007	bd	-
Ag	107	99	130	177	153	1.49	0.05	174	245	238	127	1260	184	615	757	128	172	138	165
Ba	137	126	9	123	7	120	2	117	2	105	0	120	1	124	2	119	3	101	2
Pb	208	0.517	0.063	0.416	0.034	0.573	0.093	0.392	0.070	0.507	0.011	0.614	0.048	0.446	0.043	0.473	0.070	0.492	0.051
U	238	0.020	0.002	0.023	-	bd	-	0.106	0.145	bd	-	bd	-	bd	-	0.156	-	0.022	-
La	139	1.12	0.04	1.09	0.03	1.16	0.00	1.11	0.04	1.08	0.00	1.09	0.01	1.06	0.04	1.11	0.03	1.04	0.04
Ce	140	1.82	0.06	1.76	0.05	1.87	0.07	1.94	0.09	1.78	0.02	1.76	0.06	1.76	0.04	1.82	0.05	1.71	0.01
Pr	141	0.200	0.015	0.194	0.020	0.206	0.022	0.193	0.026	0.179	0.015	0.184	0.003	0.197	0.020	0.197	0.013	0.181	0.001
Nd	146	0.867	0.101	0.857	0.081	0.908	0.015	0.828	0.082	0.879	0.001	0.807	0.026	0.851	0.046	0.915	0.028	0.826	0.111
Sm	147	0.168	0.026	0.181	0.039	0.106	0.006	0.194	0.044	0.209	0.073	0.183	-	0.166	0.044	0.171	0.013	0.152	0.001
Eu	151	0.389	0.030	0.379	0.043	0.366	0.010	0.411	0.045	0.368	0.010	0.376	0.033	0.381	0.040	0.396	0.034	0.376	0.026
Gd	157	0.135	0.020	0.129	0.034	bd	-	0.166	0.028	0.109	-	0.109	-	0.176	-	0.140	0.016	0.115	-
Tb	159	0.016	0.003	0.018	-	0.014	-	0.026	0.005	bd	-	0.012	0.000	0.013	-	bd	-	0.022	-
Dy	163	0.079	0.013	0.101	0.008	bd	-	0.101	0.021	0.063	-	bd	-	0.065	0.011	0.084	0.010	0.074	0.022
Ho	165	0.019	0.007	0.014	-	bd	-	0.023	0.003	bd	-	bd	-	bd	-	0.010	-	bd	-
Tm	169	bd	-	bd	-	0.009	-	0.031	0.014	bd	-	bd	-	bd	-	bd	-	bd	-

		D		D		E		E1		E1		E1		E1		E1	
		Ref2288		Ref2289		Ref10809		Ref8114		Ref8111		Ref8109		Ref8110		Ref8113	
		"Congo", Tucson 2006		"Congo", Tucson 2006		Hong Kong market, unknown		Tibet, Litto, ICA Show Dubai 2008		Tibet, Litto, ICA Show Dubai 2008		Tibet, Litto, ICA Show Dubai 2008		Tibet, Litto, ICA Show Dubai 2008		Tibet, Litto, ICA Show Dubai 2008	
		avg(2)	stdev	avg(2)	stdev	avg(2)	stdev	avg(2)	stdev	avg(2)	stdev	avg(2)	stdev	avg(2)	stdev	avg(2)	stdev
Li	7	24.0	0.5	17.0	0.4	10.7	0.6	10.5	0.3	88.7	8.1	7.81	0.49	76.3	1.9	8.1	0.4
Na	23	38050	354	38200	141	39050	636	37600	424	39250	212	36850	212	38750	636	37200	141
Mg	24	480	4	489	5	487	8	478	4	449	1	482	2	481	12	479	3
Al*	27	147000	-	147000	-	147000	-	147000	-	147000	-	147000	-	147000	-	147000	-
Si	29	266750	2333	276100	3394	274500	1980	275950	1344	271200	4384	266800	2970	271500	283	282900	990
K	39	3715	35	3780	28	3945	64	3675	78	4140	0	3535	7	3955	49	3590	28
Ca	42	62750	354	63900	141	63700	283	64050	71	62400	424	63350	495	64250	212	65200	141
Sc	45	0.340	0.022	0.344	0.052	0.433	0.003	0.293	0.049	0.309	0.018	0.266	0.013	0.408	0.063	0.411	0.083
Ti	49	351	6	358	1	350	6	356	13	358	8	352	0	355	2	351	3
V	51	1.43	0.01	1.37	0.06	1.40	0.00	1.38	0.01	1.35	0.02	1.35	0.02	1.38	0.05	1.39	0.04
Mn	55	28.8	0.0	28.9	0.2	29.3	0.1	28.8	0.1	27.6	0.1	28.9	0.4	28.5	0.1	29.5	0.4
Fe	57	2625	7	2635	35	2680	28	2605	35	2740	42	2600	28	2640	14	2645	35
Co	59	0.404	0.025	0.454	0.025	0.391	0.035	0.502	0.090	0.420	0.001	0.433	0.083	0.422	0.030	0.451	0.050
Ni	60	bd	-	bd	-	0.242	-	bd	-	bd	-	bd	-	0.587	-	bd	-
Cu	65	412	18	401	8	966	175	565	14	418	-	508	1	909	11	448	4
Zn	66	3.07	0.04	3.21	0.03	3.18	0.76	2.79	0.35	2.99	0.21	2.98	0.38	3.50	0.62	2.95	0.04
Ga	71	15.8	0.1	16.0	0.1	16.1	0.2	15.6	0.2	16.3	0.4	15.6	0.1	15.6	0.1	16.0	0.2
Ge	72	0.690	0.086	0.613	0.244	0.755	0.299	0.494	0.125	0.864	0.033	0.622	0.143	0.611	0.103	0.643	0.030
Rb	85	0.657	0.024	0.726	0.027	0.687	0.041	0.692	0.000	0.758	0.003	0.594	0.027	0.694	0.028	0.717	0.034
Sr	88	1020	0	1003	11	1055	7	1002	11	1015	22	987	1	1015	7	1055	21
Y	89	0.126	0.009	0.135	0.013	0.136	0.013	0.135	0.005	0.135	0.012	0.143	0.002	0.148	0.030	0.163	0.008
Zr	90	0.043	-	0.039	0.001	0.035	-	0.056	0.003	bd	-	bd	-	bd	-	0.046	0.013
Ag	107	bd	-	bd	-	0.078	-	0.095	-	bd	-	bd	-	bd	-	bd	-
Ba	137	115	2	118	1	119	2	117	1	136	2	115	3	125	2	117	0
Pb	208	0.444	0.030	0.468	0.016	0.525	0.062	0.432	0.025	0.533	0.086	0.454	0.010	0.605	0.040	0.507	0.015
U	238	bd	-	bd	-	bd	-	bd	-	bd	-	bd	-	bd	-	bd	-
La	139	1.02	0.03	1.08	0.03	1.09	0.03	1.05	0.04	1.09	0.01	1.07	0.01	1.10	0.01	1.08	0.01
Ce	140	1.71	0.00	1.74	0.08	1.79	0.04	1.71	0.01	1.78	0.01	1.71	0.04	1.82	0.08	1.82	0.12
Pr	141	0.185	0.001	0.191	0.003	0.197	0.018	0.186	0.008	0.188	0.011	0.212	0.001	0.204	0.001	0.208	0.010
Nd	146	0.873	0.129	0.838	0.004	0.957	0.117	0.825	0.103	0.849	0.092	0.876	0.019	0.885	0.040	0.927	0.132
Sm	147	0.139	0.013	0.148	-	0.146	0.028	0.211	0.078	0.175	0.109	0.146	0.003	bd	-	0.182	-
Eu	151	0.366	0.045	0.326	0.018	0.397	0.008	0.372	0.008	0.409	0.040	0.359	0.006	0.407	0.004	0.350	0.019
Gd	157	0.083	-	0.114	-	0.139	-	0.116	-	bd	-	0.114	-	bd	-	0.162	-
Tb	159	bd	-	0.014	-	bd	-	bd	-	bd	-	bd	-	bd	-	bd	-
Dy	163	bd	-	0.079	-	0.070	-	bd	-	0.064	-	bd	-	0.060	-	bd	-
Ho	165	bd	-	bd	-	bd	-	0.181	-	bd	-	0.011	-	bd	-	bd	-
Tm	169	bd	-	bd	-	bd	-	bd	-	bd	-	bd	-	bd	-	bd	-

Tab An10 Chemical compositions of copper-bearing andesine from different sources in the market (in µg/g, averaged)

		E2	E2	E2	E2	E2	E2	E2	E2	E2	E2	E2	E2	E2	E2	E2	E2
		2011-051496	2011-051501	2011-051507	2011-051511	2011-051522	2011-051526	2011-051531	2011-051506	2011-051489	2011-051530	2011-051520	2011-051495	2011-051534	2011-051525	2011-051486	2011-051524
		vivid red	vivid red	vivid red	vivid red	vivid red	vivid red	vivid orangey red	orangey red	orangey red	orangey red	pastel bluish green	green	green	color-changing deep bluish green to	color-changing bluish green to orangy red	color-changing bluish green to brownish
		avg(2)	avg(2)	avg(2)	avg(2)	avg(2)	avg(2)	avg(2)	avg(2)	avg(2)	avg(2)	avg(2)	avg(2)	avg(2)	avg(2)	avg(2)	avg(2)
Li	7	8.86	7.99	7.41	8.26	6.39	9.38	8.50	11.6	9.18	25.0	7.63	6.79	7.61	8.10	8.16	26.1
Na	23	34350	35850	34100	35900	36000	35750	34350	34550	36600	34800	33850	35550	34250	35850	35200	35450
Mg	24	478	481	484	482	458	480	478	463	471	477	463	465	478	467	462	474
Al*	27	147000	147000	147000	147000	147000	147000	147000	147000	147000	147000	147000	147000	147000	147000	147000	147000
Si	29	256000	261000	258300	267750	264450	254850	253700	262850	268500	260350	250100	256850	258900	263550	264950	261800
K	39	3370	3810	3450	3665	3580	3830	3745	3375	3760	3500	3340	3535	3500	3775	3445	3515
Ca	42	65750	65400	65150	66350	64150	65250	66350	64700	63850	65750	64400	63600	65600	65650	65800	64900
Sc	45	0.375	0.376	0.345	0.510	0.320	0.353	0.378	0.315	0.405	0.354	0.452	0.419	0.331	0.425	0.361	0.442
Ti	49	369	356	347	362	362	341	343	353	364	371	339	349	335	350	358	360
V	51	1.45	1.48	1.32	1.29	1.62	1.28	1.28	1.36	1.50	1.40	1.17	1.36	1.18	1.25	1.44	1.61
Mn	55	28.7	29.4	29.6	29.6	28.0	28.9	28.7	28.6	28.1	30.1	29.6	28.4	28.8	28.9	28.9	28.3
Fe	57	2585	2590	2500	2710	2675	2370	2365	2540	2665	2655	2420	2580	2420	2680	2640	2570
Co	59	0.505	0.559	0.515	0.514	1.04	0.599	0.494	0.462	0.447	0.473	0.508	0.503	0.426	0.503	0.518	0.557
Ni	60	0.450	bd	bd	bd	bd	0.415	0.490	bd	0.576	bd	0.642	bd	bd	bd	bd	bd
Cu	65	514	493	509	523	350	679	482	468	571	368	371	468	528	532	576	555
Zn	66	10.8	3.25	2.84	5.85	2.57	4.00	5.51	4.69	5.85	3.96	9.96	9.15	4.22	5.06	5.78	3.48
Ga	71	15.0	15	13.8	15.4	15.5	14.8	15.8	15.3	14.6	15.2	15.1	15.4	25.3	13.7	14.6	16.0
Ge	72	0.716	0.568	bd	bd	0.980	0.592	0.990	0.736	0.567	0.864	6.42	0.597	0.808	0.784	0.633	0.901
Rb	85	0.646	0.565	0.719	0.713	0.751	0.748	0.720	0.665	0.972	0.775	0.897	0.649	0.731	0.697	0.573	0.691
Sr	88	1060	1110	1100	1130	1140	1060	1130	1095	1135	1075	1110	1090	1100	1080	1130	1155
Y	89	0.153	0.162	0.149	0.122	0.145	0.191	0.184	0.136	0.145	0.164	0.151	0.133	0.311	0.121	0.164	0.148
Zr	90	0.076	bd	bd	bd	bd	0.046	0.081	0.097	bd	0.056	bd	0.076	0.174	bd	bd	bd
Ag	107	bd	bd	bd	bd	bd	bd	bd	bd	0.088	bd	bd	bd	bd	bd	bd	bd
Ba	137	112	116	117	110	116	98.5	124	116	115	114	101	114	125	95.5	115	118
Pb	208	3.41	0.501	0.406	1.35	0.543	0.620	2.49	1.08	2.61	0.741	3.70	2.85	1.45	0.638	2.77	0.592
U	238	bd	bd	bd	bd	bd	0.046	bd	bd	bd	0.021	0.023	bd	0.068	0.057	bd	bd
La	139	1.08	1.13	1.14	1.13	1.15	1.15	1.22	1.10	1.18	1.13	1.09	1.11	1.18	1.11	1.18	1.16
Ce	140	1.76	1.85	1.87	1.86	1.71	1.79	1.85	1.70	1.80	1.67	1.70	1.77	1.89	1.86	1.81	1.82
Pr	141	0.200	0.214	0.218	0.180	0.196	0.194	0.162	0.193	0.219	0.223	0.160	0.201	0.311	0.237	0.232	0.203
Nd	146	0.923	0.799	0.899	0.965	0.957	0.807	0.816	0.951	0.904	1.00	0.929	0.934	0.775	1.16	0.807	0.877
Sm	147	0.235	0.197	bd	0.169	bd	0.208	0.189	0.237	bd	0.173	bd	0.182	0.165	bd	bd	0.125
Eu	151	0.440	0.492	0.355	0.467	0.360	0.400	0.436	0.446	0.426	0.360	0.435	0.428	0.412	0.348	0.486	0.325
Gd	157	bd	bd	bd	0.175	bd	0.165	bd	bd	bd	0.149	bd	bd	bd	bd	bd	bd
Tb	159	bd	bd	bd	bd	bd	0.034	bd	bd	bd	0.035	bd	bd	0.085	bd	bd	bd
Dy	163	bd	bd	bd	bd	bd	0.090	0.109	0.102	bd	bd	bd	bd	0.156	bd	bd	bd
Ho	165	bd	bd	bd	bd	bd	bd	0.034	0.026	bd	0.038	bd	bd	0.025	bd	bd	bd
Tm	169	bd	bd	bd	bd	bd	bd	bd	bd	bd	bd	bd	bd	bd	bd	bd	bd

Tab An11 Chemical compositions of copper-bearing andesine from the market 2011 (in µg/g, averaged)

				F2		F3		F4		G		G		G		G		G	
		Ref8028		Desert Sun		Ponderosa		Modoc's Eye		Ref10678		Ref10681		Ref10688		Ref10680		AA-Xian_1	
		Oregon		Oregon		Oregon		Oregon		Inner Mongolia, Litto, diffusion-treated		Inner Mongolia, Litto, diffusion-treated		Inner Mongolia, Litto, diffusion-treated		Inner Mongolia, Litto, diffusion-treated		Diffusion-treated, Abduriyim	
		avg(2)	stdev	avg(85)	stdev	avg(22)	stdev	avg(70)	stdev	avg(2)	stdev	avg(2)	stdev	avg(2)	stdev	avg(2)	stdev	avg(2)	stdev
Li	7	2.54	0.34	8.97	1.72	20.5	1.5	13.7	5.6	30.6	4.5	15.2	0.6	12.4	0.2	21.6	0.3	17.3	1.5
Na	23	24550	212	21067	532	18859	678	21639	668	39400	283	37750	71	37650	71	38650	212	37450	919
Mg	24	771	21	860	14	792	14	867	32	480	3	474	1	484	8	480	1	468	-
Al*	27	147000	-	147000	-	147000	-	147000	-	147000	-	147000	-	147000	-	147000	-	147000	-
Si	29	228800	1980	225275	9143	210495	6558	225456	7433	281050	212	273150	4313	279700	2828	294850	3182	265150	7000
K	39	970	1	437	35	338	19	398	19	4095	21	3760	42	3725	21	3745	35	3695	64
Ca	42	80700	707	88746	2991	77491	1757	80430	1806	61200	141	62100	424	62150	212	63250	71	64150	212
Sc	45	0.392	0.054	0.407	0.072	0.386	0.057	0.309	0.070	0.295	0.017	0.285	0.011	0.322	0.035	0.381	0.104	0.403	0.064
Ti	49	205	2	154	10	132	5	140	4	366	6	355	6	339	2	352	13	347	2
V	51	2.20	0.07	2.08	0.15	1.83	0.16	1.98	0.19	1.39	0.03	1.21	0.01	1.33	0.04	1.30	0.06	1.38	0.10
Mn	55	35.8	0.1	33.0	1.3	34.5	0.7	35.6	0.9	27.8	0.8	28.6	0.6	28.8	0.1	29.7	0.3	28.9	0.2
Fe	57	3090	28	2516	89	2552	77	2599	75	2655	7	2715	21	2500	14	2560	14	2575	21
Co	59	0.511	0.019	0.543	0.074	0.530	0.085	0.575	0.194	0.495	0.034	0.409	0.004	0.426	0.029	0.356	0.011	0.398	0.058
Ni	60	0.322	-	1.01	0.61	1.47	0.66	1.37	0.94	bd	-	bd	-	bd	-	0.696	-	0.346	-
Cu	65	13	9	91	17	174	41	79	62	723	73	658	42	563	2	616	14	520	4
Zn	66	2.78	0.09	2.77	0.59	2.59	1.52	2.07	0.73	2.84	0.16	2.89	0.63	2.91	0.08	2.48	0.68	2.52	0.61
Ga	71	14.2	0.4	11.8	0.5	10.3	0.4	11.2	0.5	15.9	0.1	15.9	0.1	15.0	0.1	15.7	0.7	15.0	0.3
Ge	72	0.849	0.192	0.681	0.210	0.582	0.125	0.697	0.214	0.774	0.142	0.589	0.174	0.654	0.039	0.868	0.187	0.759	0.182
Rb	85	0.100	0.004	0.157	0.080	0.084	0.099	0.103	0.066	0.717	0.023	0.656	0.030	0.713	0.002	0.686	0.006	0.648	0.035
Sr	88	493	8	300	9	358	8	335	15	1055	7	1035	7	1040	14	1085	7	1003	10
Y	89	0.174	0.010	0.168	0.017	0.147	0.017	0.137	0.019	0.143	0.002	0.121	0.006	0.118	0.011	0.123	0.005	0.131	0.016
Zr	90	0.035	-	0.034	0.013	0.066	0.051	0.043	0.012	bd	-	bd	-	bd	-	0.290	-	bd	-
Ag	107	bd	-	0.119	0.060	0.102	0.073	0.11	0.07	bd	-	bd	-	bd	-	bd	-	bd	-
Ba	137	59.1	1.3	12.0	1.1	9.9	0.8	11.0	0.5	130	2	124	1	98.0	1.1	110	2	115	-
Pb	208	0.300	0.049	0.303	0.189	0.134	0.093	0.162	0.158	0.594	0.059	0.406	0.009	0.365	0.059	0.392	0.005	0.427	0.052
U	238	bd	-	0.030	0.036	0.010	0.003	0.064	0.090	bd	-	bd	-	bd	-	0.023	0.003	0.087	-
La	139	0.345	0.009	0.267	0.033	0.199	0.013	0.218	0.028	1.11	0.01	1.10	0.04	0.92	0.02	0.97	0.03	1.05	0.06
Ce	140	0.653	0.048	0.521	0.059	0.386	0.026	0.460	0.099	1.76	0.01	1.74	0.11	1.63	0.05	1.69	0.02	1.74	0.00
Pr	141	0.080	0.004	0.089	0.128	0.051	0.014	0.069	0.034	0.185	0.017	0.190	0.026	0.171	0.004	0.182	0.006	0.185	0.031
Nd	146	0.443	0.019	0.302	0.056	0.280	0.049	0.310	0.097	0.841	0.043	0.833	0.063	0.705	0.075	0.837	0.115	0.822	0.124
Sm	147	0.099	-	0.096	0.028	0.082	0.015	0.128	0.041	0.147	-	0.110	0.008	0.118	-	0.170	-	0.160	-
Eu	151	0.204	0.011	0.148	0.033	0.115	0.022	0.140	0.034	0.538	0.216	0.383	0.036	0.385	0.027	0.370	0.013	0.365	0.001
Gd	157	bd	-	0.082	0.021	0.080	-	0.126	0.047	0.114	-	0.179	-	bd	-	bd	-	0.103	-
Tb	159	0.012	-	0.017	0.010	0.033	0.045	0.023	0.013	0.019	-	bd	-	bd	-	bd	-	bd	-
Dy	163	bd	-	0.055	0.016	0.047	0.011	0.069	0.025	0.078	0.014	bd	-	bd	-	0.105	-	bd	-
Ho	165	bd	-	0.015	0.007	0.013	0.001	0.017	0.008	0.013	-	0.015	-	0.013	-	bd	-	bd	-
Tm	169	bd	-	0.014	0.012	0.014	-	0.015	0.009	bd	-	bd	-	bd	-	bd	-	bd	-

Tab An13 Chemical compositions of diffusion-treated andesine and untreated andesine from Inner Mongolia (in µg/g, averaged)

				G		G1		G2		K		H		H	
		17402478		17402477		AA-Xian		AA-Shenzhen 2		10722-Cu		10722-1_colorless		Ref10785	
		diffusion-treated, Eric Braunwart		diffusion-treated, Eric Braunwart		diffusion-treated, Xian factory		diffusion-treated, Shenzhen		Cu diffusion experiment Inner Mongolia, Emmett		Inner Mongolia, Emmett		Inner Mongolia, colorless	
		avg(42)	stdev	avg(10)	stdev	avg(60)	stdev	avg(27)	stdev	avg(4)	stdev	avg(4)	stdev	avg(2)	stdev
Li	7	13.7	2.7	23.6	2.2	18.6	1.8	18.8	2.2	7.59	0.99	7.90	0.69	2.94	0.47
Na	23	38840	1104	42010	1481	40350	938	38852	589	38275	960	36475	250	37100	141
Mg	24	494	9	492	20	492	20	476	34	391	46	490	6	481	1
Al*	27	147000	-	147000	-	147000	-	147000	-	147000	-	147000	-	147000	-
Si	29	277474	8614	264590	11443	284073	7525	275281	5724	245500	5958	251125	3958	285450	212
K	39	3537	135	4278	116	3691	157	3616	89	3280	141	4233	21	3655	35
Ca	42	65305	678	63020	933	64118	644	65193	1402	65825	655	65250	1173	64300	707
Sc	45	0.296	0.162	0.328	0.072	0.358	0.055	0.362	0.073	0.407	0.104	0.432	0.028	0.314	0.017
Ti	49	342	6	370	6	358	5	362	7	345	9	334	5	342	2
V	51	1.39	0.08	1.56	0.34	1.55	0.12	1.45	0.07	3.25	1.92	1.36	0.10	1.20	0.01
Mn	55	31.0	0.8	29.3	0.8	31.3	1.1	29.7	2.3	22.4	4.7	30.8	0.7	29.7	0.3
Fe	57	2562	63	2880	77	2843	124	2773	51	2488	17	2445	19	2425	7
Co	59	0.440	0.054	0.547	0.120	0.545	0.259	0.456	0.084	0.469	0.076	0.406	0.027	0.386	0.012
Ni	60	0.397	0.114	0.448	-	0.933	0.653	0.536	0.344	7.36	5.40	0.263	-	bd	-
Cu	65	606	168	1002	71	602	58	553	45	3490	1708	0.556	0.106	0.978	0.117
Zn	66	2.89	0.41	3.27	0.58	2.99	0.49	3.10	0.81	28.68	15.28	3.02	0.34	2.82	0.04
Ga	71	16.0	0.6	17.0	0.6	17.1	0.6	16.7	0.3	15.0	0.4	15.3	0.5	15.0	-
Ge	72	0.765	0.183	1.012	0.174	0.823	0.181	0.737	0.165	0.809	0.065	0.820	0.090	0.765	0.069
Rb	85	0.764	0.062	0.850	0.075	0.759	0.119	0.702	0.049	0.785	0.070	0.724	0.035	0.688	0.002
Sr	88	1102	22	1085	31	1099	30	1134	30	1063	28	1050	24	1075	7
Y	89	0.138	0.013	0.164	0.025	0.142	0.018	0.148	0.017	0.148	0.026	0.139	0.025	0.132	0.029
Zr	90	0.054	0.007	-	-	0.065	0.020	0.068	0.017	131	170	0.028	0.016	bd	-
Ag	107	0.445	0.515	0.134	-	0.199	0.161	0.089	0.028	bd	-	bd	-	0.067	-
Ba	137	97.6	1.9	142	5	117	2	120	2	98.9	2.2	98.7	2.7	97.6	1.1
Pb	208	0.304	0.038	0.472	0.107	0.375	0.073	0.399	0.095	0.649	0.088	0.367	0.060	0.369	0.037
U	238	0.033	0.028	0.245	0.301	0.310	0.971	1.43	3.61	0.125	0.160	0.005	0.008	bd	-
La	139	1.02	0.03	1.16	0.05	1.08	0.04	1.12	0.05	1.05	0.09	1.08	0.02	1.03	0.04
Ce	140	1.72	0.06	1.93	0.12	1.84	0.07	1.88	0.07	1.70	0.03	1.80	0.09	1.63	0.01
Pr	141	0.180	0.012	0.198	0.020	0.186	0.019	0.186	0.015	0.168	0.015	0.185	0.013	0.166	0.006
Nd	146	0.807	0.089	0.904	0.117	0.851	0.104	0.861	0.100	0.846	0.050	0.776	0.084	0.769	0.155
Sm	147	0.173	0.035	0.247	-	0.177	0.044	0.188	0.048	0.107	0.057	0.164	0.030	0.122	-
Eu	151	0.363	0.039	0.409	0.054	0.389	0.041	0.408	0.039	0.371	0.073	0.380	0.052	0.379	0.033
Gd	157	0.146	0.041	0.186	0.045	0.147	0.038	0.135	0.045	0.087	0.023	0.133	0.023	0.106	-
Tb	159	0.018	0.004	0.041	0.017	0.021	0.003	0.019	0.002	0.012	0.002	0.001	0.002	bd	-
Dy	163	0.096	0.021	0.188	0.066	0.094	0.027	0.088	0.012	0.063	0.053	0.032	0.022	bd	-
Ho	165	0.014	0.001	0.021	0.005	0.020	0.007	bd	-	0.006	0.005	0.008	0.008	bd	-
Tm	169	bd	-	0.022	0.009	0.022	0.006	bd	-	0.002	0.000	0.001	0.002	bd	-

Lit.An01 Abduriyim A. (2009) A mine trip to Tibet and Inner Mongolia: Gemological study of andesine feldspar. News from Research: www.gia.edu/research-resources/news-from-research/andesine-mines-Tibet-Inner-Mongolia.pdf, Sept. 2010.

Lit.An02 Abduriyim, A. (2009) Gem News International: Visit to andesine mines in Tibet and Inner Mongolia. Gems & Gemology, Vol. 44, No. 4, Winter, pp. 369–371.

Lit.An03 Abduriyim, A. (2009) The characteristics of red andesine from the Himalaya Highland, Tibet. Journal of Gemmology, Vol. 31, No. 5–8, pp. 283–298.

Lit.An04 Abduriyim, A. & Kobayashi, T. (2009) Gem News International: Gemological properties of andesine collected in Tibet and Inner Mongolia. Gems & Gemology, Vol. 44, No. 4, Winter, pp. 371–373.

Lit.An05 Abduriyim A., Laurs B.M. (2010) Additional field research on Tibetan andesine. G&G, Vol. 46, No. 4, pp. 310–311.

Lit.An06 Abduriyim A. and Laurs B.M. (2010) New Field Research Confirms Tibetan Andesine. www.gia.edu/research-resources/.../Tibetan-andesine.pdf

Lit.An07 Abduriyim A., McClure S.F., Rossman G.R , Leelawatanasuk T., Hughes R.W., Laurs B.M., Lu R., Isatelle F., Scarratt K., Dubinsky E.V., Douthit T.R., Emmett J.L. (2011) Research on gem feldspar from the Shigatse region of Tibet," G&G, Vol. 47, No. 2, in preparation.

Lit.An08 Audetat, A., Gunther, D., and Heinrich, C.A., (1998), Formation of a magmatic-hydrothermal ore deposit: Insights with LA-ICP-MS analysis of fluid inclusions: Science, v. 279, p. 2091-2094 (46)

Lit.An09 Bruker (1999) SMART and SAINT-Plus. Versions 6.01. Bruker AXS Inc., Madison, Wisconsin, USA.

Lit.An10 Emmett J., Douthit T. (2009) Copper diffusion of plagioclase. News from Research, www.gia.edu/research-resources/news- from-research/Cu-diffusion-Emmett.pdf, Aug. 21.

Lit.An11 Federman D. (2006) Gem Profile: Andesine feldspar. Modern Jeweler, www.modernjeweler.com/print/Modern-Jeweler/Andesine-Feldspar/1$52, March.

Lit.An12 Fitzgerald, J.D.F., Parise, J.B., Mackinnon, I.D.R. (1986) Average structure of an An48 plagioclase from the Hogarth Ranges. American Mineralogist, 71, 1399-1408.

Lit.An13 Fontaine GH, Hametner K, Peretti A, Günther D. (2010) Authenticity and provenance studies of copper-bearing andesines using Cu isotope ratios and element analysis by fs-LA-MC-ICPMS and ns-LA-ICPMS. Analytical and Bioanalytical Chemistry Volume 398, Numbers 7-8, 2915-2928.

Lit.An14 Fontaine, G., Hametner K., Günther D. and Peretti A. (2009) Identification Test for Copper-bearing Gemstones (Copper-Andesine and Paraiba-type Tourmalines) Using Copper-Isotope Ratio Determinations by Femtosecond Laser Ablation-MC-ICPMS. Abstract. www.gemresearch.ch/news/Copper-isotope/Copper.htm

Lit.An15 Fritsch E. (2002) Gem News International: Red andesine feldspar from Congo. G&G, Vol. 38, No. 1, 94-95.

Lit.An16 Guillong M. and Günther D. (2001) Quasi 'non-destructive' laser ablation-inductively coupled plasma-mass spectrometry fingerprinting of sapphires. Spectrochimica Acta Part B-Atomic Spectroscopy, 56.1219-1231.

Lit.An17 Guilmette, C., Hebert, R., Dupuis, C., Wang, C.S., and Li, Z.J. (2008) Metamorphic history and geodynamic significance of high-grade metabasites from the ophiolitic melange beneath the Yarlung Zangbo ophiolites, Xigaze area, Tibet: Journal of Asian Earth Sciences, v. 32, p. 423-437.

Lit.An18 Günther D. and Hattendorf B. (2005) Solid sample analysis using laser ablation inductively coupled plasma mass spectrometry. Trac-Trend. Anal.Chem. 24(3): 255-265.

Lit.An19 Günther D., Frischknecht R. and Heinrich, C. A. (1997) Capabilities of a 193nm ArF Excimer Laser for LA-ICP-MS Micro Analysis of Geological Materials. J. Anal. At. Spectrom., 12: 939-944.

Lit.An20 Günther, D., Audétat, A., Frischknecht, A., Heinrich, C.A. (1998) Quantitative analysis of major, minor, and trace elements in fluid inclusions using laser ablation-inductively coupled plasma mass spectrometry J. Anal. At. Spectrom., 13, 263-270 (39)

Lit.An21 Guillong, M., Latkoczy, Ch., Jung Hun Seo, Günther, D., Heinrich, Ch. A. (2008) Determination of sulfur in fluid inclusions by laser ablation ICP-MS J. Anal. At. Spectrom., 23, 1581-1589.

Lit.An22 Hattendorf B., Latkoczy C. and Günther D. (2003) Laser ablation-ICPMS. Anal. Chem., 75(15): 341A-347A.

Lit.An23 Hofmeister, A.M., and Rossman, G.R. (1985), Exsolution of metallic copper from Lake County labradorite: Geology, v. 13, 644-647.

Lit.An24 Hughes R.W. (2010) Hunting Barack Osama in Tibet: In search of the lost andesine mines. www.ruby-sapphire.com/tibet-andesine.htm, Nov. 3.

Lit.An25 James R. (2008a) Sunrise over Oregon. www.yourgemologist.com/ISGForumsBoard/showthread.php?t=5566, Apr. 17.

Lit.An26 James R. (2008b) ISG report on the diffusion treatment of andesine! www.yourgemologist.com/ISGForumsBoard/showthread.php?t=5569, Jul. 23.

Lit.An27 Japan Germany Gemmological Laboratory (2008) Brief photo report from Tibet about andesine mine. <http://www.sapphire.co.jp/jggl/433.htm>

Lit.An28 Jewellery News Asia (2009) New copper isotopes method for testing copper-bearing gemstones. Show Daily. Hong Kong Convention and Exhibition Center. September 23, p. 6.

Lit.An29 Johnston, C.L., Gunter, M.E., and Knowles, C.R. (1991) Sunstone labradorite from the Ponderosa mine, Oregon: Gems & Gemology, v. 27, p. 220-233.

Lit.An30 Kratochvil G. (2008) The Great andesine scam. www.jewelcutter.com/articles/andesine_scam.htm, May 17.

Lit.An31 Krzemnicki M.S. (2004) Red and green labradorite feldspar from Congo. Journal of Gemmology, Vol. 29, No. 1, pp. 15-23.

Lit.An32 Laurs B.M. (2005) Gem News International: Gem plagioclase reportedly from Tibet. G&G, Vol. 41, No. 4, pp. 356-357.

Lit.An33 McClure, S.F. (2009) Observations on Identification of Treated Feldspar. GIA, News from Research, Sept. 10. <http://www.gia.edu/research-resources /news-from-research/identification-treated-feldspar.pdf>

Lit.An34 McDowell FW (1983) K-Ar dating: Incomplete extraction of radiogenic argon from alkali feldspar. Chemical Geology, 41, 119-126.

Lit.An35 Milisenda C., Furuya M. & Haeger T. (2008) A study of treated labradorite-andesine feldspars. Proceedings of the 2nd International Gem and Jewelry Conference GIT2008, 283–284.

Lit.An36 Prost, M.A., (2000), Its Day in the Sun: Colored Stone, v. 13, 10-15.

Lit.An37 Rose, C., and Rose, J., (1998), The Spice of Light: Lapidary Journal, v. 51, 14-18.

Lit.An38 Roskin G. (2008) JCK web exclusive: The andesine report. Jewelers' Circular-Keystone, posted November 12. <http://www.jckonline.com/article/291011-JCK_Web_Exclusive_The_Andesine_Report.php>

Lit.An39 Rossman, G. (2009) The Red Feldspar Project. California Institute of Technology, 8 pp. <http://www.gia.edu/research-resources/news-from-research/chemical-analyses.pdf>

Lit.An40 Rossman, G.R. (2011) The Chinese red feldspar controversy: Chronology of research through July 2009. Gems & Gemology, Vol. 47, No. 1, pp. 16–30.

Lit.An41 Sheldrick, G.M. (1996) SADABS. University of Göttingen, Germany.

Lit.An42 Sheldrick, G.M. (2008) A short history of SHELX. Acta Crystallographica, A64, 112-122.

Lit.An43 Ulrich, T., Günther, D., Heinrich, C.A. (1999) Gold concentrations of magmatic brines and the metal budget of porphyry copper deposits Nature, 399, 676-679.

Lit.An44 Thirangoon, K. (2009) Effects of Heating and Copper Diffusion on Feldspar: An Ongoing Research. GIA, News from Research, May 29, 29 pp. <http://www.gia.edu/research-resources/news-from-research/heating-diffusion-feldspar.pdf>

Lit.An45 Villa I.M., Hermann J., Müntener O., Trommsdorff V. (2000) 39Ar-40Ar dating of multiple zoned amphibole generations (Malenco, Italian Alps). Contributions to Mineralogy and Petrology, 140, 363-381.

Lit.An46 Villa I.M., Ruggieri G., Puxeddu M., Bertini G. (2006) Geochronology and isotope transport systematics in a subsurface granite from the Larderello-Travale geothermal system (Italy). Journal of Volcanology and Geothermal Research, 152, 20-50.

Lit.An47 Wang W., Lan Y., Lu T., Jiang W., Chen C., Li Q., Chen Z., Xie J. (2010) Letters to the Editors: Geological field investigation on the reported occurrence of 'red feldspar' in Tibet. Gems & Jewellery, Vol. 19, No. 4, 44-45.

About the Authors

Dr Peretti FGA FGG is Director of international GRS laboratories in Switzerland, Thailand, Hong Kong and Sri Lanka. GRS Gemresearch Swisslab AG, P.O. Box 3628, CH-6002 Lucerne, Switzerland.

adolf@peretti.ch

Prof. Villa is Professor for Isotope Geology and Geochronology at the Institute of Geological Sciences, University of Bern, Switzerland.

igor@geo.unibe.ch

Prof. Günther is Professor for Trace Elements and Microanalysis at the Laboratory for Inorganic Chemistry, ETH Zurich, Switzerland.

guenther@inorg.chem.ethz.ch

K. Hametner is Research Assistant for Laser Ablation-ICP-MS on gems at the Laboratory for Inorganic Chemistry, Günther Group, ETH Zurich, Switzerland.

hametner@inorg.chem.ethz.ch

L. Dorta is PhD student at the Department of Chemistry and Applied Biosciences Laboratory of Inorganic Chemistry, Günther Group, ETH Zurich, Switzerland.

Dr Fontaine, previously at the Laboratory for Inorganic Chemistry, Günther Group, ETH Zurich, Switzerland.

W. Bieri (Msc. EarthSc., FGA) is Research Gemologist at GRS Gemresearch Swisslab Ltd., Lucerne, Switzerland.

wbieri@gemresearch.ch

M. Meier (Msc. EarthSc.) is PhD student at the Department of Geosciences, University of Fribourg.

mario.meier@unifr.ch

Acknowledgments

This report would not have been possible without the contribution of samples from two of the expedition members (Dr Ahmadjan Abduriyim and Richard W. Hughes) to the new mines in Tibet in 2010. Also, they donated additional diffusion-treated samples from different sources. For the samples from Oregon and pictures from the Oregon mines, we are grateful to the support and consultation by Mariana Photiou (FGA), owner of mining claims in Oregon and in her own words "a promoter of good ethics and environmentally sound mining operations". The Dust Devil Mine operators donated samples and Don Buford consulted us on Oregon sunstone qualities and production. Their warm welcome at the Tucson show in 2011 was very motivating. She donated samples and provided the pictures from the Oregon mines and gemstones. Prof. Thomas Armbruster analyzed our samples for crystal structures and formulated the technical part on page 35-37. Prof. B. Grobety from the University of Fribourg facilitated the access to the SEM laboratory. Marco Cheung from Litto Gems Company provided pictures from some of the mines in Tibet (Yu Lin Gu, Zha Lin and Bainang) and helped organizing the GRS expedition to Tibet in 2009. Daniel Lam was very cooperative in organizing the Tibet expedition and translations in China. Litto Gems sponsored material from Inner Mongolia, old and new mines in Tibet and King Star Jewelry (Hong Kong) provided samples as well. We thank Glenn Lambrecht (Research Group Rock Water Interaction, Institute of Geological Sciences, University of Berne) and Dr Eric Reusser (IMP ETH ZH) for Raman spectroscopy, Sumeth Tanthadilok for graphics and artwork and Mr. Saleem Michael for preparing this report for the internet at www.gemresearch.ch.

Red andesine from different collection points in Tibet have been tested for authenticity. Copper-bearing red andesine from the so-called new mines in Tibet (first reported in 2010) can be discriminated from diffusion-treated counterparts using high-resolution analytical techniques and methods.

The geological process of Tibetan andesine formation involved the circulation of sulfur-rich fluids that enriched Copper in the feldspars, producing a characteristic natural chemical signature.

The authenticity protocol used in this work is based on elemental fingerprints, isotopic ratio determinations of copper and argon, and micro chemical fluid inclusion analyses.

Our measurements for hand-collected materials from the old mines (first reported in 2008) partly confirm them as authentic. Instead, most of the faceted gem quality stones in the market overlap with the chemical fingerprints of diffusion-treated andesine. The authenticity remains undeterminable unless destructive methods can be used for testing.

GRS GEMRESEARCH SWISSLAB

6002 Lucerne, Switzerland.
www.gemresearch.ch

Online Version

Order this book

ISBN 978-3-9523867-0-5

978-3-9523867-0-5